The molecular role of spatacsin : regulating endolysosomal function at the level of endoplasmic reticulum-endolysosomes contact sites

Alexandre Pierga

THESE

Pour obtenir le grade de docteur délivré par

SORBONNE UNIVERSITE

Ecole doctorale Cerveau, Cognition et Comportement (ED 158)

Spécialité Neurosciences

THE MOLECULAR ROLE OF SPATACSIN: REGULATING ENDOLYSOSOMAL FUNCTION AT THE LEVEL OF ENDOPLASMIC RETICULUM-ENDOLYSOSOMES CONTACT SITES

Par Alexandre Pierga

Dirigée par Frédéric Darios

Présentée le 24 janvier 2022

Devant le jury composé de :

Dr BOMONT Pascale	Rapporteur
Pr REID Evan	Rapporteur
Dr DANGLOT Lydia	Examinateur
Dr DELEVOYE Cédric	Examinateur
Dr POTIER Marie-Claude	Examinateur
Dr DARIOS Frédéric	Directeur de thèse

Résumé grand public en français

Cette étude porte sur les maladies du neurone moteur et sur les liens entre dysfonctions cellulaires et mort neuronale. Nous travaillons sur une forme génétique de maladie du neurone moteur causée par des mutations du gène SPG11. Ces mutations conduisent à la perte de fonction de la protéine codée par ce gène, la spatacsine. Notre objectif est de comprendre comment des défaillances cellulaires causées par la perte de fonction de spatacsine peuvent conduire à l'apparition d'une maladie chez les patients.

D'après des études récentes, la fonction de la spatacsine est liée aux compartiments d'élimination des déchets cellulaires : les lysosomes. Ces organelles sont sphériques mais ont la capacité de former des tubules avec leur membrane, afin de procéder à la formation de nouveaux lysosomes. En absence de spatacsine, leur fonctionnement se dérègle entrainant la mort des neurones. Le but de ce projet est d'identifier quelle est la fonction de la spatacsine dans la formation des tubules.

Nous nous intéressions à la capacité qu'ont les lysosomes, lieux de la dégradation cellulaire, à déformer leur membrane et à devenir allongés ou tubulaires. Or, nous avons découvert que cette capacité à se déformer repose sur l'action de notre protéine d'intérêt : la spatacsine.

La spatacsine est une protéine qui ne déforme pas elle-même la membrane des lysosomes. Son rôle est de mettre en relation d'autres protéines pour permettre cette déformation. Pour réaliser son action, la spatacsine a une position stratégique. Elle se trouve dans l'organelle le plus imposant de la cellule : le réticulum endoplasmique. Et si la spatacsine a la capacité de réguler la fonction des lysosomes, c'est car le réticulum endoplasmique et les lysosomes sont par endroits extrêmement proches. On appelle ces zones des zones de contacts, elles ont été récemment mises en lumières par de nombreux travaux qui démontrent leur implication dans de diverses fonctions de régulation des mécanismes cellulaires.

Par sa présence à ces zones de contact entre réticulum et lysosomes, la spatacsine interagit avec d'autres protéines qui vont déformer la membrane des lysosomes. La spatacsine interagit également avec certaines protéines pour en dégrader d'autres. Ainsi elle orchestre à l'interface entre le réticulum et les lysosomes l'action d'une machinerie complexe qui permet aux lysosomes de se déformer, de se déplacer et de se positionner dans la cellule.

A court terme, il apparait important de relier ce que nous avons découvert du fonctionnement de la régulation de la dynamique des lysosomes par la spatacsine à la mort neuronale. Dans un second temps, l'objectif sera d'agir sur le mécanisme que nous avons identifié, afin de prévenir la dysfonction des lysosomes. Prévenir la dysfonction lysosomale permettra potentiellement de prévenir la mort neuronale.

Le défi est de relier les différentes échelles d'études, c'est-à-dire de réussir à transposer le savoir acquis dans nos modèles d'étude cellulaire à l'échelle d'un éventuel traitement qui empêcherait la mort neuronale due à l'absence de spatacsine. Ainsi, un mécanisme prévenant la mort neuronale en culture devra être transposé à l'échelle d'un organisme entier, sur notre modèle de souris, puis à l'échelle du patient humain, si toutes les étapes préliminaires sont franchies avec succès.

Résumé de la thèse en français

Notre objectif durant ce projet a été de définir la fonction moléculaire de la spatacsine et sa localisation cellulaire qui restent mal connues. L'identification de la fonction moléculaire de la spatacsine permettra une meilleure compréhension des mécanismes cellulaires à l'origine de la mort neuronale dans des modèles de maladie du neurone moteur.

Nous avions trois objectifs principaux afin de déterminer la fonction moléculaire de la spatacsine.

1° Tout d'abord il apparaissait important de définir la localisation subcellulaire de la spatacsine qui reste controversée. Notre objectif était d'identifier à quelle(s) membrane(s) se lie la spatacsine et nos résultats préliminaires semblait indiquer qu'elle était principalement localisée au niveau du réticulum endoplasmique, ce que nous avons confirmé.

2° Ensuite, notre deuxième objectif était d'identifier comment la spatacsine pouvait réguler la formation de lysosome tubulaires et notre hypothèse était que cette régulation était liée à la formation de zones de contact entre le réticulum endoplasmique et les lysosomes.

3° Notre troisième et dernier objectif consistait à identifier le rôle de la spatacsine dans la régulation de la dégradation ubiquitine-dépendante. En effet, nos résultats préliminaires indiquaient que la spatacsine interagissait avec plusieurs protéines de la voie ubiquitine-protéasome pour réguler la formation de lysosomes tubulaires.

Notre premier objectif dans ce projet était de préciser la localisation subcellulaire de la spatacsine. Grâce à l'utilisation de techniques de microscopie à super-résolution, nous avons pu observer que la spatacsine, exprimée avec un tag permettant sa détection dans des fibroblastes de souris, se localise au niveau du réticulum endoplasmique. Ce résultat a été confirmé par d'autres expériences que nous avons menées et qui reposaient sur le fractionnement subcellulaire de cerveaux de souris. Par des méthodes de centrifugations différentielles et d'isolation de compartiments à l'aide de gradients, nous avons pu montrer que la spatacsine était enrichie au niveau de la fraction subcellulaire contenant le réticulum endoplasmique. Enfin, nous avons également pu montrer que la spatacsine était fortement associée à la membrane du réticulum endoplasmique car seuls de forts détergents la solubilisent.

Notre second objectif concernait le rôle de la spatacsine dans la régulation de la dynamique des lysosomes tubulaires et l'éventuelle implication de contacts entre le réticulum endoplasmique et les lysosomes dans cette régulation. Nous avons montré en observant les lysosomes tubulaires en live imaging sur cellules intactes et exprimant des protéines fluorescentes, que la spatacsine, via son domaine C-terminal régulait la formation de lysosomes tubulaires mais également leur vitesse de déplacement et leur durée de vie. Nous avons également montré que cette altération des propriétés des lysosomes tubulaires avait pour conséquence une redistribution des lysosomes plus proches du noyau en absence de spatacsine.

Les lysosomes tubulaires ont une relation privilégiée avec le réticulum endoplasmique. Des approches de super-résolution et de live imaging ont permis de montrer

que les lysosomes tubulaires sont extrêmement proches du réseau de réticulum endoplasmique et que leur déplacement se fait le long de ce réseau. De plus il apparaît que les contacts entre le réticulum endoplasmique et les lysosomes sont altérés en absence de spatacsine. Au niveau de ces zones de contacts, la spatacsine réticulaire interagit avec son partenaire lysosomal, la spastizine. La spastizine est une protéine dont la mutation perte de fonction cause une forme de paraplégie spastique héréditaire, la forme SPG15, qui est très similaire à la forme SPG11 sur laquelle nous travaillons. Nous avons également pu mettre en évidence que la spastizine interagit avec la Kinésine KIF13A, qui est un moteur moléculaire et qui permet de former les lysosomes tubulaires et de promouvoir leur mouvement. L'interaction entre spatacsine et spastizine au niveau des zones de contacts entre le réticulum endoplasmique et les lysosomes est donc extrêmement importante pour la formation de lysosomes tubulaires.

Enfin, pour notre troisième objectif concernant le rôle de la spatacsine dans la dégradation dépendante de l'ubiquitine, nous avons montré grâce à une méthode innovante de criblage basée sur l'analyse d'image automatisée, que la spatacsine interagissait avec des protéines liées à la dégradation ubiquitine-dépendante pour réguler la formation de lysosomes tubulaires. Ainsi, la spatacsine a la capacité d'interagir via son domaine C-terminal avec la protéine UBR4 pour dégrader un autre de ses partenaires lysosomaux : AP5z1. Cette dégradation est nécessaire pour éviter que AP5z1 soit trop présent aux lysosomes, et par son interaction avec la spatacsine, empêche celle-ci d'interagir avec son autre partenaire la spastizine. En effet, perturber l'interaction spatacsine-spastizine, empêche le recrutement de la spastizine aux lysosomes et empêche la formation de lysosomes tubulaires. Nous avons également pu montrer que l'interaction spatacsine-spastizine était dépendante de l'architecture du réticulum endoplasmique car perturber celle-ci empêche l'interaction entre les deux protéines.

A la suite de ce projet, qui a permis d'identifier de nouvelles fonctions de la spatacsine dans la régulation de la dynamique des lysosomes tubulaires d'une part et qui a identifié de nouvelles fonctions pour les contacts lysosomes-réticulum endoplasmique d'autre part, il apparait important de continuer à investiguer le rôle de la spatacsine.

Nous avons fait des progrès significatifs dans la compréhension des mécanismes moléculaires impliquant la spatacsine, et de nombreuses questions sont soulevées par ces nouveaux résultats. Il apparaît tout d'abord important de savoir si ces mécanismes de régulation de la fonction lysosomale sont les mêmes dans les modèles neuronaux. En effet, ce sont les neurones qui sont le plus affectés par la pathologie SPG11. Ainsi, nous pourrons évaluer si ces fonctions de la spatacsine sont liées à l'apparition de la neurodégénérescence.

De plus, afin de mieux comprendre le mécanisme de régulation de la formation des lysosomes tubulaires par la spatacsine, certains tests sont nécessaires comme identifier comment le système répond à divers stress cellulaires. Enfin, il apparaît important d'identifier par quels mécanismes nous pourrions compenser l'absence de spatacsine sur la formation des lysosomes tubulaires afin de voir s'il est possible de prévenir la neurodégénérescence liée à la dysfonction lysosomale dans la paraplégie spastique de type 11.

ABSTRACT

The loss of spatacsin, involved in hereditary spastic paraplegia type SPG11, causes lysosomal dysfunction. The molecular function of spatacsin has, thus far, remained elusive. Here, we used a combination of trained neural networks and targeted image analysis coupled to an siRNA screen to show that spatacsin function is associated with ubiquitin-mediated proteolysis. We demonstrated that spatacsin controls lysosome morphology and dynamics by acting at the contact sites between the Endoplasmic Reticulum (ER) and lysosomes and that this regulatory function of spatacsin relies on ubiquitin-dependent degradation of AP5Z1.

Spatacsin is required for the formation and dynamics of tubular lysosomes. We identified a pool of lysosomes with a tubular shape that corresponds to dynamic lysosomes.

The highly dynamic tubular lysosomes we observed in mouse fibroblasts were strongly associated with the ER. Consistent with this finding, spatacsin was localized to the ER and interacted with lysosome-localized spastizin at the contact sites between the ER and lysosomes. Our data show, for the first time, that proteins acting at contact sites between the ER and lysosomes regulate the motility of lysosomes along the ER network. We identified AP5Z1, known to interact with spatacsin and localized in lysosomes, as a protein degraded in a ubiquitin- and spatacsin-dependent manner to regulate tubular lysosome formation and motility. However, spatacsin required several of its partners, such as UBR4, to mediate AP5Z1degradation.

Importantly, the interaction of spatacsin with its partners, spastizin and AP5Z1, is modulated by the morphology of the ER network and could thus play a role in coupling ER morphology to lysosome function.

We thus identify spatacsin as a protein present at contact sites between the ER and lysosomes that is critical for the coordination of lysosome trafficking with ER network morphology.

THE MOLECULAR ROLE OF SPATACSIN: REGULATING ENDOLYSOSOMAL FUNCTION AT THE LEVEL OF ENDOPLASMIC RETICULUM-ENDOLYSOSOMES CONTACT SITES

Contents

INTRODUCTION

I. Context of Study

a) The growing need to tackle neurodegenerative diseases

Neurodegenerative diseases constitute a major discipline of interest as the world population gets older. According to the World Health Organization & United Nations, there will be two billion people over the age of 60 in 2050 (against one billion in 2020). Among diseases that come with ageing, Alzheimer's Disease is the most frequently diagnosed. It is stated that it affects 5% of adults over 65 and up to 50% of adults over 85 years old (Cummings, 2004). On top of the distress caused by the disease itself on individuals, with symptoms such as apathy, anxiety, depression, sleep disorders, etc. (Ritchie and Lovestone, 2002), the cost for society of the care of patients is enormous. In 2015, the global societal cost of dementia was estimated to be 818 billion of dollars (Ritchie and Lovestone, 2002). It is therefore one of the challenges of the 21st century to better understand the mechanisms of neurodegeneration.

For the most frequent neurodegenerative diseases such as Alzheimer, the etiology is unknown: it is thus difficult to study their physiopathology and to develop therapeutic strategies. In contrast, there are many rare neurodegenerative diseases of identified genetic origin. In these cases, the etiology is a known gene mutation, allowing development of relevant models to study these diseases. My thesis focuses on a group of rare neurodegenerative diseases, Hereditary Spastic Paraplegias.

b) Hereditary Spastic Paraplegias (HSP)

HSP prevalence & common mechanisms with other neuro-degenerative disorders

HSP constitute a family of neurodegenerative diseases with a genetic origin. They are rare (with an estimated prevalence of 3-9/100 000 in Europe/North America) (Blackstone, 2012; Blackstone et al., 2011) but their study is important for the patients and also to understand the mechanisms of the onset and the progression of neurodegenerative diseases in general. Indeed, there are common cellular mechanisms that are affected between Hereditary Spastic Paraplegias and more frequent diseases such as Alzheimer Disease, Parkinson disease or Huntington disease. Whether it is at the level of lysosomal dysfunctions (Ferguson, 2019; Lie and Nixon, 2019; Neefjes and van der Kant, 2014; Schreij et al., 2016), at the level of mitochondrial dysfunctions (Kwong et al., 2006), endoplasmic reticulum regulation (Chiurchiù et al., 2014), lipid accumulation (Sipione et al., 2020) or microtubule disruption (Zempel and Mandelkow, 2015).

One of the particularity of Hereditary Spastic Paraplegias is that the disease can occur at any age, due to the number of different genes that are affected, but the onset is more common in childhood or early adulthood (Erfanian Omidvar et al., 2021).

Classification of HSPs

HSP present a high variability of symptoms, but they are characterized by a common feature: the degeneration of the pyramidal tract, also known as cortico-spinal tract (See **Figure 1**). This tract is involved in the control of voluntary movements and is formed by the axons of neurons of the motor cortex projecting towards motoneurons of the spinal cord (Blackstone, 2012). Degeneration of the pyramidal neurons results in the development of a pyramidal syndrome with lower limb spasticity that will worsen with the disease progression. The degeneration of the tract happens in a retrograde pattern, causing an axonopathy, so the lower limbs are the first to be affected (Deluca et al., 2004).

Common symptoms

The pyramidal syndrome is characterized by a spasticity of the lower limbs. Patients have a motor weakness that can go up to paralysis. Spasticity corresponds to a muscular stiffness caused by muscle hyper contractibility, which is normally inhibited by the cortico-spinal tract.

Other symptoms can be observed in HSP patients along the pyramidal syndrome, constituting complex forms of HSP. These symptoms and include ataxia, dementia, cognitive impairment, neuropathy, epilepsy, etc. (Fink, 2013; Harding, 1983; Lo Giudice et al., 2014) – (see **Figure 1**) . The only treatments available for patients are targeting the muscle contraction to limit the spasticity, but no curative treatment of the disease exists so far.

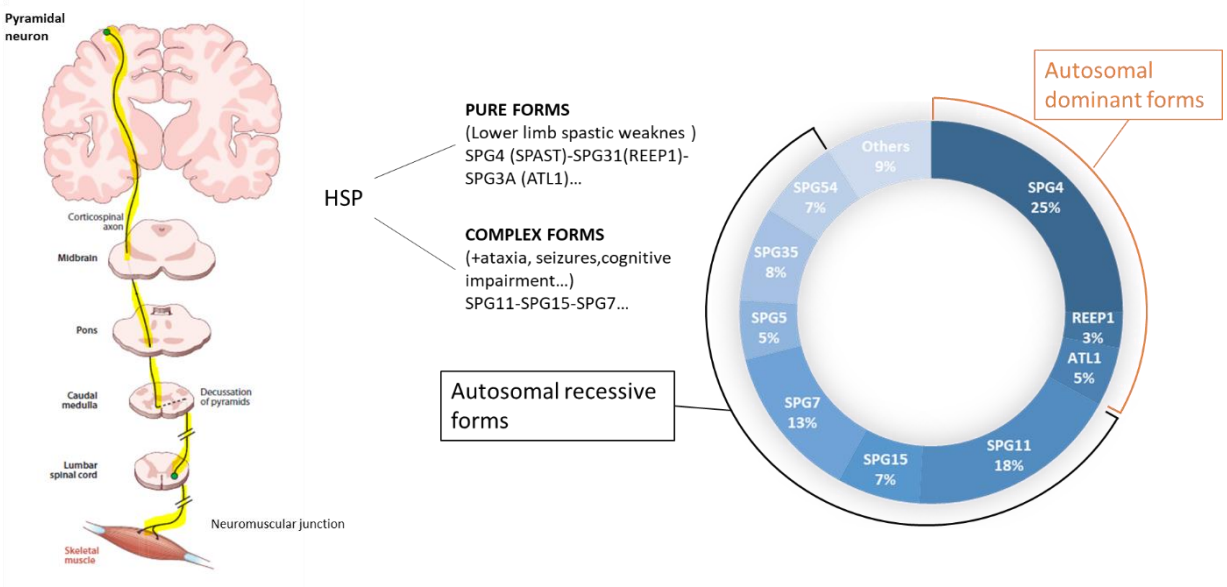

Figure 1: Left: Scheme showing the cortico-spinal tract in yellow (adapted from (Blackstone, 2012)). **Right:** Prevalence of complex and pure forms of HSP (*From Blackstone et al, 2011-2012-2018 + Ghaedi et al, 2019)*

Over 80 SPG genes have been identified to be causing forms of HSP when mutated explaining the variability of symptoms. The transmission of the disease can be autosomal recessive or dominant (see **Figure 1**). Among these diversity of genetic causes for HSP, there are also several different cellular pathways that are affected by mutations responsible for HSPs.

c) Cellular pathways impaired in Hereditary Spastic Paraplegias

Several cellular pathways have been shown as altered in HSPs such as Endoplasmic Reticulum Shaping, the endolysosomal pathway, transport of cargoes or mitochondrial function. My goal is not to list all organelles or pathways affected by HSP proteins mutations as it has been done extensively and in details by fellow researchers (Blackstone, 2012; Blackstone et al., 2011; Toupenet Marchesi et al., 2021).

HSP proteins involved in Endoplasmic Reticulum shaping

Traditionally, the proteins of HSP pure forms have been associated with the Endoplasmic Reticulum (ER). Spastin (SPG4), for example, is an ATPase that severs microtubules (Connell et al., 2009) but its isoforms starting at methionine M1, that has the particularity to have an hairpin domain, is located to the ER and participates to its morphogenesis (Park et al., 2010). It appears that Spastin cooperates with GTPase Atlastin1 (SPG3A)(Rismanchi et al., 2008) and with REEP1 (SPG31) to ensure that the structure of the ER is properly formed, especially at the level of the ER-tubular network and the formation of three-way junctions (Park et al., 2010). As lipid droplets are formed at the ER (Walther et al., 2017), the loss of the HSP proteins involved in the ER morphogenesis have consequences on the lipid droplets biogenesis (Klemm et al., 2013; Papadopoulos et al., 2015).

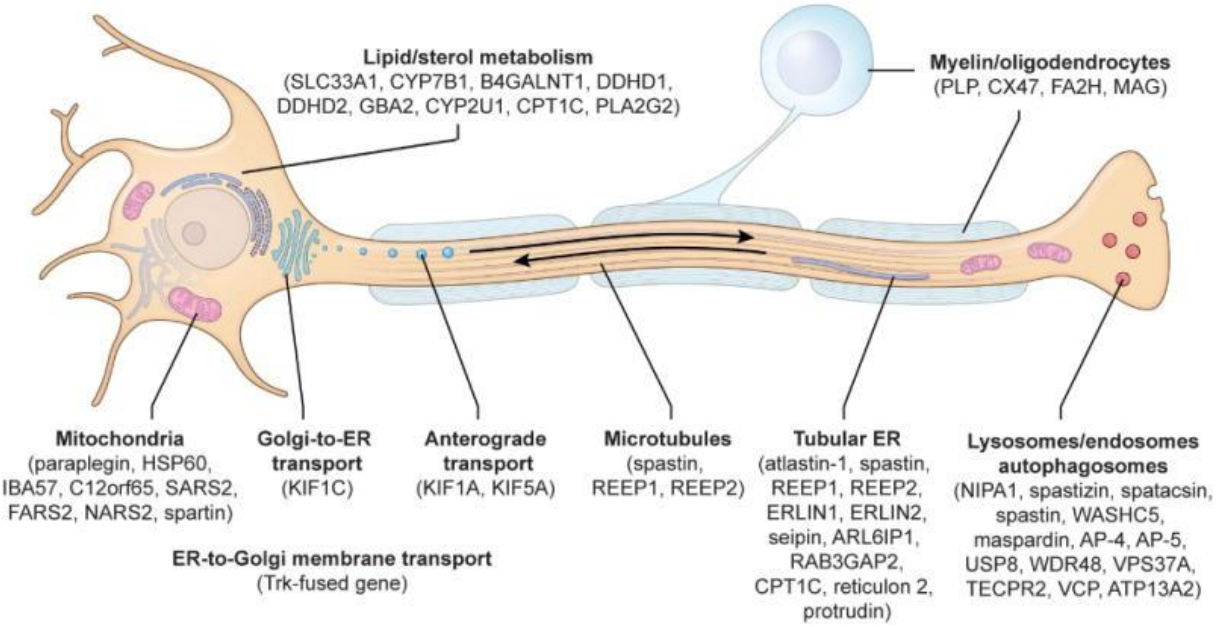

Figure 2 : HSP proteins are represented in multiple cellular pathways (Blackstone, 2012).

HSP proteins involved in endo-lysosomal pathway

Another example of a cellular compartment that is commonly affected by HSP proteins mutations is the endolysosomal compartment. Showing that there are multiple levels of interaction between organelles and that the loss of one protein doesn't have only one type of consequence, the loss of Spastin has an impact on endosomal fission as well (Allison et al., 2013). These cases of multiple organelles dysfunctions in the cell help researchers identify new pathways of regulation & interactions between organelles. Lysosomal defects caused by mutations of ER proteins have been also identified in SPG8 (strumpellin) and SPG31 (REEP1) HSP forms (Allison et al., 2017a).

The lysosomal compartment fails to renew itself in SPG11 and SPG15 (Chang et al., 2014a). This leads to lysosomal accumulation in SPG11 and SPG15 HSPs (Branchu et al., 2017; Khundadze et al., 2013a) and SPG48 HSP also presents some forms of lysosomal accumulation (Khundadze et al., 2019a).

HSP proteins & mitochondria

The paraplegin protein (SPG7) is localized at the mitochondria and its absence is responsible for mitochondrial defect (Casari et al., 1998). ER-protein REEP1 is also involved at the level of the mitochondria as it facilitates the formation of contacts between the ER and mitochondria and this plays a role in neurodegeneration (Lim et al., 2015). The protein Spartin (SPG20) is localized to mitochondria (Lu et al., 2006), and it has been reported as playing a role in mitochondrial metabolism (Ring et al., 2017) and in mitochondrial respiratory chain (Spiegel et al., 2017).

HSP proteins and cellular transport

The motor protein, KIF5A (SPG10) is promoting axonal transport of mitochondria, which is very important for the survival of motor neurons (Karle et al., 2012). Spastin (SPG4), that we mentioned earlier, is involved in cellular polarization, by interacting with protrudin and regulates bone morphogenetic protein receptor trafficking in the cell (Connell et al., 2020). Other kinesins KIF1A (SPG30) and KIF1C (SPG58) that are involved in cargo transport at neurites are mutated in forms of HSPs (Caballero Oteyza et al., 2014; Citterio et al., 2015)

Hereditary Spastic Paraplegias constitute a family of very diverse disorders, they share however several symptoms. Similarly, the proteins mutated in forms of HSP are implicated in a few different cellular pathways and similarities between disorders emerge, several main themes are found between pathologies. Therefore, studying the cellular mechanisms involved in the disease development of a given HSP is also potentially relevant for the study of other HSPs or neuronal pathologies.

II. Hereditary Spastic Paraplegia Type SPG11

a) A complex form of HSP

Symptoms

The type SPG11 of HSP is the most frequent autosomal recessive HSP (Tesson et al., 2015) and it is indissociable from a clinician point of view from the SPG15 type (Hanein et al., 2008a). It is a complex form of HSP meaning that patients can have several other symptoms additional to the pyramidal syndrome (de Souza et al., 2017). The most frequent symptoms additional to the pyramidal syndrome are a cognitive impairment, a thinning of the corpus callosum, ataxia (a lack of muscle control or coordination of voluntary movements), visual impairment etc. (see **Figure 3**).

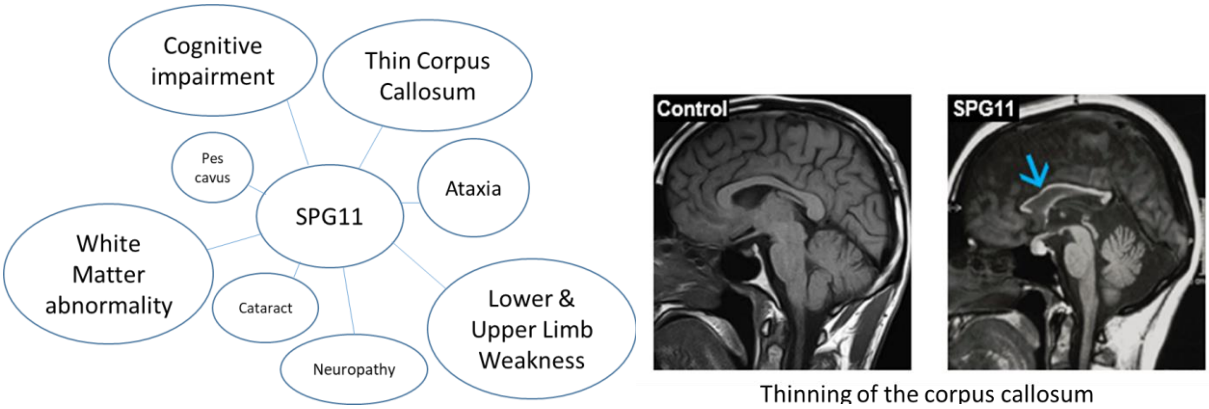

Figure 3: Symptoms of HSP type SPG11. **Left**: Frequent symptoms associated to SPG11 HSP. **Right**: illustration of thinning of the corpus callosum in SPG11 HSP (blue arrow) that can be observed by MRI (Boukhris et al., 2008).

Mutations of SPG11 have been associated to other diseases

Variability of symptoms in SPG11 led to classification of SPG11 patients as suffering from Amyotrophic Lateral Sclerosis (ALS) or Charcot-Marie Tooth disease (CMT). For ALS, it constitutes a rare subset of the disease with a genetic origin and a juvenile onset as typical age of onset of regular ALS is normally 55-75 years and the origin of the disease is mainly sporadic (Denora et al., 2016a; Orlacchio et al., 2010). The theme of clinical overlap between HSP and forms of amyotrophic lateral sclerosis has been discussed as they have in common to show prominent upper motor neurons signs (Fink, 2001; Strong and Gordon, 2005). For Charcot-Marie Tooth, this neuropathy shows damage to peripheral nerves and in particular the ones controlling lower limb muscles and mutations of SPG11 gene can cause such clinical features (Montecchiani et al., 2016).

b) Cellular biology of SPG11 HSP

b.1 spatacsin: the product of SPG11 gene

Most mutations observed in SPG11 patients are missense mutations (Stevanin et al., 2008), suggesting that the disease is due to the loss of function of the SPG11 gene product spatacsin. Spatacsin is a 2443 amino acids protein in human (280 kDA) (Stevanin et al., 2007a). This long protein -the median length of protein in *H. Sapiens* is 375 a.a (Brocchieri and Karlin, 2005)- is of unknown structure, only putative domains have been identified and are represented in **Figure 4** (Cogo et al., 2020; Hirst et al., 2013a; Stevanin et al., 2007a).

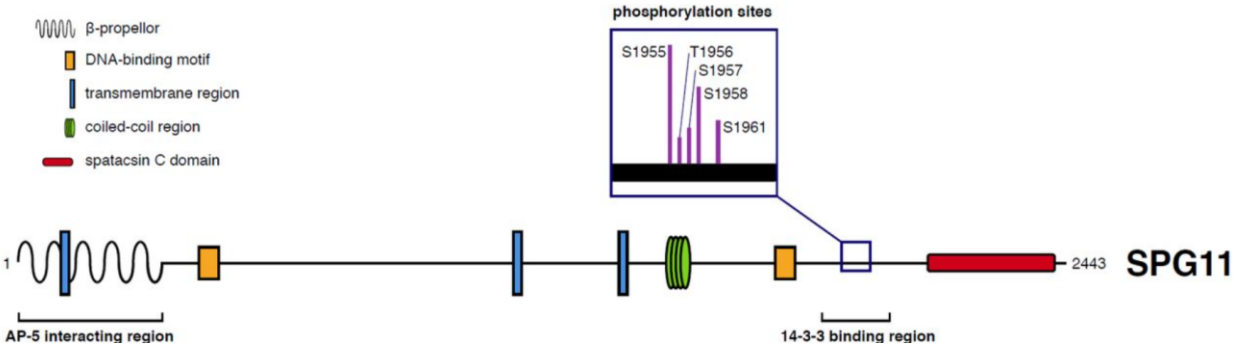

Figure 4 : Representation of the putative domains of spatacsin Protein (Cogo et al., 2020)

One particularly interesting domain of spatacsin might be its Cter domain also known as "Spatacsin_C" domain. In a recent study, it has been proposed that this domain that was conserved through evolution might have a tertiary structure homologous to VPS16_C protein (Alexander L. Patto and O'Kane, 2020). This could bring us information on a potential function for this domain as VPS16 is known to be part of the HOPS complex and to participate in endolysosomal transport (Alexander L. Patto and O'Kane, 2020).

b.2 Cellular localization of spatacsin

Sucellular localization of spatacsin has been largely investigated, but it is still debated. Spatacsin is expressed at very low endogenous levels in cells and the antibodies against it are poorly specific. From the literature, when using anti-spatacsin antibodies, it seems that spatacsin cellular localization is cytoplasmic, with a granular pattern (see **Figure 5**).

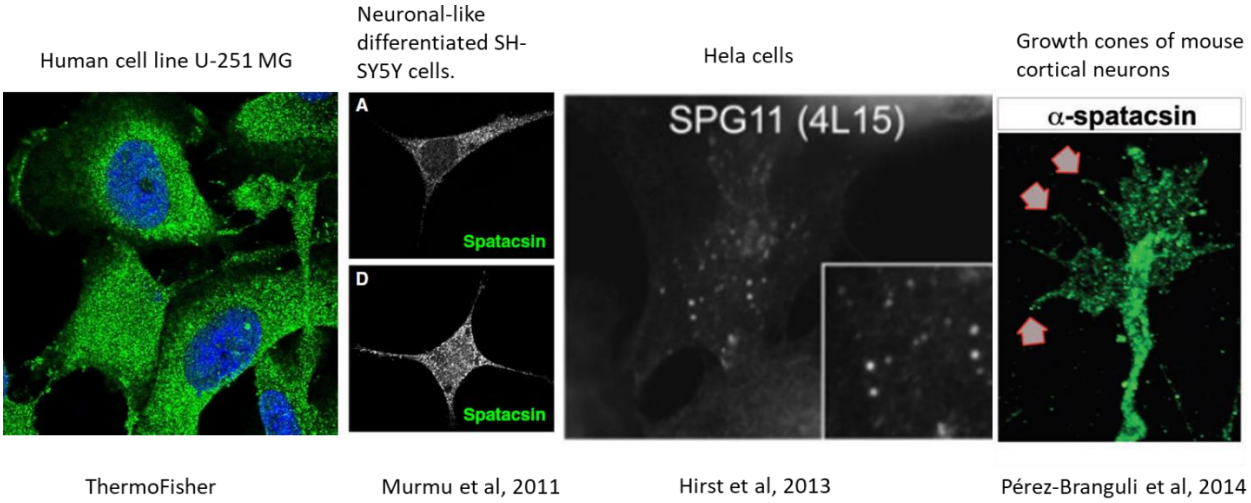

Figure 5: Subcellular localization of spatacsin in various cell types using antibodies against spatacsin (Hirst et al., 2013a; Murmu et al., 2011a; Pérez-Brangulí et al., 2014)

This diffuse localization does not give precise information on spatacsin sub-cellular compartment association, it can be sometimes seen as colocalizing with ER (Cogo et al., 2020; Murmu et al., 2011a) or cytoskeleton (Murmu et al., 2011a; Pérez-Brangulí et al., 2014).

Using over-expressed constructs of spatacsin coupled to a tag or cell lines stably expressing tagged spatacsin show a diffuse and granular cytoplasmic staining pattern (see **Figure 6**).

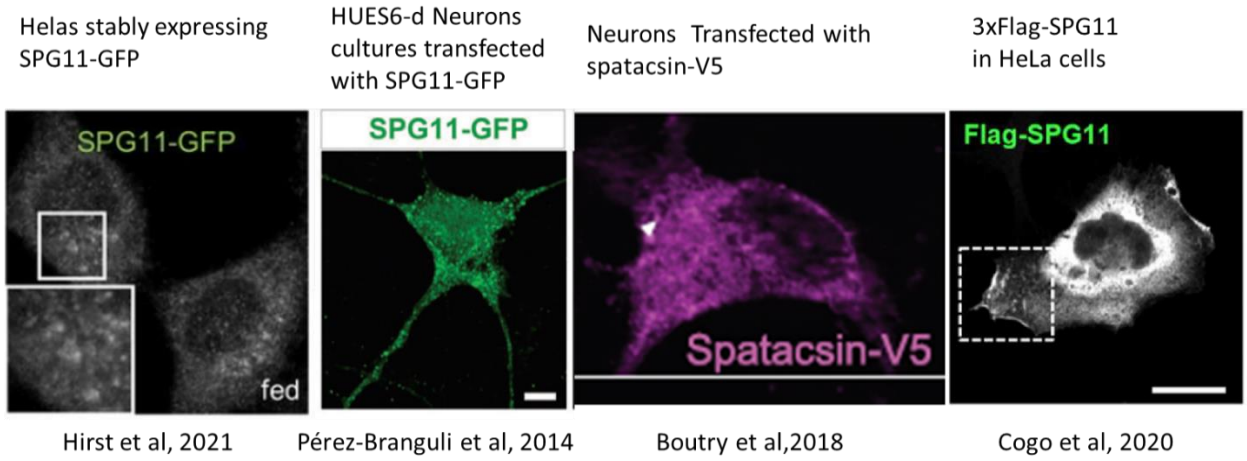

Figure 6: Subcellular localization of spatacsin in various cell types expressing a tagged spatacsin (Boutry et al., 2018; Cogo et al., 2020; Hirst et al., 2021a; Pérez-Brangulí et al., 2014).

The precise subcellular localization of spatacsin remains vague, but there is a convergence in the literature pointing toward a partial and transitory localization of spatacsin at the endolysosomal compartment (Boutry et al., 2018; Hirst et al., 2021a, 2013a; Schröder et al., 2007; Wyant et al., 2018). Indeed it seems that spatacsin can be recruited to lysosomes either in starvation conditions (Hirst et al., 2021a; Wyant et al., 2018) or in conditions of lipid accumulation in lysosomes (Boutry et al., 2018), see **Figure 7**.

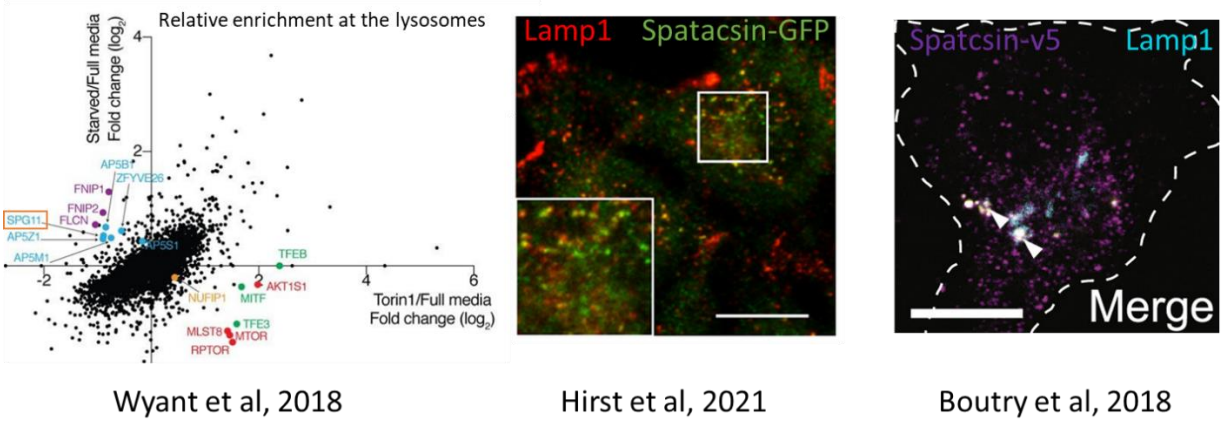

Figure 7 : Spatacsin is enriched at the lysosomes in response to different cellular stresses (Boutry et al., 2018; Hirst et al., 2021a; Wyant et al., 2018).

b.3. Spatacsin 's role at the endolysosomal compartment

Endolysosomal compartment is enlarged in absence of spatacsin

Besides spatacsin partial localization at the endolysosomes, there have been several studies pointing toward a role of spatacsin at the level of the late endosomes/lysosomes (see **Figure 6**). One of the first study on SPG11 patients fibroblasts showed an enlargement of the endolysosomal compartment (stained by LAMP1 Lysosomal protein) in absence of spatacsin, compared to healthy controls (Renvoisé et al., 2014). In another study on Hela cells, in starvation (i.e., a culture medium depleted from amino acids), cells acquired an enlarged endolysosomal compartment after 6h of starvation. After 24h, the compartment normally returns to its original size but this does not happen in absence of spatacsin (Chang et al., 2014), showing that spatacsin is required for lysosomes recovery.

Spatacsin is involved in Lysosome Recycling during Autophagy

Autophagy is an evolutionarily conserved process by which cytoplasmic proteins and organelles are catabolized (Mizushima and Komatsu, 2011) During starvation, the protein mTOR (mammalian target of rapamycin), a nutrient-responsive kinase, is inhibited, and this induces autophagy. In autophagy, autophagosomes envelop and sequester intracellular components and then fuse with lysosomes to form autolysosomes, which degrade their contents to regenerate nutrients. The regulation of autophagy in response to nutrients abundance is dependent on mTOR signaling, which is inhibited during initiation of autophagy.

Reactivation of mTOR happens after prolonged starvation and attenuates autophagy and generates proto-lysosomal tubules. The lysosomes renew themselves via a process of membrane budding and formation of tubes followed by fission to form new proto lysosomes. This process is called Autophagic Lysosomal Reformation (ALR) (Yu et al., 2010)(see **Figure 8**).

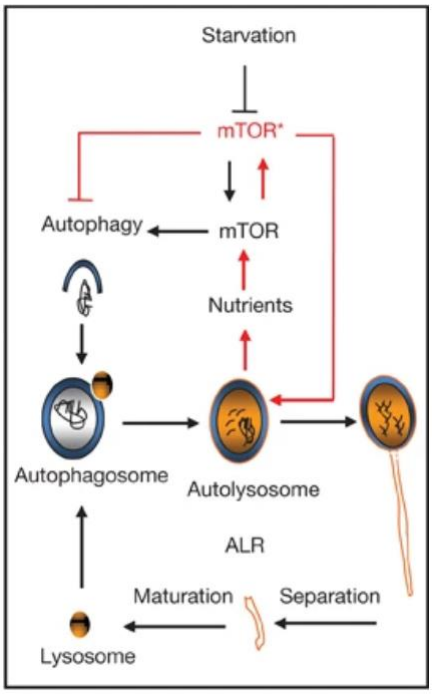

Figure 8 : Autophagic Lysosomal Reformation during prolonged starvation (Yu et al., 2010).

In absence of spatacsin, less tubules are observed emanating from lysosomal membrane in starvation conditions and this results in an impairment of the reformation of the lysosomes pool leading ultimately to a lysosome depletion (Chang et al., 2014a). These results indicate that spatacsin has a role in the process of reforming new membranes from the lysosomes in starvation conditions.

b.4. Dysfunctions in the clearance of degradation-destined cargoes

Accumulation of autophagosomal content in absence of spatacsin

An impressive convergence of data in the literature of SPG11 HSP indicates that in absence of spatacsin, there is an accumulation of autophagosomes membrane marker (LC3-II) or autophagosomes content (p62) (See **Figure 9**). Whether it was measured by counting the amount of vesicles positive for these markers or by measuring global levels of these proteins, virtually all studies showed an impairment in absence of spatacsin (Boutry et al., 2018; Branchu et al., 2017; Chang et al., 2014a; Khundadze et al., 2021; Renvoisé et al., 2014; Vantaggiato et al., 2019; Varga et al., 2015). This indicates that the content that was destined for degradation was not normally degraded by the cell in absence of spatacsin.

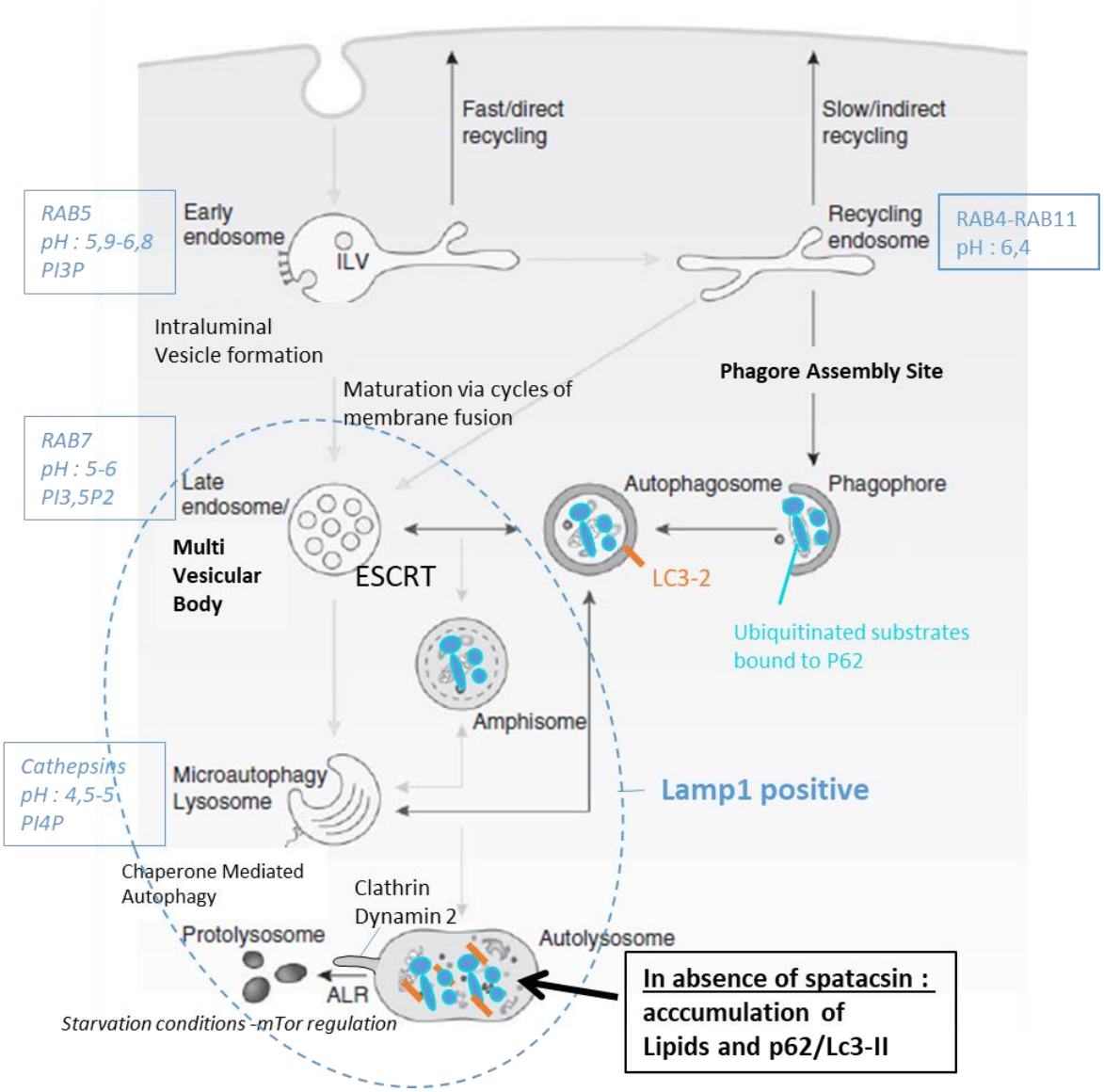

Figure 9 : Endosome biogenesis & autophagy pathways to the lysosome, adapted from (Reggiori and Klumperman, 2016).

No alteration of lysosomal degradation capacity in absence of spatacsin

Interestingly, in vitro assays testing lysosomal degradation agree that there is no enzymatic alteration of the lysosomes in absence of spatacsin and that nor their acidification nor degradative capacities are altered (Branchu et al., 2017; Chang et al., 2014a; Renvoisé et al., 2014; Varga et al., 2015). However, it is still possible that some enzymatic activities of lysosomes are altered in vivo. Measuring such activities in vivo is challenging and has not been evaluated in SPG11 models.

The cargo degradation defects observed in absence of spatacsin could also be explained by a default of autophagosomes – lysosomes fusion (Khundadze et al., 2021). Moreover, other types of accumulation of cargoes have been observed in the brain of SPG11 patients such as ubiquitin aggregates in granular lysosome like structures or P62/TDP43 accumulation resembling amyotrophic lateral sclerosis lesions (Denora et al., 2016a) (Mori et al., 2021).

b.5. The role of lipids in lysosomal clearance in SPG11 HSP

In a Spg11 knockout mouse model, along with accumulation of autophagic degradation content, a lack of lipid droplets accompanied with a slower lipid clearance from the lysosomes was observed (Branchu et al., 2017). This was confirmed in following studies where the nature of the lipid accumulation was identified as simple gangliosides such as GM2 and cholesterol (Boutry et al., 2019a, 2018). Interestingly, the accumulation of lipids was linked to lysosomal membrane recycling processes dependent of spatacsin, dynamin and clathrin which seemed to share many features with autophagic lysosomal reformation but occurred in basal conditions (Boutry et al., 2019a, 2018).

A direct correlation was found between the accumulation of ganglioside GM2 and autophagic marker p62 accumulation: as GM2 levels went up in lysosomes so did p62 levels. Decreasing GM2 levels with miglustat, an inhibitor of glucosylceramide synthase used to treat Gaucher disease, resulted in P62 level decrease in lysosomes (Boutry et al., 2018)-see **Figure 10**. This indicates that the potential clogging of the lysosomal compartment with lipids complicates the degradative action of lysosomes and prevents the clearance of substrates.

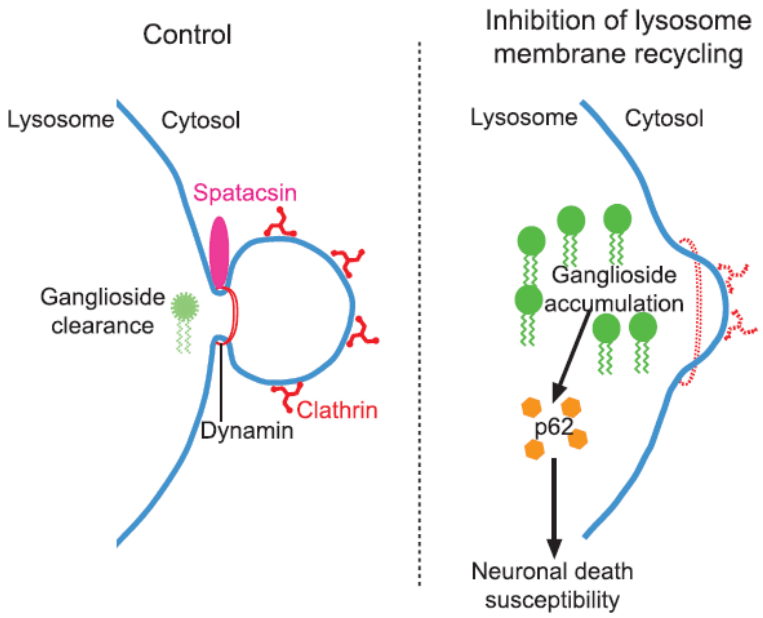

Figure 10 : Ganglioside accumulation promotes cargo destined for autophagy accumulation in lysosomes (Boutry et al., 2018).

Similar features have been observed in a group of disorders called Lysosomal Storage Disorders (LSD) such as Niemann-Pick type C or Sandhoff disease (Breiden and Sandhoff, 2019; Sandhoff and Harzer, 2013, p. 201; Vanier, 2010). Although the proportions of lipid accumulation in lysosomes is smaller in SPG11 HSP compared to the other LSDs, a similar link between these accumulations and neurodegeneration has been observed.

b.6. Linking Spg11-related cellular defects to neurodegeneration

Mouse models of Spg11$^{-/-}$ mice have shown an impairment of the motor and cognitive phenotype in absence of spatacsin (Branchu et al., 2017; Khundadze et al., 2021; Varga et al., 2015). These studies confirm that the loss of SPG11 leads to neuronal loss, notably in motor cortex. The use of Zebrafish models where SPG11 was invalidated using morpholinos showed that they developed a motor phenotype as well and had a perturbed axonal growth (Boutry et al., 2018; Martin et al., 2012). Moreover, these degenerative phenotypes seemed to be linked to ganglioside accumulation in neurons (Boutry et al., 2018). Indeed, lowering GM2 levels with miglustat in zebrafish knockdown for Spg11 improved the motor phenotype and lowering GM2 by miglustat or miRNA against GM3 synthase prevented death of Spg11$^{-/-}$ neurons (Boutry et al., 2018).

Other studies on neuronal models derived from induced pluri-potent stem cells lacking spatacsin observed neurite growth abnormalities (Pérez-Brangulí et al., 2014), proliferation defects in Neuronal Progenitors Cells (NPCs) (Mishra et al., 2016) and altered cell cycle in NPCs along with premature neurogenesis in organoids (Pérez-Brangulí et al., 2019). These defects seemed to be linked to a deregulation of the Wnt/GSK3β pathway based on a transcriptomic analysis that was performed on SPG11 patient cell lines (Mishra et al., 2016). In consequence, a proposed strategy adopted was to inhibit GSK3β signaling using the drug Tideglusib. The neurites abnormal growth, the premature neurogenesis and the NPCs proliferation defects were all rescued by Tideglusib treatment (Mishra et al., 2016; Pérez-Brangulí et al., 2019; Pozner et al., 2018). GSK3β is a kinase that is implicated in numerous cellular pathways (Wu and Pan, 2010) but reports have shown its implication in lysosomal biogenesis via nuclear translocation of Transcription Factor EB (TFEB) (Parr et al., 2012). It is possible that Tideglusib may be acting on lysosomal function considering that TFEB signaling was altered in cells lacking spatacsin (Boutry et al., 2019a).

The lysosomal dysfunctions causing an accumulation of undegraded material likely causes degeneration of motor neurons of the cortico-spinal tract as they are more fragile than other cells. Moreover, they don't divide and rely more than other cells on their autophagic degradation capacity to remove unwanted cellular materials.

Even if spatacsin is involved in lysosomal function and neurodegeneration, its precise cellular role remains unknown. Investigating its relationship with two other HSP proteins AP5z1 (SPG48) and spastizin (SPG15), that interact with spatacsin, provides more information on its potential role.

c) AP5z1 and spastizin, interactors of spatacsin and their link to endolysosomal dysfunctions

AP5z1 (along with other AP5 subunits) and spastizin were reported to interact with spatacsin for the first time in a study that was screening for proteins implicated in DNA damage and repair (Słabicki et al., 2010a, p. 5). If downregulating AP5z1 and spastizin made cells more sensitive to DNA damage, downregulating spatacsin had no effect on this parameter even if spatacsin was found be phosphorylated

by ATM upon DNA damage in a previous study (Matsuoka et al., 2007). AP5z1 and spastizin are encoded by genes mutated in SPG48 and SPG15 (Hanein et al., 2008a; Słabicki et al., 2010a).

AP5 is a member of the family of adaptor protein complexes

Adaptor protein complexes are known to associate with clathrin (for AP1, AP2 and AP3) and to recognize various cargoes to concentrate them in vesicular carriers (Park and Guo, 2014) (see **Figure 11**). AP1 has been reported to play a role in somato-dendritic sorting, AP2 in pre & post-synaptic endocytosis and AP3 in sorting of synaptic vesicles, underlining their importance for the functioning of neurons and explaining why mutations affecting these complexes lead to neurodegenerative disorders (Guardia et al., 2018). AP4 and AP5 are expressed in smaller proportions compared to other AP complexes and have less clear molecular role (Hirst et al., 2013b).

AP5z1 and spastizin form a protein complex with spatacsin

Spatacsin, spastizin and AP5z1 were proposed to interact in stochiometric proportions to form a protein complex (an hexametric complex, as AP5z1 is associated to 3 other subunits of the AP5 complex - see **Figure 11**)(Hirst et al., 2013a). Moreover, it appears that stability of the proteins of the complex are interdependent. Indeed, downregulating SPG11 by siRNA leads to an important loss of spastizin and downregulating SPG15 leads to spatacsin loss. However, downregulation of SPG11 or SPG15 only leads to moderate loss of AP5z1 and downregulation of SPG48 had no effect on spatacsin or spastizin levels (Branchu et al., 2017, p. 217; Hirst et al., 2013b; Khundadze et al., 2013a; Renvoisé et al., 2014; Vantaggiato et al., 2019; Varga et al., 2015). At least for the spatacsin-spastizin co-dependence, it seems that the regulation of their protein levels isn't transcriptional as there is no alteration of SPG11-mRNA in a Spg15 $^{-/-}$ mouse model (Khundadze et al., 2013a).

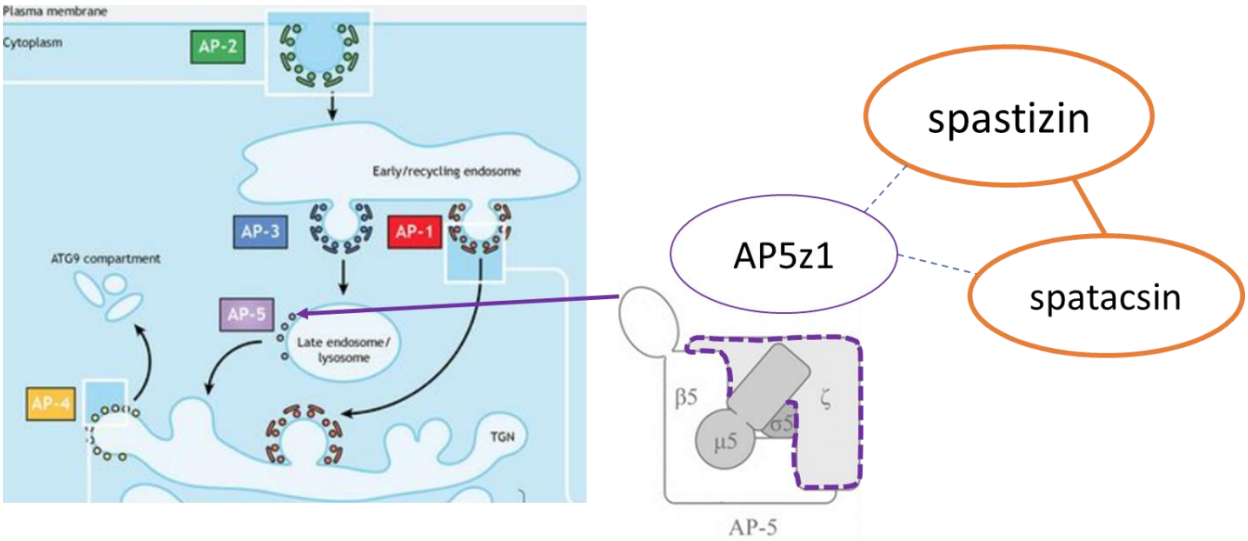

Figure 11: The hexametric complex of HSP proteins: AP5z1/spatacsin/spastizin in the realm of AP complexes (Sanger et al., 2019).

The existence of this AP5z1/spatacsin/spastizin complex where partners are interdependent might explain the similarities that were observed concerning the functions of these HSP proteins.

AP5z1 and spastizin sub-cellular localization

Like spatacsin, it seems that AP5z1 and SPG15 are rather cytoplasmic proteins that are recruited to the endo/lysosomal compartment upon starvation (Chang et al., 2014a; Hirst et al., 2021a, 2013b, 2011a; Wyant et al., 2018) (see **Figure 12**). However, one study reports the existence of an AP5z1 isoform that is nuclear (Słabicki et al., 2010a) and another one indicates that AP5z1 is not enriched in heavy membranes fractions that are enriched in endolysosomal marker Lamp1 but rather in the membrane fraction containing early endosomes marker EEA1 (Khundadze et al., 2013a).

For spastizin, one study observed its localization to the midbody of cells (Sagona et al., 2010a) and another to the early endosomes with only partial localization to the endolysosomes (Khundadze et al., 2013a). One of the particularity of spastizin is to possess a FYVE domain that grants it the ability to bind Phosphatidylinositol-3-phosphate (PI3P) (Sagona et al., 2010a). All studies on spastizin agree that its localization is dependent on the FYVE domain. Indeed, when a mutation is introduced in the FYVE domain, spastizin becomes completely cytoplasmic and is no longer recruited to membranes (Chang et al., 2014a; Khundadze et al., 2013a; Sagona et al., 2010a).

The same phenomenon of spastizin cytoplasmic re-localization is observed when cells are treated with wortmannin, an inhibitor of phosphoinositide 3 kinases, preventing the phosphorylation of PtdIns (Chang et al., 2014a; Khundadze et al., 2013a) (see **Figure 12**). This indicates that the ability of spastizin to be located to membranes is dependent on its ability to bind PI3P. A recent study shows that expression of a construct containing the spastizin FYVE domain alone results in its localization to early endosomes membranes where PI3P is the most enriched and that the localization of spastizin at late endosomes/lysosomes is to be explained by the rest of the protein sequence and maybe by interaction with spatacsin (Hirst et al., 2021a).

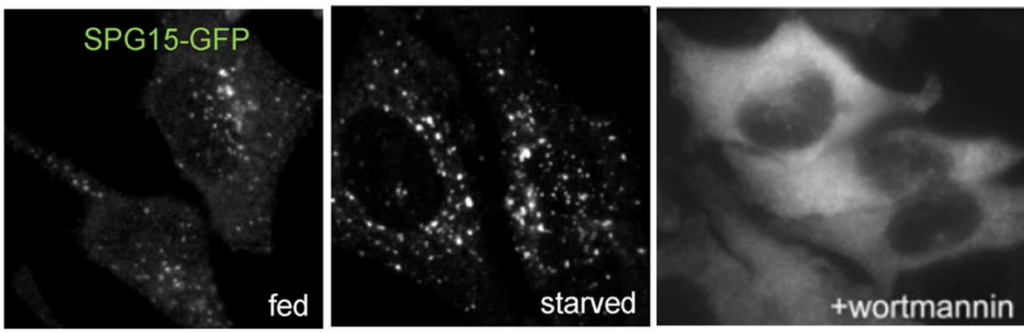

Figure 12 : Subcellular localization of spastizin (Hirst et al., 2021, 2013).

Loss of AP5z1 and spastizin cause endolysosomal defects.

Fibroblasts of SPG15 patients have an enlarged endo/lysosomes compartment (Renvoisé et al., 2014) and cells depleted of SPG15 or AP5z1 have an alteration of autophagic lysosomal reformation causing accumulation of undigested cargoes in the cells (Chang et al., 2014a; Khundadze et al., 2019a). This is probably explaining why both knocked-out mouse models for SPG15 or AP5Z1 present aberrant accumulation of non-degraded material in their lysosomal compartment (Khundadze et al., 2019a, 2013a). As we have seen previously in $Spg11^{-/-}$ model these accumulations of material in the lysosomes of neurons are linked to neurodegeneration and both $Ap5z1^{-/-}$ and $Spg15^{-/-}$ mouse models present an alteration of their motor phenotype (Khundadze et al., 2019a, 2013a).

Again, no alteration of lysosomal hydrolase activity were observed in in vitro assays for Ap5z1$^{-/-}$ model (Khundadze et al., 2019a) and a moderate increase (less than 50% by Western Blot assay) of Cathepsin D activity is reported at 16 months in Spg15$^{-/-}$ model (Khundadze et al., 2013a). Interestingly, a double knocked-out model for SPG11 & SPG15 present similar endolysosomal defects that as Spg11$^{-/-}$ or Spg15$^{-/-}$ models (Khundadze et al., 2021) underlining that both proteins are implicated in the same cellular mechanisms regulating endolysosomal pathway.

Potential roles of spastizin in cytokinesis and autophagosome maturation

If they share a lot of characteristics with spatacsin in terms of endolysosomal transitory localization and implications in the endolysosomal system, AP5z1 and spastizin also have their particularities. An early study on spastizin showed that it is a key player in cytokinesis by interacting with PI3P at the level of the midbody. This localization of spastizin to the midbody is dependent of its interaction with molecular motor from the Kinesin family : KIF13A (Sagona et al., 2010a).

Another study tried to explain the endolysosomal defects observed in absence of spastizin by showing that it interacts with early endosomes RAB5 GTPase and recycling endosome RAB11 GTPase (see **Figure 9**). On top of these interactions, they showed that spastizin was also interacting with Beclin1/RUBCN/UVRAG complex, which is involved in autophagosome maturation & endosome motility. Therefore, the lack of spastizin would result in less early endosome-late endosome fusion causing a latter alteration of the endolysosomal pathway (Vantaggiato et al., 2019). These data might find supporting literature in a study conducted on a Zebrafish model invalidated for spastizin homolog that showed an accumulation of RAB11 positive vesicles (Kanagaraj et al., 2014).

Role of AP5z1 in lysosomal enzymes sorting

AP5z1 is involved in protein sorting from the Golgi toward the endolysosomes especially for sorting of M6PR (Hirst et al., 2018a). Indeed, an alteration of Mannose 6-Phosphate Receptor (M6PR) trafficking was observed in absence of AP5Z1 (Hirst et al., 2011a) and M6PR clustering was observed upon AP5z1 downregulation (Hirst et al., 2015). Mannose 6 phosphate is a sugar added in the Golgi to cargoes destined to early endosomes, it will bind to M6P Receptor. Then the substrate-receptor complex enters clathrin coated vesicles from Golgi to early endosomes. This route is important for lysosomal enzymes targeting from the ER, then from Golgi to the endolysosomal compartment. So, an alteration of the M6PR pathway could in part explain some of the aberrant accumulation of material in lysosomes. On top of M6PR traffic alteration, the Ap5z1$^{-/-}$ mouse model showed an aberrant Golgi structure at 16 months and accumulation of constitutive Golgi proteins in the lysosomes (Khundadze et al., 2019a).

AP5z1, spastizin, spatacsin share many features, in terms of the cellular defects that are observed in the HSPs that are associated to mutations of their coding genes. Indeed, the three knocked-out mouse models had an impaired motor phenotype and lysosomal aberrant accumulations. Whether the proteins always exist in a protein complex or only transitory is unknown, but it appears that their molecular role are interdependent. The extent of the interdependence and the regulation of their interaction remains to be more investigated.

d) Involvement of the lysosomes in neurodegenerative disorders

If we consider a broader scale than Hereditary Spastic Paraplegias, lysosomes constitute a compartment particularly vulnerable to failure in neurodegenerative disease (Nixon, 2013). Neurons, as postmitotic cells are particularly dependent of the lysosomal system. Moreover, they are further challenged by their extreme geometric asymmetry. The cell's rely on two proteolytic clearance systems, the Ubiquitin Proteasome System (UPS) and the autophagic pathway (Berke and Paulson, 2003; Goldberg, 2003).

The two systems share the use of adaptor proteins such as ubiquitin and p62, and lysosomal degradation is upregulated when proteasome activity is inhibited, highlighting that the two pathways are interdependent (Sitte et al., 2000).

With ageing, there is an increased need for degradation of damaged organelles, but the proteolysis capacity of the cells decreases. As a result : lipofuscin aggregate presence in lysosomes is linearly correlated with age in various organisms (Brunk and Terman, 2002). This might explain why lysosomal dysfunction appear to be connected to age. But at the other end of the spectrum, lysosomal phenotypes can also be caused by a variety of genetic conditions altering the degradative pathway.

Alzheimer's Disease

A direct genetic link between lysosomal dysfunction and Alzheimer Disease (AD) are mutations of PS1 (Presenilin), the most common cause of early-onset familial AD (Sherrington et al., 1995). The role of PS1 in lysosome acidification has been confirmed in various systems (Wolfe et al., 2013), and recent evidence has shown that normalizing lysosomal acidification fully reverses defective autophagy and lysosome function in PS1-deficient cells (Coen et al., 2012).

In several AD mouse models, various lipid storage materials such as cholesterol or sphingolipids accumulate in endolysosomal compartments, reminding of defects observed in lysosomal storage disorders or HSP. These lipid accumulations can promote lysosome deacidification and prevent the processing and clearance of Amyloid Precursor Protein (APP) and its metabolites (Karaca et al., 2014). Another major risk factor for AD, lipoprotein ApoE4, increases levels of intracellular A-beta peptide (Aβ) when it is overexpressed, enlarges lysosomes and alters their morphology and causes neurodegeneration (Belinson et al., 2008).

Fronto Temporal Dementia

Fronto Temporal Dementia (FTD) is the second most common dementia in people younger than 65 years (Onyike and Diehl-Schmid, 2013). Mutation of GRN is responsible for FTD, and it has been observed,– in mice models & patients– that there are enlarged lysosomal vesicles and lipofuscin accumulations in absence of GRN (Ahmed et al., 2010; Valdez et al., 2017). Moreover, GRN-deleted mice have increased levels of TMEM 106B, a lysosomal protein which is known as a risk factor for FTD (Brady et al., 2013). This TMEM protein regulates the morphology of lysosomes, the degradation of endocytosed cargo & lysosomal trafficking (Brady et al., 2013).

Another cause of FTD is the gene encoding Valosin-Containing Protein (VCP, also known as p97) (Watts et al., 2007). VCP regulates endolysosomal sorting of endocytosed ubiquitinated cargoes (Ritz et al., 2011) and its mutation is known to disrupt selective autophagy. VCP depletion or the expression of mutant VCP in cell models causes immature autophagosomes containing ubiquitinated substrates to accumulate (Tresse et al., 2010).

Lysosomal Storage Disorders (LSDs)

LSDs can be caused by a loss of function of hydrolytic enzymes at the lysosomes causing an accumulation of the substates. For example, in Gaucher disease, the loss of glucocerebrosidase activity results in accumulation of ceramides, causing additional defects such as autophagosome-lysosome fusion and autophagic lysosome reformation impairment (Magalhaes et al., 2016; Osellame et al., 2013). But the cause for LSDs can also be the loss of the transporter to the lysosome of the enzyme, which is the case for mucopolysaccharidoses (Jeyakumar et al., 2005). There can also be a loss of the transporter of the substrate for example NPC, a cholesterol transporter from the lysosomes whose loss of function results in massive cholesterol accumulation in the lysosomes (Carstea et al., 1997; Loftus et al., 1997).

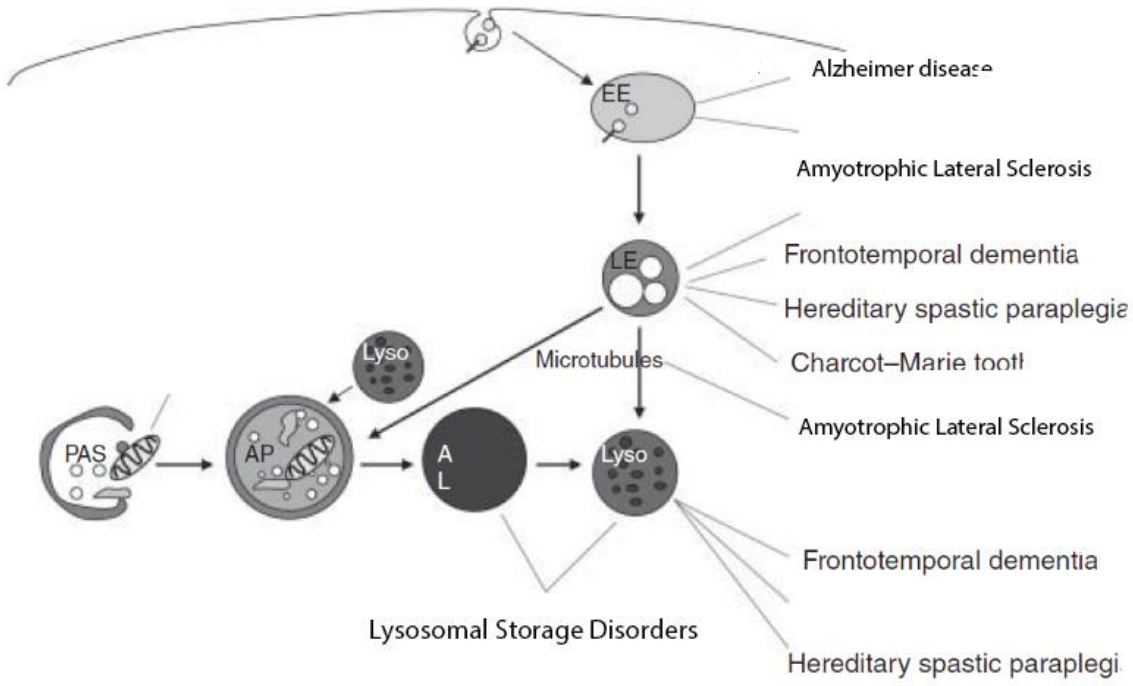

Figure 13 : Links between the endolysosomal pathway and neurodegenerative disorders (Reggiori and Klumperman, 2016). EE : Early Endosomes. LE : Late Endosomes. PAS : Phagophore Assembly Site. AL : Autolysosome. AP :autophagosome.

The aim of this far from exhaustive catalog of neurogenerative disorders that have a lysosomal component to the disease is to show that beyond SPG11 pathology there is a real challenge on the broader scale to solve the mysteries of lysosomal dysfunctions that appear to be relevant for many patients.

e) Other cellular alterations in absence of spatacsin

There is a dominant part of the literature on SPG11 HSP focusing on lysosomal function, but other organelles start to draw the attention. For example, mitochondrial transport alteration has been reported in neurites of SPG11 patient derived neurons (Güner et al., 2021), and a problem of mitochondrial fission has been reported in neurons lacking AP5z1 or spastizin (Denton et al., 2018).

In their screening of potential interactors of SPG11, recent studies have highlighted a potential role for spatacsin at the level of the proteasome, the cytoskeleton and t-RNA synthases (Alexander L. Patto and O'Kane, 2020, p. 202). The cytoskeleton seemed to be altered in neuronal model lacking SPG11 as the cells contained more acetylated tubulin (Pérez-Brangulí et al., 2014).

One of the most interesting results for my work during my PhD was the study showing that there was a global calcium homeostasis alteration in the cells lacking spatacsin (Boutry et al., 2019a)-**See Annex-1.**

This alteration of calcium homeostasis is caused by an excessive entry of extracellular calcium via a process called Store Operated Calcium Entry (SOCE). In this process, upon low levels of calcium in the Endoplasmic Reticulum (ER), the ER will contact the Plasma Membrane (PM) to import calcium from the extracellular space. These ER-PM contacts are modified by a change of cholesterol balance at the plasma membrane which results from an impaired cholesterol homeostasis in the cells caused by the absence of spatacsin. In this work, we were able to show that calcium homeostasis and cholesterol homeostasis, notably at the lysosomes, are linked in a co-regulation cycle. It appears that progressive clogging of the lysosomes in absence of spatacsin plays a role in these processes and that calcium levels indirectly regulate lysosomal function by playing on master lysosome regulator TFEB translocation to the nucleus (see **Figure 14)**.

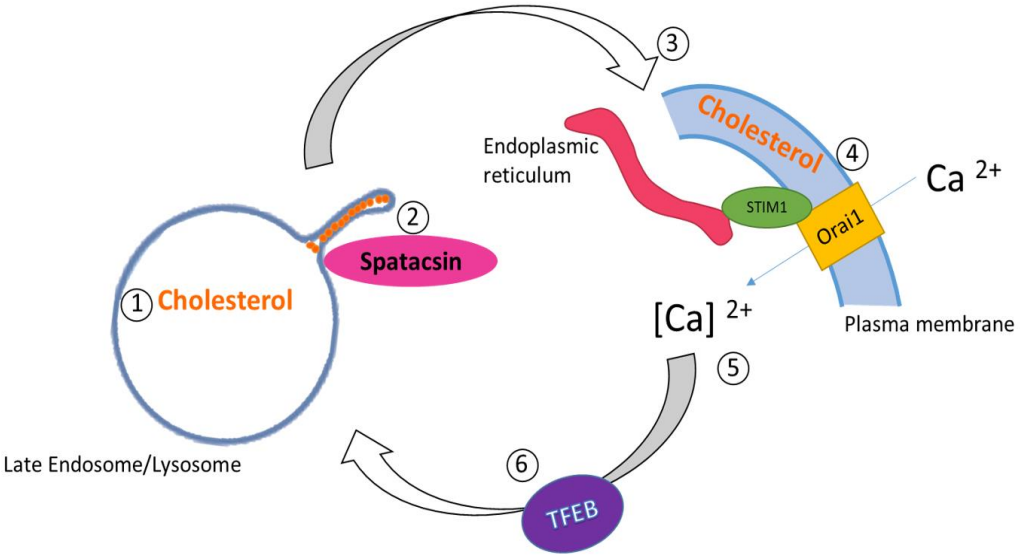

Figure 14: A cycle of linked phenomena leading to cholesterol accumulation in lysosomes in absence of spatacsin.

1) Cholesterol accumulates in absence of spatacsin
2) Cholesterol is less exported from lysosomes via membrane tubulation because of spatacsin lack
3) Lack of cholesterol export toward Plasma Membrane (PM) changes its cholesterol composition
4) Cholesterol decrease at the PM triggers ER-PM contacts between STIM1 and Orai1 stimulating import of extracellular calcium
5) Cytosolic calcium levels are increased upon excessive extracellular calcium entrance
6) TFEB regulated by calcium dependent activity of calcineurin is translocated to the nucleus & modifies lysosomal function

These results underline that the cell is a dynamic system, where organelles and pathways interact at multiple levels. What is also particularly interesting here is that the thematic of calcium homeostasis, lipid homeostasis, and ER-contacts with the PM point toward a role of ER in the cellular phenotypes associated with SPG11 loss of function. Inter-organelles contacts are extremely important in the regulation of multiple cellular pathways, especially at the level of endosomes-ER contacts.

The consequences of spatacsin loss of function have been widely investigated, but the molecular role of spatacsin remains unknown. Investigating inter-organelle interface may help to elucidate this role.

III. Endoplasmic Reticulum contacts with Endosomes and Lysosomes

The endoplasmic reticulum is the biggest organelle of the cell, it is very dynamic and has been at the center of the recent literature produced on membrane contacts between organelles. I will discuss what has been discovered concerning membrane contact sites of the ER with organelles. My focus will be on contacts between ER and the endo/lysosomal compartment as we are interested especially in it to investigate spatacsin molecular role.

a) What constitutes a contact between two organelles?

Since the 1950s, electronic microscopy observations have shown that membranes of different organelles can be in proximity (see **Figure 15**). In the 1980s, it appeared that protein bridges could exist between these membranes (Kawamoto et al., 1986). One of the first elucidated protein bridges between organelles was the contact between vacuolar protein Vac8 and nuclear envelope protein Nuj1 in yeast (Pan et al., 2000).

A protein-protein interaction between two membranes constitutes a tether and is an actual physical bond that can withhold some tension. Contacts of the sorts can exist between all organelles and have 3 principal functions, which can be cumulated (Bord, 2016) -see **Figure 15** :

1) Forming a physical bridge between two membranes to maintain them together
2) Transferring small molecules such as ions or lipids in a non-vesicular way
3) Coordinating the function of contact machineries

It is important to note that in such contacts, membranes of organelles do not fuse and that the distance between membranes is estimated to be between a few nanometers up to forty nanometers. Also, even if the membranes are not fused, the contacts are still quite strong as some of them can even resist fractionation experiments (Vance, 1990; Williamson et al., 2015).

Moreover, strong modification of organelle shape by osmotic shock does nots abolish contacts between membranes especially between the ER and respectively plasma membrane, endosomes, lysosomes, mitochondria, peroxisomes and lipid droplets (King et al., 2020). Interestingly, this study also revealed that the nature of lipid domains present at sites of contact between organelles may vary from one contact to another. Ordered lipid domains are found at contact sites between ER and mitochondria for example while disordered domains are found at contact sites between ER and lysosomes or peroxisomes (King et al., 2020).

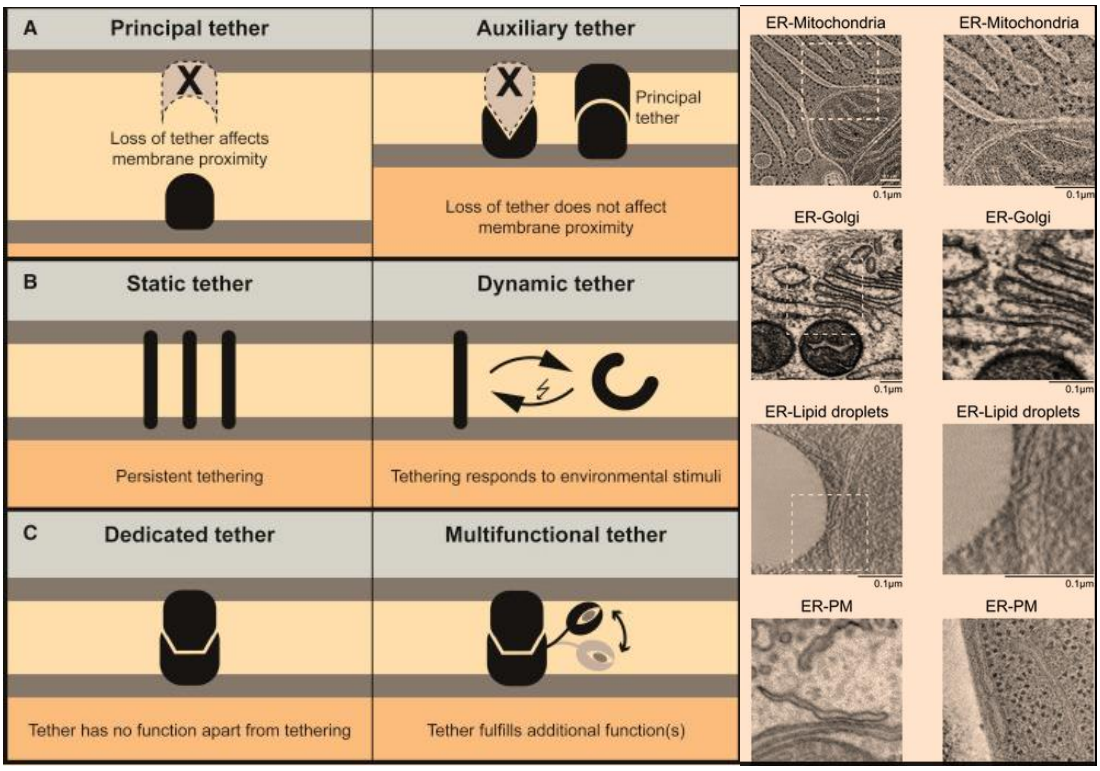

Figure 15. **Left:** Different categories of tethers exist and have various functions. **Right :** Electronic microscopy of Contacts between the ER and other organelles, from (Bord, 2016; Wu et al., 2018).

b) The ER: the major organelle for membrane contacts sites

According to a recent publication studying extensively contact sites in cells, most contacts found between organelles are between the ER and any other organelle (Valm et al., 2017) (see **Figure 16**). To explain this finding, they measured the volume that is occupied in the cells by the ER. The ER accounts for "only" 35% of the cell volume at a given time point, but being a very dynamic compartment, in only 15 min it was observed that it had occupied about 97% of the cell volume at least transiently. Still according to this publication, the ER makes most contacts with mitochondria, then the lipid droplets, the peroxisomes, the lysosomes/endosomes (they used a Lamp1 staining) and the Golgi came last (see **Figure 16**).

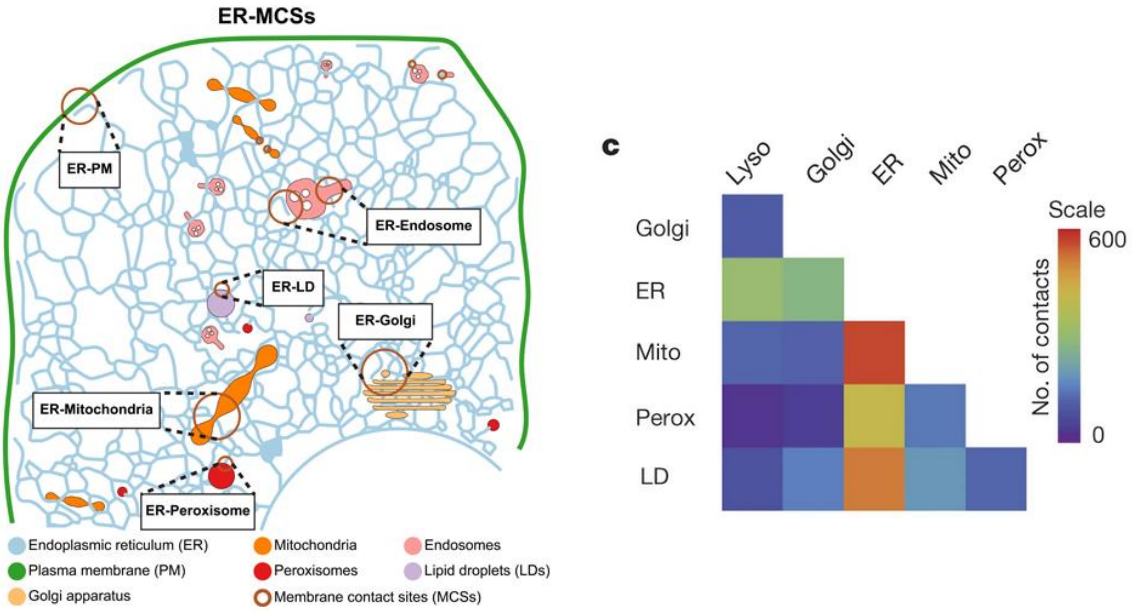

Figure 16. **Left**: The ER makes contacts with multiple organelles in the cell. **Right :** Quantification of the number of contacts between the different organelles, from (Valm et al., 2017; Wu et al., 2018).

Other organelles can also make contact between one another such as lysosome with mitochondria or with peroxisomes as we can see on **Figure 16** but far less than with the ER.

c) Roles of membrane contacts sites at the interface between ER and other organelles

Extensive reviews have listed and analyzed the functions of contact sites between the ER and other organelles (Helle et al., 2013; Phillips and Voeltz, 2016; Prinz, 2014; Prinz et al., 2020; Wu et al., 2018). We will focus more on ER-lysosomes contacts but first it seems important to mention the functions that are important for the other contacts of the ER.

c.1 Phosphoinositides at membrane contact sites of the ER with other compartments

Phosphoinosites are lipids that are rare and dynamic and are involved in the regulation of transfers of lipids and other functions taking place at ER contact sites with other membranes.

They are amphiphilic, with the polar head toward the cytosol and the hydrophilic tail in the lipid bilayer. There are 8 different phosphoinositides (see **Figure 17**). Phosphoinositides are obtained by phosphorylation or dephosphorylation of other phosphoinositides. These conversions are performed by 34 identified phosphatases and 20 kinases, some of which are causing forms of Charcot-Marie Tooth disease

or cilipoathies when mutated. This regulatory machinery allows for a fine tuning of the regulation of vesicular trafficking via phosphoinositides signaling (Dickson and Hille, 2019).

Phosphatidylinositol (PI) is the precursor of all phosphoinositides species. It is synthetized in the ER, and is then transported to the other membranes by vesicular transport or non-vesicular transport via lipid transfer proteins at contact sites.

PI3P is enriched at the early endosomes. Protrudin and FYCO1, which are involved in lysosome movement, both have a FYVE domain that allow them to bind to PI3P(Pankiv et al., 2010; Raiborg et al., 2015).

PI4P is increased at the plasma membrane and the Golgi.

PI5P is a very rare phosphoinosited found in the nucleus and plasma membrane.

PI(3.5)P2 is a late endosomes/lysosomes phosphoinositides that can only be synthetized by PIKFyve kinase. It regulates endosomal fission and fusion processes to maintain membrane homeostasis. It also induces the release of cortactin from the endosomal actin network, to regulate membrane trafficking and membrane curvature (N. H. Hong et al., 2015).

PI(3.4)P2 is a very rare phosphoinositide found at the plasma membrane and endocytic compartment.

PI(4.5)P2 is the most abundant phosphoinositide and is found principally at the plasma membrane.

PI(3.4.5)P3 is a very rare phosphoinositide which very tightly regulated and is found mostly at the plasma membrane.

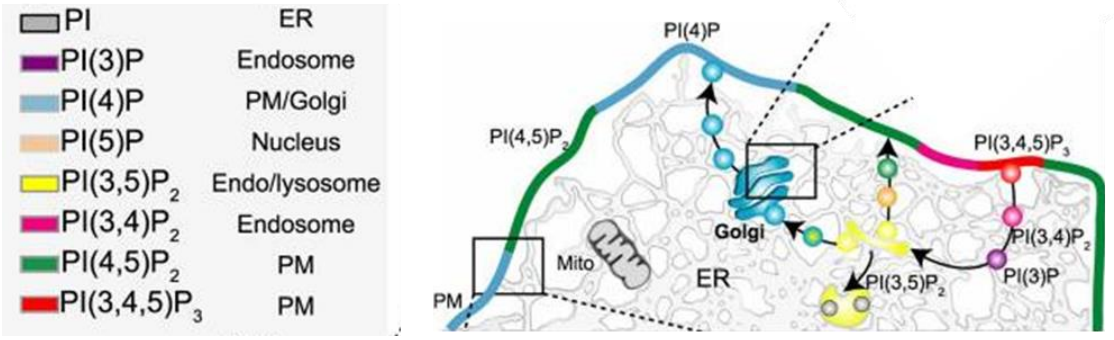

Figure 17 : The different phosphoinositides of the cell and their main subcellular localization (Dickson and Hille, 2019)**.**

c.2 ER contacts with the plasma membrane (PM)

The plasma membrane does not fit the definition of an organelle but the contacts it makes with the ER have shown to be important for several functions. First, contacts formed between the ER protein Stim1, and the PM Orai1 calcium channel are required to perform Store Operated Calcium Entry (mentioned before as being altered in SPG11 HSP). This replenishment of the ER Calcium store from the extracellular space is indeed dependent of the existence of membrane contact sites.

Lipid exchanges also take place between the two membranes, for example TMEM24 triggers an exchange of phosphatidylinositol from the ER to the PM in response to a change in calcium flux (Sun et al., 2019). Similarly ORP5/8 (oxysterols related binding proteins) are recruited at contacts between the ER and the PM to promote PI4P transfer to the ER in exchange of phosphatidylserine (Sohn et al., 2018).

ORP5 & ORP8 are proteins of the ER membrane that mediate the counter-transport of PI4P for phosphatidylserine at ER-plasma membrane contac sites. They recognize PI4P via their PH domain and their ORD domain transfers phosphatidylserine from the ER to the plasma membrane. PI4P is then hydrolysed at the ER membrane to maintain the PI4P gradient that drives the lipid exchange (Chung et al., 2015).

Synaptotagmins of the ER E-Syt2/3 form contact sites with the plasma membrane by binding PI(4.5)P2 found at the plasma membrane (Giordano et al., 2013). Moreover, the contact sites between ER and the plasma membrane are required for delivery of Phosphatidyinositol from the ER to the plasma membrane as a precursor for synthesis of PI4P and PI(4.5)P2. This contact is regulated by Nir2/3 proteins (Chang and Liou, 2015)

c.3 ER and mitochondria

ER forms the most contacts with mitochondria, principally to transfer it some of its calcium via its IP3R receptor channel. The calcium efflux is received at the mitochondria level by VDAC channel (Szabadkai et al., 2006). IP3 receptor is itself regulated by the exposure to reactive oxygen species at the membrane contacts between ER and mitochondria (Lock et al., 2012). The linkage of ER and mitochondria is regulated by the dynamin-like protein mitofusin (de Brito and Scorrano, 2008). ER regulates the mitochondrial dynamics in the cell via the Miro protein and DRP1 promoting fission of the mitochondrial compartment (Murley et al., 2013).

The ER contacts with mitochondria promotes the recruitment of actin/myosin on site resulting in the constriction of mitochondria. ER also facilitates the recruitment of fission machinery at the contact area promoting mitochondria fission (Friedman et al., 2011) (See **Figure 18**). In addition, via the ER-Mitochondria Encounter Structure (ERMES), exchanges of lipids like phosphatidylserine and phosphatidylcholine are happening at ER-mitochondria contact sites (Lahiri et al., 2014). The ER-mitochondria lipid exchanges at contact sites are also required to synthesize phosphatidylethanolamine, an essential constituent of membranes (Kainu et al., 2013).

c.4 ER and Golgi

Golgi and ER exchange mainly lipids at the level of their contact sites, these lipid transfers are mediated by lipid transfer proteins recruited to contact sites (Peretti et al., 2008). ER and Golgi exchange ceramides via CER transferase (Kawano et al., 2006) and also sterols and PI4P (Mesmin et al., 2013). PI4P is bound by two other proteins that have PH domains : ceramide transporter (CERT) and oxysterol binding protein (OSBP1). Both proteins bind VAPs at the ER and PI4P at the Golgi forming a membrane contact site.

CERT will then be able to transfer ceramide from the ER to the Golgi and OSBP1 will transfer cholesterol from ER to Golgi as well (Peretti et al., 2008). It has also been found that OSBP1 mediates a back transfer of PI4P from the Golgi to the ER where it will be dephosphorylated to provide energy for sterol transfer (Mesmin et al., 2013).

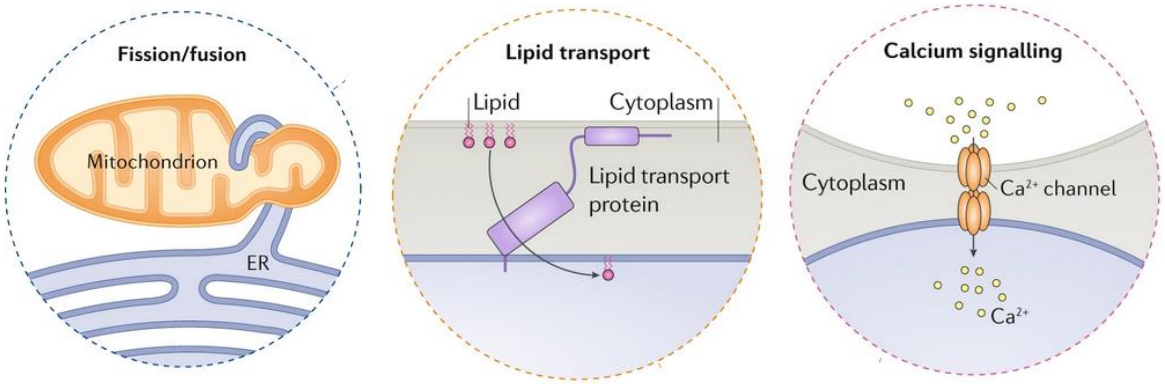

Figure 18 : The different functions of membrane contact sites (Prinz et al., 2020).

c.5 ER and Lipid droplets

At the level of lipid droplets contacts with ER, the triglyceride synthesis is regulated by FATP1 (Xu et al., 2012). These storage organelles have only a monolayer surrounding them, and it is sometimes in continuity with the ER membrane at the level of contacts, constituting an exception in the realm of membrane contact sites. Seipin is also an important protein localized at the level of ER contact sites with a role in the regulation of the morphology of lipid droplets (Salo et al., 2016).

c.6 ER and peroxisomes

Peroxisomes lipid synthesis is happening in partnership with the ER via regulation of VAPs and ACBD5 at ER-peroxisomes contact sites (Hua et al., 2017), it appears that these contacts also regulate the position of peroxisomes in the cell (Wang et al., 2018).

ER contacts with other organelles are involved in the regulation of lipid transfer, in calcium flux, in organelle fission and positioning. These functions are often under the control of Phosphoinositide regulation. The role of ER at membrane contact site appears relevant for the cellular defects observed in absence of spatacsin (**see Introduction -I**). Since loss of spatacsin has been shown to alter lysosome function (Renvoisé et al., 2014), but also some ER function (Boutry et al., 2019a), we will now more specifically focus on the ER-lysosome contacts.

d) Focus on ER- lysosomes contacts

d.1 Lysosome positioning & movement

How do lysosomes & endosomes move in the cell?

The function of lysosomes relies on their ability to move and to be at the right place in the cell. At steady state, there is a pool of relatively static lysosomes that are found close to the cell nucleus, where the Micro Tubule Organizing Center (MTOC) is located. This pool of lysosomes will fuse with autophagosomes or multi-vesicular bodies containing content destined for degradation. A second pool of lysosomes is found at the periphery of the cell, they are more dynamic and can be involved in other functions such as plasma membrane repair (Cabukusta and Neefjes, 2018)(see **Figure 19**).

The positioning of lysosomes is dependent on their ability to move, which is based on molecular motors: Kinesins (moving particles toward the cell periphery) and Dynein (moving particles toward the nucleus). The molecular motors move on a microtubule network, their displacement requires energy (under the form of ATP or GTP) (Cabukusta and Neefjes, 2018).

Lysosomes position in the cell can be modified by a variety of parameters. The cell response to nutrient abundance via the mTor pathway for example changes lysosomal position. Starvation of cells or use of Torin inhibitor of mTor result in activation of autophagy, and this is linked to a peri-nuclear clustering of lysosomes. Reinstituting nutrient rich conditions redistributes lysosomes toward the periphery (Ba et al., 2018; Korolchuk et al., 2011). Moreover, the activation of TFEB, lysosomal transcription factor, by trehalose, causing an altered lysosomal biogenesis, results in a perinuclear clustering (Ba et al., 2018).

The lysosomes also rely on calcium signaling for the movement and positioning in the cells via TRPML1 lysosomal channel flux (Li et al., 2016). In addition, PI3P is also involved in the regulation of vesicular transport by binding to Rab7 and LC3 via the adaptor protein FYCO1 (Pankiv et al., 2010). Finally, mTorC1 activity in autophagy regulation is also dependent on PI3P and lysosomal positioning, underlining how inter-dependent the parameters ruling lysosomal dynamics are (Hong et al., 2017).

Both the ER and the endosomes are very dynamic compartments, however, it has been shown that membrane contact sites are maintained during transport of organelles on the microtubular network (Friedman et al., 2010). This conservation of membrane contact sites permits the regulation of lysosomal movement by the ER, via several proteins. The ER-Lysosome association is close to microtubules (see **Figure 19**) and the contact between ER and Lysosomes favors long-distance transport, if lysosomes are not associated with the ER, they are more likely to undergo a diffusive movement than a directed one (Guo et al., 2018).

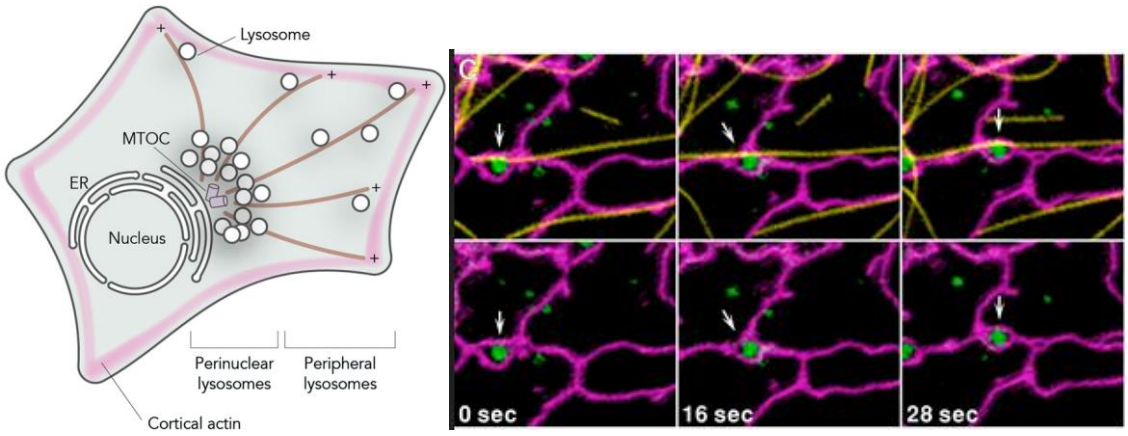

Figure 19. Left: Two principal clusters of lysosomes exist in the cell and move on cytoskeleton. **Right:** Lysosomes long-distance transport on microtubules is associated with ER contact, Green=late endosomes/lysosomes marker Lamp1, Magenta=ER marker Sec61β, Yellow=microtubules marker α-tubulin (Cabukusta and Neefjes, 2018a; Guo et al., 2018).

Lysosomes movement regulation

Several mechansisms regulating lysosome dynamics have been described.

First, we can cite ORP1L, a cholesterol sensor that is present on lysosomes, and will change its conformation based on cholesterol levels in the lysosomal membrane. ORP1L can bind VAP at the ER on one end and Rab7 at the Late Endosomes/Lysosomes (referred as lysosomes) on the other end. When cholesterol levels are low, ORP1L promotes the movement of lysosomes toward the cell periphery while when cholesterol levels are higher, it will promote their localization toward the cell center (Johansson et al., 2005; Rocha et al., 2009a)(see **Figure 20**). Interestingly, ORP1L has also been shown to be involved in autophagosome movement which is important for their proper fusion with lysosomes (Wijdeven et al., 2016).

Another example of a well identified protein of ER-lysosomes contacts that drives lysosomal position is Protrudin. Indeed, Protrudin is an ER transmembrane protein interacting with the Rab7/PI3P/FYCO1 complex mentioned before. Protrudin promotes the loading of FYCO1 on kinesins and therefore promotes Lysosomes movement toward the cell periphery (Raiborg et al., 2015a)(see **Figure 20**).

At the opposite of protrudin, RNF26 is a ubiquitin ligase localized in the ER that is preventing both early endosomes and late endosomes movements. RNF26 binds and ubiquitinates p62, therefore triggering the binding of early endosomes adaptor ESP15 and late endosomes adaptor TOLLIP on ubiquitinated p62 and trapping vesicles at the ER, close to the nucleus, where RNF26 is located. Upon de-ubiquitination of p62 by USP15, particles are released and can spread again throughout the cell (Jongsma et al., 2016a). Very recently, another example of a restricting role of the ER in the lysosomes movement has been discovered via the sorting nexin SNX19 that tethers lysosomes to the ER by binding PI3P (Saric et al., 2021).

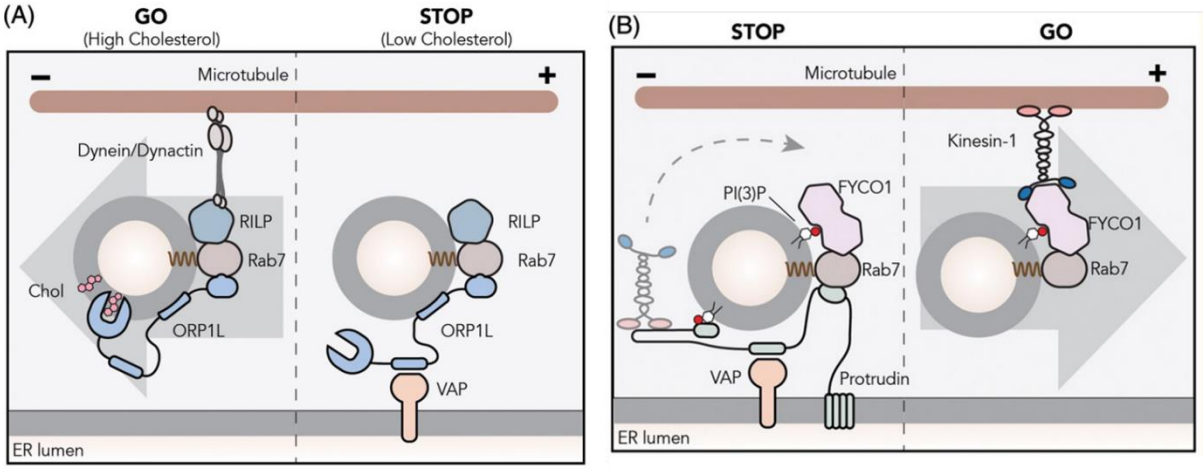

Figure 20. Left: Regulation of lysosomal movement by ER-lysosomes contact via VAP-ORP1L interaction. **Right:** Regulation of lysosomal movement by ER-Lysosome contact via protrudin/Rab7/FYCO1 interaction (Cabukusta and Neefjes, 2018a).

To conclude, ER-Lysosome contact proteins can regulate lysosome movement toward the cell periphery or the cell center depending on the cellular environment. But lysosomal movement also regulates ER-architecture, by “hitchhiking” of ER-tubules on lysosomes to form new three way junctions (Guo et al., 2018; Spits et al., 2021a) and this reshaping action of lysosomes on ER tubular network is also regulated by cell nutrient availability (Lu et al., 2020).

d.2 Lipid trafficking at the ER-lysosomes contacts

Lipids are delivered to lysosomes by endocytosis, and their breakdown in late endosomes lysosomes is happening thanks to hydrolases. Most lipid degradation products are used by the cell to create new lipids. For example, in human fibroblasts, 90% of the sphingoid base is recycled after degradation and 10 % synthesised. The fatty acids produced by degradation in lysosomes can also be used to produce energy (Gillard et al., 1998).

Cholesterol handling at the lysosomes and lipid transporters

Cholesteryl esters are digested by lysosomal acid lipases and this releases cholesterol. The absence of acid lipase activity causes Wollman disease, a disorder of cholesteryl ester storage (Du et al., 1998). Cholesterol however is not catabolized in lysosomes, and its main pathway for clearance from the body is conversion to bile salts in hepatocytes and excretion (Dawson, 2015). Niemann-pick disease develops if cholesterol transporters to the lysosomes NPC1 or NPC2 are impaired. NPC2 is in the lysosome lumen and brings cholesterol to NPC1 on the lysosome surface. In Niemann pick disease, there is an accumulation of cholesterol, sphingomyelin and gangliosides in lysosomes of neurones (Walkley and Vanier, 2009).

Cholesterol is so far the only lipid that was identified to be exchanged at ER-endosomes contacts. Cholesterol, as other lipids, is insoluble and can be transported either by vesicular transport or by non-vesicular transport at the level of a contact site also called “channeling”. This channeling of lipids is based on the presence of Lipid Transport Proteins (LTPs)(Wong et al., 2019). The LTPs will bind to the lipid at the donor membrane and deliver it across the contact space to the acceptor membrane (Lev, 2010). This form of lipid transfer is based on the binding properties of LTPs. Indeed each LTP binds specific lipids, allowing the sorting of lipid transfer at contact sites.

Moreover, the channeling rate of a given lipid is linked to the enrichment of said lipid at the contacts or it can also be driven by the abundance of its specific LTPs at contact sites, it can also be transferred againts a counter gradient of another lipid (Chiapparino et al., 2016; Wong et al., 2019) (see **Figure 21**).

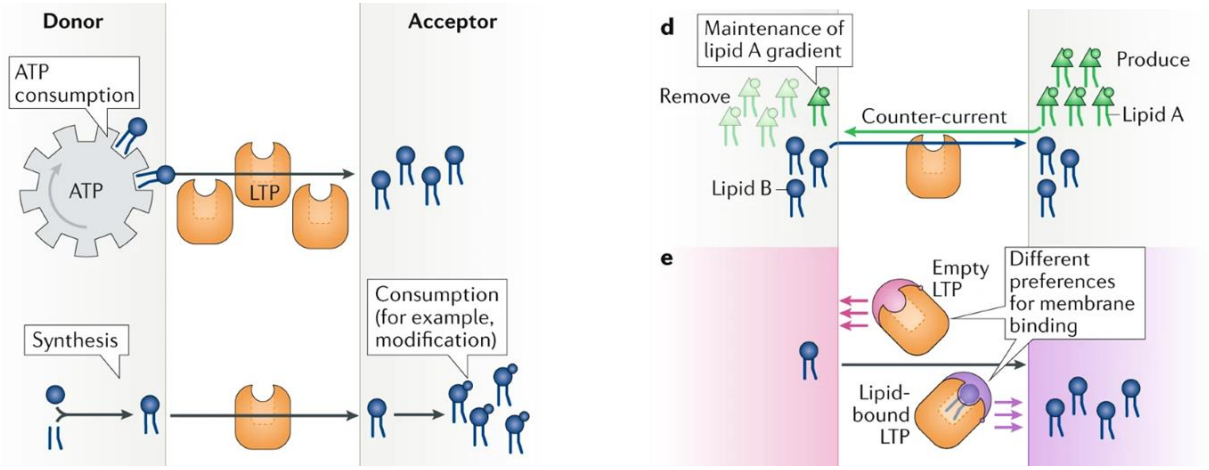

Figure 21: Different mode of actions of Lipid Transporter Proteins across membranes (Wong et al., 2019).

Regulators of cholesterol exchanges at ER-lysosomes contacts

STARD3, one of the major tether implicated in cholesterol transport at ER-endosomes interface is localized at the lysosome surface. STARD3 interacts with VAPA/B and MOSPD2, two ER resident proteins. The bridging between STARD3 and VAPs for example allows the transport of cholestrol from the ER to the late endosomes (Wilhelm et al., 2017a). Interestingly, a STARD3$^{-/-}$ mice model showed only modest cholesterol level alterations, indicating that cholesterol transport pathway are mutiple and redundent (Kishida et al., 2004) (see **Figure 22**). The STARD3-NL protein is involved in ER-late endosomes contact but does not have the ability to bind cholesterol, its ability to interact with STARD3 likely regulates the cholesterol transport at contact sites in a indirect manner (Alpy et al., 2013).

One other major protein in cholesterol exchanges at ER-endosomes contacts is late endosomes ORP1L implicated in the regulation of lysosome localization (Rocha et al., 2009a). By binding with Annexin A1 at the ER, it regulates ER-endosome cholesterol transport and this process is important for Intra Luminal Vesicles formation at muti-vesicular bodies (Eden et al., 2016). Moreover, the action of ORP1L at membrane contact sites is also operating cholesterol transfer in the opposite direction : from the endosomes to the ER (Zhao and Ridgway, 2017). This cholesterol transport by ORP1L is under the regulation of PI(4.5)P_2 and PI(3.5)P_2 which will enhance cholesterol transport by ORP1L from the ER to the lysosomes (Dong et al., 2019).

Finally, an interesting result in ER-Lysosomes cholesterol exchanges at membrane contact sites is the involment of cholesterol transporter NPC1, mutated in Niemann Pick disease. It appears that NPC1 localized at lysosomes is binding GramD1b cholesterol transporter at the ER and promotes the export of cholesterol from late endosomes/Lysosomes to the ER (Höglinger et al., 2019).

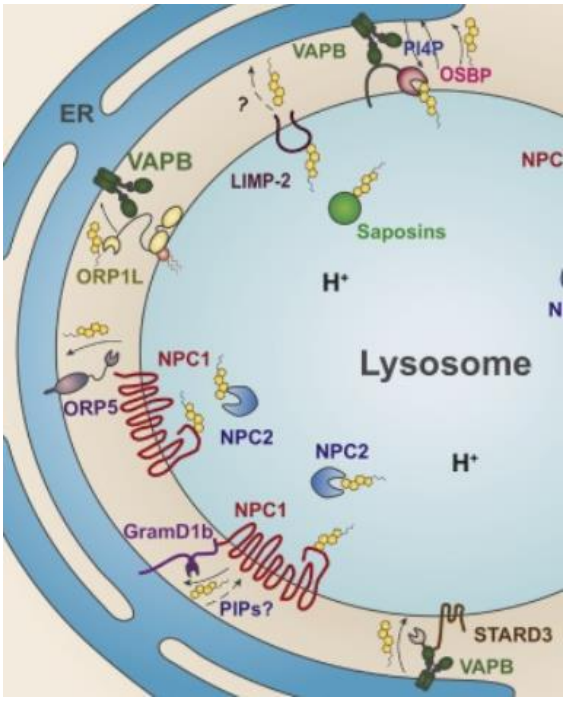

Figure 22: Multiple routes exist for cholestrol exchanges between Lysosome and ER at membrane contact sites (Meng et al., 2020).

Cholesterol exchanges at ER-Lysosome contact sites are happening via several different routes and tethers (see **Figure 22**), perturbations of these exchanges cause different defects. As we mentioned before, the absence of VAPs only cause a minor change in cholesterol at the lysosomes. However, we know that NPC1 absence causes major accumulations of cholesterol at the lysosomes and this lacks of NPC1 alo reduces the number of contacts between ER and lyso (Höglinger et al., 2019). As we have seen cholesterol homeostasis alterations in absence of spatacsin, we can wonder if these can be linked to alterations of ER-lysosomes contacts.

d.3 Calcium exchanges at ER -lysosomes contacts

Cytosolic calcium concentration is around 100 nM, which is relatively low compared to extra-cellular calcium levels going up to 2 mM. The principal calcium storage is the ER, because of its large volume and a calcium concentration of about 500 µM (Koch, 1990). The ER uptakes cytosolic calcium via SERCA pumps and releases it via IP_3 receptors, which are activated by inositol tri-phosphate (Taylor et al., 2014). The late endosomes/lysosomes have a calcium concentration similar to ER, while early endosomes have a slightly lower calcium concentration (Lloyd-Evans et al., 2010).

No channel is known in lysosomes that uptakes calcium, however calcium release occurs via TRPML and TPC channels. TRPML1 is a non-selective ion channel activated by $PI(3.5)P_2$ and which loss causes lipid accumulation in lysosomes in a lysosomal storage disorder named Mucolipidosis type IV (Bach, 2001). TRPML1 has been implicated in the regulation of numerous lysosomal functions including autophagy and autophagic lysosomal reformation regulation (Di Paola et al., 2018). TPC1/2 channels are also activated by $PI(3.5)P_2$ but are rather a Na^+ channel, they actually releases very little quantity of Ca^{2+} (P. Li et al., 2019).

TPC1 calcium channel is localized at ER-endosome contact sites, its action as a calcium channel appears to be NAADP sensitive (Kilpatrick et al., 2017). This contact is under dependence of calcium signaling as inactivation or inhibition of TPC1 results in fewer ER-endosome contacts. Lysosomes can be loaded in calcium by capturing calcium released by the IP_3Receptor of the ER (López Sanjurjo et al., 2014)(see **Figure 23**). To fulfill this purpose, IP_3R are found preferentially at ER-lysosomes contact sites. The uptake of ER calcium by the lysosome is dependent on action of V-ATPase lysosomal acidification pumps (Atakpa et al., 2018).

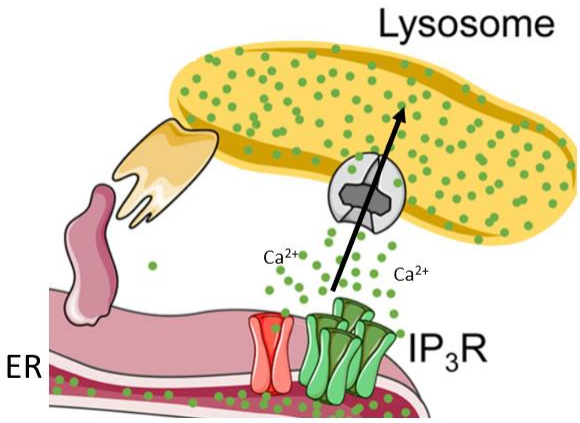

Figure 23 : Calcium is released from the ER to the lysosomes via IP_3R (Atakpa et al., 2018).

Exchanging calcium at ER-Lysosome contact sites can be used to regulate lysosomal function, for example TRPML1 channel is regulating lysosomal positioning via Ca^{2+} signaling (Li et al., 2016).

d.4 Involvement of the ER in lysosome tubulation/fission

A good balance between fission and fusion events in lysosomes is required for their proper cargo and membrane recycling balance (Freeman and Grinstein, 2018; Saffi and Botelho, 2019). There are different types of vesicular fission (see **Figure 24**) and they are dependent on the "classical" vesicle forming protein machinery, that is to say : clathrin, dynamins and Adaptor Protein (AP) complexes (Hirst et al., 2015; Miller et al., 2015; Rong et al., 2012; Schulze et al., 2013). If splitting of lysosomes by vesiculation remains poorly understood, the splitting of lysosomal tubules seems to be linked to ER action at ER-Lysosome contacts.

Autophagic Lysosomal Reformation (ALR) tubulation

First of all, as we mentioned before, lysosomes exposed to starvation undergo ALR under the regulation of mTor signaling, a process in which spatacsin and spastizin have been identified to play a role (Chang et al., 2014a). The goal of ALR is to renew the pool of lysosomes and to achieve this, there are 3 steps (Chen and Yu, 2017) (see **Figure 24**):

1) Inducing membrane deformation
2) Elongation of the emerging tube
3) Fission of the tube that will reform new lysosomes

ALR processes of tubulation are under the regulation of phosphoinositide signaling, it requires the conversion of PI4P to PI(4.5)P_2 to recruit clathrin at the membrane of the lysosomes and to connect the emerging tube to motor protein KIF5B (Rong et al., 2012). PI4P itself seems to be refraining tubulation as blocking its synthesis results in hyper tubulation (Sridhar et al., 2012). PI(3.5)P2 synthesized by PikFYVE is also necessary for ALR as when PikFYVE is inhibited, the reformation of terminal lysosomes is prevented (Bissig et al., 2017). Knowing that PI(3.5)P_2 is an activator of TRPML1 ion channel found on lysosomes, the action of PI(3.5)P_2 on tubulation can be linked to a ion efflux via TRPML1, necessary to modify the organelle osmotic properties and being able to deform its membrane (Freeman and Grinstein, 2018).

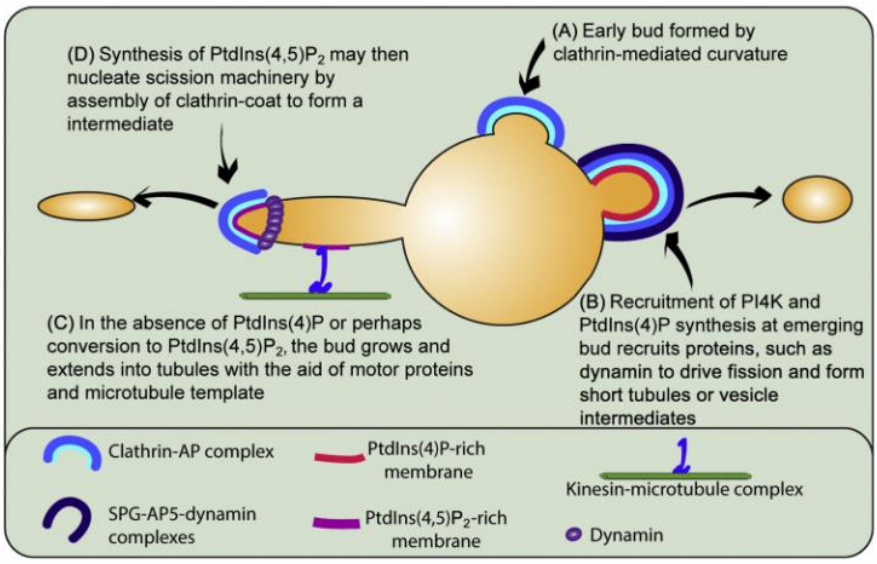

Figure 24 : Mechanisms of lysosomal tubulation and fission (Saffi and Botelho, 2019).

Non-ALR linked tubulation

We can also mention other types of membrane deformation happening in a context different from ALR. In macrophages, the lysosomal compartment is extremely dynamic as macrophages are estimated to internalize an area equivalent to their entire cell surface every 30 minutes (Steinman et al., 1976). The endolysosomal compartment is therefore under a pressure to emit tubules and vesicles that will fuse with the plasma membrane to recycle its inner membrane content. Therefore, the tubulation is very strong in macrophages upon activation of pinocytosis and it is dependent on microtubules and kinesins (Hollenbeck and Swanson, 1990; J. Swanson et al., 1987, 1987). A similar network of tubular lysosomes which is dependent on VCP activity has been more recently observed in Drosophila muscle, and appears to be linked to proper autophagosome-lysosome fusion, therefore regulating proteostasis in the cell (Johnson et al., 2015). Moreover, membrane tubulation is not happening only at the level of late endosomes/lysosomes but also at recycling endosomes, to properly sort cargo between what is destined to lysosomal degradation and what will be recycled at the ER/Golgi membrane. This tubulation requires the KIF13A kinesin (Delevoye et al., 2014, 2009).

Endosome tubule fission linked to ER action

ER forms a tubular envelope at specific contacts with endosomes, where it will promote endosome fission, similarly to what was observed for ER contacts linked to mitochondrial fission (see **Figure 25**). These sites are marked by FAM21, a retromer associated protein (Rowland et al., 2014a). The retromer is a multiprotein complex which controls cargo sorting and mediates endosome tubulation, it is involved in endosome to Golgi transport of M6P receptor (Seaman, 2012). At endosomes-ER contact sites, there is an actin assembly that requires ARP2/3 and WASH complex (see **Figure 25**). The endosome fission is dependent of TMCC1 at the ER and of CORO1C at the Endosome, although not at 100% because depletion of either protein does not completely abolish endosome fission. Once the tubular fission is completed, the cargo contained by the tube can be exported to Golgi or to other destinations (Hoyer et al., 2018). This retromer cargo export pathway is also regulated by the interaction between SNX2 (retromer) and VAPs (ER) (Dong et al., 2016).

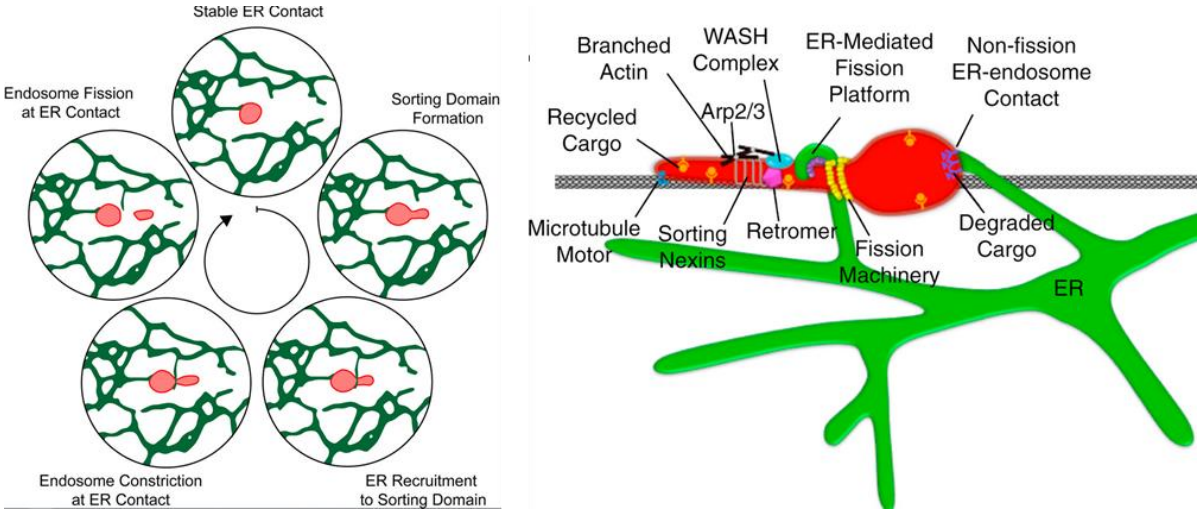

Figure 25 : ER mediates endosomal fission at ER-endosome contacts sites (Rowland et al., 2014a).

Regulation of endosomal fission

Another interesting machinery regulating endosome fission at ER contact sites is the interaction between Spastin (ER) and IST1 (endosome, associated to ESCRT). Spastin and IST1 interaction promotes fission of endosomes at ER-endosomes contacts sites but not the formation of said contacts (Allison et al., 2013). In cells depleted of Spastin, the lifetime of endosomal tubules is increased and the general endolysosomal compartment is altered, promoting axonopathy and SPG4 HSP (Allison et al., 2017a) (see **Figure 26**).

Most of the examples concerning ER regulation of endosome fission concern endosomes that are not presented as late endosomes or lysosomes. However, one can speculate that this regulation of endosome fission by ER might also play a role for late endosomes/lysosome fission. Indeed, the contacts between ER and endosomes actually increase as they mature (Friedman et al., 2013) and ER-endosomes contacts are necessary for endosome maturation. ER protrudin and late endosomes PDZ8 exchange lipid at ER-late endosomes contacts which is a necessary maturation step for the proper functioning of endolysosomal system of degradation (Shirane et al., 2020). Moreover, the Arp2/3 and WASH complex mentioned before are also involved in the construct of an actomyosin ring necessary for tubule fission at melanosomes (Ripoll et al., 2018). Finally, upon depletion of WASH complex, the endolysosomes stained by Lamp1 showed defects in tubule fission (Gomez et al., 2012).

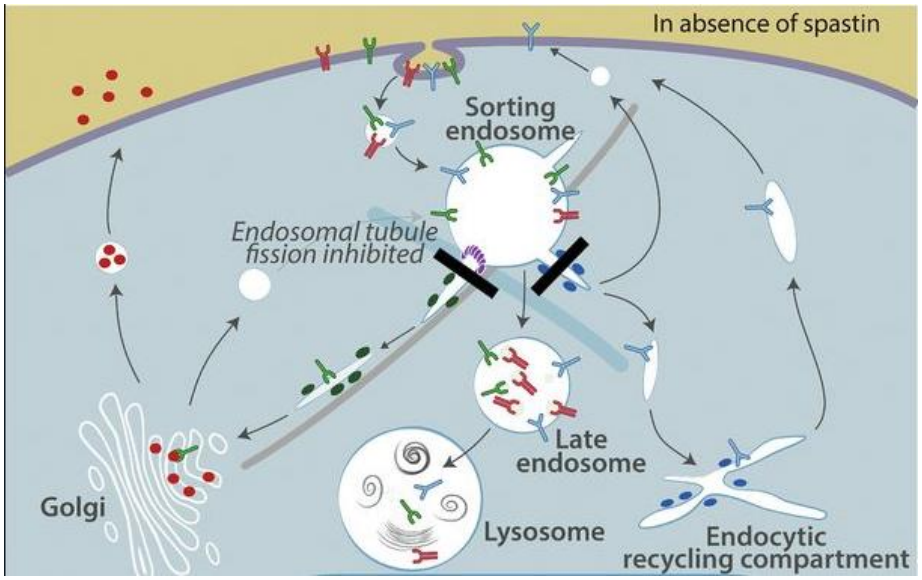

Figure 26: Lack of Spastin causes an inhibition of endosomal fission at ER-endosome contact sites which has consequences on the whole endolysosomal pathway (Allison et al., 2017).

In absence of spatacsin, there is an impairment of the lysosomal membrane recycling, and this impairment is linked to gangliosides and cholesterol accumulations in the lysosome. There is also a lack of lysosomal tubules emanating from lysosomal membrane in absence of spatacsin. Our goal will be to assess if these tubulation defects of the endo/lysosomal compartment are linked to contacts with the ER.

e) Lysosomes contacts with other compartments

As mentioned previously, most contact sites involving Endosomes/Lysosomes involve the ER, but they also contact other organelles for specific functions. For example, Lysosomes contact peroxisomes in a PI(4.5)P_2 regulated way to transfer cholesterol (Chu et al., 2015; Hu et al., 2018), an interesting mechanism for SPG11 HSP where we observed an accumulation of cholesterol in lysosomes in absence of spatacsin.

Lysosomes also make contact with mitochondria and the contact between mitochondrial FIS1 and late endosomes or lysosomes Rab7 promotes mitochondrial fission at Lysososomes-Mitochondria contact sites (Wong et al., 2018). This is a process under the regulation of cholesterol transporter ORP1L and phosphoinositide PI4P (Boutry and Kim, 2021).

There can also be endosome-endosome contacts, that are dependent on MOSPD_2 ER protein, so these endosome-endosome contacts are under a form of ER regulation. These contacts are involved in regulation of particle clustering and fusion between compartments (Di Mattia et al., 2018). Recently, it has been shown that protein tethering between organelles is involved is early steps of pore formation during events of membrane fusion, proposing a role for endosome-endosome contacts in endocytic delivery (Davis et al., 2021).

Investigating roles of spatacsin at ER-Lysosome interface promises to be interesting considering the variety of mechanisms regulated by the ER that are relevant for the cellular defects happening in absence of spatacsin. However, it is likely that not everything that spatacsin does is related to ER-Lysosome contacts, and if these contacts are impaired why not contacts between lysosomes and other compartments?

f) Regulation of membrane contact site formation

This area of the literature concerning regulation of what signals regulate the formation of membrane contact sites remains scarce, but it is a very interesting area to investigate to better understand membrane contact sites role in the cell.

One of the examples of membrane contact site regulation is that ER-Lysosome contacts are regulated via phosphorylation of the FFAT domain of VAP-binding proteins. Phosphorylation of this motif promotes the formation of ER-Lysosome contacts and cholesterol exchange (Di Mattia et al., 2020).

Contact sites between membranes can also be modified in response to various cellular stresses. In long-term ER stress response, the IP_3R-GRP75-VDAC calcium release pathway from ER to mitochondria, that we have described before, can induce apoptosis signaling. This happens by increasing Ca^{2+} flux at the ER-mitochondria junctions that will induce oxidative phosphorylation (see **Figure 27**). BCL-2 on the contrary, is an apoptosis regulating protein which reduces the calcium signaling at the membrane contact interface, while increasing ER-Mitochondria contacts to prevent apoptosis (Xu et al., 2018, p. 2).

In response to hypoxic stress, i.e. cells exposed to low O_2, there is an enrichment of FUN14 at ER-mitochondria contacts promoting mitochondrial fission (Wu et al., 2016). Also, mitochondrial dysfunction in an obesity model showed problem in ROS metabolism resulting in more ER-Mitochondria contacts (Arruda et al., 2014).

The regulation of peroxisomes-lipid droplets contacts happens via Spastin in response to oxidative stress (Chang et al., 2019) and is accompanied by the formation of early endosomes-mitochondria contacts (RAB5-Alsin) (Hsu et al., 2018). In a yeast model, it has been shown that the transfer of ceramide from ER to Golgi happens to prevent lipotoxicity of ceramide accumulation (Liu et al., 2017).

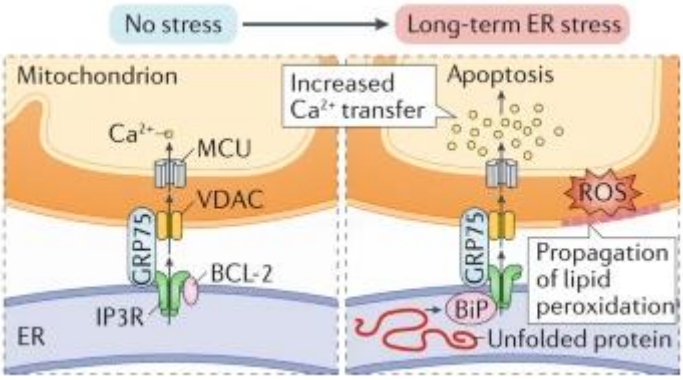

Figure 27 : Regulation apoptosis signaling by calcium flux at ER-Mitochondria contacts in response to ER stress (Prinz et al., 2020).

There is no unified function of membrane contact sites per se, as we have discussed, their roles in the cell are multiple and dynamic. The fact that various cellular stress can affect the distribution and number of these contacts and their local activity is an interesting feature of membrane contact sites. As it has been discussed by other researchers, it is possible that these contacts constitutes a conserved machinery that serves the cell in its responses to cellular stress (Molino et al., 2017).

g) Membrane contacts sites proteins involved in neurodegenerative diseases

Due to the importance of contact sites between organelles for cell physiology, it is likely that their alterations may play a role in pathological conditions. We will explore here some neurodegenerative diseases where membrane contact sites might contribute to physiopathology.

The ER–resident VAPB protein, implicated in numerous contact sites between the ER and other organelles (see before), has been found to be mutated in a form of Amyotrophic Lateral Sclerosis (ALS) (Nishimura et al., 2004). However, it is not known whether the mutation of VAPB identified as causal for ALS is affecting the ability of the protein to form membrane contact sites.

In models of Alzheimer's disease, presenilin 2 is enriched at ER-Mitochondria contact sites and regulates calcium efflux, its absence causes defects in the regulation of the ER-Mitochondria interface (Area-Gomez et al., 2012; Zampese et al., 2011).

In Parkinson's disease, alpha synuclein is found in Mitochondria Associated Membranes of ER (MAM). Mutation of alpha synuclein reduced its presence in MAM, impairing ER-mitochondria contact and promoting more mitochondrial fission (Guardia-Laguarta et al., 2014).

GM1 gangliosidosis (Landing disease), a form of lysosomal storage disorder, shows an accumulation of GM1 at the ER-Mitochondria interface in a mouse model for the disease. This causes an hyperactivation of IP_3R at the ER and a mitochondria overload of calcium, resulting in apoptosis signalling (Sano et al., 2009).

Membrane contact sites proteins mutated in Hereditary Spastic Paraplegias (HSPs)

Spastin is an ER shaping protein (Park et al., 2010), mutated in HSP type SPG4 and by interacting with endosomal IST1 (part of ESCRT sorting complex), it promotes the fission of endosomal tubules at the level of ER-endosomes contact sites. Defects in this function are linked to the apparition of HSP phenotype (Allison et al., 2017a, 2013). Interestingly, Spastin is also important for peroxisomes lipid droplets (LD) interaction (Chang et al., 2019) and for ER-LD contacts (Arribat et al., 2020), underlining the importance of ER-resident proteins at multiple levels of regulation in the cells via membrane contact sites.

Spastin interacts with Protrudin, that we mentioned earlier, to shape the ER along with other HSP proteins (Chang et al., 2013; Connell et al., 2020). Protrudin (ZFYVE 27) wa proposed to be mutated in SPG33 (Mannan et al., 2006). And we know that protrudin is an ER-resident protein, making contact with late endosomes to regulate their dynamics (Raiborg et al., 2015a).

REEP1 has also been shown to facilitate ER-mitochondria interactions (Lim et al., 2015). This ER-mitochondria interface is mediated by REEP1/2 in response to DNA damage by regulating a change of ER tubular morphology, increasing ER-mitochondria contacts and triggering apoptosis pathway activation via calcium signaling at ER- mitochondria contacts (Zheng et al., 2018).

Seipin (BSCL2), that we mentioned earlier as implicated at ER-LD contact sites, is mutated in SPG17 (Ito, 1993; Ito et al., 2008). The interesting thing about seipin, is that some of its mutations result in accumulation of the mutant Seipin in the ER, activating the Unfolded Protein Response (UPR) pathway and inducing ER stress-mediated cell death (Ito and Suzuki, 2009).

Importance of ER-lysosomes contact sites for spatacsin molecular role

In this part of the introduction concerning membrane contact sites, I wanted to emphasize on the multiple regulatory roles that the ER performs via its contacts with other organelles. By regulating organelle position, the maturation of the endolysosomal system, regulation of lipid flux or calcium flux, the ER-lysosomes interface appears extremely relevant to study regarding the phenotypes observed in absence of spatacsin.

Moreover, it appears that membrane contact sites respond to various cellular stress, which is very interesting in our model, regarding the fact that neurons are particularly vulnerable to cellular stress. Finally, it appears that several hereditary spastic paraplegia proteins are implicated in ER contacts with other organelles, and this is encouraging to place our focus on the ER-Lysosomes interface (see **Figure 28**). The next part will deal with aspects of substrate degradation regulation in the cell, especially at the ER, as SPG11 HSP is a disease of accumulation of non-degraded material.

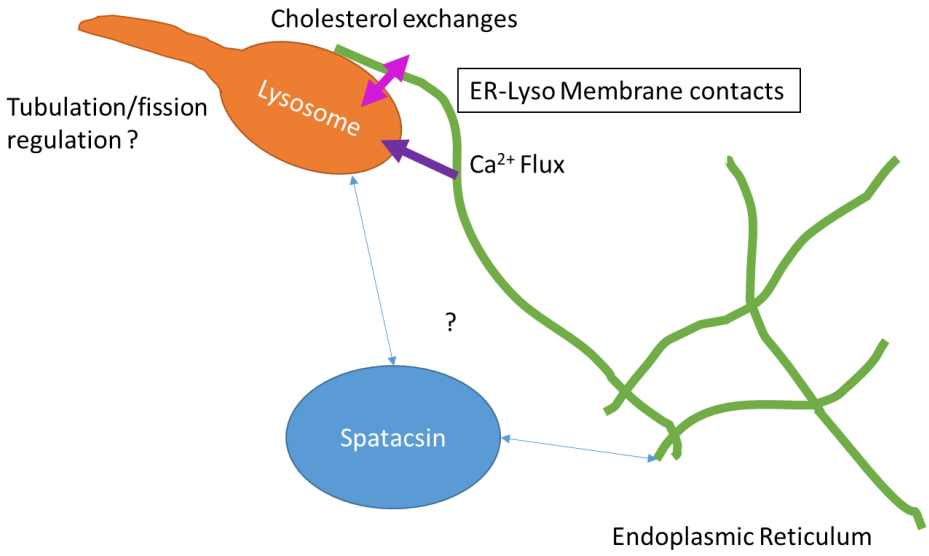

Figure 28: Can the molecular role of spatacsin be linked to ER-lysosomes contacts ?

IV. The importance of the ER in degradative pathways regulation

One of the main functions of the lysosomes is to degrade cellular components to recycle them. This can happen via autophagy as we have seen previously or via proteasomal degradation. The proteasome is a cytosolic protein complex that is, at first glance, unrelated to lysosomal dependent degradation. As preliminary data on spatacsin function led us to think that degradative processes dependent of ubiquitin were important (see **Results**), I wanted to investigate what are the main degradative pathways of the cell. Moreover, it appears that the endoplasmic reticulum (ER) is involved in the regulation of part of the ubiquitin-dependent degradation pathway, which is susceptible to link our hypothesis of a role of spatacsin at ER-lysosomes interface with a potential role in ubiquitin regulation.

a) The ubiquitin degradation pathway

Ubiquitin is a 76 amino acids protein that can be added to a substrate by specific enzymes to modulate its function and notably promote its degradation. There are 3 steps in the ubiquitination process (see **Figure 29**). First, the E1 enzyme will activate ubiquitin using ATP. Then the E2 class of enzymes will receive the ubiquitin via a thio-ester bond. Finally, E3 class of enzymes transfer ubiquitin from E2 to a lysine of the substrate.

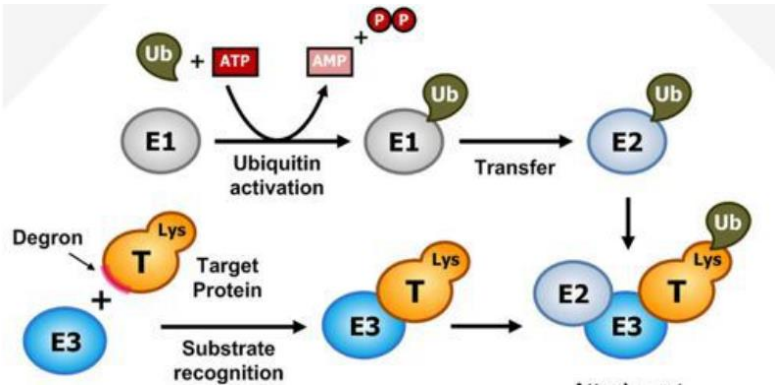

Figure 29: The three steps of ubiquitination mediated by the 3 classes of enzymes. from *https://www.creative-diagnostics.com/proteolysis-ubiquitin.html*

More than 800 E3s are believed to be encoded in the human genome, and they are divided in three major classes:

- RING finger proteins (most common)
- HECT (homologous E6-AP Cter)
- Ubox domain proteins

After the fixation of the first ubiquitin on the substrate, other ubiquitins can be added on the original ubiquitin through any of its seven Lys residues (Lys6, Lys11, Lys27, Lys29, Lys33, Lys48, and Lys63), creating polyubiquitinated substrates (see **Figure 31**). Among the eight linkages, the most prominent is Lys48 linkage, which represents up to half of all linkages and generates a proteasomal degron, i.e. a protein signaling information that will target the substrate to proteasomal degradation. Second most common is Lys63 linkage, which facilitates the autophagic degradation of protein substrates together with their associated cellular materials such as damaged mitochondria and invading pathogens (see **Figure 31**).

Ubiquitins can also be removed from the substrates by De-UBiquitinases enzymes (DUBs). About 90 DUBs have been identified so far and modulate the rate of substrate degradation by the proteasome or other destinations. There are 2 major classes of DUBs: cysteine proteases & metalloproteases.

The primary function of ubiquitination is to generate degrons on short lived proteins and misfolded/damaged proteins and thanks to the variety of E3s that exist combined to DUBs, the substrates can be very precisely addressed to their destination (Kwon and Ciechanover, 2017) (see **Figure 31**).

For example, the accepted 'canonical' signal for proteasomal recognition is a polyubiquitin chain that is anchored to a lysine residue in the target substrate and is assembled through isopeptide bonds involving lysine 48 of ubiquitin. However, homogeneous polyubiquitin chains based on linkages involving lysines 6, 11, 27, 29 and 48 can also mediate proteasomal degradation (Dammer et al., 2011).

Lysine-63-based chains have been shown to target mainly membrane proteins for degradation in the lysosome (Lauwers et al., 2010). Furthermore, some proteins can be degraded following modification by a single ubiquitin (monoubiquitylation) or multiple single ubiquitins (multiple monoubiquitylation) (Boutet et al., 2007; Kravtsova-Ivantsiv et al., 2009). A few exceptional cases have been reported, where the proteasome can degrade proteins that have not been modified by ubiquitin at all.

It is also possible that the ubiquitination of substrates does not promotes their degradation but rather is involved in signaling. On top of that, sometimes, the degron on substrates is not of ubiquitinated nature as for example in the N-end rule pathway. This pathway mediates autophagic proteolysis of substrates independently of ubiquitin chains, an arginine is fixed on the protein in N-ter that will be recognized by p62 for autophagic targeting and lysosomal degradation (Sriram et al., 2011).

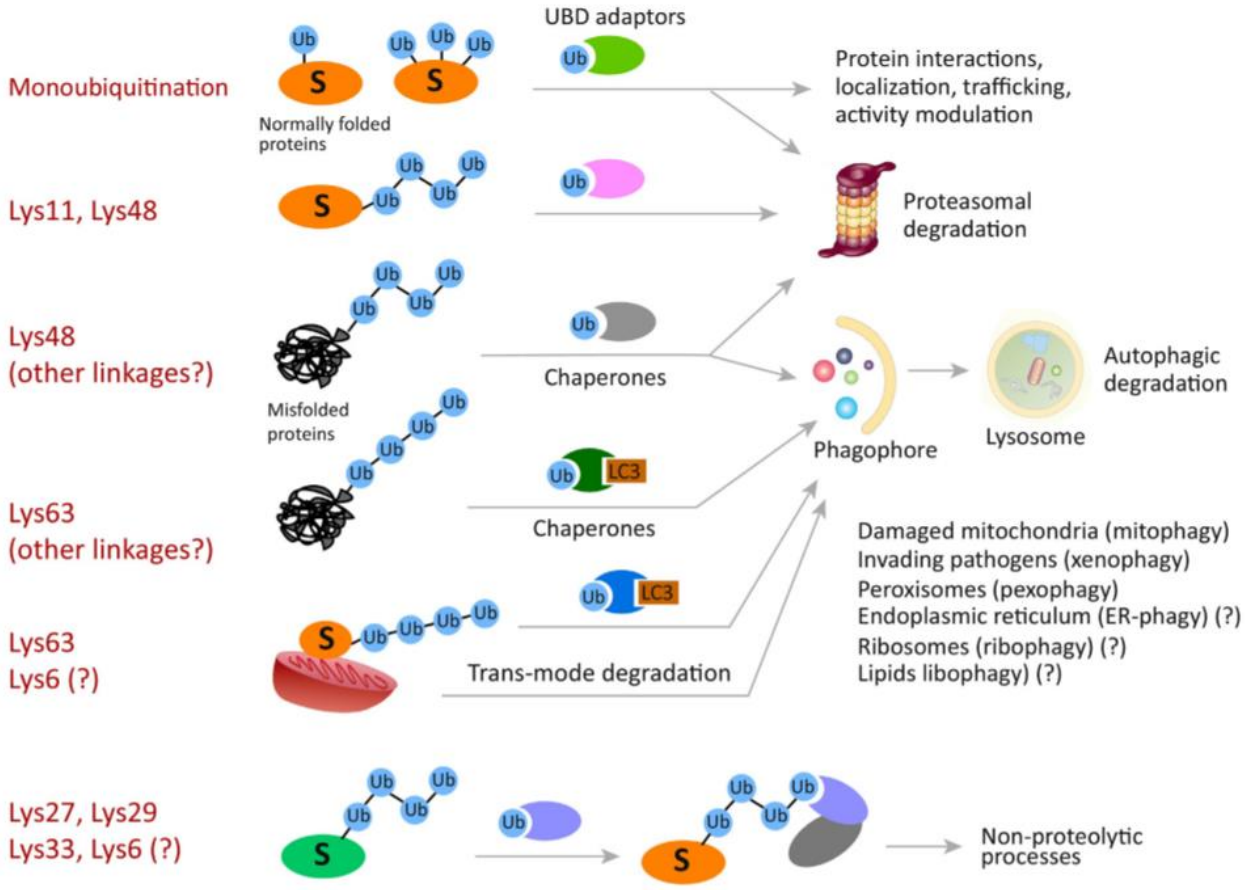

Figure 31 : The ubiquitin code for substrates targeting (Kwon and Ciechanover, 2017).

b) Proteasome and autophagy relationship for degradation

It is estimated that the proteasome is responsible for 80%-90% of the total protein degradation happening in cells, while autophagic degradation is responsible for the 10-20% remaining (Kravtsova-Ivantsiv and Ciechanover, 2012). This is however more balanced to 50-50% in non-proliferating cells such as neurons, pointing toward a more important role of autophagy in these cells (Hara et al., 2006; Liang et al., 2010)

While the ubiquitin proteasome system is recognized as a major highly specific and selective route for cellular protein degradation, autophagy is involved mostly in bulk destruction in response to stress (Cohen-Kaplan et al., 2016). Short-lived protein that are involved mostly in regulatory processes are generally degraded by the proteasome (Naujokat and Hoffmann, 2002) while long-lived proteins are preferentially degraded by autophagy (Mortimore et al., 1988).

Targeting of substrates to the proteasome

For the proteasomal degradation, ubiquitinated substrates will bind ubiquitin-associated proteins (UBA) or Ubiquitin-like proteins (UBL), which are shuttling proteins. UBA & UBL preferentially bind Lys48 ubiquitin chains, and they will carry substrates to the proteasome. Ubiquitinated substrates are delivered to 19S subunit of the proteasome, where are found ubiquitin receptors, such as Rpn1 subunit of the proteasome, that will bind the UBA/UBL associated to the substrate (Elsasser et al., 2002). Then the substrate is de-ubiquitinated at the 19S proteasome, unfolded and translocated to the proteolytic chamber of the 20S proteasome where it will be degraded (Gallastegui and Groll, 2010) (see **Figure 32**).

Targeting of substrates to the autophagosome

The delivery of cargoes destined for autophagic degradation happens via the adaptor proteins such as p62 that has an ubiquitin-binding domain (Bjørkøy et al., 2005) and has the ability to bind to Lc3-II, which is enriched at the forming autophagosome membrane (Pankiv et al., 2007) (see **Figure 32**). This process is called selective autophagy and differs from bulk autophagy where cargo internalized for degradation is not selectively shipped to the autophagosome. The formation of the autophagosome is under the control of ATG proteins, regulating autophagic degradation in the cell. P62 has a stronger affinity to bind substrate that are Lys63 ubiquitinated, but it has also been observed to target substrate to the proteasome (Babu et al., 2005).

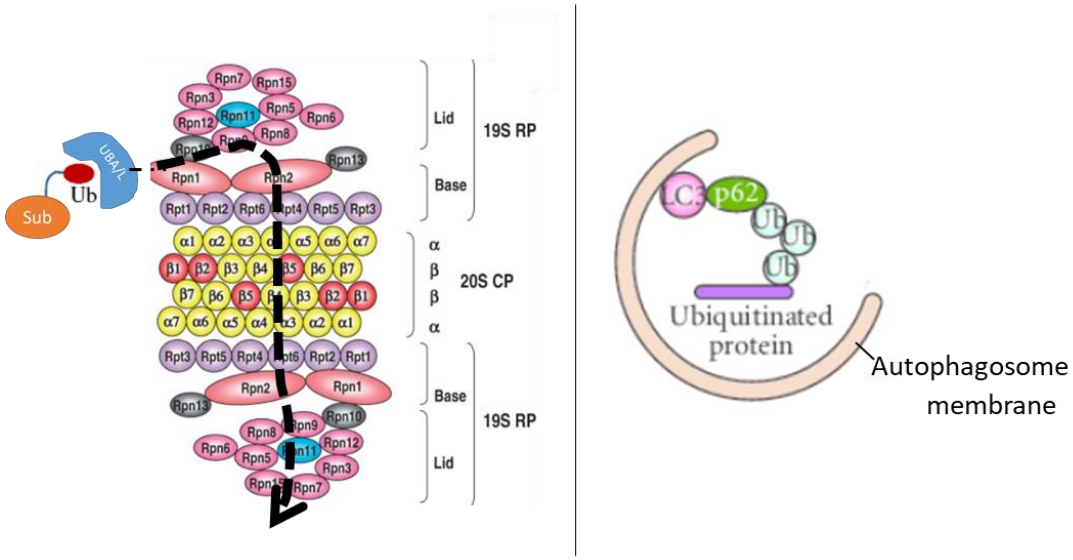

Figure 32. **Left:** The proteasome complex receiving ubiquitinated cargo bound to ubiquitin-associated proteins. (Budenholzer et al., 2017) **Right:** Targeting of ubiquitinated substrates to the autophagosome via p62 and LC3-II.

Response of the degradative systems to proteins aggregation

Degrading misfolded proteins that are soluble is generally done by the ubiquitin proteasome system. Specific misfolded proteins can be degraded by chaperone-mediated autophagy (CMA), where substrates are recognized by chaperone Hsc70 and directly delivered to lysosomes for degradation (Kiffin et al., 2004; Rothenberg et al., 2010)(see **Figure 33**).

In the case of accumulation of non-degraded misfolded proteins in cytoplasm forming an "aggresome", chaperones and proteasomes associate with aggresome to clear it. A cooperation between the two degradative systems has been observed in the case of aggresome clearance(Nanduri et al., 2015). And if the proteasome is inhibited, the number of lysosomes retained at the centrosomes close to the aggresome is higher, in order to degrade it (Zaarur et al., 2014). Some parts of the aggresome are directed to macro-autophagy, for bulk-internalization in autophagosomes that will fuse with lysosomes for degradation (Hariharan et al., 2011) (see **Figure 33**).

Proteasome inhibition has been shown to have consequences on lysosomal regulation and autophagosome biogenesis as well via TFEB and GSK3β signaling (C. Li et al., 2019; Zhan et al., 2016). As the regulators of both pathways seem to be tightly related, it seems that the ubiquitin proteasome pathway and autophagy are working in interdependent manners.

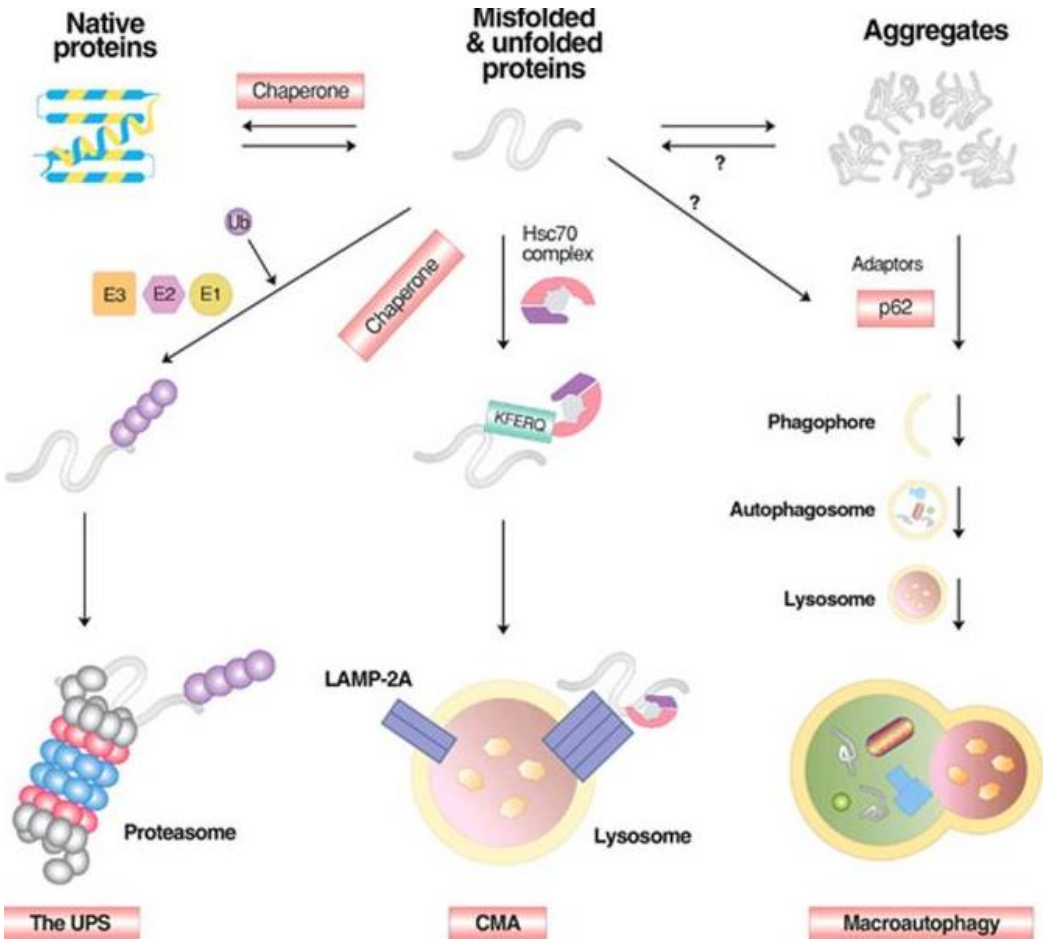

Figure 33 : Degradation of misfolded proteins requires cooperation of degradative pathways (Ciechanover and Kwon, 2015).

c) Regulation of ubiquitin proteasome pathway and autophagy by the endoplasmic reticulum

c.1 ER Associated Degradation (ERAD)

The endoplasmic reticulum (ER) receives a third of the total synthesized proteins of the cell (Kanapin et al., 2003), to catalyze specific post-translational modification such as addition of glycans, lipids, or new disulfide bonds formation in order to fold properly the proteins. The ER contains a variety of chaperones that are responsible for protein folding (Sitia and Braakman, 2003). If folding occurs improperly, proteins might aggregate in the ER which is a source of stress for the cell (Molinari et al., 2005).

Upon detection of unfolded proteins in the ER, the Unfolded Protein Response (UPR) is activated in the ER. The UPR consists in upregulating chaperones in the ER to increase its folding capacity, expand ER volume and export unfolded protein out of the ER so they can be degraded, as the ER has no degradation machinery (Oslowski and Urano, 2011; Ron and Walter, 2007).

The substrates of ERAD are targeted for retro-translocation by chaperone like lectins and are polyubiquitinated at the level of the ER-membrane (see **Figure 34**). The complexes responsible for ERAD substrates ubiquitination are E3 ligases named translocons (Mehrtash and Hochstrasser, 2019). Two major components of translocons are GP78 and HRD1, they have a wide variety of substrates (Fang et al., 2001; Zhang et al., 2015).

After ubiquitination of the ERAD substrate, p97 (VCP) /cdc48 complex is recruited to the substrate, so it can be retro-translocated and brought to the cytosol for further modifications, such as de-ubiquitinations, before being brought to the proteasome for degradation as described previously (Schuberth and Buchberger, 2005) (see **Figure 34**).

c.2 ER to Lysosome Associated Degradation (ERLAD)

Some substrates are resistant to ERAD degradation, for several reasons such as being too large or having a tendency to form aggregates (Fregno and Molinari, 2021). There is a growing list of substrates identified to be proteasome-resistant and destined to ERLAD (Fregno and Molinari, 2019).

ERLAD consists in both macro-autophagy and non-macro autophagic pathways to deliver ERAD resistant substrates to the lysosomes for degradation. Collagen for example is prone to misfolding and its degradation is enhanced by autophagy activation caused by rapamycin treatment (Ishida et al., 2009). The identification of misfolded pro-collagen is dependent on ER-chaperone Calnexin action and the ER receptor FAM134B. Together they perform the autophagy mediated quality control of procollagen. FAM134B has the ability to bind LC3-II at the autophagosome to deliver the collagen, which is complexed to calnexin, to degradation at the lysosomes (Forrester, 2019) (see **Figure 34**).

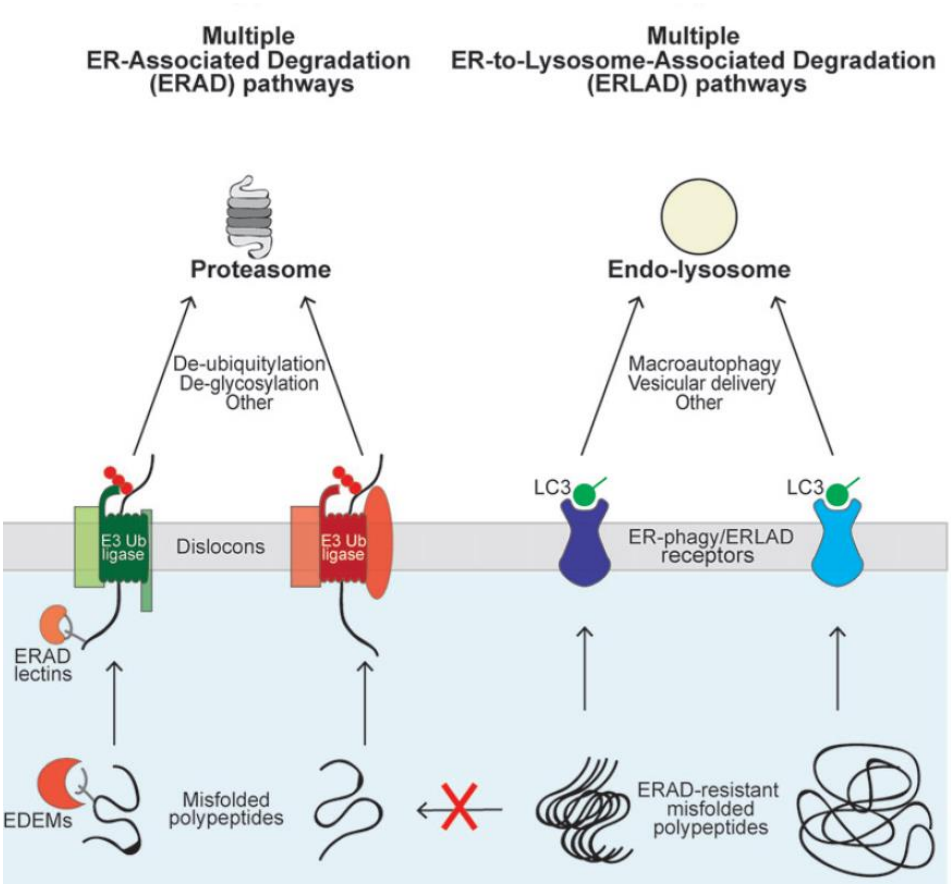

Figure 34: Mechanisms of endoplasmic reticulum regulation of misfolded protein degradation (Fregno and Molinari, 2019).

c.3 ER-phagy

The ER is an organelle that undergoes continuous recycling of its components to maintain its integrity. This can happen in basal conditions or in response to certain stress conditions (Omura et al., 1967). While ERAD is limited to degradation of proteins, autophagosomes are able to internalize entire parts of the ER by macro ER-phagy (De Leonibus et al., 2019). But ER content can also be shipped to lysosomes via vesicular delivery as seen before in ERLAD and by invagination of lysosomal membrane around ER (Schuck et al., 2014)(see **Figure 35**). This more precise sorting of ER for autophagy is mediated by various ER-phagy adaptors. For example, downregulation of FAM134B causes an enlarged ER while it fragments the ER when overexpressed (Khaminets et al., 2015).

Another ER-phagy adaptor, Sec62, is implicated in the phase of recovery following an ER stress. Indeed, the unfolded protein response (UPR), mentioned earlier, creates an excess of ER that needs to be recycled as well as excess chaperones. Sec62 role is to deliver ER components to the autolysosomal system via its LC3 interacting region (Fumagalli et al., 2016). This recovery from ER stress, named recov-ER-phagy is also relying on ESCRT sorting machinery at the late endosomes/lysosomes them to directly engulf ER components (Loi et al., 2019) (see **Figure 35**).

Atlastin 3 (ATL3) and Reticulon 3 (RTN3) are two other ER-phagy adaptors that will mediate specifically the degradation of the tubular ER upon starvation. ATL3 binds to GABARAP which is a member of the LC3 family to perform its action (Chen et al., 2019, p. 3). RTN3 and RTN3L (long isoform) are involved in ER tubule fragmentation and interact with LC3/GABARAP protein family as well (Grumati et al., 2017).

P62 adaptor is also involved in ER-phagy regulation by interacting with TRIM13 in the N-degron pathway (Ji et al., 2019)(see **Introduction IV-A**). Under stress conditions, proteins that are targeted for degradation accumulate at the ER exit sites also called ER-phagy sites. At these sites, the recruitment of the coat protein complex COPII permits the packing of ER fragments into autophagosomes (Cui et al., 2019). This is another way of regulating procollagen turnover at these exit sites (Omari et al., 2018)(see **Figure 35**).

The nuclear envelope, the lamina, which is connected to the ER, appears to be degraded by autophagy using components of the ER-phagy machinery (Mijaljica and Devenish, 2013). This form of nucleophagy appears to be important for maintaining the integrity of nuclear shape and protecting the cell from tumorigenesis (Dou et al., 2015).

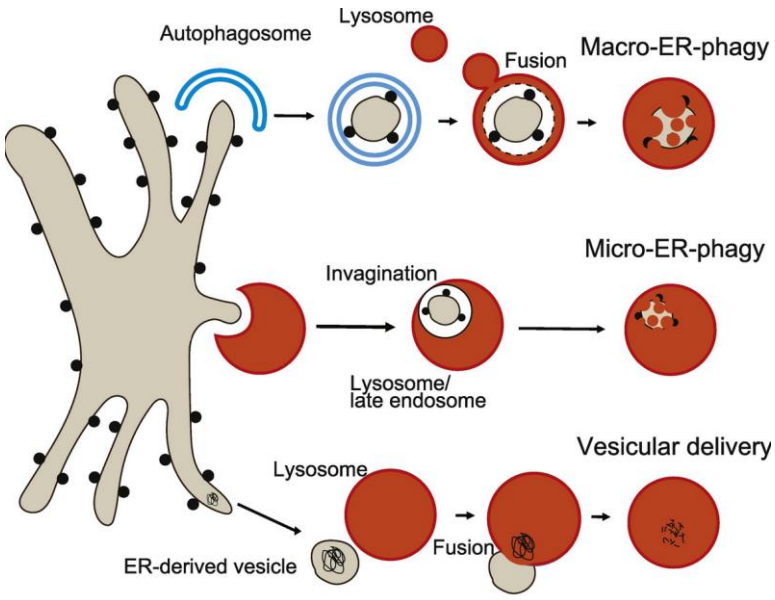

Figure 35: Different internalization of ER components by lysosomes for ER-phagy (Chino and Mizushima, 2020).

The ER cooperates with the ubiquitin proteasome pathway and the autophagic pathway to promote degradation of misfolded proteins or of other cargoes. ER is also dependent on the autophagic pathway for the degradation of its own machinery. This happens basally or in response to ER stress and highlights that organelles need to cooperate to regulate cellular homeostasis.

d) Cooperation between endoplasmic reticulum and ubiquitin pathway in non-degradative regulations

Regulation of endosomal position

We have already mentioned the interesting mechanism regulating endosomes position based on ubiquitin signaling (Jongsma et al., 2016a). The ER-located RNF26 E3 ligase can ubiquitinate p62 near the ER, recruiting the vesicles that bear ubiquitin binding domains and trapping these vesicles at the ER interface. The vesicles can be released by action of the De-ubiquitinase USP15 creating a "stop & go" mechanism to selectively trap endosomal vesicle at ER/endosome contact sites via a ubiquitin dependent machinery (see **Figure 36**).

RNF26, via its partner UBE2J1, which is an E2 ubiquitin conjugating enzyme of the ER membrane, and the use of the "stop and go" system, promotes the trafficking of EGF receptor to lysosomes (Cremer et al., 2021). This kind of mechanism adds to the complexity and the versatility of ER regulation of endosomes dynamics and help us understand how the ER/endosome contact sites can be regulated via ubiquitin signaling, an area of the literature that remains open for new mechanisms.

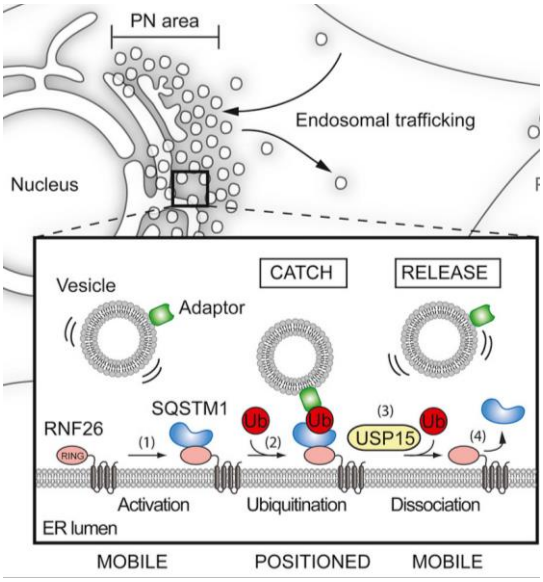

Figure 36: The "stop & go" mechanism, dependent on ubiquitin and ER to regulate endosomal position (Jongsma et al., 2016).

Regulation of collagen secretion

Another interesting example of such ubiquitin/ER collaboration is the regulation of collagen secretion via E3 ligase Cullin3 (McGourty et al., 2016). This E3 ligase has the particularity to bind with many different adaptors, here the adaptor that is involved is KLHL12. Cullin3 and KLHL12 will ubiquitinate ER-protein Sec31 under the calcium-dependent regulation of PEF1 & ALG2. This ubiquitination of Sec31 then allows the formation of large COPII coats at the ER membrane and promotes collagen vesicular secretion (see **Figure 37**).

It is very interesting to observe that the vesicle formation at the ER is under regulation of ubiquitin signaling , which was shown before by the same group (Jin et al., 2012) and calcium regulation of this process adds a level of regulation of this secretory pathway (see **Figure 37**). Interestingly this works both ways. Indeed, if Cul3 promotes vesicle formation by ubiquitination of Sec31, its de-ubiquitination by de-ubiquitinase USP8 decreases the size of the ER vesicles and prevents collagen secretion (Kawaguchi et al., 2018).

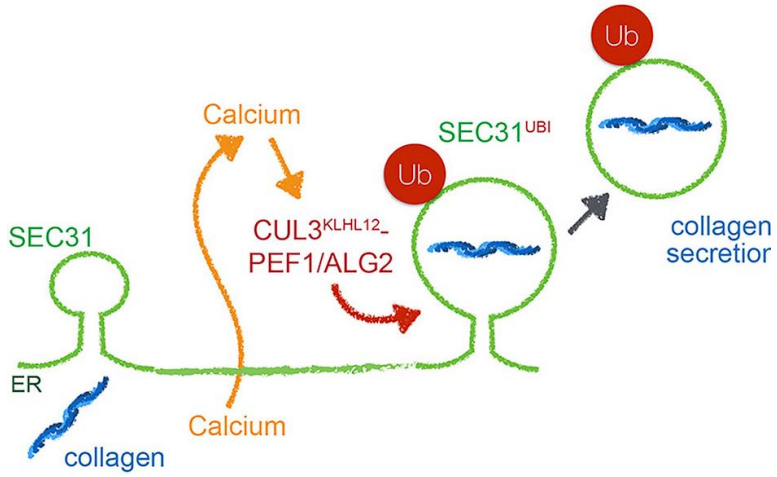

Figure 37: Collagen vesicular secretion by the ER is under regulation of ubiquitin and calcium signaling regulation (McGourty et al., 2016).

e) Dysfunctions of the degradative pathways in neurological disorders

We have discussed earlier in the first part of the introduction the links between faulty degradation of substrates at the endolysosomal compartment and neurodegenerative disorders and we will try to focus more here on the steps that precede the degradation taking place at the lysosomes or happens via other machineries of degradation.

e.1 Role of the ubiquitin proteasome pathway in neurological disorders

First, the importance of ageing in the regulation of degradative pathways can be illustrated in the way cells respond to a proteasome stress. In a study performed on rat neurons, if the proteasome is inhibited, autophagy is efficiently activated in neurons from young individuals but this is not the case for older ones, indicating that with age the pathway involved in autophagy activation is likely impaired (Gavilán et al., 2015). Ageing is linked to a general slowdown of the proteasomal activity, preventing a correct degradation of ubiquitinated substrates (Isabel and David, 2014). When proteasome is artificially activated, it delays ageing (Chondrogianni et al., 2014). Experiments have been conducted to increase proteasome activity by inhibiting de-ubiquitinase USP14, which is responsible for de-ubiquitination of cargoes docked to proteasome. Doing so speeds up the degradation of oxidized proteins, theoretically enhancing the capacity of cells to resist to oxidative stress (Lee et al., 2010). But at the same time, mutations of USP14, altering its function, lead to a neurological disease (Marshall et al., 2013).

The involvement of ubiquitin E3 ligases in neurological disorders is quite important (Lescouzères and Bomont, 2020). One of the most famous example might be E6-Ap, one of the first identified HECT E3 ligase mutated in Angelman syndrome, which is characterized by are a severe impairment of the neurological development (Kishino et al., 1997). Parkin is another famous example of E3 ligase (also known as RING, from the RING family) which is causing a form of juvenile parkinsonism when mutated (Kitada et al., 1998). CUL3 ubiquitin ligase and its many adaptors is involved in forms of giant axon neuropathy (Bomont et al., 2000), in neuronal ceroid lipofuscinosis, which is a form of lysosomal storage disorder (Staropoli et al., 2012) and in epilepsy (Azizieh et al., 2011; Van Bogaert et al., 2007).

e.2 Diseases linked to Endoplasmic Reticulum proteins regulating degradation

The ER chaperone VCP/p97, that was mentioned earlier as involved in ER-associated degradation (ERAD) is causing a multi system neurodegenerative disorder i.e., IBMPFD = Inclusion Body Myopathy / Paget disease of the bone/ Fronto Temporal Dementia. The main feature of this disorder is ubiquitin inclusions in muscle, brain, and bone tissues (Ju and Weihl, 2010). On top of that, mutation of p97/VCP also cause an impairment of autophagy, as its absence is impairing the maturation of autophagosomes (Tresse et al., 2010) and also the formation of tubular lysosomes (Johnson et al., 2015).

ER-Phagy adaptors, that we presented earlier, are also causing neurodegenerative disorders, for example, mutations of RTN3 can cause rare forms of Alzheimer's disease (Zou et al., 2018) while mutations of ATL3 cause an hereditary sensory neuropathy (Fischer et al., 2014) . Mutations of FAM134B are also the cause for another form of neuropathy (Kurth et al., 2009). It appears also that Rab7a, which is mutated in a form of neuropathy (DiVincenzo et al., 2014) is modulating ER stress and ER morphology, as when depleted, it leads to ER stress and causes ER enlargement (Mateus et al., 2018).

e.3 Hereditary Spastic Paraplegia Proteins

For HSPs, dysfunctions of the degradative pathways are happening at many levels. For example, in brain of SPG11 patients, cytoplasmic granular structures looking like lysosomes that are positive to p62 and ubiquitin staining were observed. This was revealing the accumulation of undegraded ubiquitinated cargo and reminding of lesions observed in Amyotrophic Lateral Sclerosis (ALS) (Denora et al., 2016a).

Proteins involved in ubiquitination/de-ubiquitination of substrates

Spartin (SPG20) does not have an E3 ligase activity but, by binding AIP4/AIP5 E3 ligases it recruits them to lipid droplets and regulates their turnover by promoting adipophilin ubiquitination (Edwards et al., 2009; Hooper et al., 2010). Indeed, depletion of Spartin increases the number and size of lipid droplets (Eastman et al., 2009).

ER membrane proteins Erlin1/2 (SPG62/SPG18) can bind IP_3R channels that we have seen are so important for calcium efflux from the ER toward other organelles. By interacting as a recognition factor with IP_3R they promote its polyubiquitination by RNF170 (Lu et al., 2011). RNF170 is an E3 ligase that is mutated in a form of HSP (de Sainte Agathe et al., 2021) and its ubiquitination of IP_3R regulates its degradation by ER associated degradation, (Pearce et al., 2009).

De -ubiquitinase (DUB) USP8 is mutated in Cushing disease (Reincke et al., 2015) and may also be a cause for SPG59 (Novarino et al., 2014), this DUB has the ability to interact directly with adaptor p62 and preferentially removes Lys-11 ubiquitin chains from p62 acting as a negative regulator of autophagy (Peng et al., 2019).

WD-48 (SPG60) (Novarino et al., 2014) binds USP46 and USP1, stimulating their de-ubiquitinase activity (Yin et al., 2015). USP1 has a role in autophagy regulation (Raimondi et al., 2018) and USP46 regulates trafficking of AMPA receptor, which are involved in learning & memory (Huo et al., 2015). Ubiquitin associated protein (UBAP1) is a member of the ESCRT complex which participates in cargo sorting by interacting with ubiquitinated substrates (Agromayor et al., 2012). Its mutation is responsible for endosome clustering and enlargement leading to HSP SPG80 (Lin et al., 2019).

These examples illustrate that regulation of ubiquitin-dependent pathways is relevant for the physiopathology of various forms of HSP (see **Figure 38**).

Proteins involved in ER response to stress and ER remodeling

Seipin (SPG17) that is implicated in ER-lipid droplet contacts, seems to be also involved in ER stress. Indeed, when Seipin is mutated, due to improper folding, proteins accumulate in the ER and this results in the activation of the unfolded protein response and induces cell death (Ito and Suzuki, 2009).

REEP1 (SPG31) is also linked to ER stress regulation as REEP1$^{-/-}$ mice have elevated ER stress levels. By decreasing ER stress levels using salubrinal, the motor phenotype of REEP1$^{-/-}$ mice was partially rescued linking ER stress and the development of the impaired motor phenotype of SPG31 (Wang et al., 2020, p. 1). RTN2 is an ER-shaping protein mutated in SPG12, is involved in ER architecture remodeling and upon ER stress, it binds autophagy protein ATG8 to regulate ER-phagy (Zhang et al., 2020).

Atlastin 1, remodeler of the tubular ER and cause of HSP when mutated, is under regulation of the E3 ubiquitin ligase SYVN1. Ubiquitination of ATL1 by SYVN1 prevented ATL1 GTPase activity and ER remodeling (Zhao et al., 2020). Another HSP protein under ubiquitin dependent regulation is Spastin, indeed Spastin is subject to neddylation-dependent proteasome degradation. Neddylation refers to the labelling of substrates with Nedd8 protein, an ubiquitin-like protein that activates Cullin ligases (Enchev et al., 2015) (see **Figure 38**).

Proteins involved in the degradative pathways, when mutated, cause a variety of neurological disorders, including many forms of HSP. They can be involved at every level of the regulation of degradation, whether it at the proteasome itself, at the level of chaperones regulating ER-associated degradation, ubiquitin ligases and de-ubiquitinases or ER-phagy adaptors, see **Figure 38** for an overview of HSP roles in the degradative pathways.

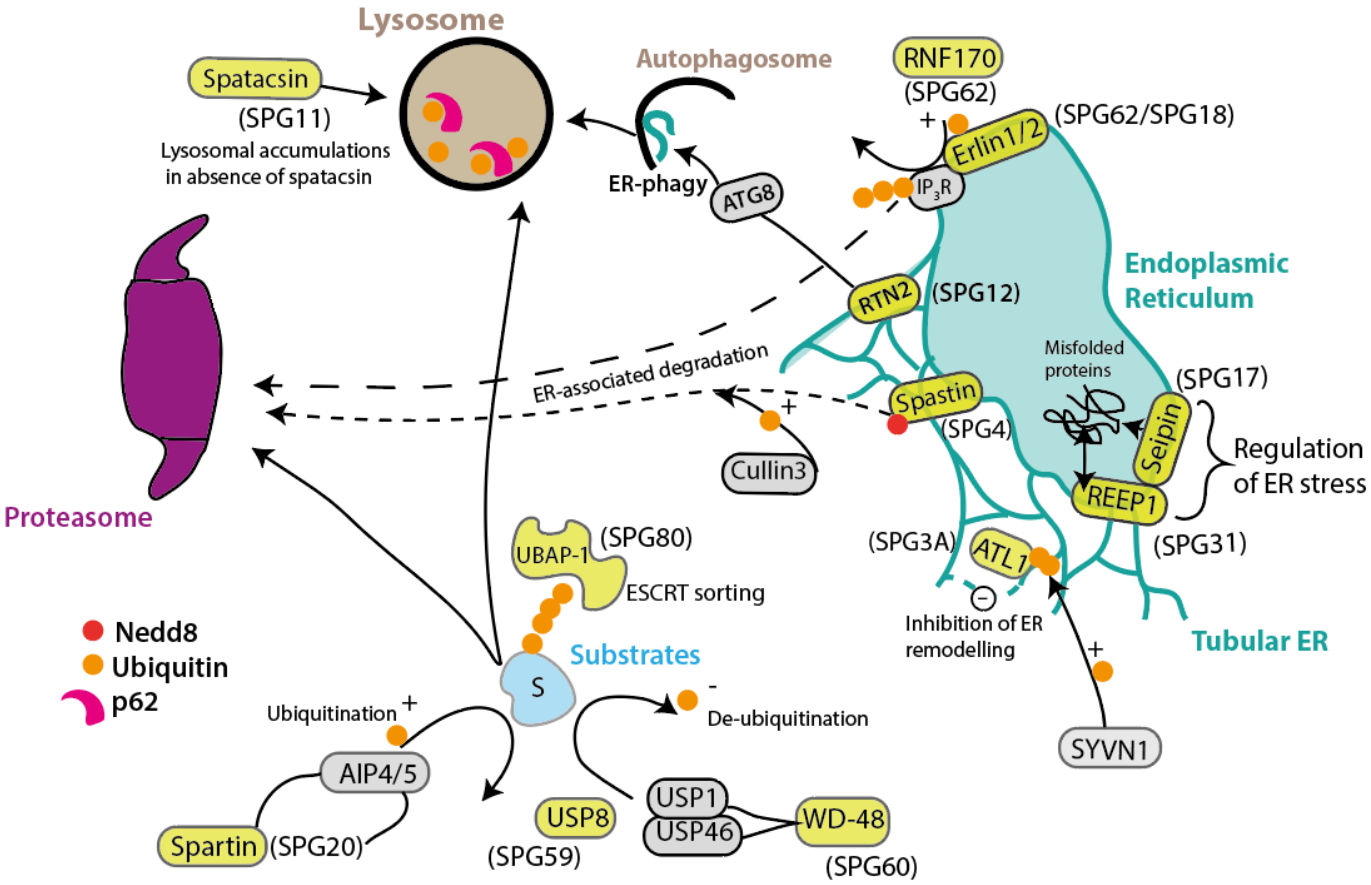

Figure 38: Hereditary Spastic Paraplegias are implicated at multiple levels of the degradative pathways.

V. Objectives of the study

We have seen in the first part of the introduction that HSPs constitute a family of neurodegenerative disorders that do not share only common symptoms but also share common cellular biology defects. SPG11 HSP is mainly characterized at the level of cell biology by lysosomal dysfunctions. Indeed, in absence of spatacsin, lysosomes fail to renew themselves, accumulate lipids such as GM2 and cholesterol and have altered calcium levels.

The endoplasmic reticulum can form membrane contact sites with all organelles of the cell and especially with lysosomes. At ER-Lysosomes interfaces, lipids such as cholesterol are exchanged, calcium is exchanged, and lysosome biogenesis and positioning are regulated. The convergence between these functions identified for ER-Lysosomes contact sites and the defects observed in absence of spatacsin led us to explore the potential implication of spatacsin at ER-Lysosomes contact sites. Moreover, spatacsin shows a diffuse pattern of localization which does not exclude it from being present at ER-lysosomes contacts.

The ER is also deeply involved in regulation of the ubiquitin proteasome pathway and in autophagic degradation of various substrates and even itself, in context of stress or not. In a yeast two hybrid screen performed on spatacsin Cter, the ubiquitin proteasome pathway was identified as playing a role in spatacsin action (see **Results**). But what could be the implication of ubiquitin-dependent proteolysis in spatacsin role at the lysosomes?

My goal in this work was to explore spatacsin molecular role to link its action at the lysosomes to a potential role at ER-Lysosomes contact sites and to ubiquitin-dependent degradation pathway (see **Figure 39**).

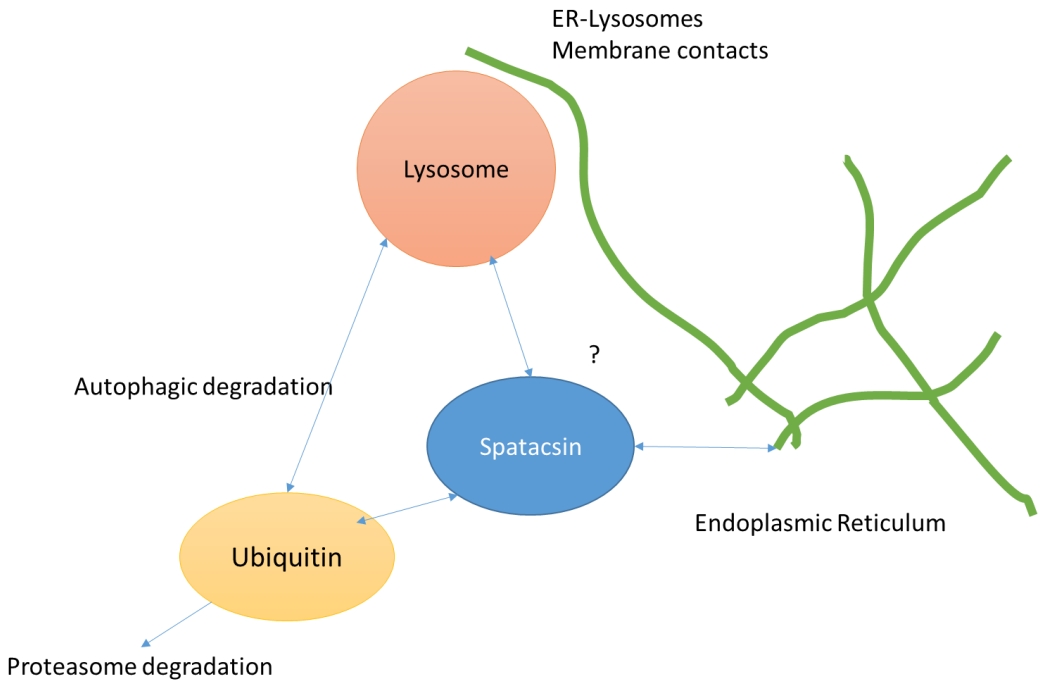

Figure 39: Key concepts of the study implicating spatacsin molecular function.

METHODS: AUTOMATED IMAGE ANALYSIS, STRENGTH & WEAKNESSES

PREAMBLE: *I will mainly discuss in the methods section my approach of image analysis during my PhD. I will detail the tools that I used and developed to perform for example automated tubular lysosome detection and tracking, which have been instrumental to my work.*

I. Principles of image analysis

a) An Image is a matrix

When you acquire an image on a confocal microscope for example, the TIFF file that you get contains much information but the principal one is an array which dimensions correspond to the size of the area you captured under the microscope (here in the example on **Figure 40:** 1027*921 pixels) and each of these pixels contains an information. The value of the pixel corresponds to the local intensity of the signal, and it is a number ranging from 0 to 255 if you are in 8 bits and from 0 to 65535 in you are in 16 bits. Having a broader range of values for your pixels allows you to capture more details in the variations of the signal.

So, you have a 1024*921 matrix that contains values ranging from 0 to 65535. In this example, we want to detect a lysosome. A lysosome corresponds to a group of pixels that have a higher value (here 5 to 20 times) than the background signal, which corresponds to the noise of the image capturing process (**Figure 40**).

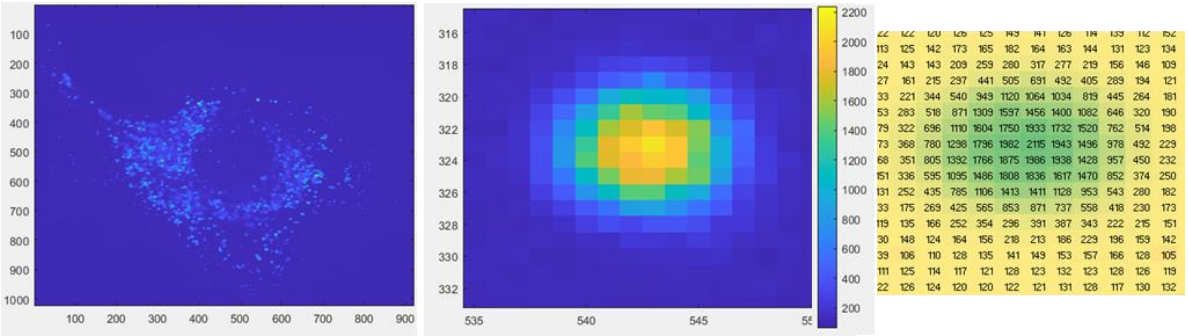

Figure 40. Left : 1024* 921 image of lysosomal staining. **Middle** : Zoom on a lysosome. **Rigth**: The same lysosome represented in an Excel sheet containing the intensity value of each pixel.

If your goal is to detect a lysosome for example, then in “matrix language” it corresponds to detecting a group of pixels that have a higher value than their surroundings. Depending on the quality of the image and the intensity of the signal, the signal to noise ratio will vary, here it is about 10 (background noise is 120, signal is over 1200, see **Figure 40**). Moreover, you can couple that to the notion of size. Indeed, for the lysosome, you know that this kind of particles is about 300 nm to 1 µm wide. Knowing the size of your pixel (here about 120 nm), if you are looking for a lysosome, you know that your group of pixels will be approximately 3 to 10 pixels wide, which corresponds to an area (if we assume it’s a circle) of about 7 pixels to 80 pixels.

b) The MATLAB software & interesting toolboxes

b.1 Binarization of images

To simplify the analysis of an image, one can binarize it. It means that your 1024*921 matrix will no longer contain values that range from 0 to 65535 but only zeros and ones. The operation of going from the original image to the binarized version is totally dependent on what you want to do. In my example of lysosome detection, by observing my image, I saw that background noise intensity is about 120-150 while lysosomal signal seems to start around 800-900. Values of signal and ratio seem sufficiently different for me to hypothesize that “all lysosomal signal is above 800”. This statement is translated in a thresholding operation, where I will artificially equal all values under 800 to zero and all values above to one. Zeros will correspond to background and ones to lysosomes. Or I can do the same thing with a threshold at 400 to capture potentially more lysosomal signal (see **Figure 41**).

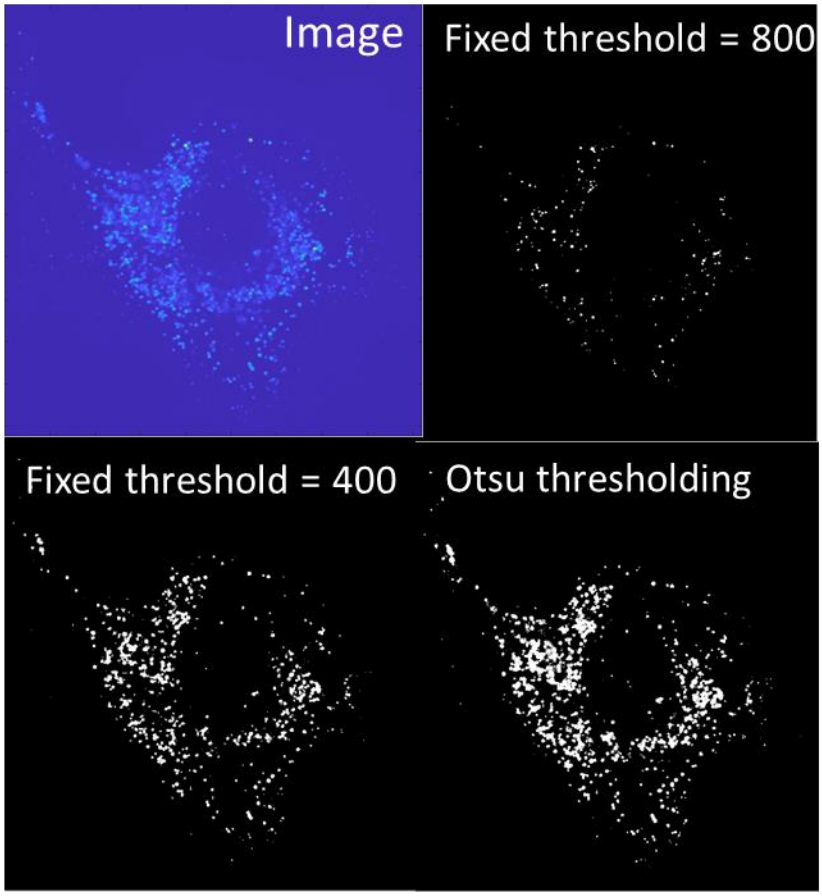

Figure 41. Upper Left : Original image. **Upper right :** Binarized image with a fixed threshold at 800. **Bottom Left :** Binarized image with a threshold at 400. **Bottom right** : Binarized image with a threshold computed by Otsu's method.

In this example, we can see that setting the threshold at 800 is probably too high and does not capture the lysosomal signal. 400 seems to be a better threshold but remains not perfect. This is where we can look into MATLAB library for more complex way to define a threshold.

Many formulas exist to calculate a threshold to distinguish an object from its background (Rogowska, 2009). I tested several thresholds and used two of them, for different applications. For lysosomal detection, I obtained the best results with the Otsu thresholding method (Otsu, 1979). The complex mathematical formulas computing this threshold value are contained in the *multithresh* function in MATLAB ("Multilevel image thresholds using Otsu's method - MATLAB multithresh - MathWorks France," n.d.). In our example, with Otsu's method, the computed threshold is 302, and it captures the lysosomal signal quite well (see **Figure 41**).

Otsu thresholding is quite convenient, and the threshold value is computed for each image very fast by MATLAB, so it proves to be a handy tool. However, if it performs quite well for lysosomes detection where signals are bright and spot-shaped, this is not the case for example if you want to detect an entire cell, which signal is more diffuse and less spot like. For cell detection, such as fibroblasts stained with cell tracker, the Kittler thresholding method gave better results (Kittler and Illingworth, 1986). See **Figure 42** for a comparison of Otsu thresholding method and Kittler for cell detection.

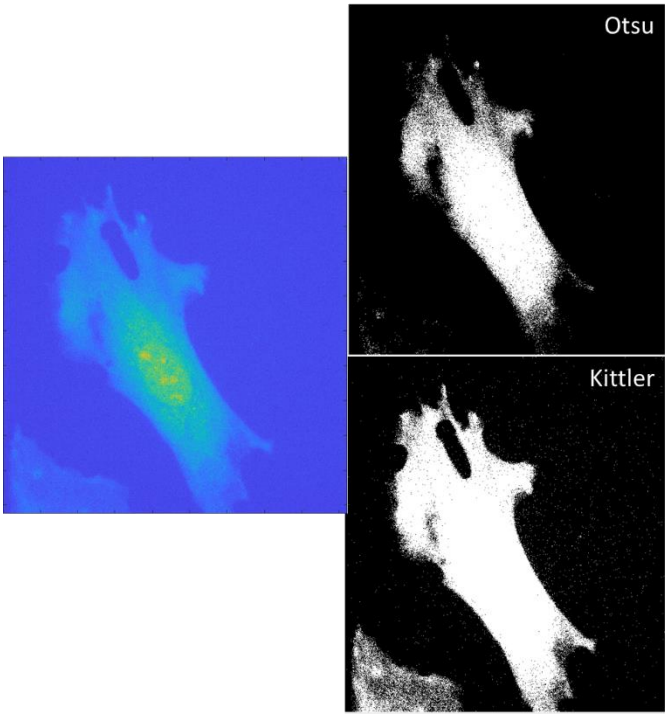

Figure 42: Comparison of Otsu and Kittler thresholding for cell detection.

b.2 Cleaning images & shape analysis

To “improve” the detection of your cell in the previous example and getting rid of the flaws of a weak signal for example, you can “clean” your image. Cleaning an image in this example starts with filling the gaps. Indeed, in the above example (**Figure 42**), you can see that some pixels are isolated. By using the function *imdilate* of MATLAB, every white pixel of the image will be surrounded by other white pixels with a thickness that you decide in the parameters of *imdilate.* Once this is done, remaining holes in the mask of the cell can be filled if they are surrounded by other white pixels using *imfill*. This can however cause artifacts of detection, creating areas that are supposed to be non-cell to be detected as cell (see red circle in **Figure 43**).

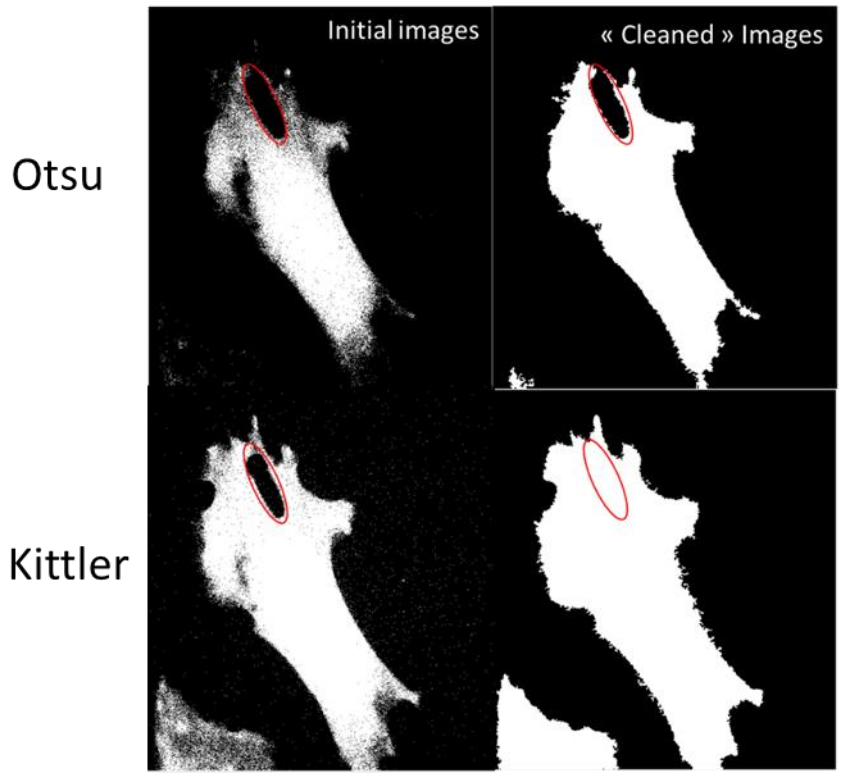

Figure 43: Cleaning cell masks using binary transformation functions and potential artifacts creation. Red circle marks an artifact of cell detection.

One of the functions that I used the most during my analysis of binary images is the function *regionprops*. As written in MATLAB documentation "regionprops returns measurements for the set of properties for each component (object) in the binary image". This function computes various parameters on each individual binary object on the image, for example, for each lysosome, it will calculate its area in pixels, its circularity (whether the object is round or not from 0 to 1), its perimeter and many other features. All this information is stored in tables in MATLAB, and to know which lysosome is which, the table contains the list of pixels of each lysosome, giving an information on what coordinates correspond to each object.

b.3 batch processing of images

One of the main advantages of automated analysis is to gain time, especially if you deal with large data sets. In MATLAB, the strategy I adopted, for example for my siRNA screening effect on lysosomal tubulation (see **Results**), was to store images in individual folders. Each folder contained the different images corresponding to the different fluorescent channels of the acquisition and based on their name a different information was extracted from them. One of the easy things to do is to use the automatic labelling that is implemented in most microscopes, in the example, the image acquired with the first wavelength is labeled “w1” while the second one is labeled “w2”. Using the *regexp* function on MATLAB you can apply a different operation on the image whether they are labeled with “w1” or “w2” (see **Figure 44**).

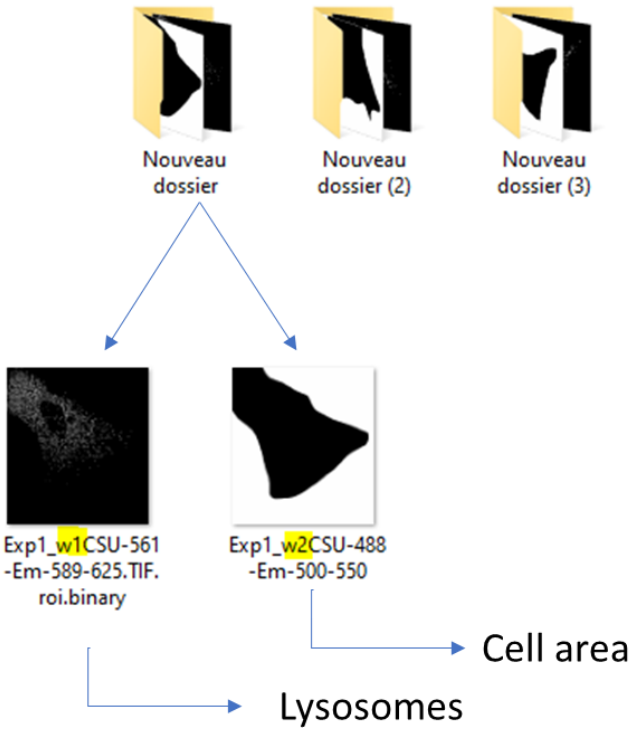

Figure 44: Principles of batch analysis using MATLAB.

If your images and folders are correctly labeled you can program MATLAB to open every folder, find images with the right label, extract information (for example how many lysosomes are present per unit area) and store it in an output table.

c) ICY spot detector

Besides thresholding tools included in MATLAB, I used the ICY spot detector (Olivo-Marin, 2002). For lysosomes detection, I generally used the scale 2 (objects around 3 pixels in size) with a sensitivity of 140. 140 is the maximum sensitivity as I wanted to detect as many particles as possible (see **Figure 45**).

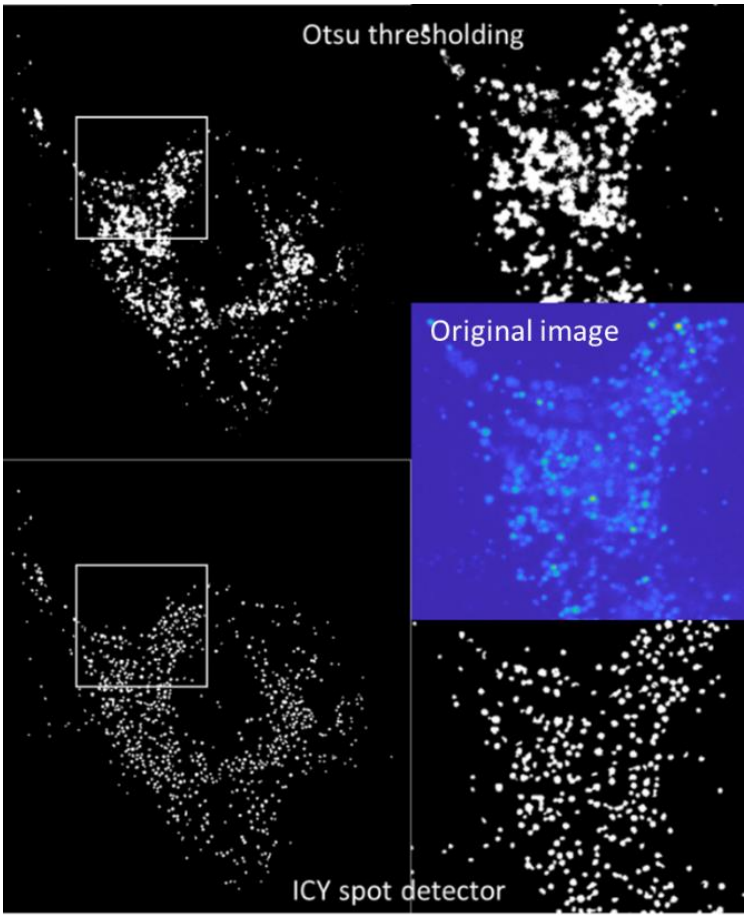

Figure 45: Comparison of lysosomal detection between Otsu thresholding method and ICY spot detector.

ICY spot detector main advantage over Otsu thresholding method is that each detected particle is individualized from the others, which is not the case with Otsu. Indeed, close lysosomes are often detected as one particle which can mislead the analysis depending on what feature you want to extract. For example, if you want to know what area is covered by the lysosomal staining, then Otsu is the better method because it captures more of the lysosomal staining, but if you want to count particles, or extract their individual properties, identify their precise localization, then ICY spot detector gives better results (see **Figure 45**).

II. Applications

a) Tubular lysosomes detection

Using the *regionprops* function, I defined by trial & error the shape of a tubular lysosome using 3 parameters. A tubular lysosome should have a circularity under 0.5 (0 is the opposite of a circle, 1 is a perfect circle), it should have an eccentricity above 0.9 (1 is a perfect straight line) and its long dimension should be at least 4 times higher than the small one. This method is quite efficient for tubular lysosome detection (see **Figure 47**).

To refine my detection of tubular lysosomes, I tried an approach to discriminate between round and tubular particles that was not fixed by an empirical decision of which parameters were relevant. I used the "Classification learner" application of MATLAB to define a mathematical model for tubular lysosome detection. To do this, I constituted a training set for my model that consisted of 12 variables (area, perimeter, eccentricity etc.) defining the shape of particles, these 12 variables were extracted by *regionprops* function.

And I labeled by hand the class of each object to accompany the 12 variables (x_1,…,x_{12}), class 1 is tubular lysosome and class 2 is round lysosome.

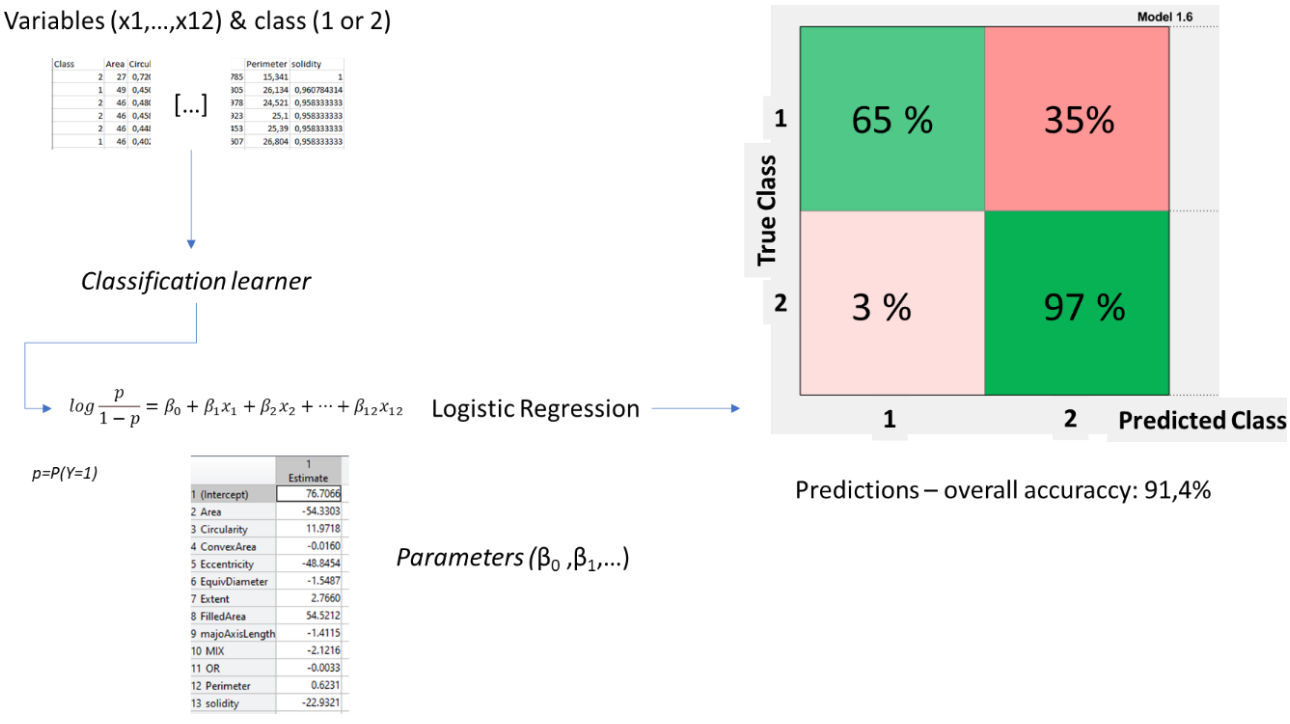

Figure 46: The classification learner application for tubular lysosome detection.

The data set was implemented in the Classification Learner interface, I had a table containing 2431 values, 401 tubular lysosomes and 2030 round lysosomes. With this table, the application tested different models and opted for a logistic regression model that gave the best accuracy results. A set of parameters *(*β_0, β_1,…) predicting the role of each variable in discriminating between round and tubular was determined (see **Figure 36**).

The overall accuracy of this model is 91.4%, meaning that once the parameters were fixed on the training set, 9 times out of 10 the particle was labeled in the correct class (tubular or round) based on the model parameters. However, if we take a closer look to the confusion matrix (see **Figure 46**), we can see that a class 2 object (a round lysosome) is classified as round 97% of time but a class 1 object (tubular) is correctly classified only 65% of times. This means that round particles are almost never mistaken as tubular but a third of tubular particles are mistaken as round. This model has an almost 0 "false positive" detecting rate but a very high "false negative" rate. Strikingly, this model detects more tubular lysosomes than the one with the fixed parameters (see **Figure 47**), showing how difficult it can be to discriminate between round and tubular lysosomes.

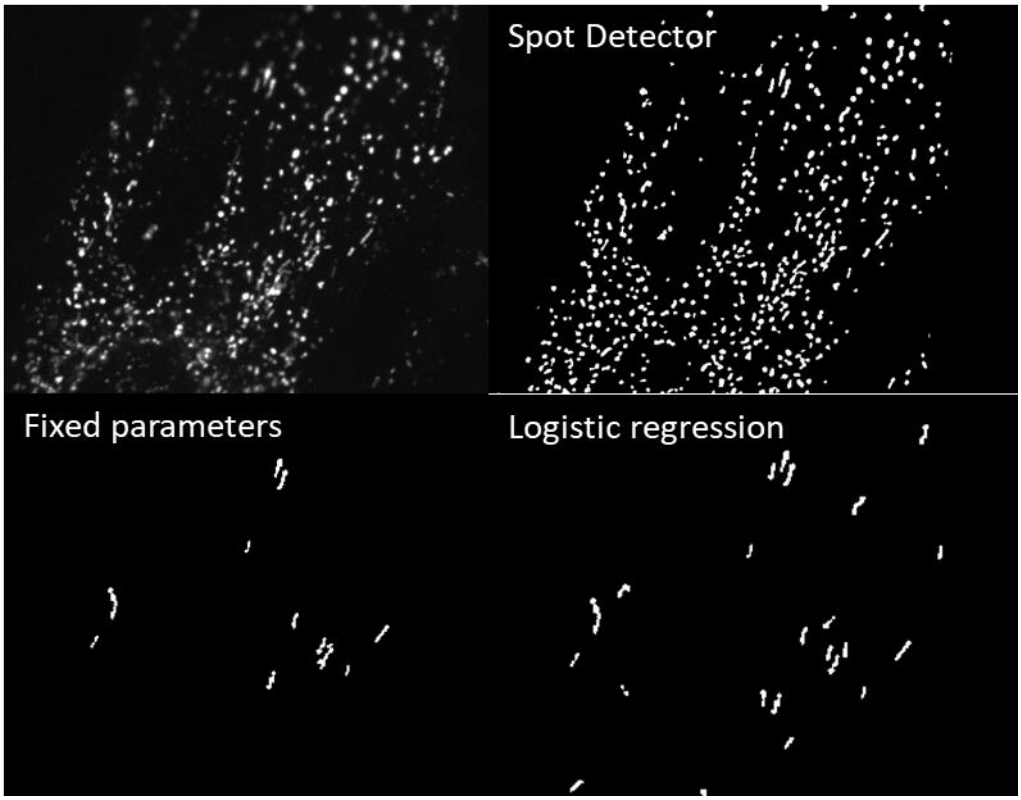

Figure 47: Comparison of different methods for tubular lysosome detection.

In the mouse embryonic fibroblast model of the lab, we know that there are less tubular lysosomes in absence of spatacsin (Boutry et al., 2019) (see **Results**). Let's compare the results obtained for tubular lysosome detection on the same cells, one Wild-Type (WT) condition and one Knocked-Out (KO) for SPG11 condition, with 3 methods: the" Fixed Parameters" method, the "Logistic regression" method and a labelling "By Hand" performed by me on images using ImageJ multipoint tool.

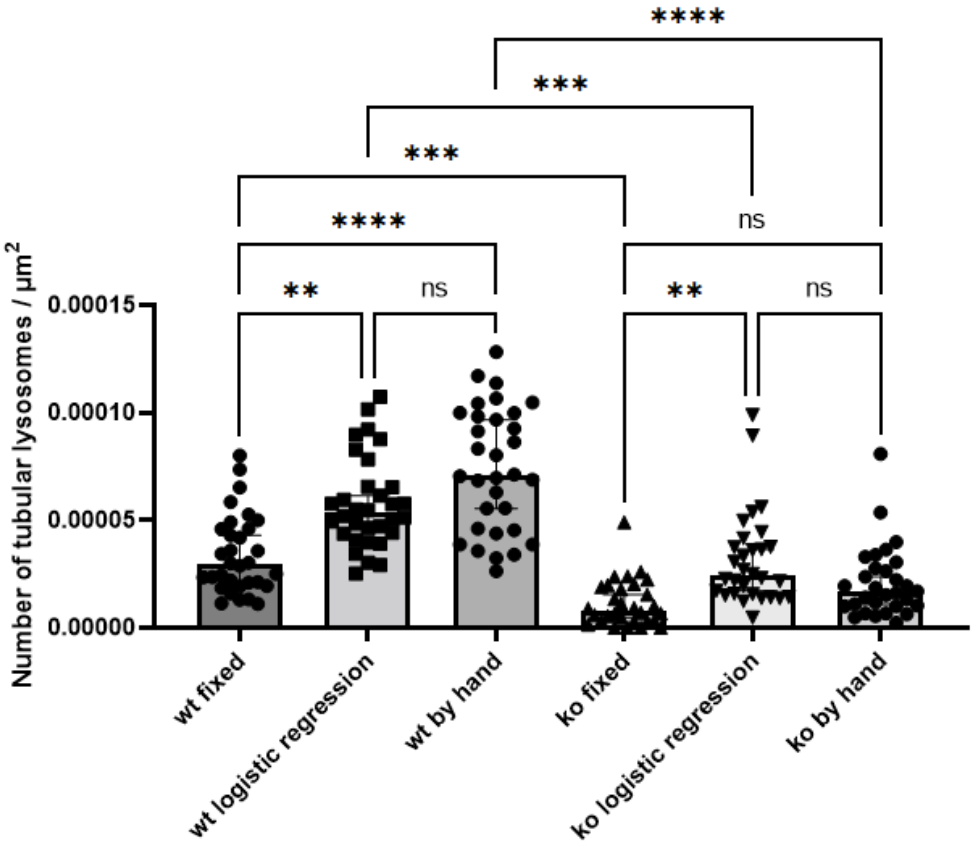

Figure 48: Comparison of tubular lysosome detection methods

We see on **Figure 48** that the automated methods missed indeed part of the tubular lysosomes compared to the "manual" one, but importantly, in all methods, the difference between WT and KO cells remained significative. This is an indicator that automated methods, although imperfect, still capture the difference in the studied parameter, and the time that is gained by the automation (a few minutes for an entire data set versus a few minutes for each cell) justifies the use of automated detection of tubular lysosomes.

The MATLAB code used for this application can be found in **Annex 2- a) .**

b) Tubular lysosomes tracking

The tracking of tubular lysosomes is built on top of the tubular lysosome detection algorithm. Indeed, to track the movement of lysosomes, it is important to detect them properly first. For particle tracking, the lysosomes are detected on the multiple images that compose the timelapse video creating a sequence of binary images containing tubular lysosomes. Then the coordinates of their centroids (identified by *regionprops)* associated with the number of the frame they are in, are exported in a table.

This table is analyzed by the *track* function that was originally written by John C. Crocker in 1998 and has been updated since (DeConinck, 2014). The *track* function will link the different centroids to form trajectories, given a maximum displacement distance between two frames that I set at the mean size of a tubular lysosome which is 2.4 µm (see **Figure 49**). The *track* function then outputs another table that contains only trajectories longer than 3 frames, with the associated coordinates of the centroids sorted in a frame-dependent order.

Then the displacement per particle was measured using Pythagoras Theorem on the coordinates of centroids (see **Figure 49**). The mean speed of particles during trajectories was obtained by the ratio of the displacement on the duration of the trajectory. The *track* function cannot compute trajectories on data sets that contain several hundreds of particles per frame, it is limited to under 100 particles, which is perfect to analyze tubular lysosome trajectories but could not be used to analyze the general movement of all lysosomes in the cell.

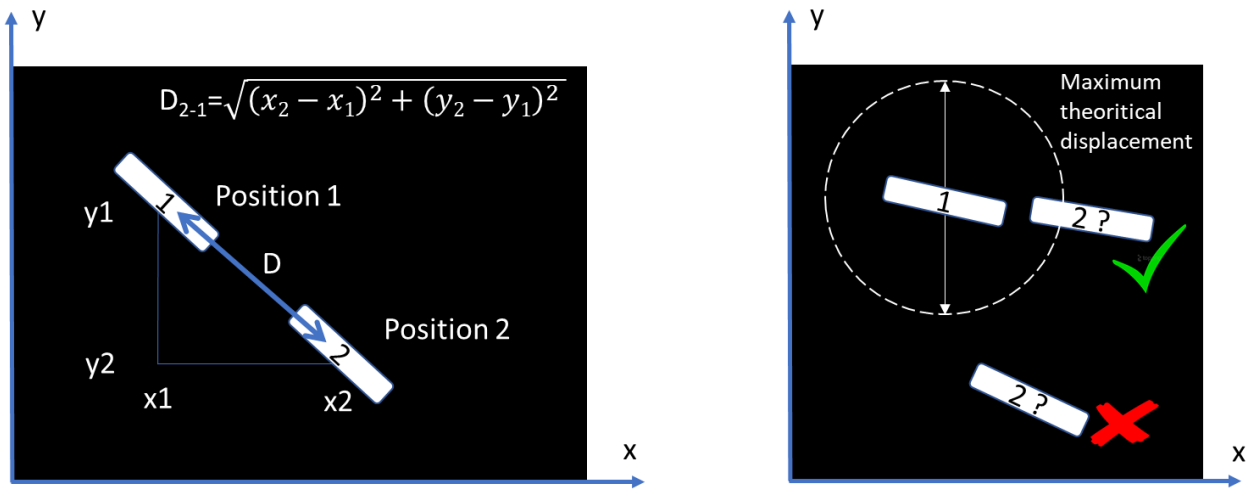

Figure 49. Left: Measuring displacement between two frames principle**. Right: M**aximum displacement between two frames for tubular lysosome detection.

I compared the results I obtained using this automated tracking method with a more manual method. I obtained the coordinates of the centroids of the tubular lysosomes using the multi-point tool of ImageJ and exported this information in a table that I analyzed similarly in MATLAB based on Pythagoras to obtain duration, mean speed and length of the trajectory.

What is striking when you compare the results obtained by the two methods is that the trajectory captured by the automated method are much shorter in duration (see **Figure 50**). You follow the trajectory of the lysosome for mean duration of 5-10 seconds with the automated detection while, by hand you can follow them for the whole 60 seconds of the timelapse video. This is explained by the fact that as we saw in the previous part, the detection of tubular lysosome is not perfect, and sometimes the tubular particle is not detected by the algorithm, creating a gap of information in the trajectory. Therefore, the automated method captures only fragments of lysosomal trajectories and not the complete sequence.

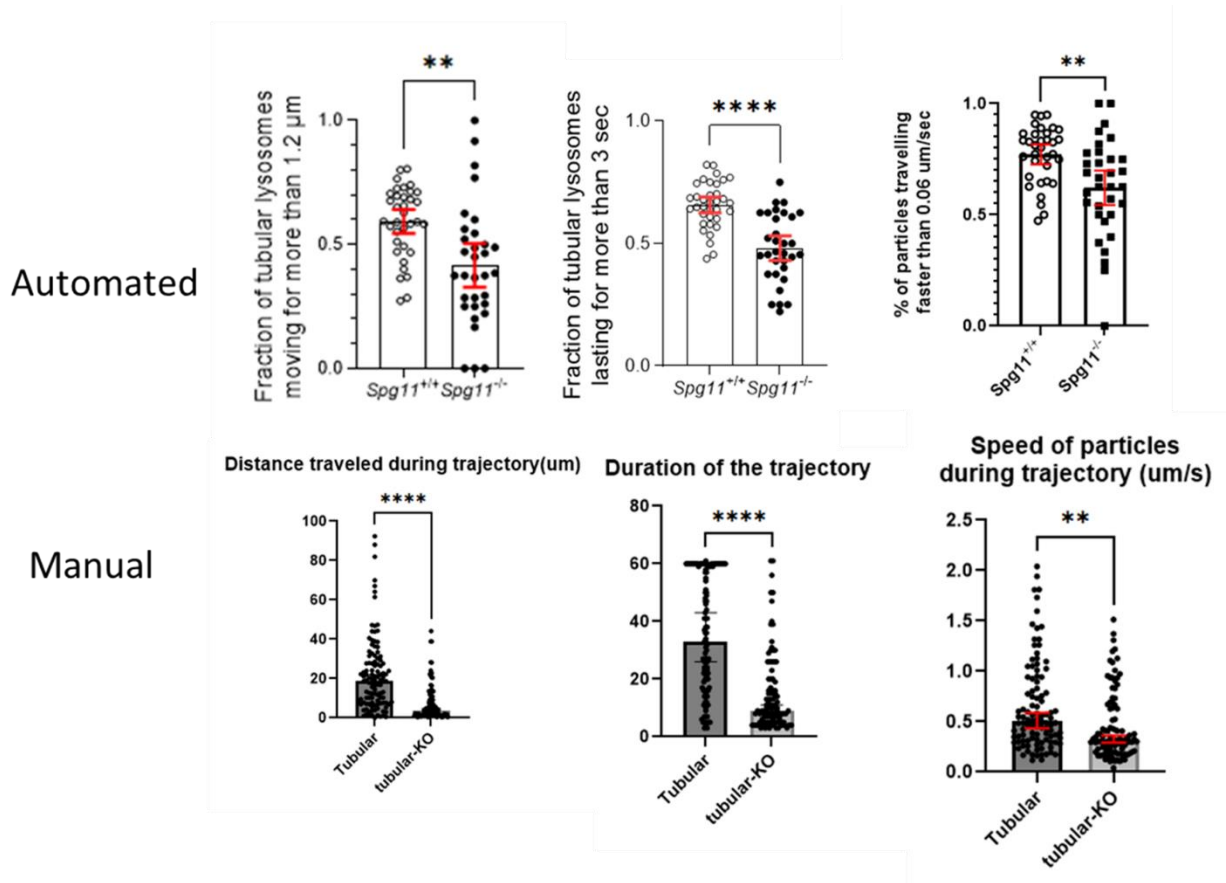

Figure 50: Comparison of tubular lysosome movement by hand or using automated tracking of particles.

However, as this detection is way faster (it takes hours to analyze the trajectories of a single cell by hand and a few minutes for an entire batch of cells by MATLAB), the data sets obtained with the automated detection method are extremely large, containing thousands of fragments of trajectories. Therefore, the data is not considered in terms of median or mean for the results obtained by the automated method but rather is proportion of particles per analyzed cell that are above a cut-off value. This also avoids the risk of having a single cell that contains many trajectories to excessively weight on the results. And the fact that we consider only fragments of trajectories explains why the values of displacement and duration are so much smaller than the one obtained with the manual methods on complete trajectories. The value obtained for the speed are however quite similar (see **Figure 50**).

Most importantly, with both methods, we measured an impairment of the displacement length, duration, and speed of tubular lysosomes in absence of spatacsin (see **Figure 50**), indicating that the automated tracking of lysosomal trajectories is suitable for our analysis.

The MATLAB code used for this application can be found in **Annex 2- b).**

c) Other applications using MATLAB

c.1 Area overlap between masks

I used this method to measure the overlapping area between the Endoplasmic Reticulum and the lysosomes. Considering the resolution limit, the overlap between the ER and the Lysosomes does not reflect a fusion of the two compartments but rather a spatial proximity.

To measure the overlap between the compartments, they must be binarized first. The ER was binarized by hand using the thresholding tool of ImageJ, all other methods failed to deliver consistent satisfactory results. The lysosomes were binarized using ICY spot detector because the goal was to measure in % the overlapping area with the ER compared to the area of each particles as not all particles are the same size (see **Figure 51**).

To determine the area of the overlap between the two compartments, every pixel that constitutes the ER mask (=1 in the binary image) is stored in a table, and this information is used to select pixels that have the exact same position in the lysosomal mask, whether they are equal to 1 or 0. This creates a third binary image that contains the intersection of the two masks and the area of each intersection is extracted using *regionprops* (see **Figure 51**).

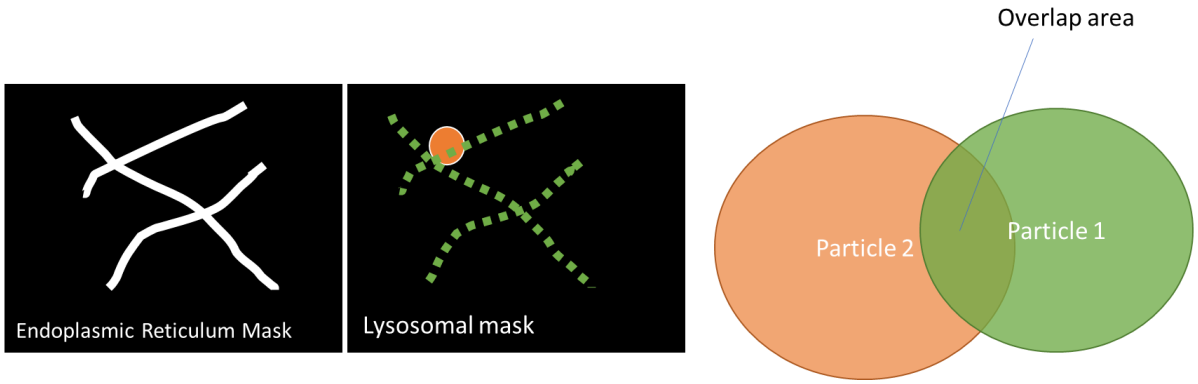

Figure 51: Illustration of the principle of area overlap.

The MATLAB code used for this application can be found in **Annex 2- c) .**

c.2 Clustering of particles around the nucleus

This analysis method was not written by me but by Raphaël Matusiak, a former engineer of the team, I only brought minor modifications to it.

The principle is to detect the centroids of all lysosomes using either *regionprops* on an image that has been binarized by ICY Spot detector or to use the *pkfnd* (peak find) function on the original grayscale image of the lysosomes. Then the distance between the centroid of each particle and the centroid of the nucleus of the cell is measured. Finally, these distances are expressed as a fraction of the maximum distance obtained between the farthest away lysosome and the nucleus (see **Figure 52**).

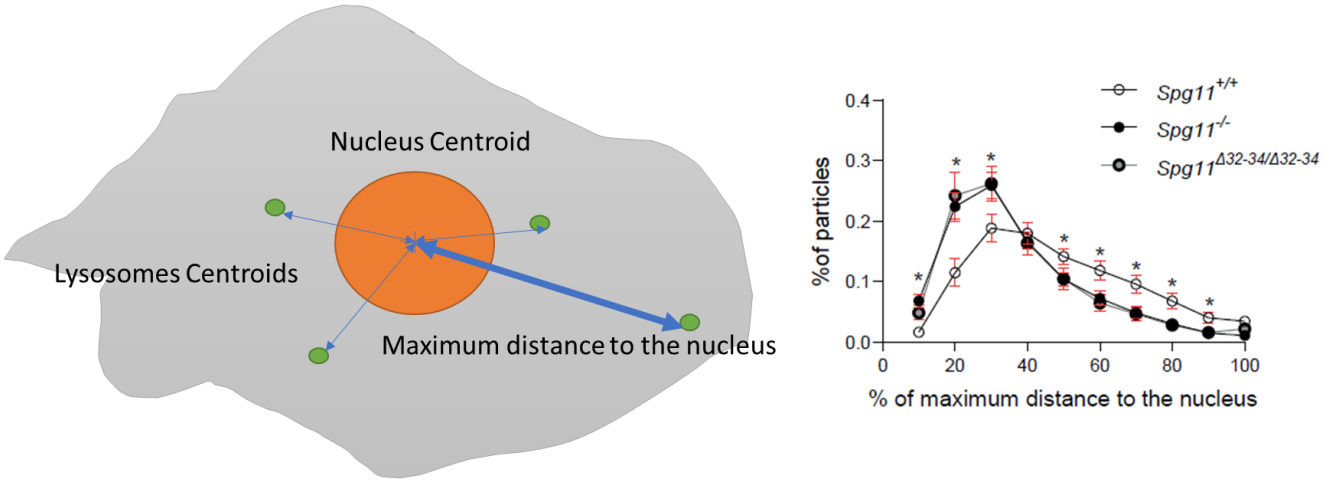

Figure 52: Measurement of particle clustering around the nucleus.

The MATLAB code used for this application can be found in **Annex 2-d) .**

c.3 Fluorescence ratio of a signal in compartments

To determine what is the proportion of fluorescent cholesterol that is contained in the lysosomes for example (Boutry et al., 2019), the fluorescence in the lysosomes needs to be compared to the total fluorescence of the cell. This can be done by hand using ImageJ, but automation of the process is also possible.

Based on what we have seen before, we can process our data set in batch with folders containing 3 images, each of them with a recognizable label. The first image is the cell stained by cell tracker that will be binarized with Kittler threshold to extract the cell mask. The second image is the lysosomal staining that will be binarized using Otsu threshold to extract the lysosomal mask. Using a conditional selection, we can extract the lysosomal mask that is contained in an individual cell. Then the fluorescence intensity in the third image is measured inside the cell mask on one side and in the lysosomal mask on the other side (see **Figure 53**).

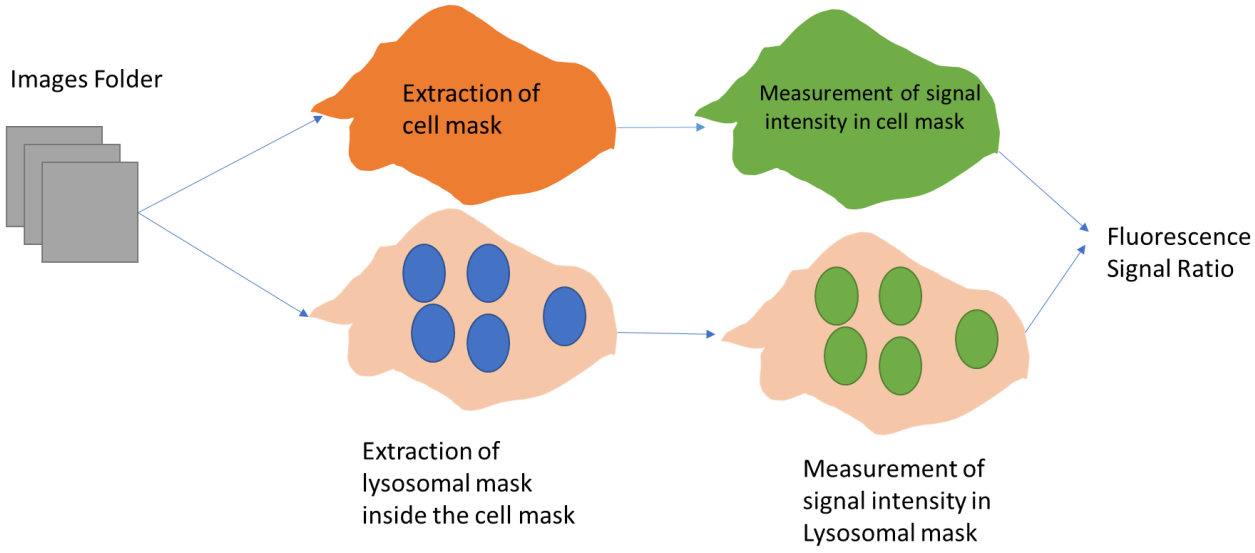

Figure 53: Principle of lysosomal ratio measurement using masks.

The noise of the fluorescence signal is measured as the signal that is outside of the cell mask after removing twice the eventual bright spots with Otsu thresholding.

Areas of both masks are extracted using *regionprops* and the formula of the fluorescence ratio is:

$$Ratio = \frac{(Lyso\ fluo - noise) * Lyso\ Area}{(Cell\ fluo - noise\ ) * Cell\ Area}$$

The MATLAB code used for this application can be found in **Annex 2-e).**

RESULTS

PREAMBLE: During my PhD, I had the opportunity to work on two papers that were submitted for publication. The first one from 2019 can be found in Annex 2 as it was part of Maxime's Boutry PhD thesis work, and I was only the second author on it.

The second paper however, that was recently submitted, summarizes the results that I obtained during my PhD thesis. I wrote the paper with Frédéric and performed most of the analyses and experiments with him. Raphaël performed the Neural Network analysis & wrote the first version of the particle clustering algorithm. Margaux took care of our mice models. Julien was involved in the characterization of the truncated spatacsin mouse model. Maxime was involved in the characterization of the lysosomal phenotype in fibroblasts in absence of spatacsin.

Article 1: Endoplasmic reticulum shape regulates lysosome motility in a ubiquitin and spatacsin-dependent manner (submitted)

Alexandre Pierga[1-4], Raphaël Matusiak[1-4], Margaux Cauhapé[1-4], Julien Branchu[1-4], Maxime Boutry[1-4], and Frédéric Darios[1-4].

1 : Sorbonne Université, F-75013, Paris, France

2 : Paris Brain Institute, ICM, F-75013, Paris, France

3 : Inserm, U1127, F-75013, Paris, France

4 : CNRS, UMR 7225, F-75013, Paris, France

Abstract

The endoplasmic reticulum (ER) forms contacts with the lysosomal compartment, regulating lysosome positioning and dynamics. However, the mechanisms regulating the formation and function of such contacts are unknown. Here, we demonstrate that spatacsin is an ER-resident protein that regulates lysosome motility, shown by the presence of tubular lysosomes. Screening for spatacsin partners required for this function showed spatacsin to act in a ubiquitin-dependent manner. spatacsin promotes the degradation of its partner AP5Z1. This in turn facilitates the interaction of spatacsin with spastizin, which allows recruitment of KIF13A to the lysosomal compartment, regulating lysosomal dynamics. Importantly, the interaction of spatacsin with spastizin occurred at contact sites between the ER and lysosomes, and tubular lysosomes, which were highly dynamic, were entangled in a network of tubular ER. Alteration of the ER network morphology impaired the interaction of spatacsin with its partners and resulted in aberrant lysosomal dynamics, showing that the ER promotes lysosome movement by its action at contact sites. Our work thus demonstrates that the integrity of the ER network is required to promote lysosome motility and spatacsin contributes to the regulation of this phenomenon in a ubiquitin-dependent manner.

Introduction

Lysosomes are membrane-limited organelles responsible for the degradation of various cellular substrates. They degrade the content of late endosomes and autophagosomes upon fusion with these subcellular compartments. In addition, they also participate in many other cellular functions, such as cell metabolism and the repair of plasma membranes, as well as adhesion and migration(Ballabio and Bonifacino, 2020). These diverse functions rely on the cellular localization of lysosomes, as well as their motility and remodeling(Hipolito et al., 2018; Pu et al., 2016). Accordingly, lysosomes are a highly dynamic subcellular compartment(Bonifacino and Neefjes, 2017). They are retrogradely transported along microtubules upon coupling to cytoplasmic dynein and move anterogradely toward the cell periphery upon coupling to various kinesins(Ballabio and Bonifacino, 2020), changing their cellular distribution. Their shape is also dynamically controlled depending on cellular needs. For example, they form a tubular network following phagocyte activation in macrophages(Hipolito et al., 2018) or tubules emanating from autolysosomes are observed during autophagy lysosome reformation (ALR) to terminate autophagy(Yu et al., 2010). Such changes in shape likely rely on the cytoskeleton and molecular motors(Boes et al., 2002; Du et al., 2016) but it is not known whether all tubular lysosomes formed in response to various cellular stimuli are equivalent.

It has recently emerged that endosomes and lysosomes not only interact with the cytoskeleton but also form functional contacts with other subcellular organelles the endoplasmic reticulum (ER). Such contacts with the ER are involved in the filling of lysosomes with Ca^{2+} or the non-vesicular transfer of lipids between the two subcellular compartments(Wang et al., 2017; Wilhelm et al., 2017b). The interactions of the ER with endosomes and lysosomes also regulate the morphology and trafficking of these subcellular compartments. For example, the interaction of endosomes and lysosomes with the ER control ER architecture by modulating the formation of the ER network at the cell periphery(Spits et al., 2021b). Conversely, the ER mediates the distribution and trafficking of endolysosomes through various mechanisms involving the proteins RNF26, protrudin, and ORP1L(Jongsma et al., 2016b; Raiborg et al., 2015b; Rocha et al., 2009b) or it can regulate the morphology of endolysosomes by promoting their fission(Allison et al., 2017b; Rowland et al., 2014b). Furthermore, the morphology of the ER regulates the trafficking of lysosomes in axons(Özkan et al., 2021). However, the control of endolysosomal dynamics is still only partially understood(Cabukusta and Neefjes, 2018b) and the molecular mechanisms linking ER morphology and lysosome function have not been elucidated.

Lysosome function is impaired in various pathological conditions, such as, for example, in neurodegenerative diseases(Oyarzún et al., 2019). Among them is hereditary spastic paraplegia type SPG11, which is due to loss-of-function mutations in the *SPG11* gene, leading to the absence of spatacsin(Stevanin et al., 2007b). The subcellular localization of spatacsin is still debated, as it has been proposed to be localized in the ER, microtubules, or lysosomes(Hirst et al., 2013a; Murmu et al., 2011b).

However, the loss of spatacsin function has been shown to impair lysosome distribution and ALR(Boutry et al., 2019b; Chang et al., 2014b), suggesting a lysosomal function for this protein. spatacsin bears a spatacsin_C domain in its C-terminus, which has been conserved throughout evolution up to plants(Alexander L Patto and O'Kane, 2020). However, this domain has no homology in the human genome, suggesting a specific function. spatacsin interacts with spastizin and AP5Z1, two proteins encoded by genes mutated in other forms of hereditary spastic paraplegia, SPG15 and SPG48, respectively(Hanein et al., 2008b; Słabicki et al., 2010b, p. 48). spastizin contains a FYVE domain, which binds to phosphatidylinositol-3-phosphate, allowing its recruitment to lysosomes(Hirst et al., 2021b). AP5Z1 is a subunit of the adaptor protein complex AP5, involved in the sorting of proteins in late endosomes(Hirst et al., 2018b). Loss-of-function mutations in *SPG11*, *SPG15*, or *SPG48* lead to the lysosomal accumulation of material(Branchu et al., 2017; Khundadze et al., 2019b, 2013b; Varga et al., 2015). However, it is not known how the absence of these proteins leads to lysosomal dysfunction and the mechanisms that regulate the interactions between these proteins have not been investigated.

Here, we show that spatacsin is an ER protein that regulates the shape and motility of lysosomes in a ubiquitin-dependent manner. We show that spatacsin-mediated degradation of AP5Z1 facilitates its interaction with spastizin, allowing the recruitment of spastizin to lysosomes. spastizin in turn recruits the motor protein KIF13A, which regulates the motility of lysosomes. We also demonstrate that this regulatory pathway is impaired when the morphology of the ER is modified by blocking the homotypic fusion of ER tubules. Overall, our data show that ER morphology can control lysosomal dynamics in a spatacsin- and ubiquitin-dependent manner.

Results

1. spatacsin is an endoplasmic reticulum-associated protein

We investigated the subcellular localization of spatacsin by transfecting mouse embryonic fibroblasts (MEFs) with a vector allowing the expression of spatacsin with a C-terminal V5 tag and determined its localization by immunostaining and confocal imaging. spatacsin-V5 showed a diffuse distribution that poorly colocalized with late endosomes and lysosomes stained with Lamp1. By contrast, spatacsin-V5 partially colocalized with the ER labelled by the expression of GFP-Sec61β (Fig 1A). V5-tagged spatacsin appeared to be mainly associated with the ER by STED imaging (Fig 1B).

We confirmed the subcellular localization of endogenous spatacsin by fractionating *Spg11*$^{+/+}$ and *Spg11*$^{-/-}$ mouse brains by differential centrifugation (Fig. 1C). spatacsin, encoded by *Spg11*, was present in all but the S3 fraction, which corresponds to soluble proteins of the cytosol. spatacsin, along with the ER transmembrane Ca^{2+} sensor STIM1 and ER chaperone GRP78, was enriched in the microsomal P3 fraction, whereas the lysosomal peptidase cathepsin D and outer mitochondrial membrane channel VDAC were enriched in the P2 fraction (Fig 1C). We then prepared lysosome and ER enriched fractions from *Spg11*$^{+/+}$ and *Spg11*$^{-/-}$ mouse brains using density gradients to complete the analysis. We detected very low levels of spatacsin in the lysosomal fraction, but the signal was stronger in the ER fraction, indicating that endogenous spatacsin is enriched in the ER (Fig. 1D).

spatacsin has been proposed to contain transmembrane regions(Stevanin et al., 2007b), which could allow its tight association with membranes. We tested this hypothesis by subjecting membrane fractions obtained from the brains of *Spg11*$^{+/+}$ and *Spg11*$^{-/-}$ mice to various extraction conditions (i.e., high salt, low pH, high pH, and detergents)(Zhu et al., 2003). spatacsin and the integral ER-membrane protein STIM1 were not released from the membranes by high salt concentration or low or high pH buffer but were solubilized by the detergent deoxycholate (Fig. 1E). Conversely, the membrane-associated protein calreticulin was released from the membranes by high salt, as well as high and low pH buffers (Fig. 1E). Overall, our data show that spatacsin is likely associated with the ER membrane by transmembrane domains(Stevanin et al., 2007b).

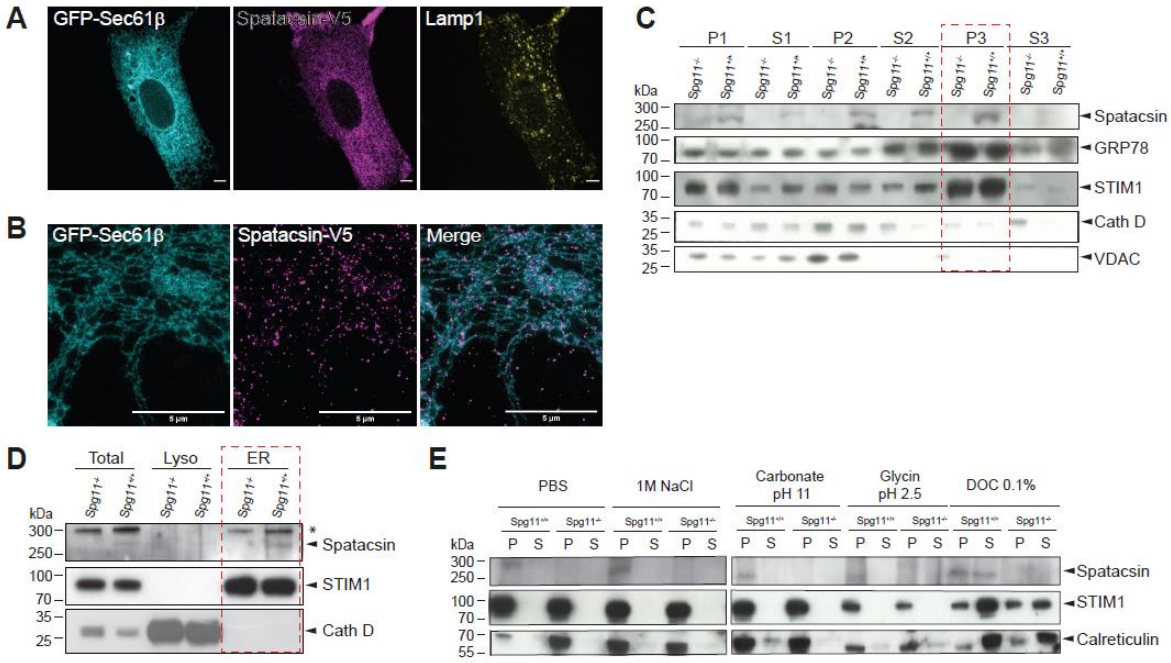

Figure 1. spatacsin is an endoplasmic reticulum protein.

A. MEFs expressing the ER marker GFP-Sec61β and V5-tagged spatacsin. Cells were immunostained with anti-V5 antibody and the lysosome marker Lamp1. Scale bar: 5 µm.

B. STED images of MEFs expressing the ER marker GFP-Sec61β and expressing V5-tagged spatacsin. Cells were immunostained with anti-V5 and anti-GFP antibodies. Scale bar: 5 µm

C. Western blot analysis of subcellular fractions prepared from Spg11$^{+/+}$ and Spg11$^{-/-}$ mouse brains by differential centrifugation. Proteins of each fraction were immunoblotted with antibodies raised against spatacsin, ER proteins STIM1 and GRP78, lysosomal protein cathepsin D (Cath D), and mitochondrial protein VDAC. Note that spatacsin was enriched in fraction P3 (highlighted in the red rectangle).

D. Western blot analysis of ER- and lysosome-enriched fractions obtained from Spg11$^{+/+}$ and Spg11$^{-/-}$ mouse brains. Immunoblots with antibodies raised against spatacsin, ER protein STIM1, and lysosomal protein cathepsin D. ER fractions are encircled by the red rectangle. The asterisk indicates nonspecific signals.

***E.** Membrane association of spatacsin. P3 fractions of Spg11$^{+/+}$ and Spg11$^{-/-}$ mouse brains were resuspended in the indicated buffers or detergents and re-fractionated into the supernatant (S) and membrane pellet (P). spatacsin was released from membranes solely with the detergent deoxycholate (DOC), like the transmembrane protein Stim1.*

2. spatacsin regulates the morphology and motility of lysosomes

The loss of spatacsin function has been shown to affect lysosome function(Boutry et al., 2019b, 2018; Branchu et al., 2017; Chang et al., 2014b; Varga et al., 2015). We transfected *Spg11*$^{+/+}$ and *Spg11*$^{-/-}$ MEFs with vectors expressing GFP-Sec61β, to label the ER, and Lamp1-mCherry, a marker of late endosomes and lysosomes (henceforth referred to as lysosomes). The absence of spatacsin had no visible impact on the morphology of the ER, as observed by live confocal imaging (Supplementary Fig. 1A). By contrast, the distribution and morphology of lysosomes was altered in *Spg11*$^{-/-}$ compared to *Spg11*$^{+/+}$ MEFs. In the absence of spatacsin, lysosomes were clustered around the nucleus (Fig. 2C, Suppl. Fig. 1B), as previously observed(Boutry et al., 2019b). Furthermore, we observed a higher number of tubular lysosomes in *Spg11*$^{+/+}$ than *Spg11*$^{-/-}$ cells (Fig. 2C-D). We also observed a higher number of tubular lysosomes in *Spg11*$^{+/+}$ than *Spg11*$^{-/-}$ fibroblasts when they were labelled with the acidic marker Lysotracker, with a pulse of Dextran-Texas Red followed by a long chase, or with DQ-BSA, which fluoresces upon degradation by lysosomal hydrolases(Marwaha and Sharma, 2017) (Supplementary Fig. 1C-D). These results suggests that tubular lysosomes represent a population of catalytically active lysosomes.

Furthermore, tracking individual lysosomes in wildtype MEFs by live imaging showed tubular lysosomes to move, on average, faster than round lysosomes (Fig. 2E). The proportion of lysosomes with a speed > 0.3 µm/sec, corresponding to microtubule-dependent movement for these organelles(Cordonnier et al., 2001), was higher among the tubular than round lysosomes (Fig. 2F), suggesting that tubular lysosomes are highly mobile and dynamic. Comparison of the speed of lysosomes in *Spg11*$^{+/+}$ and *Spg11*$^{-/-}$ MEFs showed that tubular lysosomes move faster in *Spg11*$^{+/+}$ than *Spg11*$^{-/-}$ MEFs, whereas the dynamics of round lysosomes was not affected (Fig. 2G-H). The difference in the dynamics of tubular lysosomes was validated by automated tracking, which showed tubular lysosomes to travel a longer distance in 1 min and to be longer lived in *Spg11*$^{+/+}$ than *Spg11*$^{-/-}$ MEFs (Fig. 2I-K, Supplementary Videos 1-2). We used this this method to analyze lysosomal dynamics in subsequent experiments. Overall, these data suggest that tubular lysosomes labelled in MEFs are catalytically active and highly dynamic and that spatacsin is important for the control of their formation and motility.

We then used MEFs derived from a mouse line in which exons 32 to 34 of *Spg11* are spliced out (Suppl. Fig. 2A-C) to elucidate the molecular mechanisms by which spatacsin controls these lysosomal phenotypes. Such splicing retained the reading frame and led to the expression of a protein called spatacsin$^{\Delta 32\text{-}34}$, which lacks a domain of 170 amino acids, partially deleting the conserved spatacsin_C domain (Fig. 2A, Suppl. Fig. 2A-C). Western blot analysis of brains obtained from *Spg11*$^{+/+}$, Spg*11*$^{-/-}$, and *Spg11*$^{\Delta 32\text{-}34/\Delta 32\text{-}34}$ mice showed the latter strain to express a spatacsin protein that is slightly smaller than the wildtype protein (Fig. 2B).

Overexpression of spatacsin $^{\Delta 32\text{-}34}$ with a C-terminal V5 tag in MEFs showed diffuse and ER-associated localization like that of full-length spatacsin (Supplementary Fig. 2D). Like *Spg11*$^{-/-}$ MEFS, *Spg11*$^{\Delta 32\text{-}34/\ \Delta 32\text{-}34}$ fibroblasts showed clustering of lysosomes around the nucleus and fewer tubular

lysosomes than wildtype cells (Fig. 2C-D, Suppl. Fig. 1B). The dynamics of tubular lysosomes was also altered in *Spg11*$^{\Delta 32\text{-}34/\Delta 32\text{-}34}$ MEFs (Fig. 2I-K). Overall, these results suggest that the spatacsin domain encoded by exons 32 to 34 of *Spg11* plays an important role in the formation and dynamics of tubular lysosomes.

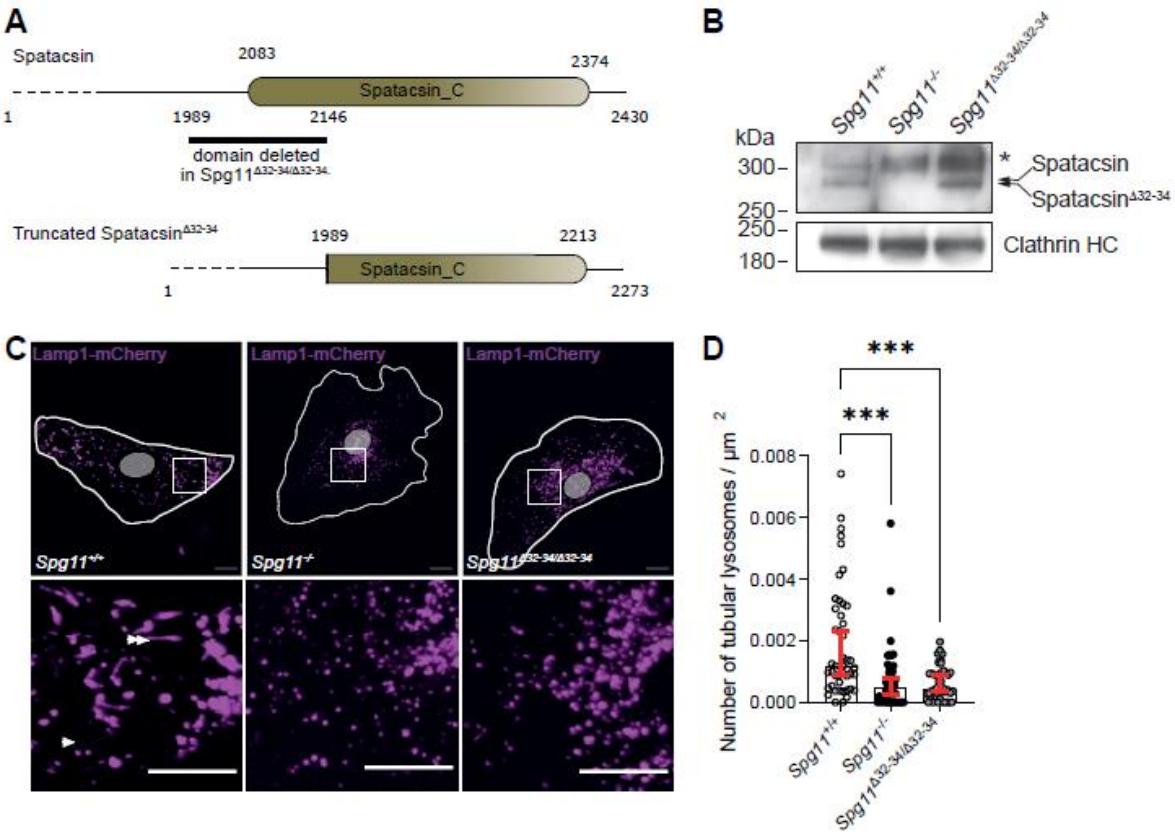

Figure 2. spatacsin regulates lysosomal dynamics and positioning

A. *Representation of the spatacsin_C domain and the region truncated in the Spg11*$^{\Delta 32\text{-}34/\Delta 32\text{-}34}$ *mouse model.*

B. *Western blot showing expression of truncated spatacsin in Spg11*$^{\Delta 32\text{-}34/\Delta 32\text{-}34}$ *mouse brain. Equal loading was validated by clathrin heavy chain (HC) immunoblotting.*

C. *Lamp1-mCherry expression in Spg11*$^{+/+}$*, Spg11*$^{-/-}$*, and Spg11*$^{\Delta 32\text{-}34/\Delta 32\text{-}34}$ *MEFs imaged by spinning-disk confocal microscopy. Note the perinuclear clustering of lysosomes in Spg11*$^{-/-}$ *and Spg11*$^{\Delta 32\text{-}34/\Delta 32\text{-}34}$ *MEFs and the presence of tubular lysosomes in Spg11*$^{+/+}$ *MEFs (white arrowheads). Scale bar: 5 µm.*

D. *Quantification of the number of tubular lysosomes in Spg11*$^{+/+}$*, Spg11*$^{-/-}$*, and Spg11*$^{\Delta 32\text{-}34/\Delta 32\text{-}34}$ *MEFs. Median and 95% CI, N = 45 cells from three independent experiments. ***P < 0.001 for both Spg11*$^{-/-}$ *and Spg11* $^{\Delta 32\text{-}34/\Delta 32\text{-}34}$ *when compared to Spg11* $^{+/+}$ *MEFs. Kruskall-Wallis test followed by Dunn's multiple comparisons test.*

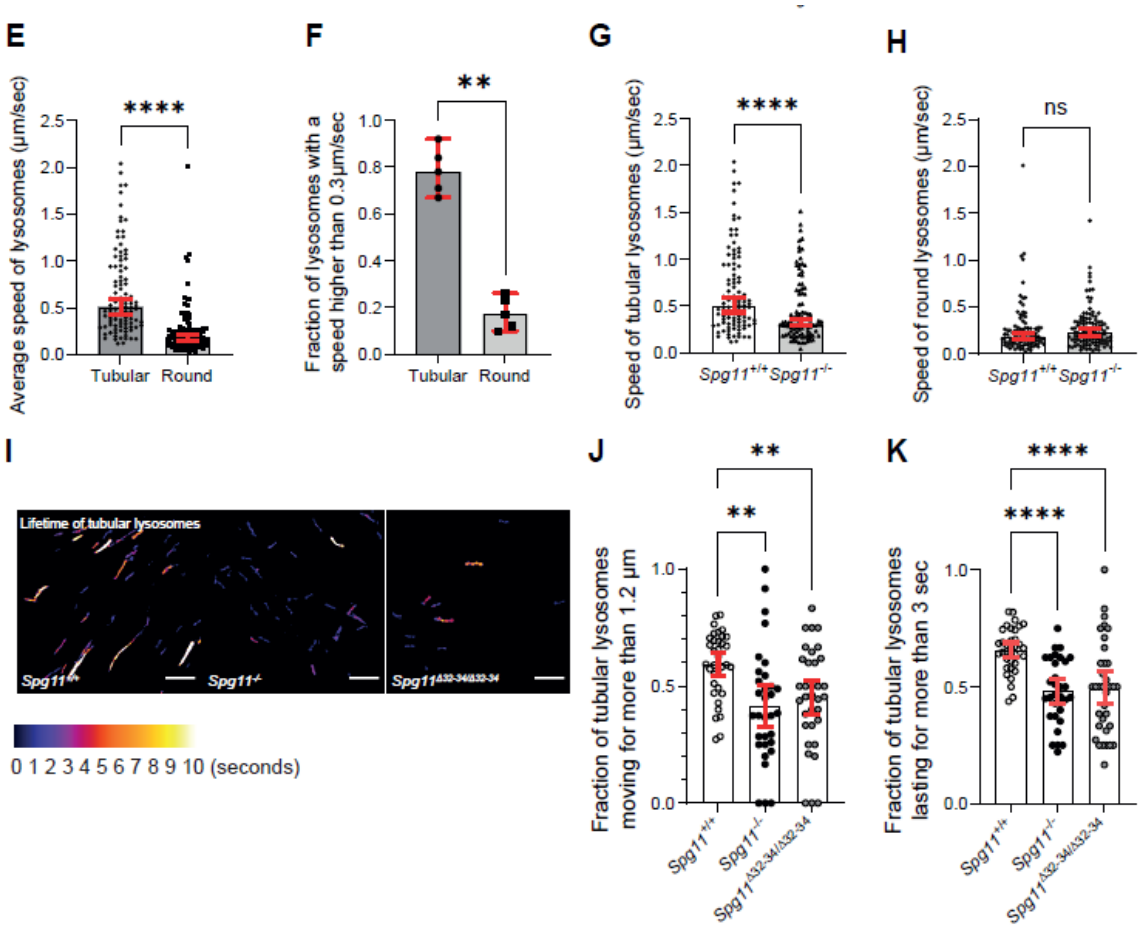

Figure 2. spatacsin regulates lysosomal dynamics and positioning (second part)

*E. Average speed of tubular and round lysosomes in wildtype MEFs. Median and 95% CI, N = 110 from five independent MEFs. ****P < 0.0001, Mann-Whitney test.*

*F. Quantification of the proportion of lysosomes with an average speed > 0.3 µm/sec according to their shape in wildtype MEFs. Median and 95% CI. **P < 0.01, Mann-Whitney test.*

*G. Quantification of the average speed of tubular lysosomes in Spg11$^{+/+}$ and Spg11$^{-/-}$ MEFs. Median and 95% CI, N > 100 from five independent MEFs. ****P < 0.0001, Mann-Whitney test.*

H. Quantification of the average speed of round lysosomes in Spg11$^{+/+}$ and Spg11$^{-/-}$ MEFs. Median and 95% CI, N = 110 from five independent MEFs. Mann-Whitney test.

I. Heatmap indicating the lifetime of tubular lysosomes during their movement obtained by projecting binary images of tubular particle detection over time. Blue indicates a shorter lifetime in seconds and red a longer lifetime. Scale bar: 5 µm.

*J. Quantification of the proportion of tubular lysosomes moving > 1.2 µm in Spg11$^{+/+}$, Spg11$^{-/-}$, and Spg11$^{Δ32-34/Δ32-34}$ MEFs. Mean and 95% CI, N = 35 cells from three independent experiments. **P < 0.01 for both Spg11$^{-/-}$ and Spg11 $^{Δ32-34/Δ32-34}$ when compared to Spg11 $^{+/+}$ MEFs. One-way ANOVA followed by Sidak's multiple comparisons test.*

*K. Quantification of the proportion of tubular lysosomes lasting < 3 s in Spg11$^{+/+}$, Spg11$^{-/-}$, and Spg11$^{Δ32-34/Δ32-34}$ MEFs. Mean and 95% CI, N = 35 cells from three independent experiments. ****P < 0.0001 for both Spg11$^{-/-}$ and Spg11 $^{Δ32-34/Δ32-34}$ when compared to Spg11 $^{+/+}$ MEFs. One-way ANOVA followed by Sidak's multiple comparisons test.*

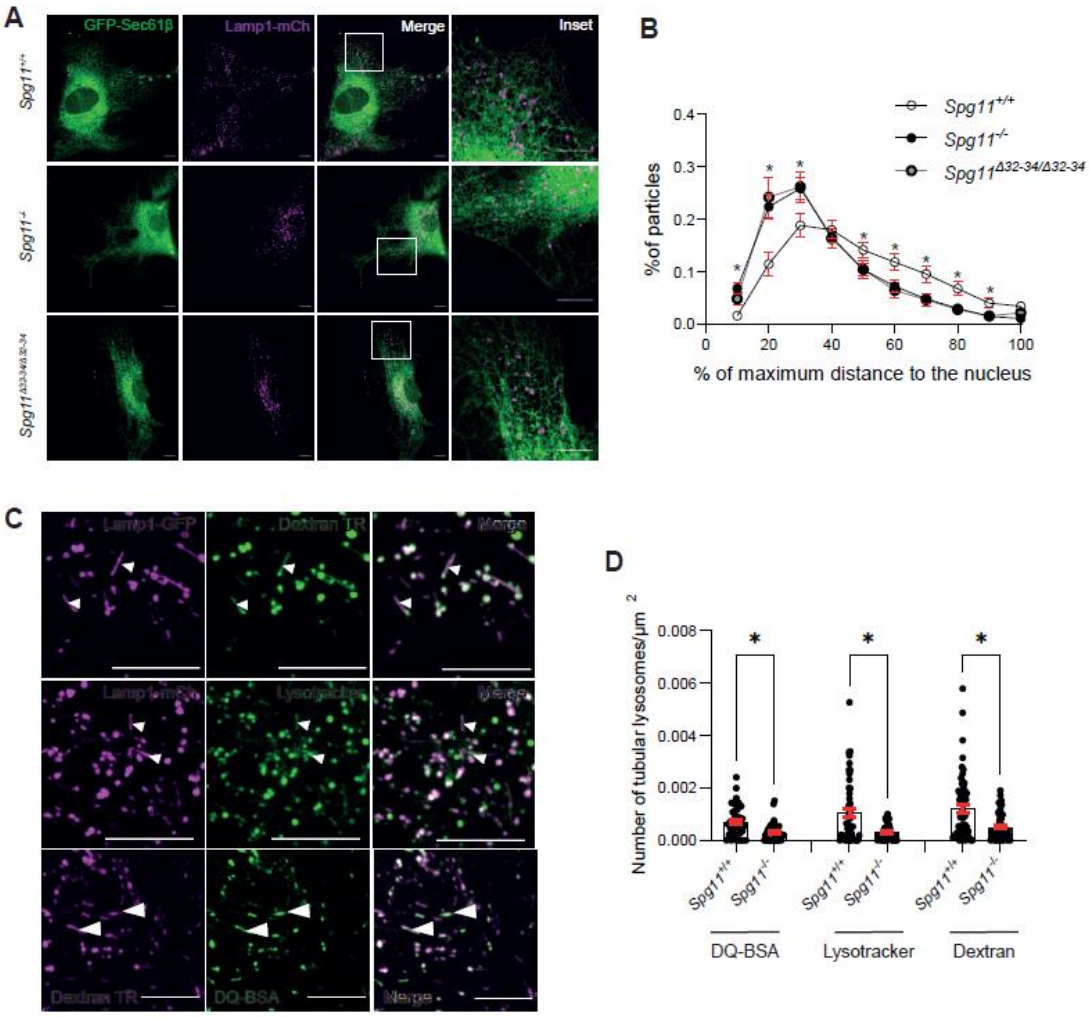

Supplementary Figure 1. spatacsin regulates the morphology, positioning, and motility of endolysosomes

A. *Live imaging of the ER marker Sec61ß-GFP and lysosome marker Lamp1-mCherry in Spg11$^{+/+}$, Spg11$^{-/-}$, and Spg11$^{Δ32-34/Δ32-34}$ MEFs. Note that the absence of spatacsin (Spg11$^{-/-}$) or expression of truncated spatacsin (Spg11$^{Δ32-34/Δ32-34}$) did not alter ER morphology. Scale bar: 5 µm.*

B. *Quantification of the distance of lysosomes from the nucleus in Spg11$^{+/+}$, Spg11$^{-/-}$, and Spg11$^{Δ32-34/Δ32-34}$ fibroblasts. Mean and 95% CI, N = 53 cells from three independent experiments. *P < 0.05 for both Spg11$^{-/-}$ and Spg11 $^{Δ32-34/Δ32-34}$ when compared to Spg11 $^{+/+}$ by Dunnett's multiple comparisons test (two-way ANOVA nonparametric test).*

C. *Live imaging of lysosomes stained with various markers in Spg11$^{+/+}$ MEFs. Note that tubular lysosomes were positive for Lamp1, Dextran-Texas Red (TR), and Lysotracker, as well as DQ-BSA, indicating that they are an acidic and catalytically active compartments. Scale bar: 5 µm.*

D. *Quantification of the number of tubular lysosomes in Spg11$^{+/+}$and Spg11$^{-/-}$ MEFs using the fluorescent markers DQ-BSA-green, Lysotracker-Green, or Dextran-Texas Red. Median and 95% CI, N > 40 cells from three independent experiments. *P < 0.05, Kruskall-Wallis test followed by Dunn's multiple comparisons test.*

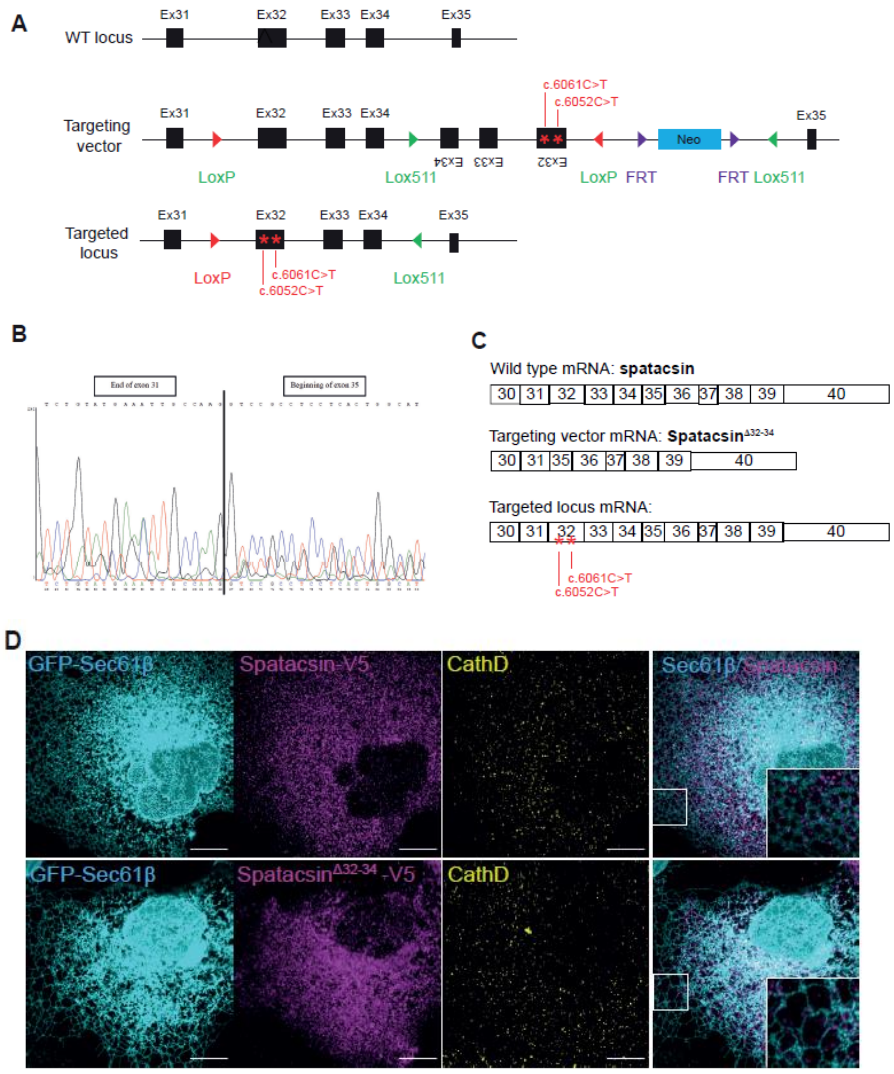

Supplementary Figure 2. Characterization of *Spg11*$^{\Delta 32\text{-}34/\Delta 32\text{-}34}$ model.

A. *Diagram showing the genomic structure of the mouse* Spg11 *gene (top), the targeting vector (middle), and the targeted locus upon excision of the neomycin resistance cassette and action of the Cre-recombinase (bottom). The mutations introduced were c.6052C > T (p. Arg2018*) and c.6061C > T (p. Gln2021*). Scheme adapted from* (Branchu et al., 2017).

B. *Sequencing of RT-PCR product obtained from the brains of homozygous mice that incorporated the targeting vector, showing the splicing of exons 32, 33, and 34.*

C. *Scheme representing the mRNA produced in a wildtype mouse, a mouse that incorporated the targeting vector, or after the action of the Cre recombinase. Note that the intermediate model expressing the floxed allele showed splicing of exons 32 to 34 with conservation of the reading frame between exons 31 and 35. It was thus equivalent to a functional deletion of exons 32 to 34, leading to expression of a protein called spatacsin*$^{\Delta 32\text{-}34}$.

D. *Immunostaining of cells expressing the ER marker GFP-Sec61β and V5-tagged spatacsin or V5-tagged spatacsin*$^{\Delta 32\text{-}34}$*. Cells were immunostained with anti-V5 antibody and the lysosome marker cathepsin D. Scale bar: 5 µm.*

3. Involvement of the ubiquitin-dependent proteolysis pathway in spatacsin-mediated regulation of endolysosomes

We next aimed to define the molecular action of spatacsin in the formation of tubular lysosomes. We thus sought to identify proteins that bind to the domain encoded by exons 32 to 34 of *Spg11*. We performed a two-hybrid screen with the C-terminal region of human spatacsin (aa 1943-2443, containing the spatacsin_C domain) and a second screen with the same C-terminal fragment in which the amino acids encoded by exons 32-34 were deleted. Comparison of the two screens identified several proteins that potentially bind directly to the domain encoded by exons 32 to 34 (Fig. 3A, Suppl. Tables 1 and 2).

Among the proteins that could potentially bind to the domain encoded by exons 32 to 34, we aimed to identify those important for the regulation of lysosome morphology. Thus, we downregulated each identified partner in wildtype MEFs using siRNA and analyzed the consequences on the lysosomes, which were imaged by spinning disk confocal microscopy after staining with Dextran-Texas Red.

We used two methods to quantify the effect of siRNA on lysosomes. First, we developed an unbiased classification method to discriminate between lysosomal staining in *Spg11*$^{-/-}$ and *Spg11*$^{+/+}$ MEFs by training a neural network that exploited all parameters of the lysosomal staining in images. The trained neural network was then used to predict the probability of the cell to be considered as a *Spg11*$^{-/-}$ fibroblast for each image of fibroblasts transfected with siRNA. In parallel, we performed a directed analysis that automatically detected tubular lysosomes. For both methods, we evaluated how well the downregulation of each candidate using siRNA in wildtype MEFs phenocopied the lysosomal phenotype of *Spg11*$^{-/-}$ MEFs. We compared the effect of each siRNA with that of three independent siRNAs downregulating *Spg11* (Fig. 3B; Supplementary Fig. 3). The neural network approach identified 28 genes and directed analysis identified 11 genes that, after downregulation by siRNA, were at least as effective as *Spg11* siRNA to phenocopy *Spg11*$^{-/-}$ MEFs (Fig. 3C, Suppl. Tables 1 and 2). Eight genes were identified by both analyses, suggesting their importance in the function of spatacsin in lysosomes.

Gene ontology analysis of the candidates identified by the two approaches suggested a role of the ubiquitin-dependent protein catabolic process and proteolysis in modulation of the lysosomal phenotype (Fig. 3C), suggesting that the action of spatacsin on lysosomes is linked to ubiquitin-dependent proteolysis. We confirmed this hypothesis by expressing mutant ubiquitin-K0, which prevents poly-ubiquitination of substrates required for degradation(Wu-Baer et al., 2003). Expression of this mutant in wildtype MEFs decreased the number of tubular lysosomes, as well as their dynamics (Fig. 3D-F), suggesting a role for ubiquitination in the control of lysosomal phenotype by spatacsin.

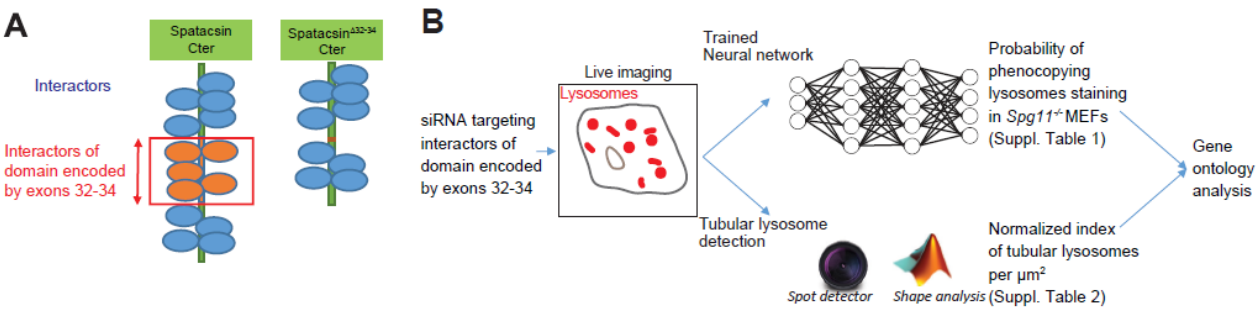

C

	Positive by Neuron network analysis (n=28)		Positive by directed analysis (n=11)		Positive for both analyses(n=8)	
GO biological processes	*P*	FDR[a]	*P*	FDR	*P*	FDR
regulation of cell morphogenesis	5.99×10^{-5}	4.51×10^{-2}				
protein modification by small protein conjugation or removal	6.93×10^{-7}	2.74×10^{-3}				
protein ubiquitination	1.66×10^{-5}	2.19×10^{-2}				
ubiquitin-dependent protein catabolic process					1.47×10^{-5}	2.59×10^{-2}
proteolysis involved in cellular protein catabolic process			4.42×10^{-6}	6.99×10^{-2}	5.72×10^{-7}	9.04×10^{-3}
proteolysis	7.77×10^{-6}	1.23×10^{-2}	5.74×10^{-6}	3.02×10^{-2}	1.52×10^{-5}	2.41×10^{-2}
organic substance catabolic process	5.93×10^{-5}	4.68×10^{-2}				

Figure 3. Ubiquitin-dependent proteolysis contributes to the regulation of the lysosome phenotype by spatacsin

A. *Scheme showing the strategy to identify interactors of the domain of spatacsin encoded by exons 32 to 34 of SPG11. Yeast two-hybrid screens were performed with the C-terminal domain of human spatacsin (aa 1943-2443) or the same domain missing exons 32 to34 as bait. Interactors specifically interacting with the spatacsin domain encoded by exons 32 to 34 (orange) were selected.*

B. *Design of the screening process for interactors of the spatacsin domain encoded by exons 32 to 34 of SPG11. Each interactor was downregulated by siRNA in wildtype MEFs, and lysosomes imaged by spinning disk confocal microscopy. The effect of the siRNAs was analyzed using an unbiased method (trained neural network) or directed analysis to quantify the presence of tubular lysosomes.*

C. *Table summarizing the pathways identified by gene ontology analysis as being significantly enriched in the list of genes identified by neural network analysis, directed analysis, or both. FDR: False discovery rate.*

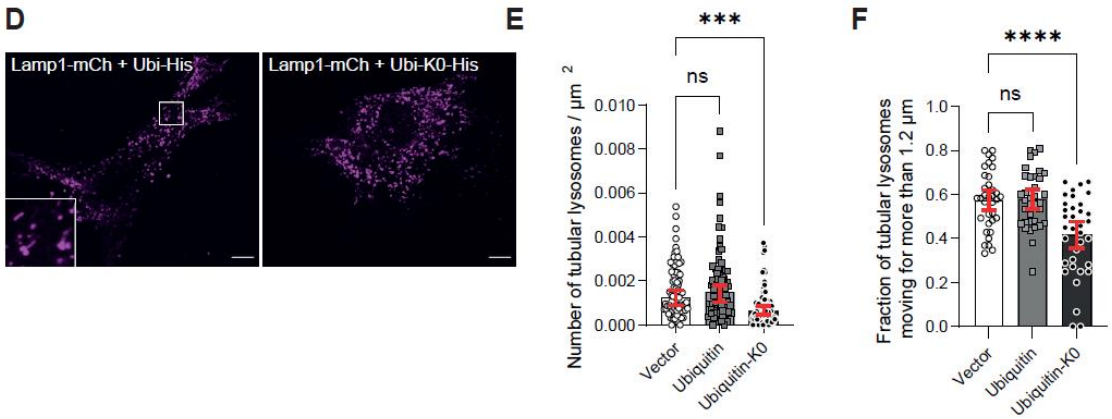

Figure 3. Ubiquitin-dependent proteolysis contributes to the regulation of the lysosome phenotype by spatacsin (second part)

D. Live images of lysosomes in wildtype MEFs co-transfected with Lamp1-mCherry and either Ubi-His or UbiK0-His. Scale bar: 10 µm.

*E. Quantification of the number of tubular lysosomes in wildtype MEFs transfected with an empty vector or vectors expressing ubiquitin or mutant ubiquitin-K0. Median and 95% CI, N = 75 cells from three independent experiments. ***P < 0.001, Kruskall-Wallis test followed by Dunn's multiple comparisons test.*

*F. Quantification of the proportion of tubular lysosomes moving > 1.2 µm in wildtype MEFs transfected with an empty vector or vectors expressing ubiquitin or mutant ubiquitin-K0. Mean and 95% CI, N = 35 cells from three independent experiments. ****P < 0.0001, **P < 0.01. One-way ANOVA followed by Sidak's multiple comparisons test.*

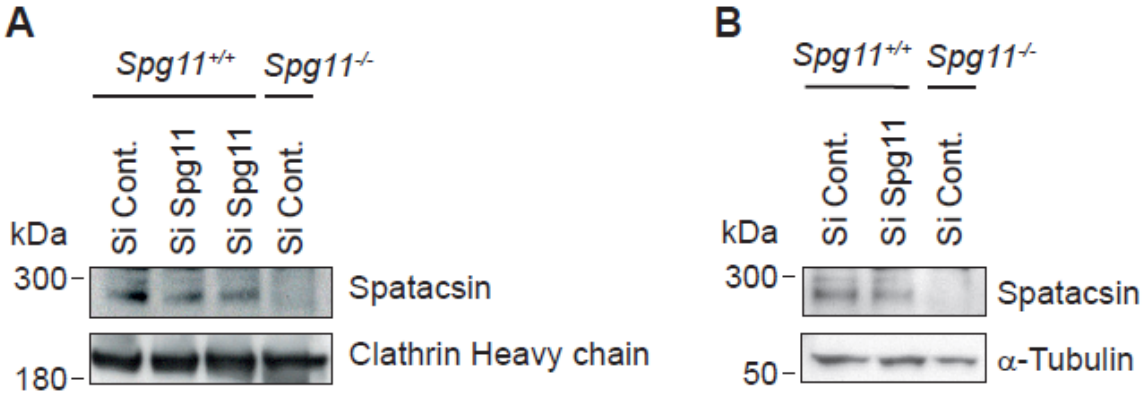

Supplementary Figure 3. Downregulation of spatacsin by siRNA.

Western blot of wildtype MEFs transfected with control siRNA or independent siRNA that downregulate spatacsin purchased from Dharmacon (A) or ThermoFisher (B). Lysate of Spg11$^{-/-}$ MEFs was used as a negative control. Equal loading was validated by clathrin heavy chain (A) or α-tubulin (B) immunoblotting.

4. spatacsin promotes the ubiquitin-dependent degradation of AP5-Z1

Our screening approach showed that the control of tubular lysosome formation and dynamics by spatacsin depends on poly-ubiquitination and proteolysis. We then aimed to identify candidate proteins that may be regulated by ubiquitination and/or proteolysis to control lysosomal phenotype. Exploration of the interactome of the spatacsin domain encoded by exons 32 to 34 revealed no binding partners with endolysosomal localization, suggesting that ubiquitin-dependent regulation may act on other proteins present in the endolysosomal system. Among spatacsin binding partners, spastizin and AP5Z1 co-immunoprecipitate with spatacsin and colocalize with lysosomes(Hirst et al., 2021b, 2013a) (Supplementary Fig. 4A; Fig. 4E). We thus investigated whether spastizin or AP5Z1 are regulated by ubiquitin-dependent proteolysis. Overexpression of spatacsin-GFP in wildtype MEFs lowered levels of AP5Z1, whereas spastizin levels were unaffected (Fig. 4A, B). Co-transfection of ubiquitin-K0 with the vector expressing spatacsin-GFP blocked this effect on AP5Z1, suggesting that spatacsin mediates poly-ubiquitin-dependent degradation of AP5Z1 (Fig. 4A, B).

The downregulation of AP5Z1 was not observed upon overexpression of spatacsin$^{\Delta 32\text{-}34}$–GFP, suggesting that the domain encoded by exons 32 to 34 contains the information that controls the degradation of AP5Z1 (Fig. 4C). Among the proteins that bind to the domain encoded by exons 32 to 34 of *Spg11* and important for lysosomal phenotype, we confirmed by co-immunoprecipitation that UBR4 interacts with the C-terminal domain of spatacsin, but not the domain lacking the fragment encoded by exons 32 to 34 of *Spg11* (Supplementary Fig. 4B). UBR4 is an N-recognin involved in the degradation of proteins with an N-Degron motif(Sriram et al., 2011). AP5Z1 is predicted to have such a motif according to the Eukaryotic Linear Motif Resource (http://elm.eu.org/index.html). Downregulation of UBR4 using siRNA led to higher amount of AP5Z1 in the presence of spatacsin-GFP (Fig. 4D) and a lower number of tubular lysosomes (Supplementary Fig. 4C), suggesting that AP5Z1 degradation may be mediated by UBR4 and that preventing AP5Z1 degradation may impair the formation of tubular lysosomes.

We next tested whether AP5Z1 levels contribute to the regulation of lysosome function by co-transfecting wildtype MEFs with Lamp1-mCherry and either a vector expressing GFP-AP5Z1 (Fig. 4E) or siRNA that downregulate AP5Z1 (Supplementary Fig. 4D). Both overexpression and downregulation of AP5Z1 decreased the number of tubular lysosomes (Fig. 4F, Suppl. Fig. 4E). GFP-AP5Z1 also affected lysosomal dynamics in control fibroblasts (Fig. 4G). Overall, these data show that AP5Z1 levels must be tightly regulated to control lysosomal dynamics and suggest that spatacsin contributes to such regulation by promoting the ubiquitin-dependent degradation of AP5Z1.

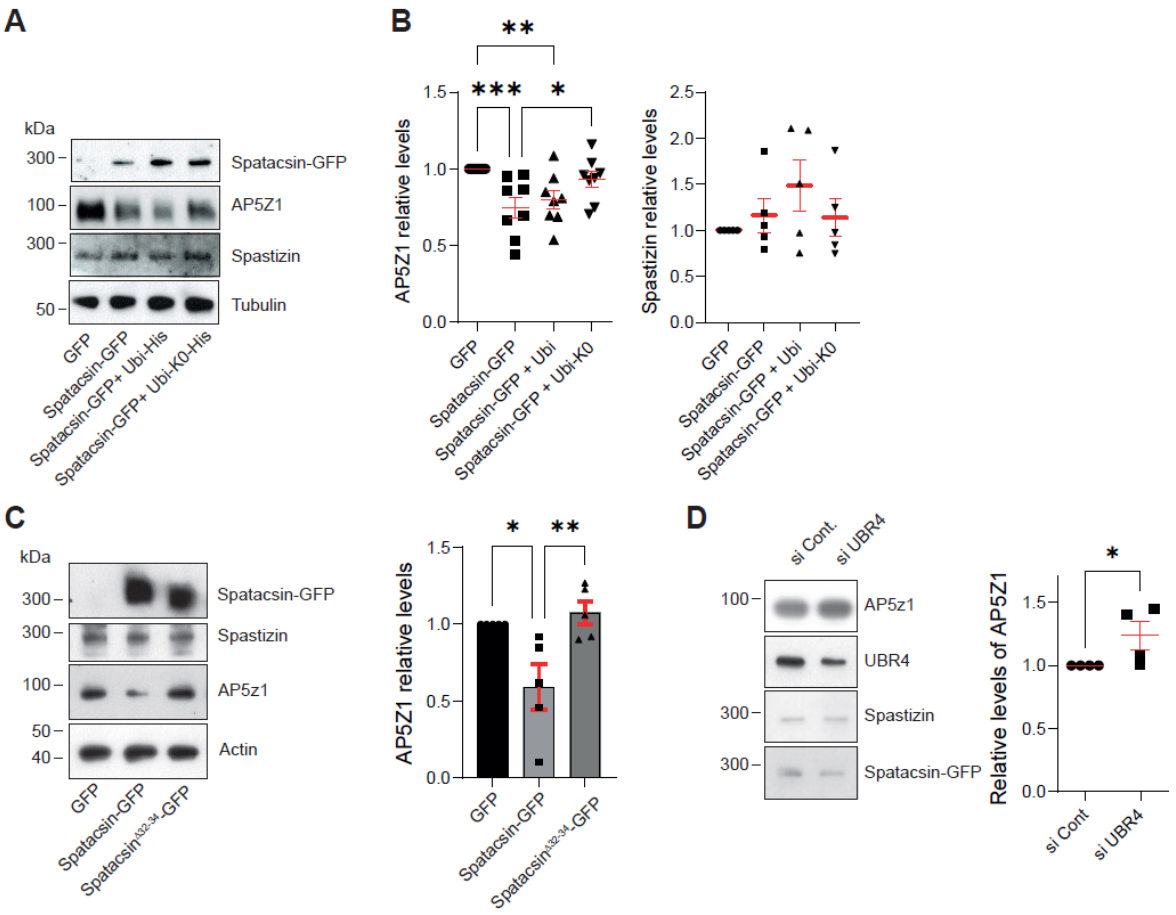

Figure 4. spatacsin promotes ubiquitin-dependent degradation of AP5Z1

A. *Western blot analysis of wildtype MEFs overexpressing spatacsin-GFP alone or together with ubiquitin or mutant ubiquitin-K0.*

B. *Overexpression of spatacsin leads to lower levels of endogenous AP5Z1. This effect was blocked by co-expression of mutant ubiquitin-K0 (Left). Levels of endogenous spastizin were not significantly affected by expression of spatacsin-GFP or ubiquitin. Mean ± SEM, *P < 0.05, **P < 0.01, ***P < 0.001, Kruskall-Wallis test.*

C. *Western blots showing levels of spatacsin-GFP, spastizin, AP5Z1, and actin in MEFs overexpressing GFP, spatacsin-GFP, or spatacsin$^{\Delta 32\text{-}34}$-GFP (Left). Right: quantification of the western blots showing that overexpression of full-length spatacsin-GFP, but not spatacsin$^{\Delta 32\text{-}34}$-GFP, leads to lower levels of endogenous AP5Z1. Mean ± SEM, *P < 0.05, **P < 0.01, Kruskall Wallis test.*

D. *Western blot showing higher levels of AP5Z1 in wildtype MEFs transfected with siRNA that downregulates the N-recognin UBR4. Mean ± SEM, *P < 0.05, Mann-Whitney test.*

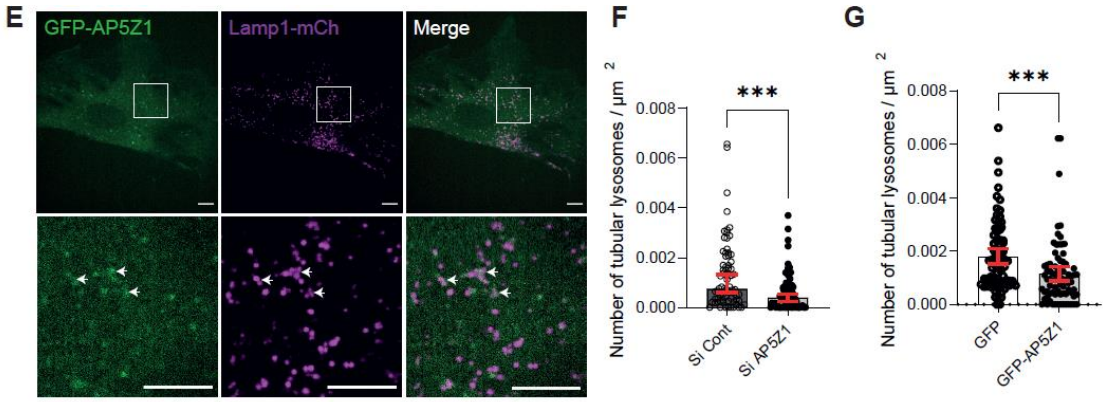

Figure 4. spatacsin promotes ubiquitin-dependent degradation of AP5Z1 (second part)

E. Live images of wildtype MEFs expressing Lamp1-mCherry and GFP-AP5Z1.Scale bar: 10 µm.

*F. Quantification of the number of tubular lysosomes in wildtype MEFs transfected with a vector overexpressing GFP-AP5Z1. Mean and 95% CI, N = 78 for cells from three independent experiments. ***P < 0.001, Mann-Whitney test.*

*G. Quantification of the proportion of tubular lysosomes moving > 1.2 µm in wildtype MEFs transfected with a vector overexpressing GFP-AP5Z1. Mean and 95% CI, N = 30 cells from three independent experiments. **P < 0.01, unpaired t-test.*

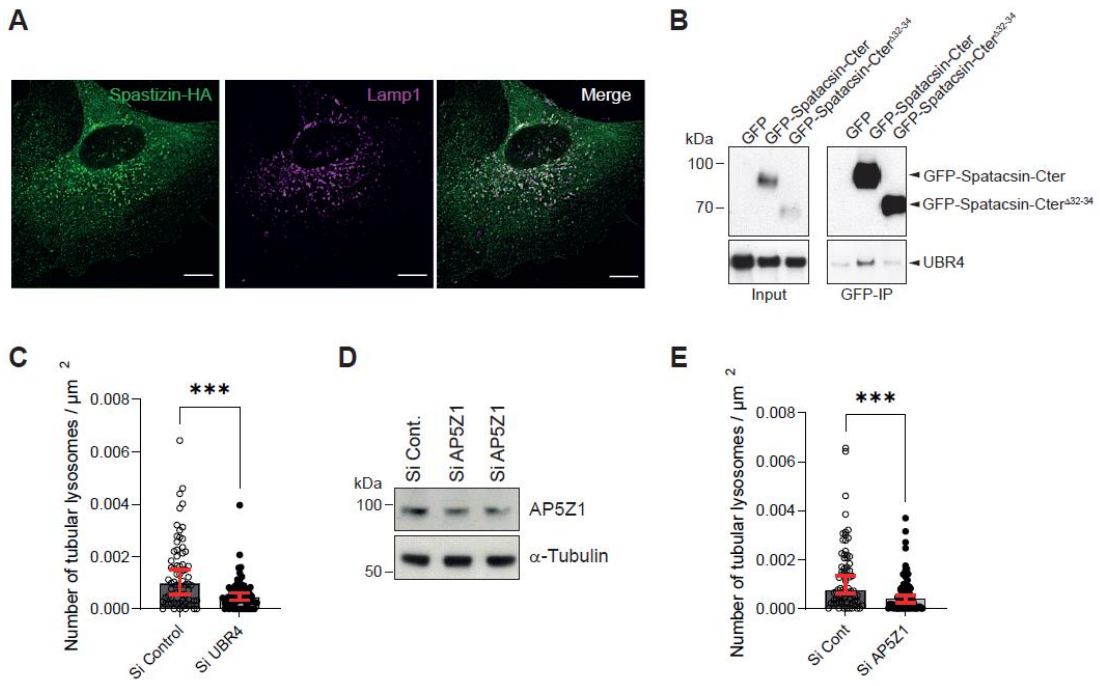

Supplementary Figure 4. spatacsin promotes ubiquitin-dependent degradation of AP5z1

A. *Wildtype MEFs expressing spastizin-HA were immunostained with anti-Lamp1 and anti-HA antibody. Note the colocalization of spastizin-HA with lysosomal marker Lamp1. Scale bar: 5 µm.*

B. *Western blots showing co-immunoprecipitation of UBR4 with the C-terminal domain of spatacsin (aa 1943-2443, GFP-spatacsin-Cter) but not the construct lacking amino acids encoded by exons 32 to 34 (GFP-spatacsin-Cter$^{\Delta 32\text{-}34}$).*

C. *Quantification of the number of tubular endolysosomes in wildtype MEFs transfected with siRNA that downregulates UBR4. Data obtained with two independent siRNAs were combined. Median and 95% CI, N = 68 cells from three independent experiments. ***P < 0.001, Mann-Whitney test.*

D. *Western blot showing downregulation of AP5Z1 48 h after transfection with two independent siRNAs. Equal loading was validated by α-tubulin immunoblotting.*

E. *Quantification of the number of tubular lysosomes in wildtype MEFs transfected with siRNA that downregulate AP5Z1. Data obtained with two independent siRNAs were combined. Median and 95% CI, N = 74 cells from three independent experiments. ***P < 0.001, Mann-Whitney test.*

5. Ubiquitin-dependent degradation of AP5Z1 promotes spastizin recruitment to lysosomes

We then evaluated the consequences of blocking spatacsin-mediated degradation of AP5Z1. Expression of Ubiquitin-K0, which prevented degradation of AP5Z1 resulted in increased interaction of AP5Z1 with spatacsin and diminished interaction of spastizin with spatacsin, as evaluated by co-immunoprecipitation (Fig. 5A-B). Thus, spatacsin-mediated degradation of AP5Z1 appears to favor the interaction of spatacsin with spastizin. We tested this hypothesis by overexpressing AP5Z1 and observed that it lowered the amount of spastizin co-immunoprecipitated with spatacsin (Fig. 5C-D). Overall, these data suggest that spatacsin contributes to the regulation of AP5Z1 levels by promoting its degradation, thus favoring the interaction of spatacsin with spastizin.

spatacsin is required to recruit spastizin to lysosomes(Hirst et al., 2021b). Accordingly, we observed weaker colocalization of spastizin-GFP with Lamp1-mCherry in *Spg11*$^{-/-}$ than *Spg11*$^{+/+}$ MEFs by live imaging (Suppl. Fig 5A-B). Thus, spatacsin-mediated AP5Z1 degradation may regulate the localization of spastizin to lysosomes. Overexpression of AP5Z1 or preventing its degradation by the expression of ubiquitin-K0 in wildtype MEFs, significantly decreased the localization of spastizin-GFP to lysosomes (Fig. 5E). Overall, these data suggest that spatacsin-mediated ubiquitin-dependent degradation of AP5Z1 contributes to lysosomal localization of spastizin.

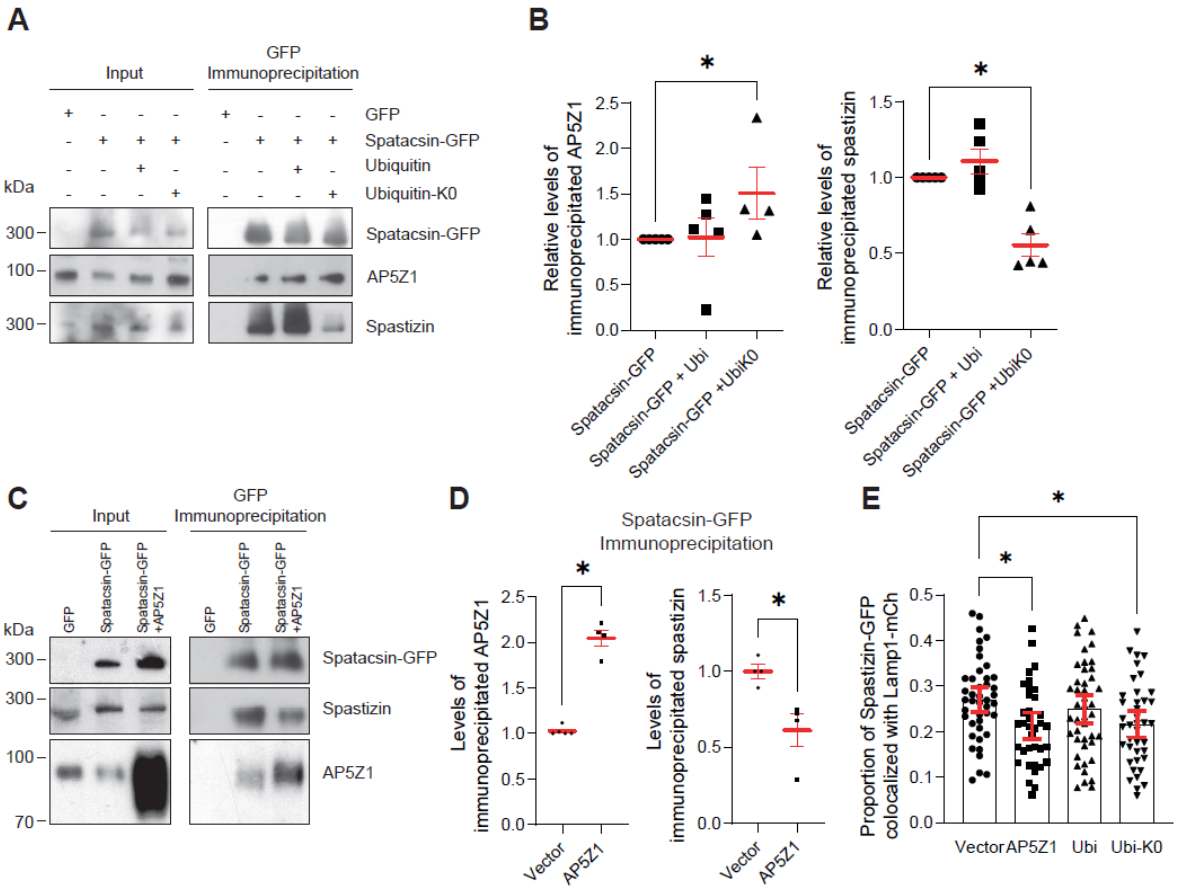

Figure 5. AP5Z1 regulates spastizin recruitment to lysosomes

A. *Western blots showing that the interaction of spatacsin-GFP with AP5Z1 and spastizin is modulated by the expression of mutant ubiquitin-K0.*

B. *Quantification of immunoprecipitation showing that ubiquitin-K0 increases the amount of AP5Z1 and decreases the amount of spastizin immunoprecipitated with spatacsin-GFP. Mean ± SEM, *P < 0.05, Kruskall-Wallis test.*

C. *Western blots showing that the interaction of spatacsin-GFP with spastizin decreases when AP5Z1 is overexpressed.*

D. *Quantification of immunoprecipitation showing that overexpression of AP5Z1 increases the interaction of spatacsin-GFP with AP5Z1 and decreases the interaction of spatacsin-GFP with spastizin. Mean ± SEM, *P < 0.05, Mann-Whitney test.*

E. *Quantification of the proportion of spastizin-GFP colocalized with Lamp1-mCherry in wildtype MEFs overexpressing AP5Z1, ubiquitin, or ubiquitin-K0. Mean and 95% CI, N > 36 cells from three independent experiments. *P < 0.05, one-way ANOVA followed by Sidak's multiple comparison test.*

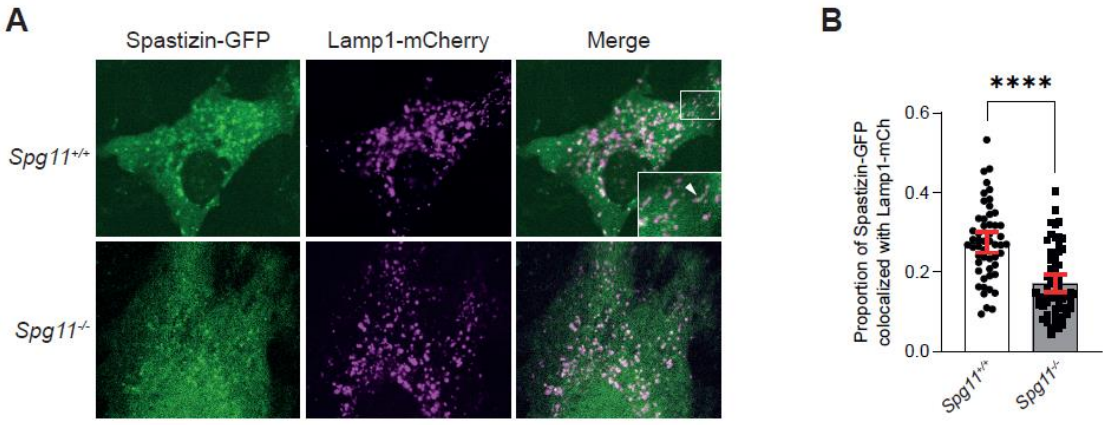

Supplementary Figure 5. spatacsin is required for lysosomal localization of spastizin

A. *Expression of spastizin-GFP and Lamp1-mCherry in Spg11$^{+/+}$ and Spg11$^{-/-}$ MEFs. Note the localization of spastizin-GFP along the tubular lysosomes in Spg11$^{+/+}$ MEFs (arrowheads in insert), and the absence of colocalization of spastizin-GFP with lysosomes in Spg11$^{-/-}$ MEFs. Scale bar 10 µm.*

B. *Quantification of the proportion of spastizin-GFP colocalized with Lamp1-mCherry in Spg11$^{+/+}$ and Spg11$^{-/-}$ MEFs. Mean and 95% CI, N > 50 cells from three independent experiments. ****P < 0.0001, unpaired T-test.*

6. spastizin regulates tubular lysosome motility

Live imaging showed that spastizin-GFP is localized along tubular lysosomes (Inset Suppl. Fig. 5A), suggesting that it may play a role in lysosome motility. We tested this hypothesis by downregulating its expression using siRNA (Fig. 6A). Downregulation of spastizin resulted in a decrease in the number of tubular lysosomes (Fig. 6B). Treatment of MEFs with the PI3 kinase inhibitor wortmannin prevented the lysosomal localization of spastizin (Fig. 6C) and decreased the number of tubular lysosomes and their dynamics (Fig. 6D). These results suggest that recruitment of spastizin to lysosomes is required to mediate their motility.

spastizin has been shown to interact with the motor protein KIF13A(Sagona et al., 2010b). Transfection of MEFs with a vector expressing KIF13A-YFP showed it to be partially colocalized with Lamp1 immunostaining (Fig. 6E). Overexpression of the mutant KIF13A-ST-YFP, devoid of the motor domain(Delevoye et al., 2014b) but capable of interacting with spastizin (Supplementary Fig. 6), prevented the formation of tubular lysosomes and altered their dynamics (Fig. 6F).Overall, these results suggest that spastizin mediates the recruitment of KIF13A to lysosomes to control the formation of tubular lysosomes and their motility.

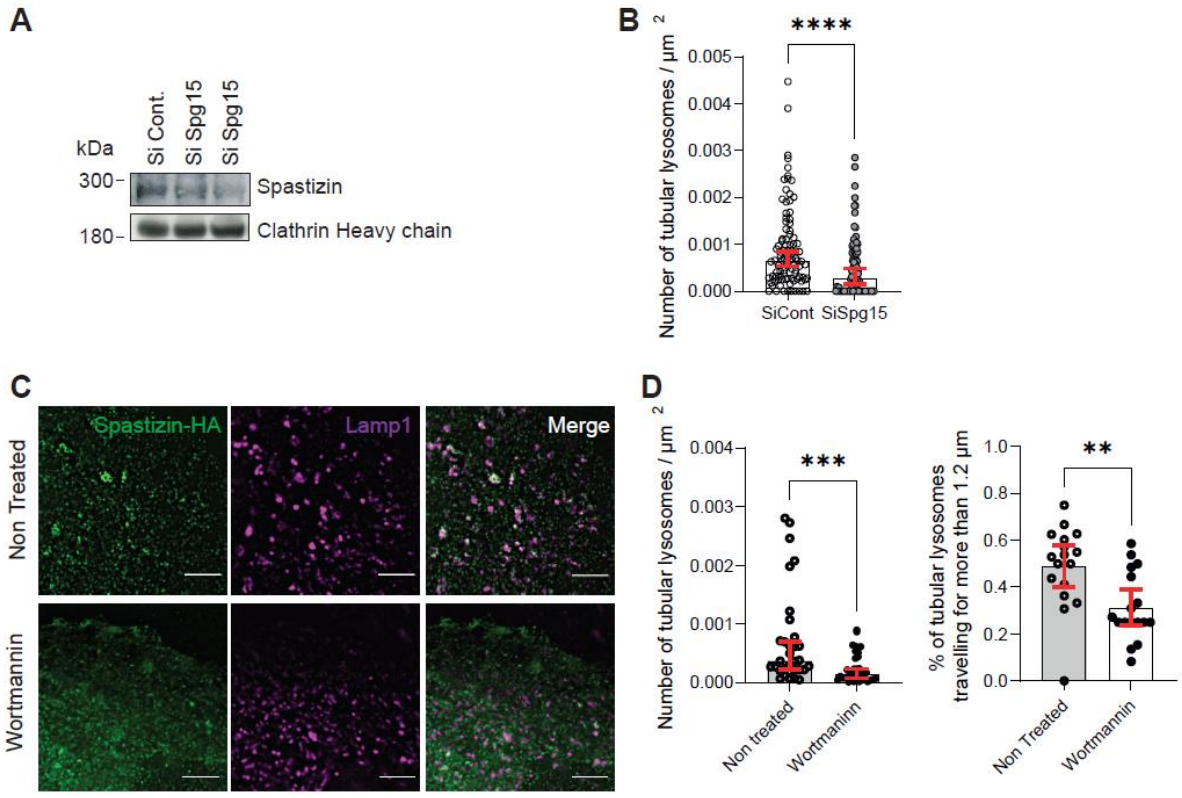

Figure 6. spastizin regulates lysosome morphology and dynamics

A. *Western blot showing downregulation of spastizin 48 h after transfection of wildtype MEFs with siRNA. Equal loading was validated by clathrin heavy chain immunoblotting.*

B. *Quantification of the number of tubular lysosomes in wildtype MEFs transfected with siRNAs that downregulate spastizin. Data obtained using two independent siRNAs were combined. Median and 95% CI, N = 92 cells from three different independent experiments. ****P < 0.0001, Mann-Whitney test.*

C. *Images of wildtype MEFs expressing spastizin-GFP and Lamp1-mCherry treated with 100 nM wortmannin for 1 h. Note the loss of colocalization of spastizin-GFP and Lamp1-mCherry upon wortmannin treatment. Scale bar: 5 µm*

D. *Left: quantification of the number of tubular lysosomes in wildtype MEFs treated with wortmannin. Median and 95% CI, N = 32 cells from three different independent experiments. ***P = 0.0009, Mann-Whitney test. Right: proportion of tubular lysosomes moving > 1.2 µm (right) in wildtype MEFs treated with wortmannin. Median and 95% CI, N = 17 cells from three different independent experiments. **P = 0.014, Mann-Whitney test.*

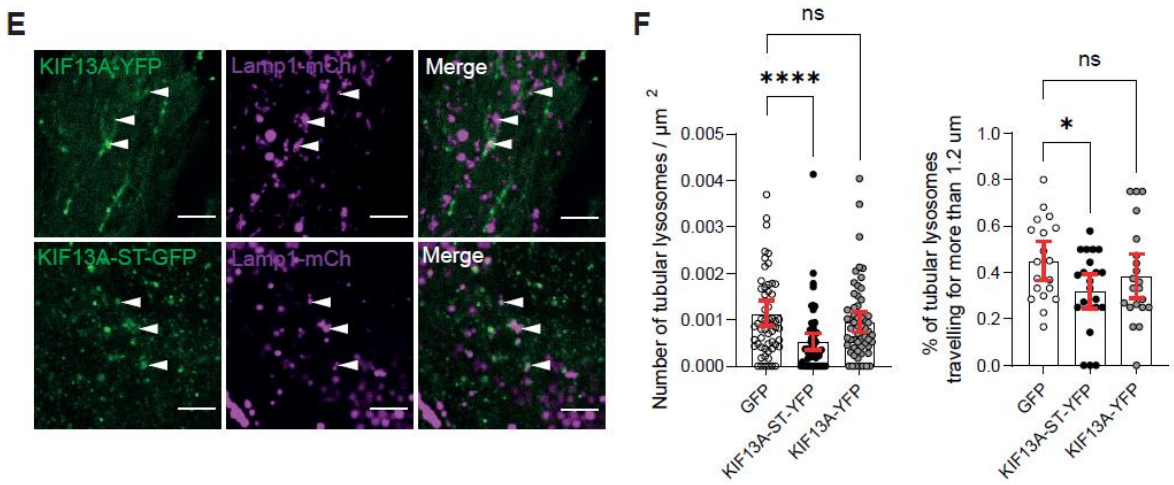

Figure 6. spastizin regulates lysosome morphology and dynamics (second part)

E. Images showing the partial colocalization of Lamp1-mCherry with KIF13A-YFP and mutant KIF13A-ST-YFP lacking the motor domain. Scale bar: 5 µm.

*F. Left: quantification of the number of tubular lysosomes in wildtype MEFs transfected with wildtype KIF13A or mutant KIF13A-ST. Median and 95% CI, N = 58 cells from three different independent experiments. ****P < 0.0001, Kruskall-Wallis test. Right: proportion of tubular lysosomes moving > 1.2 µm in wildtype MEFs transfected with wildtype KIF13A or mutant KIF13A-ST. Mean and 95% CI, N = 22 cells from three different independent experiments. *P < 0.05, one-way ANOVA, Dunnett's multiple comparisons test.*

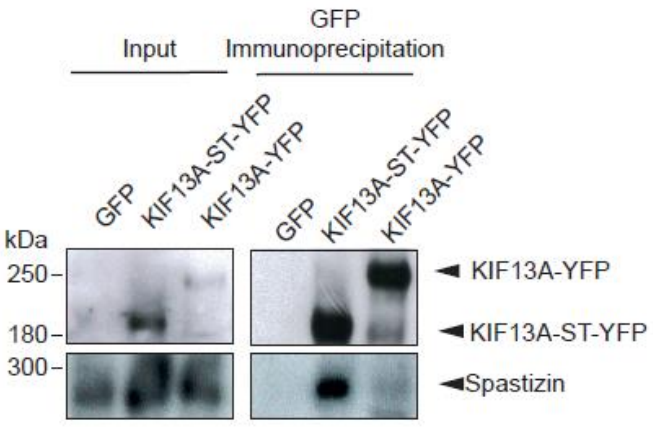

Supplementary Figure 6. Interaction of spastizin with KIF13A

Western blots showing co-immunoprecipitation of spastizin-HA with KIF13A-YFP or mutant KIF13A-ST-YFP (devoid of the motor domain).

7. The ER is a platform to promote the formation of tubular lysosomes and regulate their motility

Our data, thus far, suggested that spatacsin mediates the degradation of AP5Z1 in a ubiquitin-dependent manner, facilitating the interaction of spatacsin with spastizin and allowing the recruitment of spastizin to lysosomes, thus contributing to regulate the formation and dynamics of tubular lysosomes. We next aimed to determine the localization of the interaction between ER-associated spatacsin and spastizin. A proximity-ligation assay in MEFs transfected with spatacsin-V5 and spastizin-HA showed the interaction of spatacsin with spastizin to occur at lysosomes labelled by Lamp1 immunostaining (Fig. 7A). This suggests that the interaction of spatacsin with spastizin occurs at contact sites between the ER and lysosomes.

Based on our results, we analyzed the interaction of lysosomes with the ER network. The analysis of live images of MEFs expressing Lamp1-mCherry and GFP-Sec61 showed ~85% of Lamp1-mCherry-positive particles to be in contact with the ER. However, consideration of only highly motile tubular lysosomes increased the proportion that was in contact with the ER to approximately 95% (Fig. 7B-C). Moreover, the overlap of lysosome and ER staining was greater for tubular lysosomes than round lysosomes, suggesting that they were in closer proximity to the ER. (Fig. 7D). Live imaging showed that tubular lysosomes move along the ER tubular network (Fig. 7E, Suppl. Video 3), also suggesting that tubular lysosomes are closely associated with the ER network. Accordingly, STED microscopy showed that the tubular lysosomes were entangled in a network of ER tubules (Fig. 7F). Overall, these data show that dynamic tubular lysosomes are strongly associated with the ER tubular network.

Given the strong association of dynamic tubular lysosomes with the ER network, we assessed whether ER network integrity contributes to lysosome morphology and/or motility. Atlastin-1 is a GTPase involved in the homotypic fusion of ER tubules, thus regulating ER network morphology(Hu et al., 2009). As previously observed, expressing a form of atlastin-1 mutated in the GTPase domain (atlastin K80A) strongly altered the morphology of the ER (Supplementary Fig. 7A-B)(Hu et al., 2009). Disruption of the ER tubular network by expression of atlastin K80A resulted in a decrease in the number of tubular lysosomes (Fig. 7G) and affected their dynamics (Fig. 7G), indicating that the integrity of the ER tubular network is necessary for tubular lysosome formation and dynamics.

Finally, we evaluated the impact of ER network alteration on AP5Z1 levels as well as on the interaction of spatacsin with its partners. Co-transfection of atlastin-K80A-myc with spatacsin-GFP prevented spatacsin-dependent degradation of AP5Z1 (Fig. 7H, Supplementary Fig. 7C). It also led to a higher amount of AP5Z1 and a lower amount of spastizin coimmunoprecipitated with spatacsin-GFP (Fig. 7H, Supplementary Fig. 7D). This observation is consistent with a role of AP5Z1 and spastizin in the regulation of tubular lysosome formation and dynamics. As spatacsin did not interact with either wildtype or the K80A variant of atlastin, the effect of atlastin on lysosome morphology and motility is likely modulated by ER network morphology.

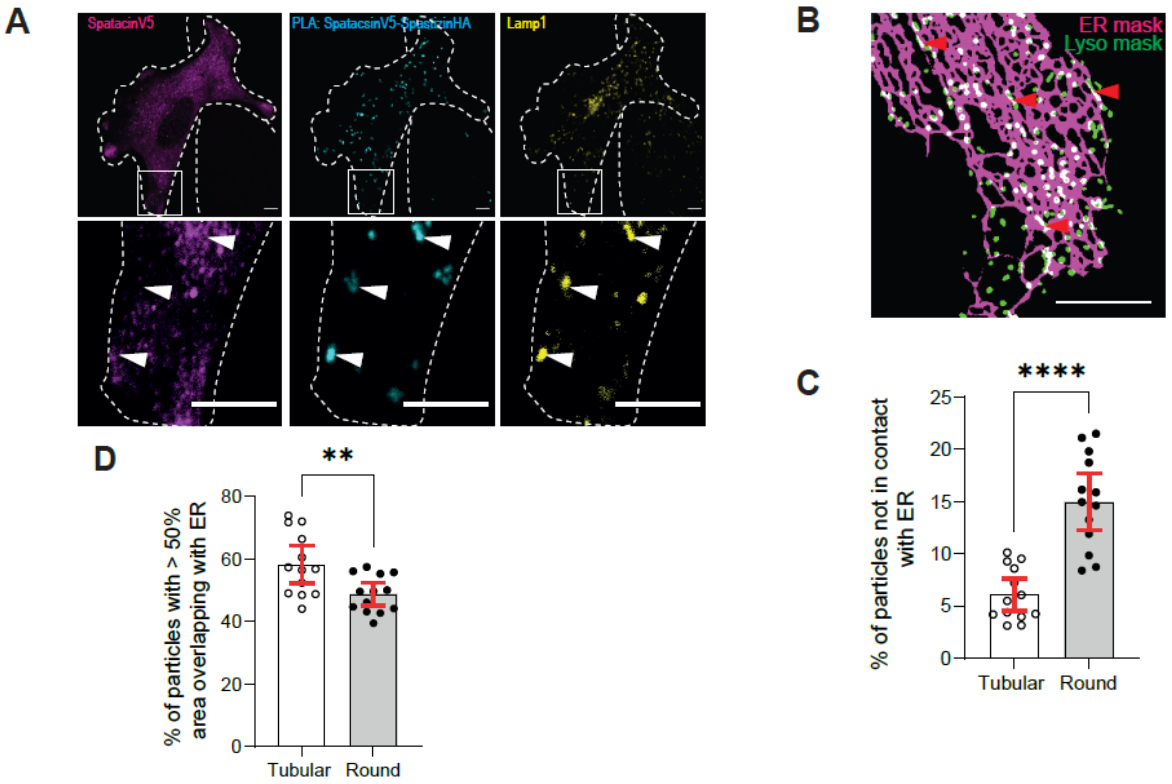

Figure 7. ER is a platform to promote the formation of tubular lysosomes and regulate their motility

A. *Proximity-ligation assay (PLA) showing the interaction between V5-tagged spatacsin and HA-tagged spastizin in wildtype MEFs. The PLA signal (cyan) is detected at the level of lysosomes immunostained with Lamp1 (arrowheads). Scale bar: 5 µm.*

B. *Binarized image of fibroblasts expressing GFP-Sec61 and Lamp1-mCherry. Note the strong overlap (white) between the ER (magenta) and lysosome (green) masks. Red arrowheads point to tubular lysosomes.*

C. *Quantification of the proportion of lysosomes free from contact with the ER depending on their shape. Mean and 95% CI, N = 13 cells from three independent experiments. ****P < 0.0001, unpaired t-test.*

D. *Quantification of the proportion of lysosomes that have an area overlapping with the ER > 50% based on their shape. Mean and 95% CI, N = 13 cells from three independent experiments. **P < 0.01, unpaired t-test.*

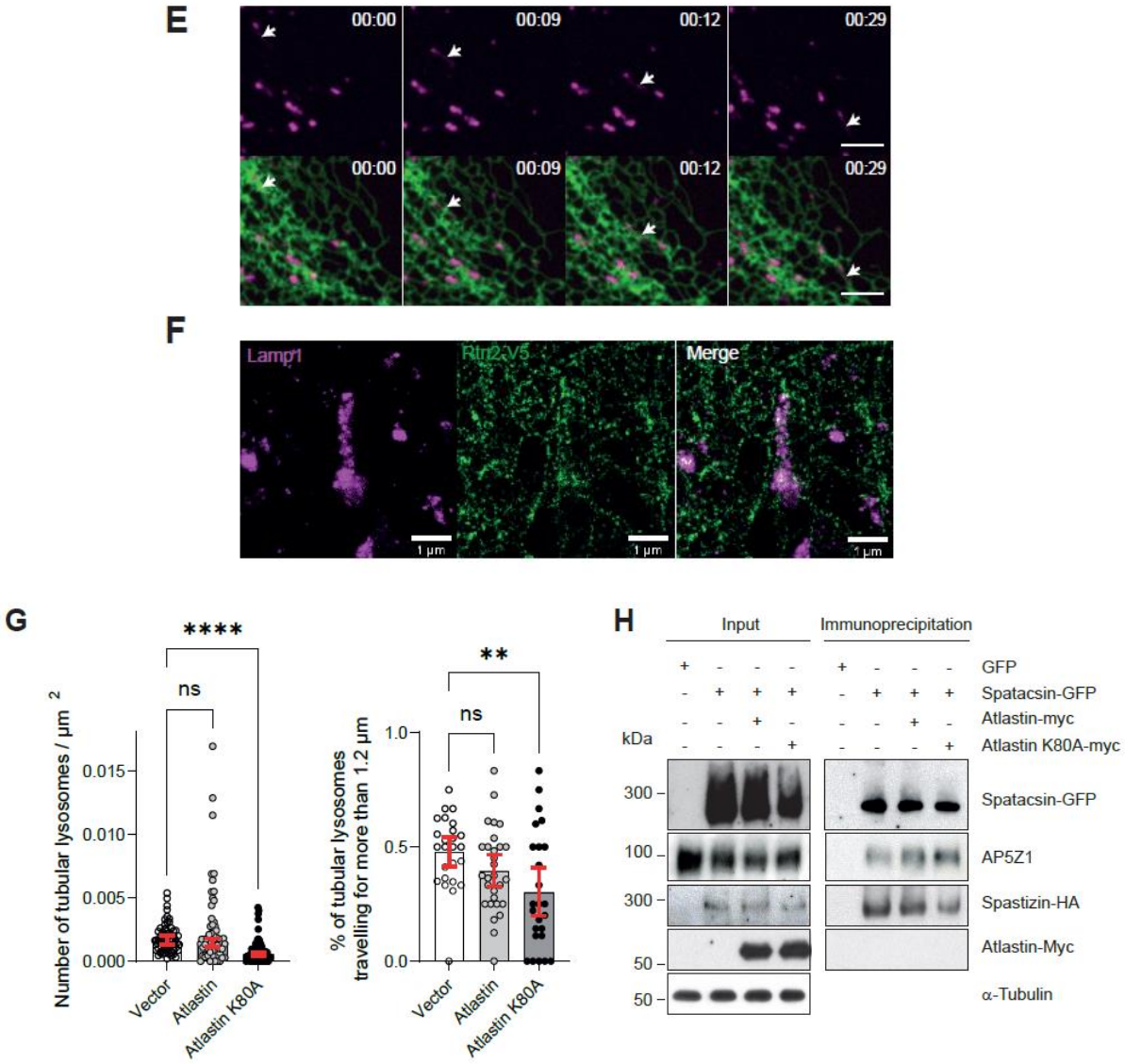

Figure 7. ER is a platform to promote the formation of tubular lysosomes and regulate their motility (second part)

E. Snapshot images of live imaging of a wildtype MEF transfected with Lamp1-mCherry (Magenta) and GFP-Sec-61β (Green). A tubular lysosome trafficking along the ER tubule network is indicated by an arrow. Scale bar: 5 µm.

F. STED image of a tubular lysosome stained with Lamp1 antibody and its close interaction with the ER tubular network stained by anti-V5 antibody targeting Reticulon2-V5 (Rtn2-V5) expressed in wildtype fibroblasts. Scale bar: 1 µm.

*G. Left: quantification of the number of tubular lysosomes in wildtype MEFs transfected with a vector overexpressing wildtype atlastin, or mutant atlastin K80A. Median and 95% CI, N = 61 cells from three independent experiments. ****P < 0.0001, Kruskall-Wallis test followed by Dunn's multiple comparison test. Right: proportion of tubular lysosomes moving > 1.2 µm. Mean and 95% CI, N = 25 cells from three independent experiments. **P = 0.0052, one-way ANOVA, Dunnett's comparison test.*

H. Western blots showing that the interaction of spatacsin-GFP with AP5Z1 and spastizin is modulated by the expression of mutant atlastin K80A.

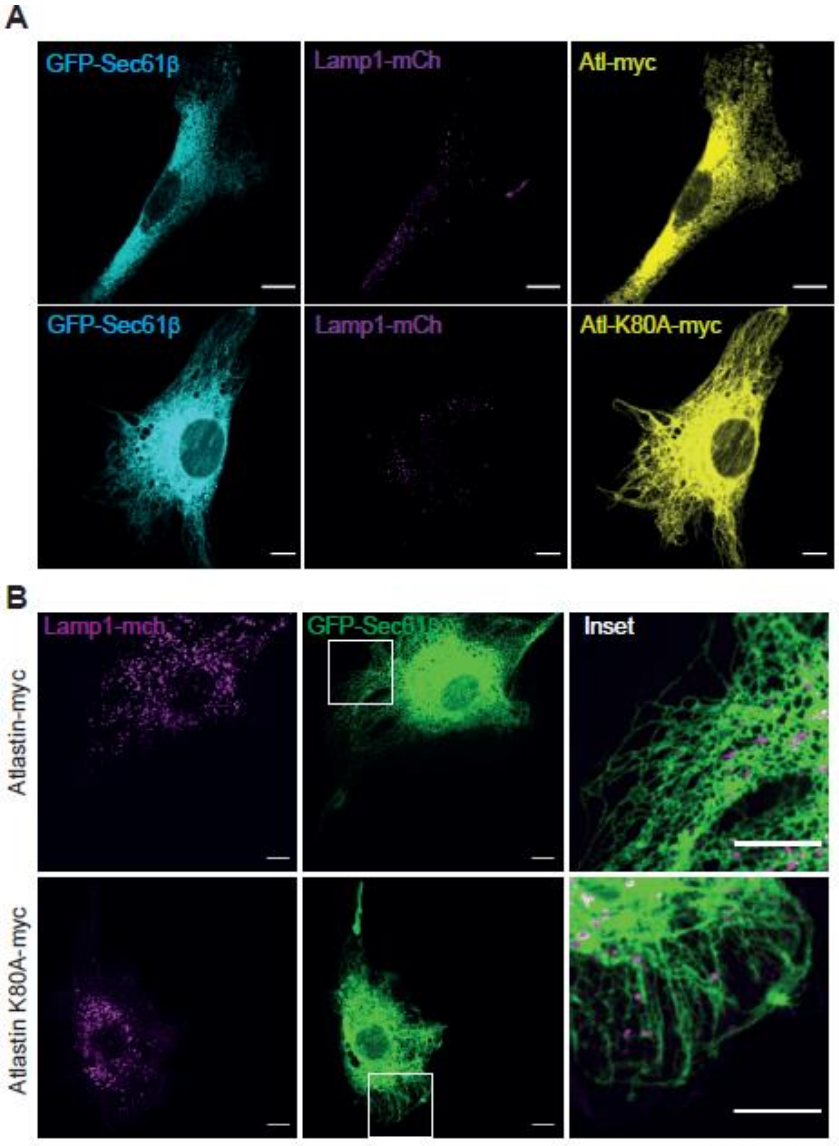

Supplementary Figure 7. Mutant atlastin K80A disrupts the ER network and lysosomal dynamics

A. *Anti-myc immunostaining of wildtype MEFs transfected with Lamp1-mCherry, GFP-Sec61□□ and either Atlastin-myc or mutant atlastin K80A-myc. All cells expressing Lamp1-mCherry and GFP-Sec61□ were positive for myc immunostaining.*

B. *Live imaging of MEFs expressing Lamp1-mCherry, GFP-Sec61□□ and either atlastin-myc or mutant atlastin K80A-myc. Note the change in ER morphology in MEFs co-transfected with atlastin K80A-myc*

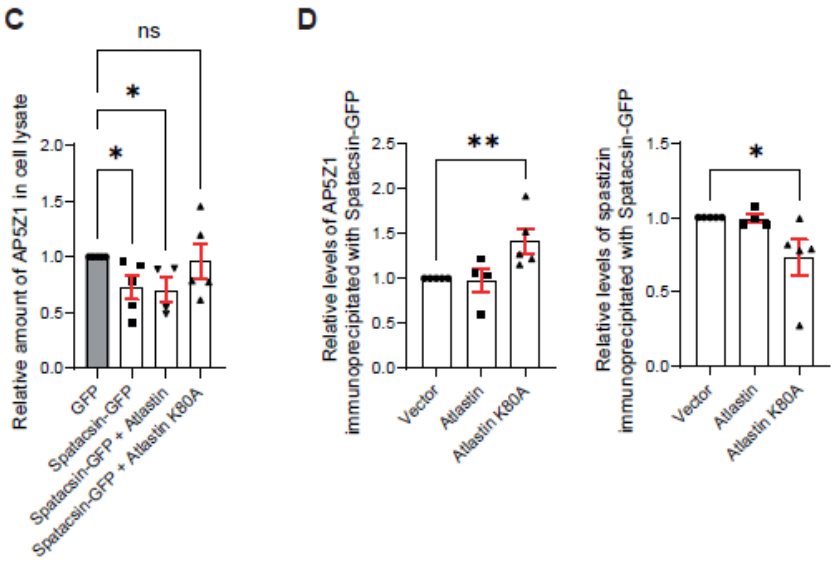

Supplementary Figure 7. Mutant atlastin K80A disrupts the ER network and lysosomal dynamics (second part)

*C. Quantification of Western blots showing that AP5Z1 levels are decreased upon expression of spatacsin GFP, which is blocked when cells are co-transfected with a vector expressing atlastin K80A. Mean ± SEM, *P < 0.05. Kruskall Wallis test.*

*D. Quantification of Western blots showing that the interaction of spatacsin-GFP with AP5Z1 and spastizin is modulated by expression of mutant atlastin K80A. Mean ± SEM, *P < 0.05, ** P< 0.01. Kruskall Wallis test followed by Dunn's multiple comparison test.*

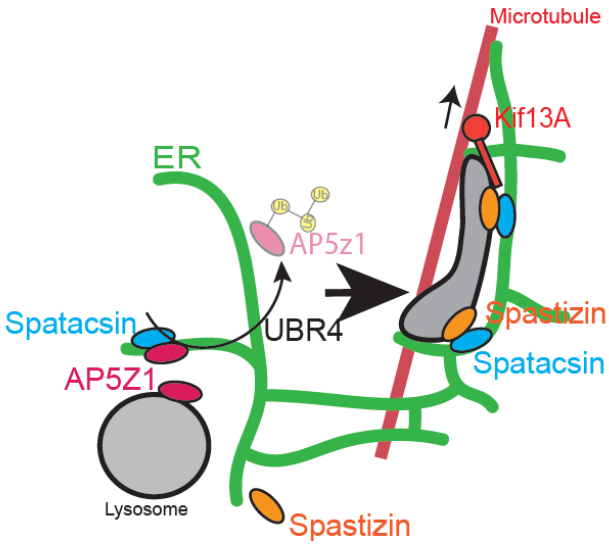

Figure 8. Scheme summarizing the molecular action of spatacsin.

Spatacsin is an ER-resident protein that mediates the degradation of AP5Z1 using accessory proteins such as UBR4. Upon degradation of AP5Z1, spatacsin can interact with spastizin at the levels of contact sites between ER and lysosomes. This allows the recruitment of the molecular motor KIF13A, which likely allows the formation of tubular lysosomes and their movement.

Discussion

The loss of spatacsin, involved in hereditary spastic paraplegia type SPG11, causes lysosomal dysfunction(Boutry et al., 2018; Branchu et al., 2017; Chang et al., 2014b; Varga et al., 2015). The molecular function of spatacsin has, thus far, remained elusive. Here, we used a combination of trained neural networks and targeted image analysis coupled to an siRNA screen to show that spatacsin function is associated with ubiquitin-mediated proteolysis. We demonstrate that spatacsin controls lysosome morphology and dynamics by acting at the contact sites between the ER and lysosomes and that this regulatory function of spatacsin relies on ubiquitin-dependent degradation of AP5Z1.

spatacsin is required for the formation and dynamics of tubular lysosomes. We identified a pool of lysosomes with a tubular shape that corresponds to dynamic lysosomes. Their mean velocity, which is > 0.3 µm/sec, is consistent with microtubule-based movement(Cordonnier et al., 2001). Furthermore, such tubular lysosomes rely on the presence of spastizin at the surface of lysosomes, which recruits the molecular motor KIF13A. KIF13A is a plus end-directed microtubule motor that allows the movement of vesicles toward the cell periphery(Nakagawa et al., 2000) and promotes the formation of tubules in recycling endosomes(Delevoye et al., 2014b). KIF13A likely contributes to the formation of tubular lysosomes by pulling on membranes, as shown in endosomes(Delevoye et al., 2016). This action may also participate in the motility of tubular lysosomes (Fig. 8). spastizin/KIF13A coupling to lysosomes by spatacsin may thus contribute to the trafficking of lysosomes toward the cell periphery and may explain the clustering of lysosomes around the nucleus when spatacsin is absent(Boutry et al., 2019b).

The formation of tubules emanating from lysosomes has also been observed after long-term starvation in ALR, a cellular process that relies on spatacsin and spastizin but appears to be independent of AP5Z1(Chang et al., 2014b). Starvation has been shown to promote lysosomal recruitment of spastizin in a Rag GTPase-dependent manner(Hirst et al., 2021b). The recruitment of spastizin to lysosomes may contribute to the formation of tubules in ALR. However, the lysosomal tubules observed in ALR and in our study may differ, as ALR tubules are catalytically inactive(Yu et al., 2010) and rely on the kinesin KIF5B for their formation(Du et al., 2016). This suggests that there are differences in lysosomal tubules that may be associated with different molecular motors possibly involved in different lysosomal functions(Pu et al., 2016).

The highly dynamic tubular lysosomes we observed in MEFs were strongly associated with the ER. Consistent with this finding, spatacsin was localized to the ER and likely interacted with lysosome-localized spastizin at the contact sites between the ER and lysosomes. Proteins present at the ER-Lysosomes contact sites, such as ORP1L, RNF26, and FYCO1, can change the cellular localization of lysosomes, depending on their molecular interactions(Jongsma et al., 2016b; Raiborg et al., 2015b; Rocha et al., 2009b). Our data show, for the first time, that proteins acting at contact sites between the ER and lysosomes regulate the motility of lysosomes along the ER network. Furthermore, the mechanisms that regulate the membrane contact sites are critical to understanding how they may respond to physiological stimuli(Venditti et al., 2021).

Our strategy of screening for the role of putative spatacsin partners in the formation of tubular lysosomes revealed an unexpected role for ubiquitin-dependent degradation in the function of spatacsin. We identified AP5Z1, known to interact with spatacsin and localized in lysosomes(Hirst et al., 2013a), as a protein degraded in a ubiquitin- and spatacsin-dependent manner to regulate tubular lysosome formation and motility. However, spatacsin required several its partners, such as UBR4, to mediate AP5Z1 degradation (Fig. 8).

AP5Z1 is a subunit of the adaptor protein complex AP5(Hirst et al., 2011b), which needs to be tightly regulated, as both its overexpression or downregulation impaired lysosome motility. Adaptor protein complexes recruit proteins to specific subcellular compartments to modulate intracellular trafficking(Sanger et al., 2019). Their activation relies on their interaction with specific cargo and transmembrane proteins. However, inactivation of these complexes is also important in the regulation of trafficking events. Phosphorylation has been proposed to inactivate AP1 and AP2 complexes(Beacham et al., 2019). AP5 may be negatively regulated by spatacsin in a ubiquitin-dependent manner through the degradation of at least one subunit of this complex. Our data suggest that AP5Z1, required for the formation of tubular lysosomes, must be degraded to allow the association of spastizin with lysosomes, which is mediated by spatacsin.

Importantly, the interaction of spatacsin with its partners, spastizin and AP5Z1, is modulated by the morphology of the ER network and could thus play a role in coupling ER morphology to lysosome function. The morphology of the ER was recently proposed to regulate the trafficking of lysosomes in the pre-axonal region to control the availability of axonal lysosomes in neurons(Özkan et al., 2021). As ER-resident spatacsin can control lysosome motility depending on ER morphology, it is possible that spatacsin could contribute to the regulation of lysosome trafficking in neurons. The absence of spatacsin in SPG11 patients and models may thus impair lysosome trafficking in axons, leading to their accumulation in the cell body. In the long term this could contribute to the lysosomal storage disorder that has been observed in *Spg11* knockout models and the brains of SPG11 patients(Boutry et al., 2018; Branchu et al., 2017; Denora et al., 2016b).

We thus identify spatacsin as a protein present at contact sites between the ER and lysosomes that is critical for the coordination of lysosome trafficking with ER network morphology. ER morphology and lysosome function are impaired in several forms of hereditary spastic paraplegia(Allison et al., 2017b; Darios et al., 2022). The results of this study, identifying a spatacsin-mediated link between ER shape and lysosome motility, may thus represent a unifying pathophysiological mechanism for a variety of hereditary spastic paraplegias.

Experimental procedures

Mouse models

The Spg11 knockout (*Spg11*$^{-/-}$) model has been previously described(Branchu et al., 2017). This model was generated by inserting two stop codons in exon 32, leading to the loss of expression of spatacsin, and can thus be considered as a functional Spg11 knockout. To obtain this mouse model, we created an intermediate model in which floxed exons 32 to 34 bearing the stop codons were inserted in the reverse orientation in intron 34(Branchu et al., 2017) (Suppl. Fig. 1A). RT-PCR of the transcripts followed by sequencing of brain and spleen samples showed this intermediate model to express the floxed allele, with the splicing of exons 32 to 34 and conservation of the reading frame between exon 31 and exon 35 (Suppl. Fig. 1B-C). It was thus equivalent to a functional deletion of exons 32-34 and was named *Spg11*$^{\Delta 32\text{-}34/\Delta 32\text{-}34}$.

Antibodies

The antibodies used for immunofluorescence and immunoblotting were rat anti-Lamp1 (clone 1D4B, Development Studies Hybridoma Bank, University of Iowa, USA, deposited by JT August), rabbit anti-V5 (Cat#8137, Sigma), mouse anti-V5 (Cat#Ab27671, Abcam), rat anti-HA (clone 3F10, Cat#**11867423001,** Merck), rabbit anti-HA (Cat#ab9110, Abcam), rabbit anti-GFP (Cat#6556, Abcam), mouse anti-Myc (clone 9E10, Development Studies Hybridoma Bank), rabbit anti-Stim1 (Cat#5668, Cell Signaling Technology), GRP78 (clone40/BiP, Cat#610978, BD Biosciences), rabbit anti-cathepsin D (Cat#Ab75852, Abcam), rabbit anti-spatacsin (Cat#16555-1-AP, ProteinTech), rabbit anti-spastizin (Cat#5023, ProSci), rabbit anti-AP5Z1 (Cat#HPA035693, Sigma), rabbit anti-calreticulin (Cat#SPA600F, Enzo Life Sciences), mouse anti-VDAC1 (Cat#Ab16814, Abcam), mouse anti-clathrin heavy chain (clone 23, Cat#610500, BD Biosciences), and rabbit anti-UBR4 (Cat#Ab86738, Abcam).

The secondary antibodies used for immunofluorescence were purchased from ThermoFisher: donkey anti-mouse IgG Alexa 488 (Cat#A21202), goat anti-rabbit IgG Alexa 555 (Cat#A21429) and goat anti-rat IgG Alexa 647 (Cat#A21247). For STED microcopy, the secondary antibodies were goat anti-rabbit IgG STAR 580 (Cat#ST580-1002, Abberior, Göttingen, Germany) and goat anti-mouse IgG STAR 635 (Cat#ST635-1001, Abberior). The secondary antibodies coupled to horseradish peroxidase used for immunoblotting were purchased from Jackson ImmunoResearch (Ely, UK): donkey anti-mouse IgG (Cat#JIR715-035-151) and donkey anti-rabbit IgG (Cat#**711-035-152**).

Plasmids

The spastizin-GFP vectors has been previously described(Hanein et al., 2008b). spastizin-HA was obtained by replacing GFP with an HA tag in the spastizin-GFP vector. A codon-optimized vector expressing human spatacsin was generated (Baseclear, Leiden, Netherlands) in a gateway compatible system (ThermoFisher). The cDNA was transferred by LR clonase into the pDest-47 vector (ThermoFisher), leading to a vector expressing spatacsin-GFP. Deletion of nucleotides 6013 to 6477 of optimized spatacsin cDNA resulted in spatacsin$^{32-34}$. C-terminal fragments of spatacsin (aa 1943-2433) and spatacsin$^{32-34}$ (aa 1943-2226) were amplified by PCR and inserted in the pDest-53 vector (ThermoFisher), leading to vectors that expressed GFP-spatacsin-Cter and GFP-spatacsin-Cter$^{32-34}$. The other plasmids used in the study were obtained from other laboratories or Addgene. GFP-Sec61 was obtained from G. Voeltz(Voeltz et al., 2006), AP5Z1-His from M Slabicki(Słabicki et al., 2010b, p. 48), ubiquitin-His and ubiquitin-K0-His from R. Baer(Wu-Baer et al., 2003), reticulon2-V5 from E. Reid(Montenegro et al., 2012), atlastin-Myc and atlastin K80A-Myc from J. Hu(Hu et al., 2009), KIF13A-YFP and KIF13A-ST-YFP from C. Delevoye(Delevoye et al., 2014b), and Lamp1-GFP (#16290) and Lamp1-mCherry (#45147) from Addgene.

siRNA

The siRNAs used to downregulate Spg11 were either On-target plus siRNAs (Dharmacon), with the sequences CAGCAGAGAGUUACGCCAA (#J-047107-09-0002) and CAGUAUGUGCCGGGAGAUA (#J-047107-12-0002), or from ThermoFisher, with the sequence GGUUCUACCAGGCUUCUAUtt (#s103130). The siRNAs used to downregulate Spg15 and AP5z1 were Silencer Select siRNAs form Thermofisher. For Spg15, the sequences were CUUCAACUCCUGCAACGAAtt (#s102537) and GAGCGAUACCAAGAGGUAAtt (#s102536). For AP5Z1, the sequences were GGAGCAGAGUAACCGGAGAtt (#s106997) and UCUGCUCCCGGGUCACUAAtt (#s106999). The siRNAs used to test the role of spatacsin interactors identified by the two-hybrid screen were Silencer Select siRNAs from ThermoFisher and are listed in Supplementary Table 3.

Subcellular fractionation of brain tissue

Mice were killed using CO_2 and the brains immediately dissected and rinsed twice in PBS at 4°C. Subcellular fractionation was performed according to a previously described procedure(Zhu et al., 2003). Dissected brains were homogenized in 0.32 M sucrose and 10 mM HEPES (pH 7.4) using a PFTE (**polytetrafluoroethylene**) pestle attached to a stirrer (Heidolph, Germany) rotating at 500 rpm. Lysates were centrifuged at 1,330 x *g* for 3 min, generating a pellet (P1) and a supernatant (S1). The S1 supernatant was centrifuged at 21,200 x *g* for 10 min, producing a pellet (P2) and a supernatant (S2). The S2 supernatant was then centrifuged at 200,000 x *g* for 1 h, generating a pellet (P3) and a supernatant (S3).

Isolation of the ER and lysosome-enriched fractions

Isolation of the ER and lysosome-enriched fractions was performed according to previously described protocols with several modifications(Bozidis et al., 2007; Graham, 2000). After killing mice using CO_2, the brains were immediately extracted and washed with PBS at 4°C. Brains were mechanically dissociated in 250 mM sucrose, 1 mM EDTA, 10 mM Hepes pH 7.4, 1 mM DTT and 25 mM KCl supplemented with a protease inhibitor cocktail (Thermofisher), as described for subcellular fractionation. Lysates were centrifuged at 800 x g for 5 min and the pellets discarded. The supernatant was centrifuged at 20,000 x g for 10 min and the resulting pellet A retained for lysosome isolation and the supernatant A for ER isolation. For lysosome isolation, pellet A was resuspended in 2 mL of the initial buffer and deposited on 10 ml of 27% Percoll solution in a 15-mL tube. After 90 min of centrifugation at 20,000 x g, the lysosomal fraction was visible close to the bottom of the tube and collected by pipetting. It was then resuspended in the initial buffer and centrifuged at 20,000 x g for 10 min. The pellet was resuspended in sample buffer and analyzed by western blotting.

To isolate the ER, supernatant A was deposited on a gradient of several sucrose solutions prepared in 10 mM Tris pH 7.4 and 0.1 mM EDTA. The sucrose concentrations of the three solutions were from the bottom up: 2 M, 1.5 M, and 1.3 M. The preparation was centrifuged for 70 min at 152,000 x g. After centrifugation, the ER-enriched fraction was found at the phase-limit between the 1.3 M sucrose solution and the 1.5 M sucrose solution. The fraction was collected and resuspended in the initial buffer and centrifuged for 45 min at 152,000 x g. The pellet was resuspended in sample buffer and analyzed by western blotting.

Membrane association assay

To determine the membrane association of spatacsin, we collected the P3 fraction obtained from the subcellular fractionation of the brains and followed a previously published protocol(Zhu et al., 2003). The membrane fraction was treated with one of the following solutions: 1 M NaCl and 25 mM phosphate buffer (pH 7.4); 100 mM glycine buffer (pH 2.8); 100 mM carbonate buffer (pH 11.0); or 1.0% sodium deoxycholate and centrifuged at 200,000 x *g* for 60 min. The final pellet and the supernatants analyzed by western blotting.

Mouse embryonic fibroblast cultures

Mouse embryonic fibroblasts were prepared using 14.5 day-old embryos obtained from the breeding of heterozygous (*Spg11*$^{+/-}$ or *Spg11*$^{+}$/$^{\Delta 32\text{-}34}$) mice as previously described(Boutry et al., 2019b). Comparisons between mutant and wildtype fibroblasts were always performed using fibroblasts originating from embryos of the same breeding. All experiments were performed with fibroblasts between passages 4 and 6.

Transfection

Fibroblasts were transfected using the NEON transfection system (ThermoFisher) with one pulse of 30 ms at 1350 V, according to manufacturer instructions. Cells (5 x 10^5) were transfected with 5 µg plasmid and used 24 h later. When we co-transfected a vector expressing a fluorescent protein together with a vector expressing a non-fluorescent protein for live imaging, we imaged cells expressing the fluorescent protein and then fixed the cells afterwards to verify that > 95% of cells expressing the fluorescent marker were also positive for the nonfluorescent protein by immunostaining. For transfection with siRNA, 50 x 10^3 cells were transfected with 1 pmol siRNA and analyzed after 48 h in culture.

Chemicals

Lysotracker Green and Red (Thermofisher) were used at 50 nM for 30 min to stain acidic lysosomes in fibroblasts. DQ-Red-BSA and DQ-Green-BSA (Thermofisher) were added to the culture medium at 2 µg/ml 1 h before imaging and then washed once with culture medium. Texas-Red conjugated dextran (10,000 MW –Thermofisher) was added to the culture medium at 100 µg/ml and the cells incubated for 4 h to allow its internalization by endocytosis and chased for 24 h to stain the lysosomal compartment. The PI3 kinase inhibitor wortmannin (Sigma) was used at 100 nM for 1 h.

Immunofluorescence

Cells were fixed in 4% PFA in PBS for 20 min and then permeabilized for 5 min in PBS containing 0.2% v/v Triton X-100. Cells were then blocked for 45 min in PBS with 5% w/v BSA (PBS-BSA) and incubated with primary antibodies in PBS-BSA overnight at 4°C. Cells were washed three times with PBS and incubated with secondary antibodies coupled to fluorophores. After three washes with PBS, glass coverslips were then mounted on glass slides using Prolong Gold antifade reagent (ThermoFisher).

Confocal microscopy

Images of immunofluorescence were acquired using an inverted laser scanning Leica SP8 confocal microscope (Mannheim, Germany) with a 63X objective N.A. 1.40. STED microscopy was performed using a Stedycon device (Abberior) mounted on an inverted Zeiss Imager M2 microscope, with a 100X objective N.A. 1.46.

For live imaging, cells were imaged at 37°C and 5% CO2 using a Leica DMi8 inverted spinning disk confocal microscope equipped with 63X objective N.A. 1.40 and a Hamamatsu Orca flash 4.0 camera. Timelapses of cells were acquired to analyze the trajectories of the lysosomes with one image taken every 1 s for 1 min.

Two-Hybrid screen

The yeast two-hybrid screen was performed by Hybrigenics (Paris, France) using an adult human cDNA brain library. The bait was either the complete 1943-2443 domain of human spatacsin or the same domain lacking the amino acids encoded by exons 32 to 34.

Image analysis

Measurement of particle clustering around the nucleus

Lysosomes were stained for the expression of Lamp1-mCherry, and images captured using a spinning disk confocal microscope. The particles were then detected and individualized using the Spot Detector plugin of ICY software. Spots were detected using a scale of three pixels and a sensitivity of 140. A size filter discarded all particles with an area < 10 pixels. The result was exported as a binary image. The distance between the centroid of each particle and the centroid of the nucleus was measured using MATLAB software, as described previously(Boutry et al., 2019b).

Tubular lysosome detection

After detecting lysosomal particles using Spot Detector, the *regionprops* function of the MATLAB Image Processing Toolbox was used to determine the shape characteristics of the particles on the binary images. Tubular lysosomes were defined as follows: circularity < 0.5, eccentricity > 0.9, and a width/length ratio > 4. The selected particles were saved in a new image. To screen the effect of siRNAs on tubular lysosomes, we defined a tubulation index, for which we normalized the number of tubular lysosomes/μm^2 to a value ranging from 0 to 1, corresponding to the average number of tubular lysosomes/μm^2 quantified in *Spg11*$^{-/-}$ and *Spg11*$^{+/+}$ fibroblasts analyzed in the same experiment.

Lysosome trajectory analysis

Analysis of the movement and trajectories of lysosomes was performed on the 60 timelapse images. First, to analyze the trajectory characteristics of round and tubular lysosomes particles, the particles were labeled by hand using the multipoint tool of Fiji software to extract their coordinates. The length of the trajectory and the mean speed were then computed using MATLAB. We then performed automated analysis solely for tubular lysosomes using MATLAB software. The *regionprops* function was used to detect the position of the centroids of tubular lysosomes during the timelapse. Once the coordinates were obtained, they were analyzed using John C. Crocker *track.pro* 'freeware' MATLAB function to determine the characteristics of the particle trajectories, considering that the maximum theoretical displacement of a particle between two frames was the approximate size of one tubular lysosome, hence 2.4 µm – 20 pixels. Then, the total distance that each particle traveled, its speed during the movement, and its lifetime were calculated.

Measurement of the area of the ER-Lysosomes overlap

The binarization of lysosomal staining was performed using Spot Detector. The binarization of ER staining was performed using the ImageJ thresholding tool. Once the two binary images were obtained, they were compared using MATLAB and the area of overlap between the two stainings per particle was measured using the *regionprops* function.

Image classification by a neural network

Lysosomes of *Spg11*$^{+/+}$ and *Spg11*$^{-/-}$ fibroblasts, as well as *Spg11*$^{+/+}$ fibroblasts transfected with siRNAs, were stained using Texas-Red conjugated dextran. Images were acquired using a spinning disk confocal microscopy, generating an image library.

To train the Spg11 classification model, Tensorflow (https://www.tensorflow.org/?hl=fr) and Scikit-learn (https://scikit-learn.org/stable/) Python libraries were used. Images of lysosomes of *Spg11*$^{-/-}$ (n = 742 cells) and *Spg11*$^{+/+}$ (n = 735 cells) MEFs were used as a database. Training and test sets were generated randomly with a test set size of 15% (111 *Spg11*$^{+/+}$ fibroblast images and 112 *Spg11*$^{-/-}$ fibroblast images). Initial images of 921x1024 pixels were resized to 224x224 pixels to reduce input size while retaining consistent information. Data augmentation was performed using flip Tensorflow functions to improve training and artificially increase the number of images. Finally, the image pixel values were normalized between 0 and 1. The transfer learning approach was used to avoid model training from scratch. The VGG16 (Simonyan and Zisserman, 2015) neural network structure was used and downloaded using the TensorFlow hub library (https://www.tensorflow.org/hub?hl=fr). VGG16 is a convolutional neural network model trained on ImageNet, which is a dataset of over 14 million images belonging to 1,000 classes. The top three layers were excluded and replaced with three other layers: one dense layer of 512 neurons, a dropout layer, and a 64-neuron layer. The final layer was the soft-max layer. The neural network was trained using a NVIDIA GeForce GTX 1050 Ti for 150 epochs, with a starting learning rate at 0.0001 and a batch size at 32. Model evaluation resulted in 79.5% total accuracy on the test set.

The trained model was used to predict the probability of the cell to be considered as a *Spg11*$^{-/-}$ fibroblast for each image of fibroblast transfected with siRNA. For each siRNA, the arithmetic mean of the probability was calculated.

Protein extraction from cells

MEFs were washed twice with PBS and lysed in 100 mM NaCl, 20 mM Tris pH7.4, 2 mM $MgCl_2$, 1% SDS, and 0.1% Benzonase (Sigma). Samples were centrifuged at 17,000 x g for 15 min and the supernatants recovered as solubilized proteins. The protein concentration was determined using the BCA assay kit (Thermofisher).

Western Blotting

Protein lysates supplemented with sample buffer (final concentration 80 mM TrisHCl pH 6.8, 10 mM DTT, 2% SDS, 10% glycerol) were separated on 3-8% Tris-acetate or 4-12 Bis-Tris gels (Thermofisher). Proteins were then transferred to PVDF membranes (Merck). Membranes were then incubated in Ponceau red for 5 min and blocked in PBS-0.02% Tween (PBST) with 5% milk for 45 min. The membranes were incubated with primary antibodies in PBST-5% milk overnight at 4°C. Secondary antibodies were conjugated with HRP (Jackson Lab) and the signals visualized using chemiluminescent substrates (SuperSignal West Dura/Femto; Thermofisher). The chemiluminescent signal was then acquired on Amersham Hyperfilm ECL. Signal intensities of the western blots were quantified using the ImageJ gel analysis plugin.

Co-immunoprecipitation

Cells were lysed on ice in 100 mM NaCl, 20 mM Tris pH7.4, 1 mM $MgCl_2$, and 0.1% NP40 supplemented with a protease inhibitor cocktail. Samples were centrifuged at 17,000 x g for 15 min at 4°C. Ten percent of the supernatant was retained, supplemented with sample buffer, and was used to monitor protein quantity for the inputs. The remaining 90% of the supernatants was incubated with 10 µL of GFP-trap beads (Chromotek, Germany) for 90 min using a rotating wheel at 4°C. Beads were washed 4 times in lysis buffer and supplemented with sample buffer with DDT. Beads and inputs were then analyzed by western blotting.

Proximity Ligation Assay

MEFs were fixed in PBS containing 4% PFA for 15 min. The Duolink Proximity Ligation Assay (PLA, Sigma) was then performed according to the manufacturer's instructions. After performing the PLA reaction, we immuno-stained the cells with fluorescent secondary antibodies to detect transfected cells and used the Prolong Gold antifade mounting medium (Thermofisher) instead of the Duolink in situ mounting medium provided with the kit.

Statistics

Data were analyzed using GraphPad Prism version 9 software. Comparisons of the ranks were performed using nonparametric tests for sample sets with $N < 10$. Mann-Whitney tests were used to compare two sets of data and Kruskall-Wallis tests to compare more than two sets of data. Data normality was assessed using the D'Agostino-Pearson test for sample sets with $N > 10$. Comparisons of the medians were performed by Mann-Whitney or Kruskall-Wallis tests for nonnormally distributed data. Comparisons of the means were performed by unpaired t-tests or ANOVA followed by Sidak's multiple comparisons test for normally distributed data.

Acknowledgments

We thank the Phenoparc, Celis, and ICM.quant core facilities of the Paris Brain Institute for their contributions. This work was supported by “Investissements d’Avenir” program [ANR-10-IAIHU-06] and [ANR-11-INBS-0011] grants and received funding from the European Research Council (European Research Council Starting [grant No 311149] to F.D.). M.B. received a fellowship from the French Ministry of Research (doctoral school ED3C). A.P. received an ARDOC fellowship from the Région Ile de France (grant 17012953; doctoral school ED3C) and a fellowship from the Fondation pour la Recherche Médicale (grant FDT202001010829).

References

1. Ballabio, A. & Bonifacino, J. S. Lysosomes as dynamic regulators of cell and organismal homeostasis. Nat Rev Mol Cell Biol 21, 101–118 (2020).

2. Pu, J., Guardia, C. M., Keren-Kaplan, T. & Bonifacino, J. S. Mechanisms and functions of lysosome positioning. Journal of Cell Science jcs.196287 (2016) doi:10.1242/jcs.196287.

3. Hipolito, V. E. B., Ospina-Escobar, E. & Botelho, R. J. Lysosome remodelling and adaptation during phagocyte activation. Cellular Microbiology 20, e12824 (2018).

4. Bonifacino, J. S. & Neefjes, J. Moving and positioning the endolysosomal system. Current Opinion in Cell Biology 47, 1–8 (2017).

5. Yu, L. et al. Termination of autophagy and reformation of lysosomes regulated by mTOR. Nature 465, 942–946 (2010).

6. Du, W. et al. Kinesin 1 Drives Autolysosome Tubulation. Developmental Cell 37, 326–336 (2016).

7. Boes, M. et al. T-cell engagement of dendritic cells rapidly rearranges MHC class II transport. Nature 418, 983–988 (2002).

8. Wang, W. et al. A voltage-dependent K+ channel in the lysosome is required for refilling lysosomal Ca2+ stores. Journal of Cell Biology 216, 1715–1730 (2017).

9. Wilhelm, L. P. et al. STARD 3 mediates endoplasmic reticulum-to-endosome cholesterol transport at membrane contact sites. EMBO J 36, 1412–1433 (2017).

10. Spits, M. et al. Mobile late endosomes modulate peripheral endoplasmic reticulum network architecture. EMBO Rep 22, (2021).

11. Jongsma, M. L. M. et al. An ER-Associated Pathway Defines Endosomal Architecture for Controlled Cargo Transport. Cell 166, 152–166 (2016).

12. Raiborg, C. et al. Repeated ER–endosome contacts promote endosome translocation and neurite outgrowth. Nature 520, 234–238 (2015).

13. Rocha, N. et al. Cholesterol sensor ORP1L contacts the ER protein VAP to control Rab7–RILP–p150Glued and late endosome positioning. Journal of Cell Biology 185, 1209–1225 (2009).

14. Allison, R. et al. Defects in ER–endosome contacts impact lysosome function in hereditary spastic paraplegia. J. Cell Biol. 216, 1337–1355 (2017).

15. Rowland, A. A., Chitwood, P. J., Phillips, M. J. & Voeltz, G. K. ER Contact Sites Define the Position and Timing of Endosome Fission. Cell 159, 1027–1041 (2014).

16. Özkan, N. et al. ER – lysosome contacts at a pre-axonal region regulate axonal lysosome availability. Nat Commun 12, 4493 (2021).

17. Cabukusta, B. & Neefjes, J. Mechanisms of lysosomal positioning and movement. Traffic 19, 761–769 (2018).

18. Oyarzún, J. E. et al. Lysosome motility and distribution: Relevance in health and disease. Biochimica et Biophysica Acta (BBA) - Molecular Basis of Disease 1865, 1076–1087 (2019).

19. Stevanin, G. et al. Mutations in SPG11, encoding spatacsin, are a major cause of spastic paraplegia with thin corpus callosum. Nat Genet 39, 366–372 (2007).

20. Murmu, R. P. et al. Cellular distribution and subcellular localization of spatacsin and spastizin, two proteins involved in hereditary spastic paraplegia. Molecular and Cellular Neuroscience 47, 191–202 (2011).

21. Hirst, J. et al. Interaction between AP-5 and the hereditary spastic paraplegia proteins SPG11 and SPG15. Mol Biol Cell 24, 2558–2569 (2013).

22. Boutry, M. et al. Loss of spatacsin impairs cholesterol trafficking and calcium homeostasis. Commun Biol 2, 380 (2019).

23. Chang, J., Lee, S. & Blackstone, C. Spastic paraplegia proteins spastizin and spatacsin mediate autophagic lysosome reformation. J. Clin. Invest. 124, 5249–5262 (2014).

24. Patto, A. L. & O'Kane, C. J. Distant homologies and domain conservation of the Hereditary Spastic Paraplegia protein SPG11/ALS5/spatacsin. http://biorxiv.org/lookup/doi/10.1101/2020.03.08.982389 (2020) doi:10.1101/2020.03.08.982389.

25. Hanein, S. et al. Identification of the SPG15 Gene, Encoding spastizin, as a Frequent Cause of Complicated Autosomal-Recessive Spastic Paraplegia, Including Kjellin Syndrome. The American Journal of Human Genetics 82, 992–1002 (2008).

26. Słabicki, M. et al. A Genome-Scale DNA Repair RNAi Screen Identifies SPG48 as a Novel Gene Associated with Hereditary Spastic Paraplegia. PLoS Biol 8, e1000408 (2010).

27. Hirst, J., Hesketh, G. G., Gingras, A.-C. & Robinson, M. S. Rag GTPases and phosphatidylinositol 3-phosphate mediate recruitment of the AP-5/SPG11/SPG15 complex. Journal of Cell Biology 220, e202002075 (2021).

28. Hirst, J., Itzhak, D. N., Antrobus, R., Borner, G. H. H. & Robinson, M. S. Role of the AP-5 adaptor protein complex in late endosome-to-Golgi retrieval. PLoS Biol 16, e2004411 (2018).

29. Branchu, J. et al. Loss of spatacsin function alters lysosomal lipid clearance leading to upper and lower motor neuron degeneration. Neurobiology of Disease 102, 21–37 (2017).

30. Khundadze, M. et al. A mouse model for SPG48 reveals a block of autophagic flux upon disruption of adaptor protein complex five. Neurobiology of Disease 127, 419–431 (2019).

31. Khundadze, M. et al. A Hereditary Spastic Paraplegia Mouse Model Supports a Role of ZFYVE26/SPASTIZIN for the Endolysosomal System. PLoS Genet 9, e1003988 (2013).

32. Varga, R.-E. et al. In Vivo Evidence for Lysosome Depletion and Impaired Autophagic Clearance in Hereditary Spastic Paraplegia Type SPG11. PLOS Genetics 11, e1005454 (2015).

33. Zhu, P.-P. et al. Cellular Localization, Oligomerization, and Membrane Association of the Hereditary Spastic Paraplegia 3A (SPG3A) Protein Atlastin. J. Biol. Chem. 278, 49063–49071 (2003).

34. Boutry, M. et al. Inhibition of Lysosome Membrane Recycling Causes Accumulation of Gangliosides that Contribute to Neurodegeneration. Cell Reports 23, 3813–3826 (2018).

35. Marwaha, R. & Sharma, M. DQ-Red BSA Trafficking Assay in Cultured Cells to Assess Cargo Delivery to Lysosomes. BIO-PROTOCOL 7, (2017).

36. Cordonnier, M.-N., Dauzonne, D., Louvard, D. & Coudrier, E. Actin Filaments and Myosin I Alpha Cooperate with Microtubules for the Movement of Lysosomes. MBoC 12, 4013–4029 (2001).

37. Wu-Baer, F., Lagrazon, K., Yuan, W. & Baer, R. The BRCA1/BARD1 Heterodimer Assembles Polyubiquitin Chains through an Unconventional Linkage Involving Lysine Residue K6 of Ubiquitin. Journal of Biological Chemistry 278, 34743–34746 (2003).

38. Sriram, S. M., Kim, B. Y. & Kwon, Y. T. The N-end rule pathway: emerging functions and molecular principles of substrate recognition. Nat Rev Mol Cell Biol 12, 735–747 (2011).

39. Sagona, A. P. et al. PtdIns(3)P controls cytokinesis through KIF13A-mediated recruitment of FYVE-CENT to the midbody. Nat Cell Biol 12, 362–371 (2010).

40. Delevoye, C. et al. Recycling Endosome Tubule Morphogenesis from Sorting Endosomes Requires the Kinesin Motor KIF13A. Cell Reports 6, 445–454 (2014).

41. Hu, J. et al. A Class of Dynamin-like GTPases Involved in the Generation of the Tubular ER Network. Cell 138, 549–561 (2009).

42. Nakagawa, T. et al. A Novel Motor, KIF13A, Transports Mannose-6-Phosphate Receptor to Plasma Membrane through Direct Interaction with AP-1 Complex. Cell 103, 569–581 (2000).

43. Delevoye, C. et al. BLOC-1 Brings Together the Actin and Microtubule Cytoskeletons to Generate Recycling Endosomes. Current Biology 26, 1–13 (2016).

44. Venditti, R., Wilson, C. & De Matteis, M. A. Regulation and physiology of membrane contact sites. Current Opinion in Cell Biology 71, 148–157 (2021).

45. Hirst, J. et al. The Fifth Adaptor Protein Complex. PLoS Biol 9, e1001170 (2011).

46. Sanger, A., Hirst, J., Davies, A. K. & Robinson, M. S. Adaptor protein complexes and disease at a glance. J Cell Sci 132, jcs222992 (2019).

47. Beacham, G. M., Partlow, E. A. & Hollopeter, G. Conformational regulation of AP1 and AP2 clathrin adaptor complexes. Traffic 20, 741–751 (2019).

48. Denora, P. S. et al. Motor neuron degeneration in spastic paraplegia 11 mimics amyotrophic lateral sclerosis lesions. Brain aww061 (2016) doi:10.1093/brain/aww061.

49. Darios, F., Coarelli, G. & Durr, A. Genetics in hereditary spastic paraplegias: Essential but not enough. Current Opinion in Neurobiology 72, 8–14 (2022).

50. Voeltz, G. K., Prinz, W. A., Shibata, Y., Rist, J. M. & Rapoport, T. A. A Class of Membrane Proteins Shaping the Tubular Endoplasmic Reticulum. Cell 124, 573–586 (2006).

51. Montenegro, G. et al. Mutations in the ER-shaping protein reticulon 2 cause the axon-degenerative disorder hereditary spastic paraplegia type 12. J. Clin. Invest. 122, 538–544 (2012).

52. Bozidis, P., Williamson, C. D. & Colberg-Poley, A. M. Isolation of Endoplasmic Reticulum, Mitochondria, and Mitochondria-Associated Membrane Fractions from Transfected Cells and from Human Cytomegalovirus-Infected Primary Fibroblasts. Current Protocols in Cell Biology 37, (2007).

53. Graham, J. M. Isolation of Lysosomes from Tissues and Cells by Differential and Density Gradient Centrifugation. Current Protocols in Cell Biology 7, (2000).

54. Simonyan, K. & Zisserman, A. Very Deep Convolutional Networks for Large-Scale Image Recognition. arXiv:1409.1556 [cs] (2015)

Gene name	siRNA#1	siRNA#2	Mean
ENC1	**0.48**	**0.45**	**0.47**
EEf1D	**0.70**	0.19	**0.45**
EP400	**0.40**		**0.40**
ARHGEF6	**0.50**	**0.28**	**0.39**
PSMD2	**0.37**	**0.39**	**0.38**
RNF31	**0.43**	**0.26**	**0.35**
YWHAH	0.20	**0.47**	**0.33**
ANXA7	**0.34**	**0.32**	**0.33**
ARIH2	**0.22**	**0.42**	**0.32**
HIPK2	**0.37**	**0.27**	**0.32**
EXOC7	**0.37**	**0.26**	**0.31**
COPS4	**0.42**	0.19	**0.31**
SMARCE1	**0.24**	**0.34**	**0.29**
VCPIP1		**0.28**	**0.28**
LDHA	**0.31**	**0.23**	**0.27**
UBR4	**0.30**	**0.24**	**0.27**
MKRN3	0.17	**0.35**	**0.26**
KDM5D	**0.26**	**0.25**	**0.25**
MAP3K11	**0.29**	0.19	**0.24**
SPG7	**0.23**	**0.23**	**0.23**
SPTBN1	0.20	**0.26**	**0.23**
ALDOA	0.20	**0.26**	**0.23**
MYCBP2	0.10	**0.33**	**0.22**
USP8	**0.27**	0.16	**0.21**
TRIP12	0.20	**0.23**	**0.21**
USP14	**0.29**	0.13	0.21
MOAP1	0.16	**0.24**	0.20
NEFL	**0.23**	0.17	0.20
PDS5B	0.20	0.17	0.18
PIK3CB	0.10	**0.26**	0.18
CARS2	**0.23**	0.13	0.18
IFT172	**0.23**	0.10	0.16
VPS8	0.13	0.19	0.16
TIAM1	0.17	0.13	0.15
TRP53BP1	0.10	0.20	0.15
PBXIP1	0.13	0.10	0.11
BLZF1	0.06	**0.23**	0.14
FRY	0.17	0.10	0.13
IFI30	0.07	0.20	0.13
DMAP1	0.10	0.16	0.13
SPARCL1	0.13	0.11	0.12
KCTD9	0.19	0.03	0.11
CLU	0.10	0.10	0.10
KCNAB2	0.10	0.07	0.08
TTC8	0.03	0.03	0.03

Supplementary table 1**.** *Unbiased analysis of the effect of siRNAs that downregulate genes encoding putative binding partners of the domain of spatacsin encoded by exons 32-34 of SPG11. The scores represent the probability of phenocopying Spg11$^{-/-}$ MEFs (see methods). Bold indicates genes that are at least as efficient as three independent Spg11 siRNAs (SPG11#1: 0.36, SPG11#2: 0.2, SPG11#3: 0.26).*

Gene name	siRNA#1	siRNA#2	Mean
PSMD2	**0.08**	**0.37**	**0.22**
UBR4	**0.17**	**0.31**	**0.24**
ARHGEF6	**0.42**	**0.14**	**0.28**
EEf1D	**0.39**	**0.28**	**0.34**
IFT172	**0.31**	**0.40**	**0.36**
FRY	**0.34**	**0.46**	**0.40**
BLZF1	**0.42**	**0.42**	**0.42**
USP8	**0.38**	**0.47**	**0.42**
TRIP12	0.56	**0.35**	**0.46**
KDM5D	**0.36**	0.60	**0.48**
ENC1	0.71	**0.38**	**0.55**
RNF31	0.67	**0.48**	0.57
COPS4	**0.48**	0.7	0.59
VCPIP1		0.59	0.59
EXOC7	0.72	**0.47**	0.60
KCTD9	0.62	0.62	0.62
TTC8	0.72	**0.52**	0.62
SMARCE1	0.68	0.63	0.66
SPARCL1	0.73	0.58	0.66
NEFL	0.76	0.59	0.68
TIAM1	0.87	0.58	0.72
KCNAB2	0.85	0.73	0.79
USP14	0.66	0.92	0.79
TRP53BP1	0.88	0.73	0.81
LDHA	0.64	1	0.82
PDS5B	0.82	0.83	0.82
PBXIP1	**0.45**	1.29	0.87
CARS2	0.67	1.10	0.88
HIPK2	0.82	0.95	0.88
YWHAH	0.69	1.09	0.89
EP400	0.89		0.89
MYCBP2	1.07	0.80	0.93
CLU	1.22	0.66	0.94
IFI30	1.13	0.82	0.98
SPTBN1	1.09	0.97	1.03
MKRN3	1.09	0.98	1.04
DMAP1	1.41	0.68	1.05
ANXA7	1.01	1.10	1.06
ARIH2	1.12	1.10	1.11
ALDOA	1.08	1.19	1.13
MOAP1	1.10	1.15	1.13
PIK3CB	1.60	0.66	1.13
VPS8	1.20	1.08	1.14
MAP3K11	1.46	0.89	1.18
SPG7	0.92	1.55	1.23

Supplementary Table 2. *Analysis of the proportion of tubular lysosomes in control MEFs transfected with siRNA that downregulate genes encoding putative binding partners of the domain of spatacsin encoded by exons 32 to 34 of SPG11. The scores represent the normalized number of tubules (score = 1 for control MEFS, score = 0 for Spg11$^{-/-}$ MEFS). Bold indicates genes that are at least as efficient as three independent Spg11 siRNA (SPG11#1: 0.55, SPG11#2: 0.43, SPG11#3: 0.50) in decreasing the proportion of tubular lysosomes.*

Supplementary Table 3 : list of genes invalidated during the siRNA mini-screen

Location (Row-Col)	RefSeq Accession Number	Gene Symbol	Full Gene Name	Gene ID	siRNA ID	Exon(s) Targeted	Sense siRNA Sequence	Antisense siRNA Sequence
A1	NM_007438	Aldoa	aldolase A, fructose-bisphosphate	11674	s62248	6	GCAUUGUACCCAUUGUGGAtt	UCCACAAUGGGUACAAUGCca
A2	NM_009674	Anxa7	annexin A7	11750	s62362	Not Determined	GGCUAAUCGCGAUUUGCUAtt	UAGCAAAUCGCGAUUAGCCat
A8	NM_152801	Arhgef6	Rac/Cdc42 guanine nucleotide exchange	73341	s91692	19	GAUUCUUAAGGUGAUCGAAtt	UUCGAUCACCUUAAGAAUCtg
A9	NM_011790	Arih2	ariadne homolog 2 (Drosophila)	23807	s76477	Not Determined	GGAAGACGCAUGGUAGUGAtt	UCACUACCAUGCGUCUUCCag
A10	NM_025505	Blzf1	basic leucine zipper nuclear factor 1	66352	s83070	Not Determined	CGAGUACAGACAGAGAUAAtt	UUAUCUCUGUCUGUACUCGga
A11	XM_906739	Cars2	cysteinyl-tRNA synthetase 2	71941	s206416	Not Determined	CAUGCAUACUCGACAGCUAtt	UAGCUGUCGAGUAUGCAUGgc
B2	NM_013492	Clu	clusterin	12759	s64077	Not Determined	GAAGAAGUCUCUAAGGAUAtt	UAUCCUUAGAGACUUCUUCtg
B3	NM_012001	Cops4	COP9 (constitutive photomorphogenic)	26891	s77325	5	GAACGAAUCCACAAAUGAAtt	UUCAUUUGUGGAUUCGUUCtg
B5	NM_023178	Dmap1	DNA methyltransferase 1-associated protein	66233	s82845	4	GCUUCGUAGUUAUUCACGAtt	UCGUGAAUAACUACGAAGCgc
B7	NM_023240	Eef1d	eukaryotic translation elongation factor 1	66656	s83645	6,8	CACCAGCAGAGGACGAUGAtt	UCAUCGUCCUCUGCUGGUGtg
B8	NM_007930	Enc1	ectodermal-neural cortex 1	13803	s65503	2	CCAUCAACAUCUACCUGUUtt	AACAGGUAGAUGUUGAUGGag
B9	NM_029337	Ep400	E1A binding protein p400	75560	s93641	Not Determined	GAGUUGCCCUUAAUCGAUUtt	AAUCGAUUAAGGGCAACUCag
B10	NM_016857	Exoc7	exocyst complex component 7	53413	s79165	Not Determined	CAGCUGAACUUACUAAGCAtt	UGCUUAGUAAGUUCAGCUGca
B11	XM_488539	Fry	furry homolog (Drosophila)	320365	s115690	Not Determined	GACCAUUGAAAAAUACGUAtt	UACGUAUUUUUCAAUGGUCtt
C1	AK003718	Hipk2	homeodomain interacting protein kinase 2	15258	n417910	1	UCAUUUUCGUUGUAGAAAAtt	UUUUCUACAACGAAAAUGAtg
C2	NM_023065	Ifi30	interferon gamma inducible protein 30	65972	s82442	2	GAGUCAGCCUGUAUUAUGAtt	UCAUAAUACAGGCUGACUCtg
C3	NM_026298	Ift172	intraflagellar transport 172 homolog	67661	s85415	15	CAACAUUGGUACUAUCAGUtt	ACUGAUAGUACCAAUGUUGta
C4	NM_010598	Kcnab2	potassium voltage-gated channel, shaker-	16498	s68603	12	GCUCGGCAGUUCAACCUGAtt	UCAGGUUGAACUGCCGAGCca
C5	NM_134073	Kctd9	potassium channel tetramerisation domain	105440	s98464	Not Determined	CUGAAGAACUGUAAUCUCAtt	UGAGAUUACAGUUCUUCAGtt
C6	NM_011419	Kdm5d	lysine (K)-specific demethylase 5D	20592	s74014	6	CAAACAACCAGAUAAAGAAtt	UUCUUUAUCUGGUUGUUUGct
C7	NM_010699	Ldha	lactate dehydrogenase A	16828	s69141	2	GUAUCUUAAUGAAGGACUUtt	AAGUCCUUCAUUAAGAUACtg
C9	NM_022012	Map3k11	mitogen-activated protein kinase kinase	26403	s77074	10	CGUGGUACCUAGAUUCAGAtt	UCUGAAUCUAGGUACCACGtg
C10	NM_011746	Mkrn3	makorin, ring finger protein, 3	22652	s76225	1	GGAAACGUGCUGUUUAAAAtt	UUUUAAACAGCACGUUUCCct
C11	NM_022323	Moap1	modulator of apoptosis 1	64113	s82133	Not Determined	GGAUAUGAAUCCUCGGAAAtt	UUUCCGAGGAUUCAUAUCCat
D1	NM_207215	Mycbp2	MYC binding protein 2	105689	s232922	58	GCAUAGUACAUGAUGCAAUtt	AUUGCAUCAUGUACUAUGCct
D2	NM_010910	Nefl	neurofilament, light polypeptide	18039	s70560	2	ACAUCGAGAUUGCAGCUUAtt	UAAGCUGCAAUCUCGAUGUcc
D3	NM_146131	Pbxip1	pre-B-cell leukemia transcription factor	229534	s106202	10	GGACGAAUCUGGGAGCAGAtt	UCUGCUCCCAGAUUCGUCCgc
D4	NM_175310	Pds5b	PDS5, regulator of cohesion maintenance,	100710	s97646	Not Determined	CGAUAAACUAAAGGAUAUAtt	UAUAUCCUUUAGUUUAUCGgg
D5	NM_029094	Pik3cb	phosphatidylinositol 3-kinase, catalytic, beta	74769	s93108	22	CAUAGAUUUUGGGCAUAUUtt	AAUAUGCCCAAAAUCUAUGtg
D6	NM_134101	Psmd2	proteasome (prosome, macropain) 26S	21762	s74996	Not Determined	CACCCAGAUUGACAAGUAUtt	AUACUUGUCAAUCUGGGUGag
D7	NM_194346	Rnf31	ring finger protein 31	268749	s114092	15	CGGCAUUGACUGUCCGAAAtt	UUUCGGACAGUCAAUGCCGtt
D8	NM_020618	Smarce1	SWI/SNF related, matrix associated, actin	57376	s81271	Not Determined	GUGAGAGUGUGGUACCUGAtt	UCAGGUACCACACUCUCACtg
D9	NM_010097	Sparcl1	SPARC-like 1	13602	s65275	Not Determined	CACUAACACUGGAUCUACAtt	UGUAGAUCCAGUGUUAGUGtt
D11	NM_153176	Spg7	spastic paraplegia 7 homolog (human)	234847	s107971	Not Determined	CGUGCACACGUUCAACUUUtt	AAAGUUGAACGUGUGCACGga
E2	NM_175836	Sptbn1	spectrin beta, non-erythrocytic 1	20742	s74306	24,24	CGAUGUUACAAGAACGGUUtt	AACCGUUCUUGUAACAUCGtg
E3	NM_009384	Tiam1	T-cell lymphoma invasion and metastasis 1	21844	s75132	Not Determined	GGCUGUCAAUCUACGAGGAtt	UCCUCGUAGAUUGACAGCCtg
E4	NM_013735	Trp53bp1	transformation related protein 53 binding	27223	s77592	Not Determined	GUCAGGUCAUUGAACGGUUtt	AACCGUUCAAUGACCUGACtg
E5	NM_133975	Trip12	thyroid hormone receptor interactor 12	14897	s67172	17	GGGACGAGUUUAUACUAUUtt	AAUAGUAUAAACUCGUCCCag
E6	NM_198311	Ttc8	tetratricopeptide repeat domain 8	76260	s94186	5	GGAAGACCCAUAACAGGUUtt	AACCUGUUAUGGGUCUUCCag
E7	XM_980597	Ubr4	ubiquitin protein ligase E3 component n-	69116	s87461	Not Determined	CCAUCGAGAUCAGUAACAAtt	UUGUUACUGAUCUCGAUGGtg
E8	NM_021522	Usp14	ubiquitin specific peptidase 14	59025	s81807	2,2	GAAGGUGUAGAAUUGAAUAtt	UAUUCAAUUCUACACCUUCaa
E9	NM_019729	Usp8	ubiquitin specific peptidase 8	84092	s96531	12	GCGAGAACCUUUGACGAGAtt	UCUCGUCAAAGGUUCUCGCtg
E11	NM_001081366	Vps8	vacuolar protein sorting 8 homolog (S.	209018	s101999	44	CCAGAGGACUCAAUCCCAAtt	UUGGGAUUGAGUCCUCUGGat
F1	NM_011738	Ywhah	tyrosine 3-monooxygenase/tryptophan 5-	22629	s76184	Not Determined	GGGAGAAGAUUGAAAAGGAtt	UCCUUUUCAAUCUUCUCCGgg
A1	NM_007438	Aldoa	aldolase A, fructose-bisphosphate	11674	s62250	8	CCAUCAACCUCAAUGCUAUtt	AUAGCAUUGAGGUUGAUGGat
A2	NM_009674	Anxa7	annexin A7	11750	s62363	Not Determined	CUAUGAUGCCUGGAGCUUAtt	UAAGCUCCAGGCAUCAUAGta
A8	NM_152801	Arhgef6	Rac/Cdc42 guanine nucleotide exchange	73341	s91693	16	GAGUUUAAGUUGCCUACGAtt	UCGUAGGCAACUUAAACUCca
A9	NM_011790	Arih2	ariadne homolog 2 (Drosophila)	23807	s202669	Not Determined	GCAGUACACCUAUCCAUAUtt	AUAUGGAUAGGUGUACUGCag
A10	NM_025505	Blzf1	basic leucine zipper nuclear factor 1	66352	s83071	Not Determined	CCCUAUACCAGAUAUGAAAtt	UUUCAUAUCUGGUAUAGGGat
A11	XM_906739	Cars2	cysteinyl-tRNA synthetase 2	71941	s206417	Not Determined	GCAAGCUGGUCAACACGGUtt	ACCGUGUUGACCAGCUUGCca
B2	NM_013492	Clu	clusterin	12759	s201173	Not Determined	GGAGUAGGUAUAUUAAUAAtt	UUAUUAAUAUACCUACUCCct
B3	NM_012001	Cops4	COP9 (constitutive photomorphogenic)	26891	s77323	7	GGCUACUCUUUUUAAGGAUtt	AUCCUUAAAAAGAGUAGCCag
B5	NM_023178	Dmap1	DNA methyltransferase 1-associated protein	66233	s82847	3	GCCUUUUACUAACCCAGCUtt	AGCUGGGUUAGUAAAAGGCat
B7	NM_023240	Eef1d	eukaryotic translation elongation factor 1	66656	s83647	2,4	GUUUAAAAUAUGAUGAUGCAtt	UGCAUCAUCAUAUUUAAACtt
B8	NM_007930	Enc1	ectodermal-neural cortex 1	13803	s65504	2	CCCGGGUCAUUAUCAAUGAtt	UCAUUGAUAAUGACCCGGGag
B10	NM_016857	Exoc7	exocyst complex component 7	53413	s79164	Not Determined	GGAAUACAACAUGCCUAAAtt	UUUAGGCAUGUUGUAUUCCtt
B11	XM_488539	Fry	furry homolog (Drosophila)	320365	s115689	Not Determined	GAACUAUCCCUUCGACAUAtt	UAUGUCGAAGGGAUAGUUCct
C1	AK003718	Hipk2	homeodomain interacting protein kinase 2	15258	n417906	1	GCAUUGUAAAUUUAUGAGAtt	UCUCAUAAAUUUACAAUGCta
C2	NM_023065	Ifi30	interferon gamma inducible protein 30	65972	s82440	2	ACAUCACCCUGGUGCCCUAtt	UAGGGCACCAGGGUGAUGUtc
C3	NM_026298	Ift172	intraflagellar transport 172 homolog	67661	s85417	22	GCUGCGCAGAGACUACUAUtt	AUAGUAGUCUCUGCGCAGCtt
C4	NM_010598	Kcnab2	potassium voltage-gated channel, shaker-	16498	s68601	15	GGAGAACAUUGGAGCAAUAtt	UAUUGCUCCAAUGUUCUCCat
C5	NM_134073	Kctd9	potassium channel tetramerisation domain	105440	s98463	Not Determined	GCAGGAACCGAUUUAGAAAtt	UUUCUAAAUCGGUUCCUGCca
C6	NM_011419	Kdm5d	lysine (K)-specific demethylase 5D	20592	s74013	3	GGAAGAUCUUGGACCUUUAtt	UAAAGGUCCAAGAUCUUCCtc
C7	NM_010699	Ldha	lactate dehydrogenase A	16828	s69140	4	GUUCAUCAUUCCCAACAUUtt	AAUGUUGGGAAUGAUGAACTt
C9	NM_022012	Map3k11	mitogen-activated protein kinase kinase	26403	s77075	4	AGACCCUAAAGAUUACUGAtt	UCAGUAAUCUUUAGGGUCUtg
C10	NM_011746	Mkrn3	makorin, ring finger protein, 3	22652	s76226	1	GCCCGGGCAAUUGAGAGAGAtt	UCUCUCUCAAUUGCCGGGCtc
C11	NM_022323	Moap1	modulator of apoptosis 1	64113	s82132	Not Determined	GGCUUACUGCAGUUGCUGAtt	UCAGCAACUGCAGUAAGCCtg
D1	NM_207215	Mycbp2	MYC binding protein 2	105689	s232923	21	CGGCAGUCCUUUUAAUGGAtt	UCCAUUAAAAGGACUGCCGtg
D2	NM_010910	Nefl	neurofilament, light polypeptide	18039	s70562	1	GCUUCACCGUGCUAACCGAtt	UCGGUUAGCACGGUGAAGCgg
D3	NM_146131	Pbxip1	pre-B-cell leukemia transcription factor	229534	s106204	10	GAGAUUUUGUGGAUGCCUUtt	AAGGCAUCCACAAAAUCUCtg
D4	NM_175310	Pds5b	PDS5, regulator of cohesion maintenance,	100710	s97644	Not Determined	GGAACUUUAUCUAAACCUAtt	UAGGUUUAGAUAAAGUUCCtt
D5	NM_029094	Pik3cb	phosphatidylinositol 3-kinase, catalytic, beta	74769	s93109	24	GGGAAAGCUGGACUACUAAtt	UUAGUAGUCCAGCUUUCCCtg
D6	NR_027485	Psmd2	proteasome (prosome, macropain) 26S	21762	n255792	1	GAGCUGACAUUCACACUCUtt	AGAGUGUGAAUGUCAGCUCct
D7	NM_194346	Rnf31	ring finger protein 31	268749	s114094	17	GACCCUAACUGCAAGGUGAtt	UCACCUUGCAGUUAGGGUCtg
D8	AK017922	Smarce1	SWI/SNF related, matrix associated, actin	57376	n436156	1	GCACUUAGGUACCAGAUUAtt	UAAUCUGGUACCUAAGUGCtt
D9	NM_010097	Sparcl1	SPARC-like 1	13602	s65276	Not Determined	GCACGAACUUCCAAUGUAAtt	UUACAUUGGAAGUUCGUGCaa
D11	NM_153176	Spg7	spastic paraplegia 7 homolog (human)	234847	s107973	Not Determined	CAGCCGAAGAUGAACUGAAtt	UUCAGUUCAUCUUCGGCUGct
E2	NM_175836	Sptbn1	spectrin beta, non-erythrocytic 1	20742	s74307	10,10	GGAAUGAGCUCAUACGGCAtt	UGCCGUAUGAGCUCAUUCCgc
E3	NM_009384	Tiam1	T-cell lymphoma invasion and metastasis 1	21844	s75133	Not Determined	GAGAUUCUCGAGAUCAAUAtt	UAUUGAUCUCGAGAAUCUCat
E4	NM_013735	Trp53bp1	transformation related protein 53 binding	27223	s77593	Not Determined	GUCUCCGUGUUGUAGCUAAtt	UUAGCUACAACACGGAGACcc
E5	NM_133975	Trip12	thyroid hormone receptor interactor 12	14897	s67171	15	GAUUGACCUUGUUCCACGAtt	UCGUGGAACAAGGUCAAUCtg
E6	NM_198311	Ttc8	tetratricopeptide repeat domain 8	76260	s94185	3	GAAAUGAUCCUGGAUGAAAtt	UUUCAUCCAGGAUCAUUUCag
E7	XM_980597	Ubr4	ubiquitin protein ligase E3 component n-	69116	s87463	Not Determined	CACGGGAUGUUACAACAUUtt	AAUGUUGUAACAUCCCGUGAt
E8	NM_021522	Usp14	ubiquitin specific peptidase 14	59025	s81808	6,7	GGAUAAAACUUCUUCUAGUtt	ACUAGAAGAAGUUUUAUCCat
E9	NM_019729	Usp8	ubiquitin specific peptidase 8	84092	s96530	4	GCCUUAAACUAAGAUACGAtt	UCGUAUCUUAGUUUAAGGCtt
E10	NM_173443	Vcpip1	valosin containing protein (p97)/p47	70675	s89045	1	GGACGGCAGUCUAUGGUUAtt	UAACCAUAGACUGCCGUCCat
E11	NM_001081366	Vps8	vacuolar protein sorting 8 homolog (S.	209018	s202079	40	GAAAUUCACAGAAUUUGAAtt	UUCAAAUUCUGUGAAUUUCtc
F1	NM_011738	Ywhah	tyrosine 3-monooxygenase/tryptophan 5-	22629	s76183	Not Determined	GAGGGUUAUUAGUAGCAUUtt	AAUGCUACUAAUAACCCUCca

Supplementary results

a) Spatacsin cellular localization

During my PhD thesis, I performed experiments that were not included in the manuscript. I summarize here the main supplementary data that will be used for my general discussion.

Spatacsin is not a cytoplasmic protein

When overexpressed in mouse embryonic fibroblasts, Spatacsin-V5 appeared cytoplasmic and granular. To test if Spatacsin-V5 was a soluble protein contained in the cytoplasm, we performed a cytoplasmic washout of cells using the soft detergent saponin for twenty seconds and fixed the cells immediately after.

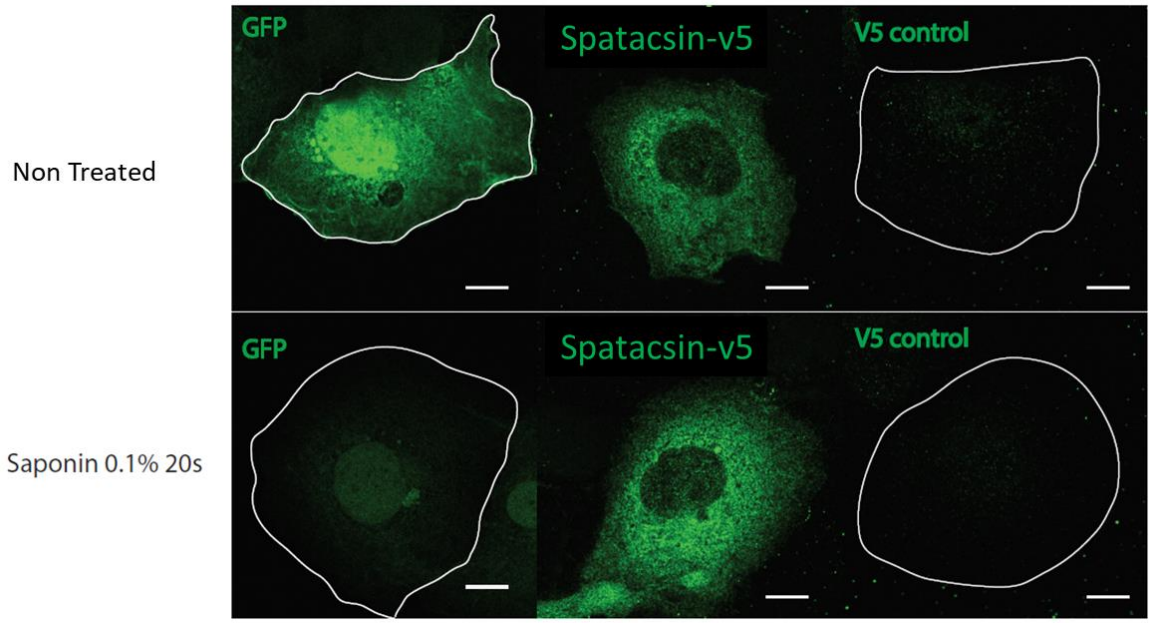

Figure 54: Fibroblasts transfected with spatacsin-v5 had their cytoplasm washed out with saponin. Spatacsin-v5 signal was unchanged after cytoplasmic washout while soluble protein GFP was completely washed out. V5-control was used to ensure that there was no non-specific signal linked to V5 tag. Scale bar 5 µm.

Spatacsin-v5 is not a soluble protein it is rather bound to membranes as removing the cytosol of cells did not change its signal.

Spatacsin is present at ER-Lysosomes contact sites

We co-stained fibroblasts transfected with spatacsin-v5 with lysosomes marker Lamp1 and ER fluorescent protein Sec61β-GFP to see if we could detect spatacsin at ER-lysosomes contact sites.

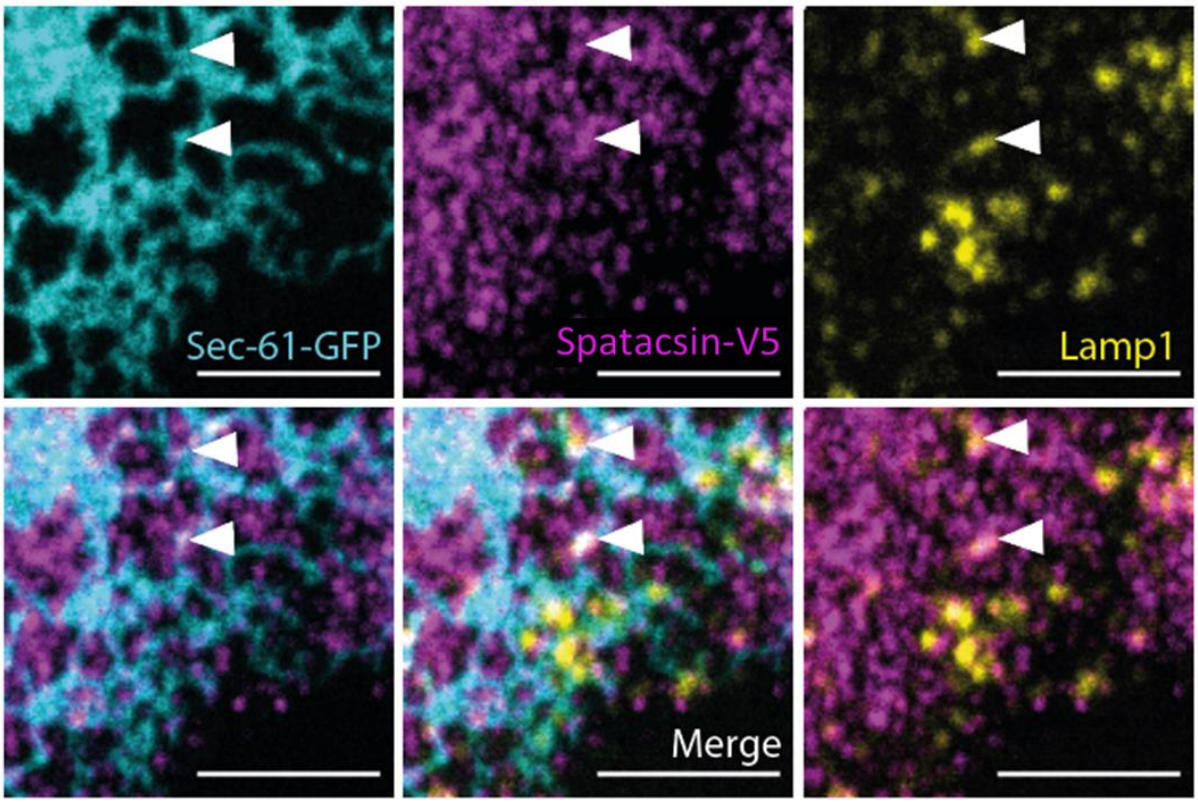

Figure 56: Spatacsin is present at ER-Lamp1 contact sites, see white arrows. Scale bar 5 µm.

Spatacsin seems to be present at ER-Lysosomes contacts. However, we do not have the STED resolution to affirm that spatacsin is present for sure at the contacts, these are confocal images.

Spatacsin/spastizin recruitment to lysosomes

According to a recent publication, spatacsin is recruited to Lamp1-positive compartment in response to nutrient stresses or inhibition of PI(3.5)P2 synthesis (Hirst et al., 2021b). We observed recruitments of spatacsin-V5 and spastizin-GFP at the lysosomes in our model for short periods of starvation (2 hours HBSS).

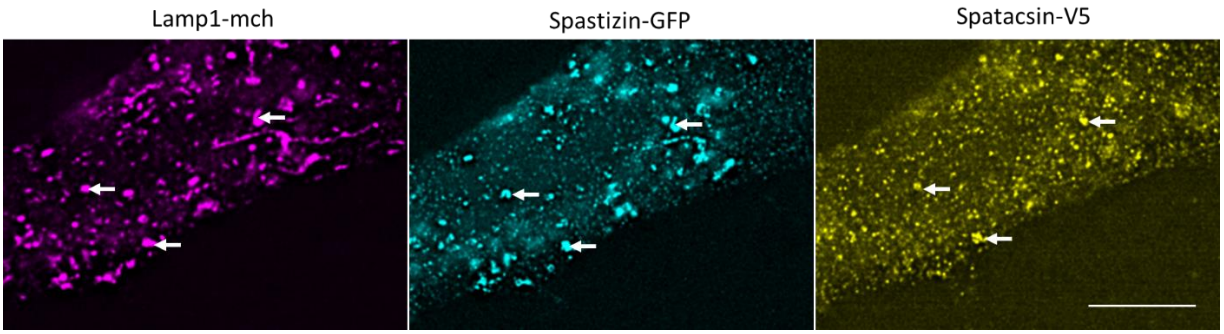

Figure 57: Spatacsin and spastizin recruitment to lysosomal compartment (white arrows) after two hours of starvation in HBSS. Scale bar 5 µm.

We also measured the effect of short starvation on tubular lysosome formation.

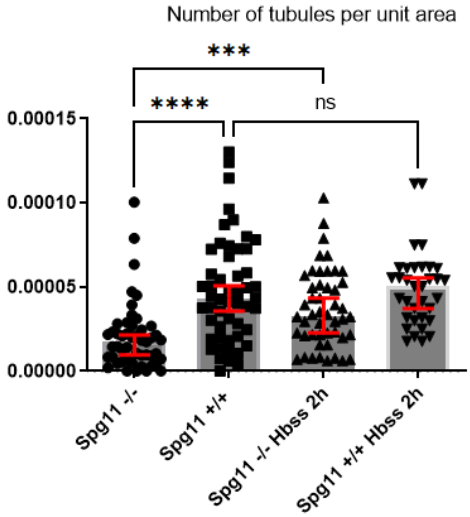

Figure 58: short starvation of fibroblasts had a positive effect on tubular lysosome formation in spatacsin depleted cells. Kruskal-Wallis test *** p<0.001.

b) Testing the effect of spatacsin recruitment to lysosomes on tubular lysosomes formation

According to (Hirst et al., 2021b), the PIKFYVE inhibitor YM20136 promotes spatacsin recruitment to lysosomes while mTorc1 inhibitor Torin has a negative effect on spatacsin recruitment to lysosomes. We therefore tested their effect on tubular lysosomes formation. Both treatments had a negative impact on tubular lysosome formation.

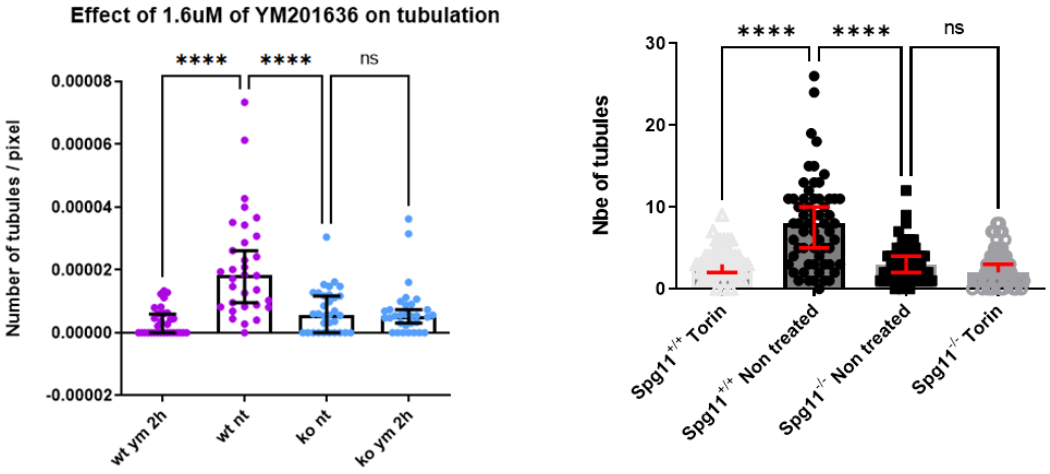

Figure 59: Number of tubular lysosomes formed in cells upon YM2016-36 and Torin treatment. Both treatments had a negative impact on tubular lysosome formation. Mann-Whitney tests **** indicates p<0.0001.

c) Tubular lysosomes properties

Tubular lysosome length is not changed in absence of spatacsin

The length of tubular lysosomes was measured in live fibroblasts cells stained with Texas Red dextran.

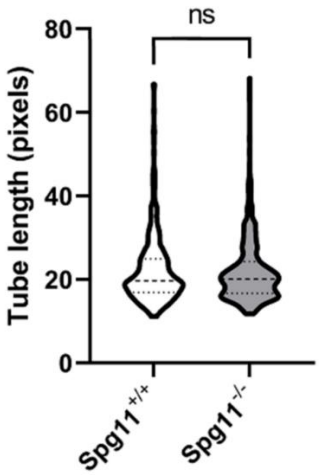

Figure 60: Tubular lysosomes length is unchanged in absence of spatacsin. Mann Whitney test.

d) ER-lysosomes contacts are modified in absence of spatacsin

Analysis of electronic microscopy images of $Spg11^{-/-}$ and $Spg11^{+/+}$ mouse embryonic fibroblasts showed that ER-Lysosomes contacts were altered in absence of spatacsin.

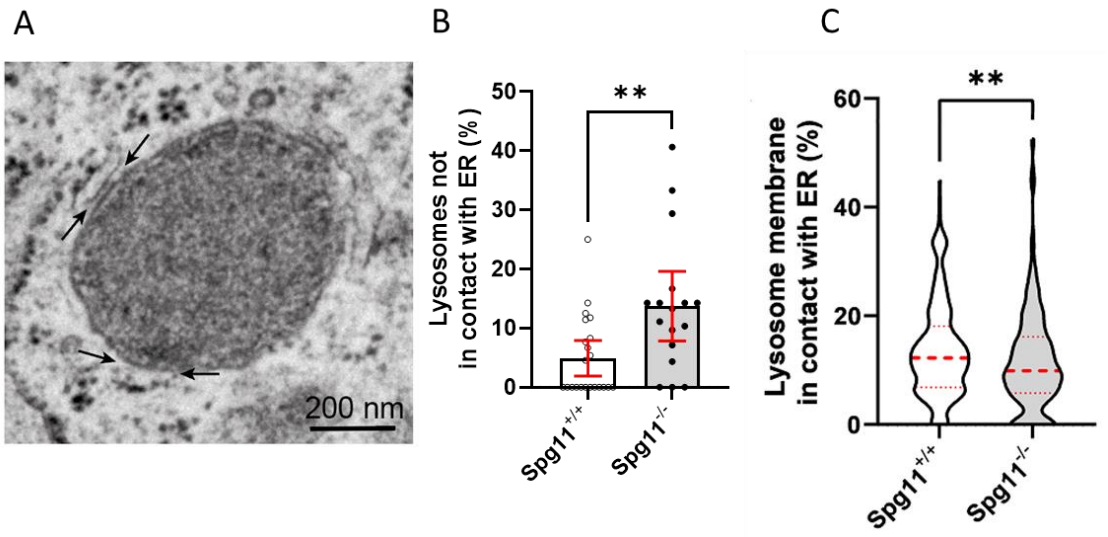

Figure 61. **A:** Illustration of membrane contact between ER and Lyso (See Arrows). **B:** The proportion of lysosomes that are not at all in contact with the ER is increased in absence of spatacsin. **C:** The proportion of membrane of the lysosomes that is in contact with the ER is also decreased in absence of spatacsin *Mann-Whitney tests p<0.01*

e) Spg11$^{\Delta 32\text{-}34/\Delta 32\text{-}34}$ mouse model

Spg11$^{\Delta 32\text{-}34/\Delta 32\text{-}34}$ mice develop a motor phenotype

We have seen in the first part of the results that spatacsin$^{32\text{-}34}$ domain is important for the function of spatacsin. The importance of the function of spatacsin$^{32\text{-}34}$ domain is shown by the fact that mice that are depleted of it, but conserve a truncated spatacsin, develop a motor phenotype resembling Spg11$^{-/-}$ motor phenotype (see **Figure 62**).

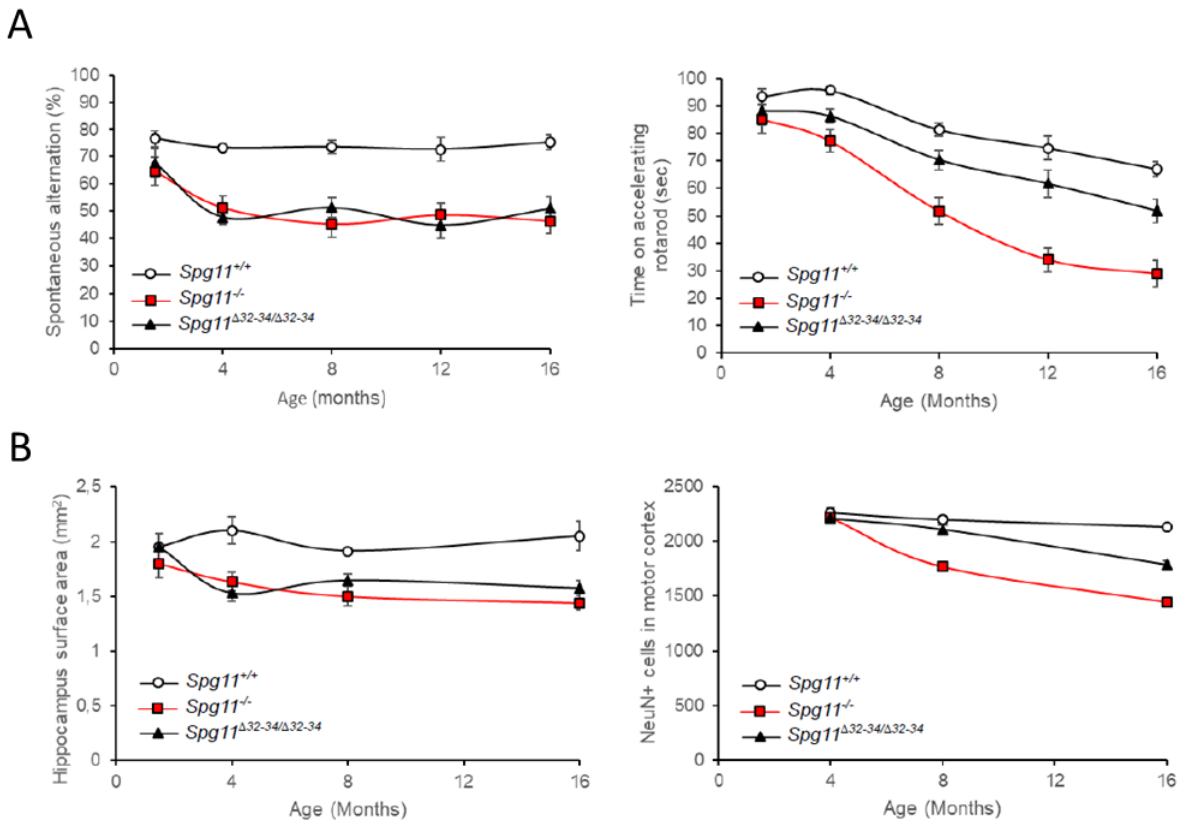

Figure 62 A: Spg11$^{\Delta 32\text{-}34/\Delta 32\text{-}34}$ mice develop a motor phenotype like Spg11$^{-/-}$mice. **B:** Neuronal loss in specific tissues of Spg11$^{\Delta 32\text{-}34/\Delta 32\text{-}34}$ mice brain Spg11$^{-/-}$mice. *Analysis performed by J.Branchu (unpublished data).*

Spg11$^{\Delta 32\text{-}34/\Delta 32\text{-}34}$ neurons accumulate gangliosides in their lysosomes

It has been recently shown that one of the hallmark of SPG11 HSP is GM2 accumulation in the lysosomes of cultured neurons in absence of spatacsin (Boutry et al., 2018). Therefore I tested if neurons that have a truncated spatacsin also accumulate ganglioside GM2.

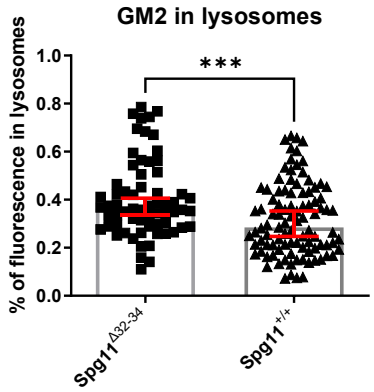

Figure 63: Cultured neurons that have a truncated spatacsin accumulate GM2 ganglioside in their lysosomes. Mann-Whitney test *** p<0.001.

f) Ubiquitin-dependent degradation of substrates alterations

Ubiquitin accumulates in cells in absence of spatacsin

Expressing ubiquitin-His in fibroblasts revealed that it forms aggregates in the cytosol of cells in absence of spatacsin. Some of the ubiquitin aggregates in absence of spatacsin colocalize with lysosomes.

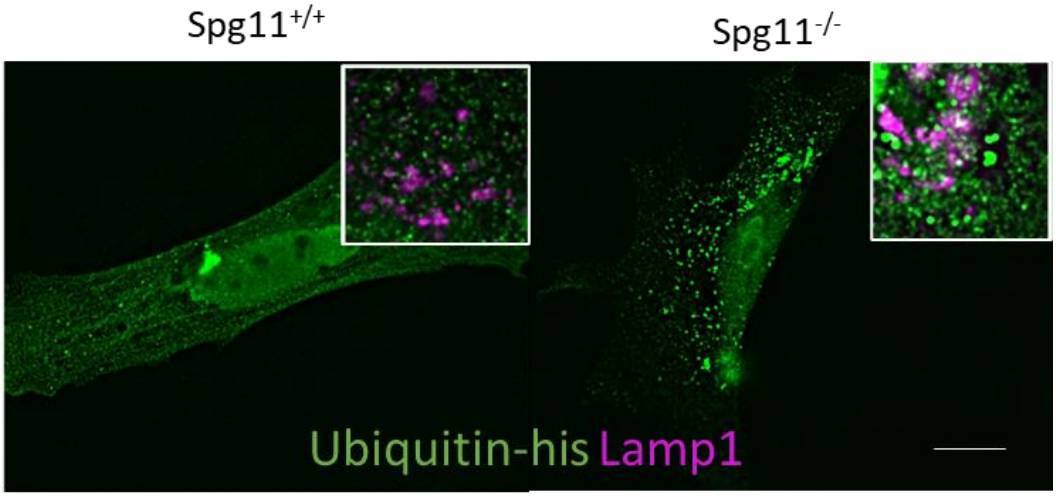

Figure 64: Ubiquitin forms cytosolic aggregates in absence of spatacsin. Insets show localization of ubiquitin aggregates respectively to lysosomal staining (Lamp1). In absence of spatacsin, some of the ubiquitin aggregates colocalize with lysosomes. Scale bar 5 µm.

Preventing poly-ubiquitination results in ubiquitin aggregation in cytosol of cells

Expression of mutant ubiquitin k0 in wild-type fibroblasts resulted in ubiquitin accumulations in the cytosol of cells. Ubiquitin accumulations colocalized partially with lysosomal staining Lamp1.

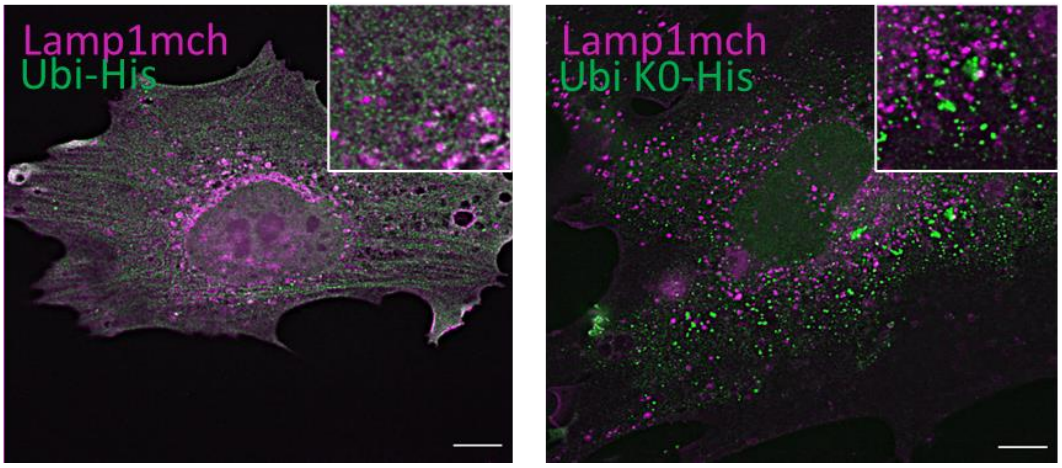

Figure 65: Mutant ubiquitin k0 forms cytosolic aggregates in wild type fibroblasts. Insets show localization of ubiquitin aggregates respectively to lysosomal staining (Lamp1). Some of the ubiquitin aggregates colocalize with lysosomes. Scale bar 5 µm.

Proteasome inhibition prevents tubular lysosome formation

Proteasome inhibitor MG-132 has a negative impact on the tubular lysosome formation in wild type cells.

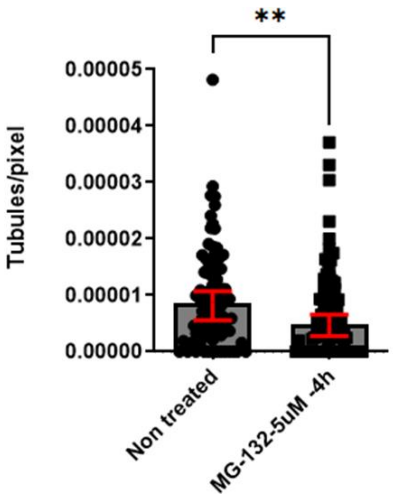

Figure 66: Inhibition of proteasome activity by MG-132 results in tubular lysosome loss. Mann Whitney test ** p<0.01.

g) AP5z1 mechanism of degradation

We have shown that AP5z1 degradation that was promoted by spatacsin was dependent on poly-ubiquitination. Therefore, to determine which degradative pathway was responsible for this degradation, we tested proteasome inhibition with MG-132 and lysosomal degradative inhibition with bafilomycin on AP5z1 levels in **Figure 67**.

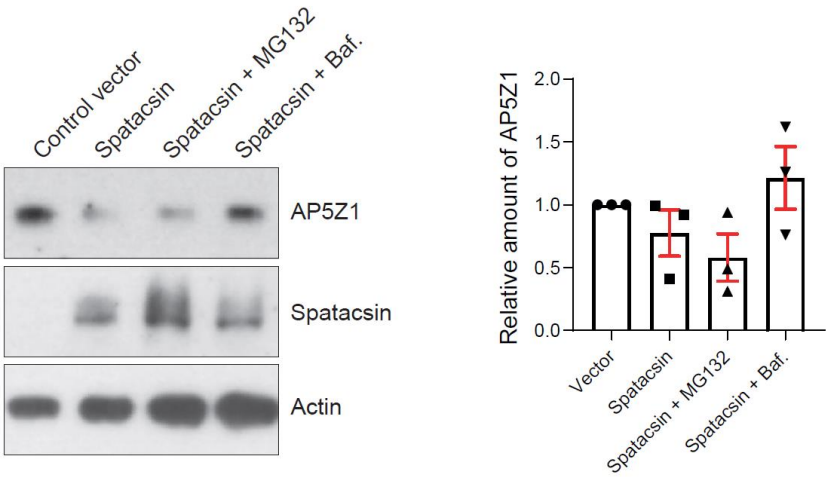

Figure 67: Variations of AP5z1 levels when degradative pathways are inhibited.

It appears that spatacsin-mediated degradation of AP5z1 is dependent on lysosomal degradative activity rather than proteasomal degradative activity.

h) AP5z1 expression and KIF13A-ST expression induce a lysosomal clustering

We overexpressed AP5z1- GFP and motor-less kinesin KIF13A-ST-GFP in wild type fibroblasts and measured the consequences on lysosomal positioning.

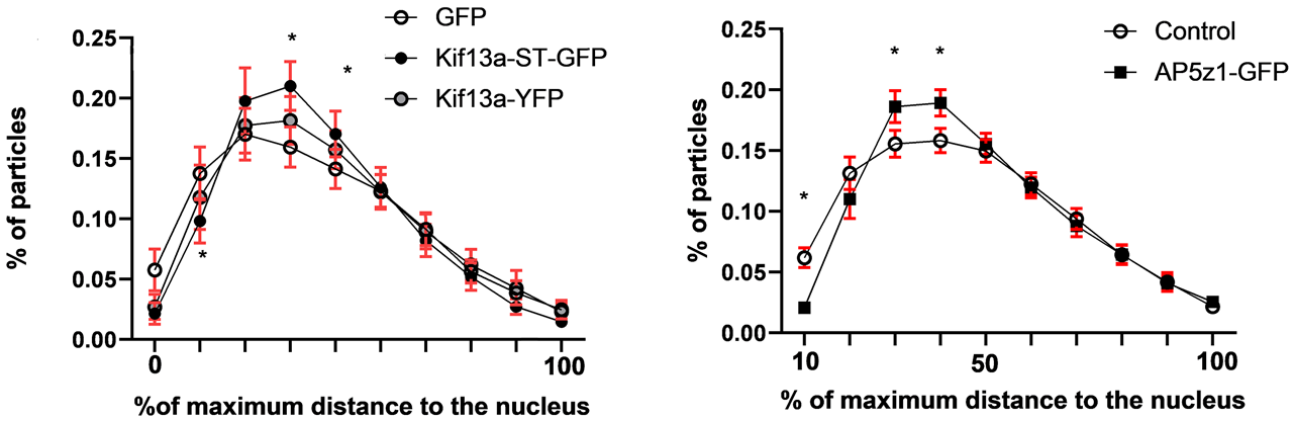

Figure 68: Lysosomal clustering when motor-less KIF13A-ST-GFP and AP5z1-GFP are expressed in wild type cells. We can see that there is a repositioning of the particles. 1-way ANOVA, * indicates p<0.01.

DISCUSSION

I. Spatacsin subcellular localization

a) Spatacsin relationship with the Endoplasmic Reticulum (ER)

In this work, to identify spatacsin subcellular localization, we fractionated mouse brains, a tissue in which spatacsin is expressed (Branchu et al., 2017), and we used spatacsin-V5 to study spatacsin localization in mouse fibroblasts.

We obtained several information from these experiments:

1) Spatacsin is not soluble & is found in the "light membranes" fraction (i.e., the pellet after 100 000g centrifugation) (see **Results Figure 1 C**).

2) Spatacsin is enriched in an ER-enriched fraction and not in a lysosomal enriched fraction (see **Results Figure 1 D).**

3) Spatacsin is very tightly attached to membranes in the "light membranes" fraction as it is quite difficult to solubilize it (only strong detergents like deoxycholate could solubilize it) (see **Results Figure 1 E**).

4) Spatacsin-V5 shows a pattern of localization that does not correspond to a cytosolic protein (see **Figure 54**). Indeed, washing out cytoplasm of cells with saponin before fixation had no effect on cellular localization of spatacsin-V5.

5) Spatacsin-V5 is also present in areas where ER and lysosomes colocalize, making it a good candidate for being a protein present at ER-lysosomes contact sites (see **Figure 56**).

What can we conclude from this? We can see on the experiments where we purified ER and lysosomal fractions (**Results Figure 1-D**) that spatacsin is not 100% an ER-located protein, some of it is still present in the lysosomal fraction. However, it appears that the majority of endogenous spatacsin in mouse brains and of spatacsin-V5 expressed in fibroblast is present in the ER. It is a possibility that spatacsin present in the lysosomal fraction corresponds to its presence at ER-lysosomes contact sites.

Spatacsin is a protein likely present at membrane contact sites between the ER and lysosomes (see **Figure 56**). We could study this ER-lysosome interface more clearly if there was a protocol to isolate it in a similar manner that it is possible to isolate the contacts between ER and peroxisomes (David et al., 2013). It would be also interesting to verify if fractionation of mouse fibroblasts expressing spatacsin-V5 would lead to similar enrichments of the tagged protein in the ER fraction. However, as spatacsin is very difficult to express, it is not certain that we would have sufficient material to perform such experiments.

b) Spatacsin localization in other models

If we compare the patterns of expression of spatacsin-V5 in mouse fibroblasts to the ones obtained in mouse neurons (Boutry et al., 2018), we see that they are very similar which indicates that spatacsin is likely an ER-protein in neurons as well. Our results on spatacsin sub-cellular localization could seem to disagree with another recent paper on spatacsin which used Hela cells expressing spatacsin-GFP under Spg11 promoter expression (Hirst et al., 2021b). Indeed, using this precise method for spatacsin sub-cellular identification they mainly develop the point that spatacsin is a lysosomal (stained by Lamp1) protein. And if the part of this paper concerning the recruitment of the protein to the lysosomes is very clear, this statement that spatacsin is only a lysosomal protein in basal conditions I must disagree with. If we look at the images (which are representative images chosen by the author) of spatacsin-GFP staining, we can clearly see that a large part of the spatacsin signal is not colocalizing with Lamp1 and that spatacsin-GFP is showing a pattern of localization very much like what we observe with spatacsin V5 (see **Figure 69**).

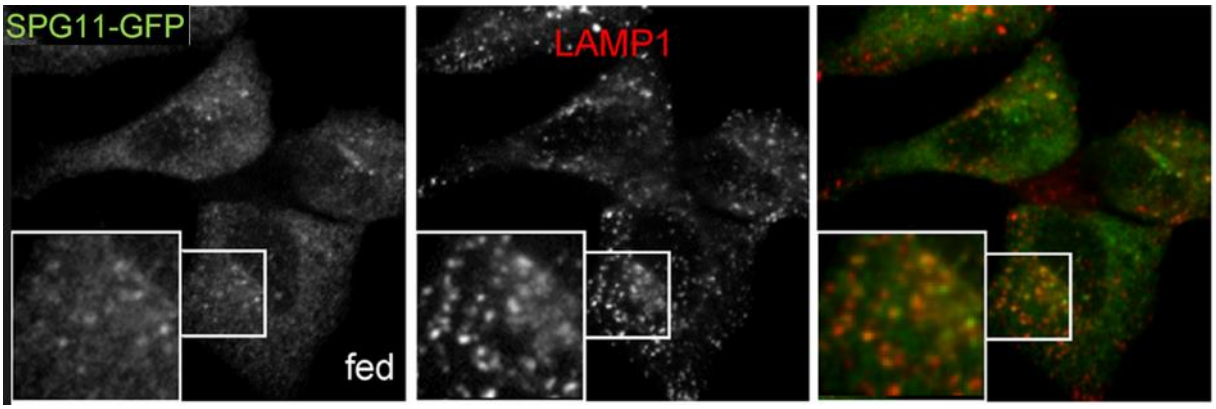

Figure 69: Spatacsin-GFP sub-cellular localization in Hela cells shows a pattern of localization that is only partially lysosomal (Hirst et al., 2021b).

Therefore, I am confident that it is an encouraging data supporting the fact that spatacsin is partially located at the lysosomes but a large part of it remains not lysosomal in basal conditions and is likely found in the ER. I will also be quite curious to see what will be the subcellular localization of endogenous tagged spatacsin by CRISPR technology (Krumm et al., 2021) as this recent paper did not include any immunofluorescence of spatacsin localization.

c) Are ER-lysosomes contacts changed in absence of spatacsin?

We have mentioned the fact that there seems to be no major alteration of the ER network in cells that lack spatacsin or that possess spatacsin$^{\Delta 32\text{-}34}$. We performed a tubular ER network morphological analysis like described in (Spits et al., 2021b), and no alteration of the number of tubular ER junctions was observed. The only alterations of the ER that we can report are the increased contacts in absence of spatacsin between ER and plasma membrane that are involved in store-operated calcium entry (Boutry et al., 2019b). Overall, we have no reason to believe that spatacsin absence has any drastic consequences on ER architecture.

However, as we have seen previously, spatacsin is present at ER-Lysosomes contacts and it is a strategic position for its involvement in tubular lysosome dynamics regulation. Tubular lysosomes have a privileged contact with the ER, making more contacts with it and being in closer proximity. STED images also showed how entangled the tubular lysosomes are in the ER network and live imaging showed that the tubular lysosomes are moving along the ER tubular network (see **Results Figure 7**).

So, is there an impairment of ER-Lysosomes contacts in absence of spatacsin? With fluorescent microscopy images, the Pearson correlation coefficient between ER and lysosomal staining as used in (Höglinger et al., 2019) showed no difference in absence of spatacsin and there was no difference in area overlap between ER and lysosomes in absence of spatacsin either.

However, if we go the resolution of electronic microscopy images, we observe that in wild-type fibroblasts, less than 8% of lysosomes are not in contact with the ER, while there is about 15% of lysosomes that are not in contact with the ER in absence of spatacsin (**Figure 61**). Moreover, the proportion of the lysosomal membrane that is in contact with the ER is lower in fibroblasts that have no spatacsin (see **Figure 61**). These results indicate that the ER-lysosomes contacts are indeed modified in absence of spatacsin, although in modest proportions.

It is then likely that spatacsin is not an essential tether for ER-Lysosomes contacts if we consider the definition proposed in other publications (Bord, 2016; Scorrano et al., 2019). Spatacsin may have a signalingfunction at ER-Lysosomes contact sites.

d) Spatacsin recruitment to lysosomes and tubular lysosome formation

A recent study on the Rag GTPase involvement in spatacsin-spastizin-AP5z1 complex recruitment to lysosomes showed that that the recruitment of the proteins to the lysosomes is dependent of mTor regulator RagC and PI3P at the lysosomes (Hirst et al., 2021b).

We cannot extract any information on the consequences of the complex recruitment on the dynamics of tubular lysosome formation from this study as it was performed on fixed cells and tubular lysosomes are lost upon regular paraformaldehyde fixation. To observe tubular lysosomes, it is necessary to perform live imaging or to use specific fixation techniques, which are listed and explained in supplementary material of (Suresh et al., 2021).

In our fibroblast model, we have observed similar recruitment of spatacsin and spastizin to lysosomes (see **Figure 57**) in conditions of amino acid deprivation. Indeed, short starvation (2h HBSS) has a positive impact on tubular lysosome formation in Spg11$^{-/-}$ cells (see **Figure 58**). However, this cannot be the result of spatacsin recruitment to lysosomes, but we have seen that spastizin is also recruited to lysosomes. Even if spastizin is greatly depleted in Spg11$^{-/-}$ cells, the recruitment of the remaining spastizin to lysosomes could explain the positive effect we observed in starvation.

It will be interesting to see if all conditions bringing the spatacsin-spastizin-AP5z1 complex to the lysosomes result in tubular lysosome formation. For now, in our model, we have measured a positive effect of starvation on tubular lysosome formation and a negative impact on tubular lysosome formation of wortmannin (see **Results Figure 6**) and mTorc1 inhibitor Torin (see **Figure 59**). These two treatments indeed prevented recruitment of proteins to lysosomes (Hirst et al., 2021b; Wyant et al., 2018). However, PIKFYVE inhibitor YM-2016-36, which increases PI3P content of lysosomes, is presented as promoting the complex recruitment to lysosomes and we have observed that it strongly inhibited tubular lysosomes formation by creating round and enlarged lysosomes (see **Figure 59**). Maybe for short treatments of YM2016-36 (15 to 20 minutes) could tubulation be promoted before the membrane tension becomes too high due to the excess fusion between lysosomes.

This data is still consistent with spatacsin being a protein of ER-Lysosomes contact sites. Indeed, we have mentioned several examples in the introduction where the formation of contacts between the ER and other organelles is under the control of phosphoinositide signaling (Chung et al., 2015; Sohn et al., 2018). Moreover, the recruitment of proteins involved in inter-organelle contacts to the area of contact has been observed in starvation conditions, with the example of ATG14 recruitment to ER-autophagosome contact in starvation (Hamasaki et al., 2013).

It would also be interesting to test is if the recruitment of spatacsin-spastizin-AP5z1 complex is dependent of endoplasmic reticulum integrity by using ATLK80A. Indeed, recent studies link the activity of RAG GTPase to ER regulation. For example, it has been shown that ER protein WDR35 regulates RagA activity to influence mTor activity (Sekiguchi et al., 2019). It has also been shown that, in a model where tunicamycin elicits ER stress, there is an increased expression of eNos which activates mTor through RagC. This mechanism will lead to the accumulation of p62 in cells, linking ER-stress and RagC regulation and potentially also spatacsin-spastizin recruitment to the lysosomes (Guha et al., 2017).

II. Regulation of lysosomes shape, motility & positioning by spatacsin

a) Physical properties of tubular lysosomes

From J. Swanson papers from the 1980s, we know that, in macrophages, tubular lysosome formation is activated upon pinocytosis (Hollenbeck and Swanson, 1990; J Swanson et al., 1987; Swanson et al., 1992). We also know from the Autophagic Lysosomal Reformation (ALR) literature that autophagy activation regulates tubulation of lysosomes (Chen and Yu, 2017; Yu et al., 2010). Recently, in macrophages, it has been shown that tubulation can be triggered via MMP9 (Matrix Metalloprotease 9) signaling, a key player in macrophage biology which activates PI3K-Akt pathway (Suresh et al., 2021).

Tubular lysosomes are different from regular lysosomes in their movement, they are more motile and require the Rab7-FYCO1 complex for their formation (Mrakovic et al., 2012). It appears that they are also less degradative than round lysosomes and present a calcium gradient higher in the lumen than in the tubular part (Suresh et al., 2021).

Moreover, to deform the lysosomal membrane during tubulation, the deformation must be physically possible. Indeed, surface membrane tension, which is dependent of the osmosis of the lysosomes, needs to be low enough so that the membrane can form a protrusion (Freeman and Grinstein, 2018; Saric and Freeman, 2021). Many factors will regulate surface membrane tension, in Freeman & al papers, they develop the argument that lysosomal channels such as TRPMLs are extremely important in regulating lysosomal osmosis and indeed, it has been shown that TRPML1 channel is regulating lysosomal positioning & motility via tubulation (Li et al., 2016).

In our model, there is no difference in tubular lysosome length in absence of spatacsin (**Figure 60**). Moreover, in cells lacking spatacsin, the number of tubular lysosomes is not completely abolished. It appears that, tubulation can be promoted by starvation (see **Figure 58**) or by modulating calcium homeostasis- (Boutry et al., 2019b) even in absence of spatacsin. So, there is no physical impossibility for cells to form tubular lysosomes in absence of spatacsin pointing again toward a role of spatacsin at the signaling level for tubular lysosome formation, and not a physical role.

b) What is the role of tubular lysosomes?

We showed that in absence of spatacsin or in presence of a truncated spatacsin in his Cter domain (removal of exons 32-34) there is:

- a loss of tubular lysosomes which are catalytically active lysosomes and not tubes emanating to reform proto lysosomes

- a loss of motility of these tubular lysosomes

- a clustering of all lysosomes close to the nucleus (see **Results-Figure 2**)

Tubular shape reflects a transitory dynamic movement

Some of these parameters seem to be linked. In our results, every time there was a loss of tubular lysosomes, the remaining tubular lysosomes where less dynamic. So, it appears that at least these two parameters are correlated. If we consider the way lysosomal movement has been described so far, the same kinesin (KIF5B-kinesin1) is involved in membrane deformation and lysosomal movement, our observations seem to be coherent with such results (Du et al., 2016; Guardia et al., 2016). Tubular lysosomes being more dynamic than the regular round lysosomes, their presence or absence is likely an indicator of the more general dynamic state of the whole lysosomal compartment. This general alteration of movement is reflected in the peri-nuclear clustering that we observed in absence of spatacsin. However, the peri-nuclear clustering of the particles was not observed every time the tubular lysosomes were lost implying that maybe there are more complex regulations for lysosomal positioning.

Tubular lysosomes for a special role in fusion with other organelles?

Several studies on tubular lysosomes point toward a specific role of this elongated compartment in the regulation of lysosomes fusion with other compartments to promote degradation of substrates, this is the case for lysosome-autophagosome fusion in macrophages (Suresh et al., 2021). This has also been observed in *Drosophila* to regulate muscle activity by regulating cellular degradative activity (Johnson et al., 2015; Murakawa et al., 2020). In *C.elegans*, the role of tubular lysosome degradative activity was linked to degradation of peroxisomes by autophagy (pexophagy) (Dolese et al., 2021). We can wonder if the tubular aspect of lysosomes is simply a transitory state linked to the promotion of their movement by kinesins and that indicates that these lysosomes are destined for fusion with other compartments of the endosomal/autophagosomal pathway.

c) Protein degradation in the cell and tubular lysosome formation

Ubiquitinated substrates are accumulating in absence of spatacsin

We have shown that ubiquitin dependent degradation of AP5z1 promoted by spatacsin was necessary for tubular lysosome formation. So, it appears that protein degradation and tubular lysosome formation are two inter-connected pathways. If we take a broader perspective than the spatacsin-mediated degradation of AP5z1, we can observe that in absence of spatacsin, there is a general alteration of the ubiquitin staining. Ubiquitin tends to aggregate in the cytoplasm of cells that lack spatacsin (see **Figure 64**). The ubiquitin-positive cytoplasmic aggregates colocalize with lysosomal staining Lamp1 (**Inset-Figure 64**) but not completely, indicating that this accumulation of ubiquitinated substrate is not specific of a lysosomal alteration. It seems to be a general alteration of ubiquitinated cargo sorting mediated by spatacsin.

Poly-ubiquitination of substrates

By using the mutant ubiquitin k0, to prevent poly-ubiquitination of substrates, we have confirmed that ubiquitin dependent degradation was required for tubular lysosome formation and dynamics. However, using ubiquitin k0 drastically changes the way substrates are degraded in the cells. Even if the lysosomal staining didn't show obvious alterations (see **Figure 65**), hundreds of substrates had their fate potentially altered (Ziv et al., 2011). This may be the reason why the lysosomes did not significantly clustered around the nucleus when ubiquitin k0 was expressed in cells (data not shown). It is possible that a multiplicity of effects was taking place in this condition.

Interestingly, the pattern of accumulation of ubiquitin in absence of spatacsin looks like the aggregation pattern that is observed when mutant ubiquitin k0 is expressed in wild-type cells (**Figure 65**). This would support a role of spatacsin in sorting of poly-ubiquitinated substrates. Proteomic approaches would be necessary to determine the nature of the whole range of proteins that aggregate and accumulate in absence of spatacsin.

The role of the proteasome

The link between degradation of ubiquitinated substrates and tubular lysosome formation is further supported by the effect of proteasome inhibitor MG-132 on tubular lysosome formation (see **Figure 66**). Indeed, blocking proteasome activity for 4h resulted in the loss of tubular lysosomes. Another inhibitor of proteasome, epoxomicin, showed similar results than MG-132 (data not shown).

Are tubular lysosomes responsible for ubiquitinated substrate delivery?

This role for tubular lysosomes has been proposed in (Johnson et al., 2015), where defective tubular lysosomes carried no ubiquitinated positive content and this resulted in a global alteration of ubiquitin dependent degradation in the cells. It would be interesting to test if our tubular lysosomes are indeed ubiquitin positive organelles to gain further information on their function. However, if we might have thought that in cells lacking spatacsin, the loss of tubular lysosomes was responsible for ubiquitin accumulation, the fact that ubiquitin k0 and MG-132 produced similar effects advocates for the opposite correlation. It rather seems that the accumulation of substrates is preventing the tubular lysosomes formation and movement. This could be explained by the prevention of AP5z1 degradation and by the fact that lysosomes probably need to uptake additional substrates to degrade, therefore changing their regular activity.

d) Relationship between lipid accumulation and tubular lysosomes

Cholesterol accumulation and the positioning of lysosomes

Previous work on lysosomes dysfunctions in absence of spatacsin focused on the impact of lipid accumulation on lysosomal function (Boutry et al., 2019a, 2018). For example, it was proposed that lysosome clustering around the nucleus was caused by an accumulation of cholesterol that will drive lysosomes toward the center of the cell in an ORP1L-dependent manner following the model developed by (Rocha et al., 2009b). However, decreasing cholesterol levels in the cell did not restore the lysosomes position toward the periphery. And as we have developed in our mechanism, it is therefore more of a problem of lysosomal dynamics that results in particle clustering, and the cholesterol accumulation reflects an impairment of cholesterol export from the lysosomes without being the cause of their mis-localization.

Lipid accumulation and membrane tension

Another interesting hypothesis that was formulated at the time was that the accumulation of lipids impaired the recycling of lysosomal membrane, similarly to what was observed in lysosomal storage disorders (Platt et al., 2012). Although, it was not clear how exactly these accumulations could perturb lysosomal reformation. When we treated cells with U18666A, the inhibitor of NPC1 that induces massive cholesterol accumulation, lysosomes were extremely enlarged and extremely round. And this is correlated to a strong decrease in membrane tubulation. The “roundness” of the lysosomes in this condition reflects an extreme surface tension, preventing the protrusion of membrane from the tensed compartment (Freeman and Grinstein, 2018).

Although U18666A cannot be washed, I have observed other conditions that can trigger round and enlarged lysosomes that have a high surface tension. This happens when cells are treated with YM-201636, inhibitor of PIKFYVE enzyme, preventing endolysosomal membrane fission (Bissig et al., 2017).It also happens if cells are treated with lysosomal acidification inhibitor bafilomycin. In both conditions, upon enlargement of lysosomes, the tubulation of lysosomes is strongly inhibited but upon washing of the drugs and restoration of a regular lysosomal size, tubulation can happen again (data not shown).

It is possible that the correlated lysosomal cholesterol decrease and tubulation restoration observed when calcium homeostasis is modified (although activating TFEB in parallel) is explained by a change of osmosis of the lysosome. This change of osmosis would allow the lysosome to deform its membrane and to export cholesterol again (Boutry et al., 2019b), rather than a cholesterol decrease would allow lysosomal membrane deformation, especially considering the modest proportions of the cholesterol accumulation in lysosomes of these cells (Boutry et al., 2019b).

e) Lysosomal calcium and tubulation

It was shown that in absence of spatacsin, store operating calcium entry is responsible for elevated lysosomal calcium levels (Boutry -unpublished data). As we have seen that ER has the ability to transfer calcium to lysosomes (Atakpa et al., 2018), we can wonder if the increased lysosomal calcium levels come from an increased ER-lysosomal calcium transfer at contact sites between ER and lysosomes. And as spatacsin is localized at these contacts, we can wonder if it is having a role in regulating this calcium transfer from the ER to lysosomes, maybe via some of its partners.

Moreover, as TRPML1 releases less calcium in absence of spatacsin (Boutry -unpublished data), the lysosomal calcium levels are less decreased upon TRPML1 activation, and these alterations can be problematic for osmosis of lysosomal compartment and local calcium signaling. The activity of TRPML1 channel has direct consequences on the ability of the lysosomal membrane to deform (Li et al., 2016).

f) Kinesin(s) involvement in lysosomal positioning

Interaction in fibroblasts of KIF13A and spastizin

According to one of the first study on spastizin, it interacts with KIF13A to regulate its transport to midbody for cytokinesis (Sagona et al., 2010). We verified this interaction by immunoprecipitation; it is not extremely strong but both proteins are expressed at low levels and are difficult to detect. The interaction is stronger between spastizin and the motor-less KIF13A-ST.

When expressed in mouse fibroblasts, KIF13A shows a tubular recycling endosomes enrichment as described in (Delevoye et al., 2014a). We can observe some KIF13A at lysosomes, but it is far from most of it. KIF13A devoid of motor domain was much more enriched at lysosomes which could explain its better interaction with lysosomal spastizin. Or this could be explained by the fact that spastizin interacts with the "Stalk" part of KIF13A and not the motor domain, and the presence of the motor domain might perturb the interaction (see **Figure 70**).

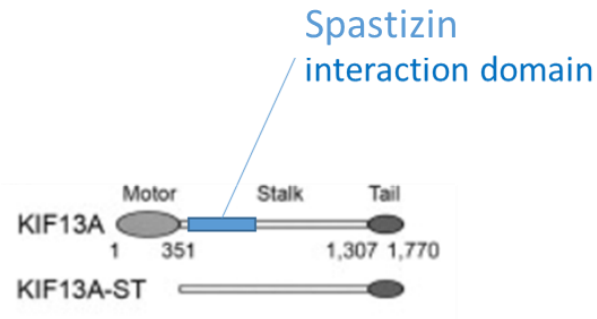

Figure 70: spastizin interacts with KIF13A and KIF13A-ST (Delevoye et al., 2014b; Sagona et al., 2010b)

KIF13A has been shown to regulate sorting of lysosomal enzymes and is involved in endosomal positioning (Delevoye et al., 2009; Nakagawa et al., 2000), so it is rather an interesting kinesin for regulation of lysosomal positioning.

KIF13A contribution to lysosomal positioning

The clustering of lysosomes induced when we express KIF13A-ST is intermediate compared to the clustering we observe in absence of spatacsin, and the same effect happens when we overexpress AP5z1 which prevents spatacsin interaction with spastizin and therefore KIF13A action (see **Figure 68 and Figure 71**). It is likely that tubular lysosomes movement and positioning is not reliant only on KIF13A but rather on several kinesins (such as KIF5B or others).

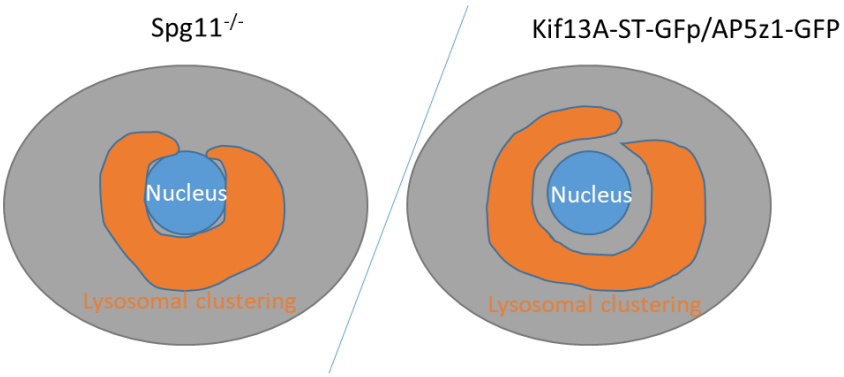

Figure 71: perinuclear clustering of lysosomes is slightly different when "motor-less" KIF13A is expressed compared to cells lacking spatacsin.

It would be interesting to test the effect of downregulation of other kinesins such as KIF5B in our model to see what the effect on tubular lysosome dynamics and positioning in the cell would be. Moreover, it has been shown that lysosomal movement is not the same considering the kinesin they travel with (Guardia et al., 2016). It is therefore possible that different classes of tubular lysosomes exist depending on which kinesin they bind to, similarly to what was proposed in a recent publication (Suresh et al., 2021). This adds a layer of complexity in the regulation of cellular movement of tubular lysosomes.

III. The importance of Spatacsin_C domain

We have shown that spatacsin regulates tubular lysosomes formation & dynamics, and that these function of spatacsin was dependent on the presence of the domain encoded by its exons 32 to 34. This 3 exons long domain overlaps with Spatacsin_C domain which is a conserved domain of the protein.

a) Potential structure of Spatacsin_C domain

"Spatacsin_C" domain has been conserved throughout evolution and has a potential structure homology with the Cter domain of VPS16 (Alexander L. Patto and O'Kane, 2020). Interestingly, mutations of VPS16 result in lysosomal abnormalities in patients with dystonia or with mucopolysaccharidosis, a form of lysosomal storage disorder (Sofou et al., 2021; Steel et al., 2020, p. 16). This lysosomal phenotype could be linked to the function of VPS16 in the autophagosome-lysosome fusion, (Jiang et al., 2014; Wartosch et al., 2015). A similar defect in lysosome-autophagosome fusion in absence of spatacsin has been proposed by another publication on $Spg11^{-/-}/Spg15^{-/-}$ model (Khundadze et al., 2021). We have not observed similar defects when we considered the total lysosomal population in our cells in absence of spatacsin but this might require additional attention and investigation especially regarding tubular lysosomes and their fusion with other compartments.

b) $Spg11^{\Delta 32\text{-}34/\Delta 32\text{-}34}$ mouse model

Mice that express the truncated spatacsin $^{\Delta 32\text{-}34/\Delta 32\text{-}34}$ develop a neuronal loss and a motor phenotype that strongly resembles the motor phenotype acquired by mice depleted of spatacsin (see **Figure 62**). This tells us that spatacsin function in tubular lysosome formation & regulation of their dynamic which is dependent on spatacsin$^{32\text{-}34}$ domain is linked to neurodegeneration.

We also observed accumulation of Ganglioside GM2 in lysosomes in the brain of $Spg11^{\Delta 32\text{-}34}$ mice and in cultured neurons (see **Figure 63**). This is like what was observed in (Boutry et al., 2018) showing that spatacsin$^{32\text{-}34}$ domain is important for the regulation of lysosomal function.

c) Diversity of identified spatacsin$^{32-34}$ partners

Performing a siRNA mini-screen on spatacsin$^{32-34}$ domain interactors

There was a very large number of proteins (about 80) that were identified to interact with the C-Ter part of spatacsin (a.a. 1943-2443). Yeast 2 hybrid technique for protein-protein interaction identification is producing a lot of false positive results (Zhang et al., 2010), and most of the interactions with spatacsin were rated "D" so potentially resulting of false-positive interaction. Considering the interactors that were specific of the spatacsin$^{32-34}$ domain helped shorten the list of spatacsin interactors that might be involved in tubular lysosome formation regulation.

Taking advantage of the generated data set to perform a non-biased analysis

One of the shortcomings of the siRNA mini screen that I performed was that I decided arbitrarily which parameter I was going to measure (i.e., the number of tubular lysosomes) to evaluate the consequences of each siRNA. The number of tubular lysosomes observed per cell is variable from one day to the other but the tubular lysosome loss in absence of spatacsin is always visible. This led me to normalize the number of tubular lysosomes observed in each condition to the controls of each batch of conditions. This strategy allowed me to have tubulation scores that we could rank and compare no matter the day the experiment was performed.

And in parallel, I had generated this large data set of images of lysosomes with many Spg11$^{+/+}$ and Spg11$^{-/-}$ conditions (about 750 images for each condition) that were my controls for each batch of siRNA that were tested. So, there came the idea to perform an unsupervised analysis by training a neural network. There was however not enough images to train a neural network, so we had to artificially increase the number of images by cropping them or rotating them, which is a common practice in neural network training (Shorten and Khoshgoftaar, 2019).

The short list of interactors of spatacsin Cter involved in tubular formation

Once the neural network was able to differentiate between Spg11$^{+/+}$ and Spg11$^{-/-}$ conditions, we could perform a new classification of the siRNAs effects. The comparison of the results obtained by the 2 approaches showed convergences & some differences, likely because the neural network considers more parameters than the directed analysis. But overall, we obtained a final shortlist of genes (see **Figure 72**).

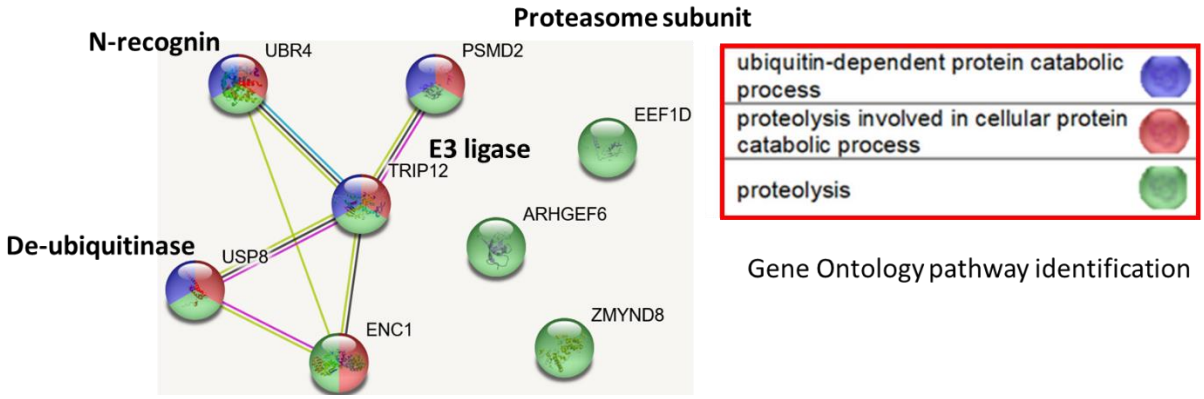

Figure 72: The short list of the 8 spatacsin[32-34] potential interactors important for tubular lysosome formation after comparing both method of analysis, and their involvement in different pathways.

UBR4 and its multiple potential roles

We have shown that UBR4 was involved in spatacsin mediated degradation of AP5z1, but UBR4 has been studied for other interesting functions. UBR4 interacts with microtubules and the endoplasmic reticulum in neurons (Shim et al., 2008, p. 600) and it is interestingly causing Episodic Ataxia when mutated (Conroy et al., 2014). On top of that, UBR4 binds to calmodulin to regulate calcium homeostasis in neurons (Belzil et al., 2013) and forms meshwork structures with clathrin contributing to membrane morphogenesis (Nakatani et al., 2005). All these features of UBR4 make it a very interesting interactor of spatacsin, especially at the level of ER-Lysosomes contact sites.

Other potentially interesting interactors of spatacsin

We have identified a role of UBR4 in AP5z1 ubiquitin-dependent degradation, but we have not investigated what might be the potential link between the other interactors and tubular lysosome formation. While PSMD2 and USP8 seem to be involved in ubiquitin dependent protein degradation, the rest of the interactors seemed hardly related to the mechanism we have identified, and it is likely that they are involved more indirectly in tubular lysosome formation.

PSMD2 encodes the subunit Rpn1 of the proteasome, which is involved in the recognition and docking of ubiquitin and ubiquitin like domains (Shi et al., 2016). USP8 is a hereditary spastic paraplegia gene (Novarino et al., 2014). The protein has a de-ubiquitinase activity and spatacsin is interacting with USP8 at its de-ubiquitinase domain, maybe spatacsin could be under the regulation of ubiquitin signaling and de-ubiquitinated by USP8? It has also been shown that USP8 is important for endosomal integrity and, in its absence, ubiquitinated proteins accumulate in endosomes (Row et al., 2006).

d) Comparison of different interactomes of spatacsin

We have identified many potential interactors of spatacsin Cter domain using the yeast 2 hybrid screening technique. Two other recent publications on *BioRxiv* published potential interactors of spatacsin using different techniques.

The first paper used a mass spectrometry approach to identify interactors of a GFP-Spatacsin_C construct expressed in Mel-2 cell line of *Drosophila* (Alexander L. Patto and O'Kane, 2020). They performed two screens based on the promoter they used to express the spatacsin construct. This approach identified membrane trafficking proteins and several aminoacyl-tRNA synthetases as potential interactors of Spatacsin_C domain.

The second paper identified interactors by mass spectrometry from a pull-down of interactors of a spatacsin-Flag construct that was exposed to a lysate of murine brain (Cogo et al., 2020). They identified a subset of 14-3-3 proteins as physiological interactors of spatacsin, which interaction is modulated by PKA-dependent phosphorylation of spatacsin at Ser1955.

The three interactomes identify tens to hundreds of potential interactors of spatacsin. The common proteins that were identified between the different screens are listed in **Figure 73**.

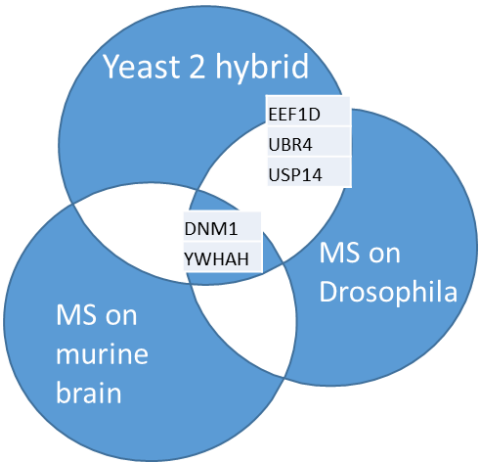

Figure 73: Common potential interactors of spatacsin in three interactomes

The only two common proteins identified by the three approaches were Dynamin1 and YWHAH. We have confirmed interaction of Dynamin1 with spatacsin by co-immunoprecipitation (Boutry et al., 2018), and Dynamin1 is a neural specific dynamin involved in membrane fission of organelles (Lee et al., 2016). This points toward a potential role of spatacsin in membrane fission via Dynamin1, which is particularly interesting as preliminary data indicate that there might be an excessive fission of the tubular lysosomes in absence of spatacsin.

YWHAH is an adaptor of the 14-3-3 protein family which is involved in regulation of its binding protein through interaction with phosphorylated motifs (Cogo et al., 2020). According to the study, spatacsin phosphorylation by PKA enzyme would promote its interaction with YMHAH and promote its re-localization from the plasma membrane to the rest of the cell. Phosphorylation of spatacsin is an interesting parameter to consider concerning its potential regulation.

The fact that spatacsin has so many potential interactors is quite a surprising result, considering that it is expressed at very low endogenous levels. It is nonetheless possible that it is one of the features of spatacsin to have the capacity to interact with many proteins, like adaptor proteins for example. Moreover, the overlap between interactomes is very small so there is a strong chance that there are a lot of false positive interactors in these data. It is interesting to note that UBR4 that we have identified in our mechanism and confirmed interaction with spatacsin by co-immunoprecipitation is found in another interactome.

IV. Spatacsin mechanism of action with interactors spastizin & AP5z1

We have shown in our study that both spastizin and AP5z1 were necessary for spatacsin regulation of tubular lysosome formation and dynamics.

Spatacsin$^{\Delta 32\text{-}34}$ does not interact with spastizin and AP5z1

We observed that truncated spatacsin does not interact by co-immunoprecipitation with AP5z1 and spastizin. This might explain why the lysosomal defects observed with truncated spatacsin are so resembling the ones of cells devoid of spatacsin, as spatacsin interaction with spastizin and AP5z1 is paramount for tubular lysosome formation as we have shown.

Ubiquitin-dependent degradation of AP5z1 promoted by spatacsin

We have shown that the regulation of AP5z1 levels must be precise as too much or too little AP5z1 results in tubular lysosome loss and in tubular lysosome dynamics alteration. But how is AP5z1 degraded?

We tested the effect of preventing proteasomal degradation with MG-132 and preventing lysosomal acidification with bafilomycin on spatacsin promotion of AP5z1 degradation (see **Figure 67**).

These results, that need to be confirmed, seem to indicate that AP5z1 degradation would be taking place in the lysosomes rather than at the proteasome. If it verifies that AP5z1 is indeed degraded at the lysosomes, it poses an interesting challenge as the protein is normally at least partially located at lysosomal membrane. It is possible that AP5z1 is shipped from one lysosome to another for degradation or that it needs to be relocated to the cytosol to be degraded but then we don't know how this could be happening.

While the downregulation of UBR4 led to increased levels of AP5z1, downregulation of potential interactor USP8 led to reduced levels of AP5z1 and to lesser interaction with spatacsin. It is therefore possible that spatacsin-AP5z1 interaction is mediated by other interactors of spatacsin such as USP8, in an antagonist regulation of UBR4 regulation. There are maybe different layers of complexity in the mechanism of spatacsin promotion of degradation of AP5z1 mediated by proteins of the ubiquitin-proteasome pathway.

Spatacsin-spastizin interaction at ER-lysosomes contact sites

If it is so important to degrade AP5z1, it is to prevent it from reducing spastizin-spatacsin interaction by competitive interaction. Moreover, blocking this spastizin-spatacsin interaction prevents spastizin recruitment to lysosomes, a result coherent with what was observed recently in another study (Hirst et al., 2021b). Accordingly, we observed that in Spg11$^{-/-}$ cells, overexpressed spastizin is not efficiently recruited to lysosomes compared to when spatacsin is present. In Spg11$^{-/-}$ cells, AP5z1 levels are decreased by about 50%, so the mis localization of spastizin there is not linked to AP5z1 excess but to the lack of spatacsin. This shows that AP5z1 mediation of spastizin localization is only happening via its interference in spatacsin-spastizin interaction. Indeed, downregulating AP5z1 had no effect on spastizin localization at the lysosomes (Hirst et al., 2021b).

Proximity ligation assay showed that spatacsin-spastizin interaction is happening only at the lysosomes. This interaction is happening likely at membrane contact sites between ER and lysosomes as we know spatacsin is present in majority at the ER, while spastizin is enriched at lysosomes. This ER-lysosome specific interaction is supported by the fact that modifying ER-architecture with ATLK80A diminishes this spatacsin-spastizin interaction. It appears also that this modification of ER prevents spatacsin degradation of AP5z1, which would suggest that this degradation is also dependent on a functional ER-lysosome contact. It would be interesting here to quantify if ATLK80A induces a loss of ER-lysosome contacts and if it has consequences on the sub-cellular localization of spatacsin, spastizin and AP5z1.

During this study, we learned a lot on spatacsin molecular role and its regulation of the tubular lysosomes formation. However, with every answered question come several new ones. We are not yet at the point where we understand everything of spatacsin molecular role and new challenges and questions await for future studies on spatacsin.

V. Shortcomings of the study

a) The use of non-neuronal model

Spatacsin is expressed in the whole body, although its loss affects mostly neuronal cells as observed in SPG11 HSP patients (Deluca et al., 2004) and in Spg11-/- mice (Branchu et al., 2017). During this study, we used Mouse Embryonic Fibroblasts (MEF) as a model to study the molecular role of spatacsin. Fibroblasts are a relatively undifferentiated mesodermal derived cell type found in abundance in connective tissue and responsible for the secretion of extracellular matrix (Garfield, 2010). Primary fibroblasts obtained from mice embryos are much easier to culture than neurons. The main advantage of using MEFs is that, granting that you obtain the genotype you want in your breeding, you can have a pair of cell lines in a single dissection, one wild type and one Spg11$^{-/-}$ that are extremely close genetically. MEFs grow fast in culture, they can be frozen for later use and can be easily electroporated, a transfection technique that I used a lot during this study for gene downregulation or gene over-expression. Spg11$^{-/-}$ MEFs show no obvious alteration of proliferation, only the lysosomal phenotype that we mentioned was observed.

Neuronal cultures are much more complicated to handle to perform the same experiments as MEFs, but they do reflect more accurately the pathology associated with spatacsin loss of function. For example, MEFs do not accumulate ganglioside GM2 that was associated with neurodegenerative phenotype in mice and zebrafish (Boutry et al., 2018) in their lysosomes. Monoculture of neurons issued from mouse embryos remain an imperfect model as well, as it does not reflect the real complexity of the brain, nor does it reflect of the extreme architecture of axons of the pyramidal tract that are affected by spatacsin loss of function. It was shown that Spg11$^{-/-}$ neurons are most susceptible to cellular death when exposed to glutamate (Boutry et al., 2018) but I also observed that after 15 days of culture, they die more than Spg11$^{+/-}$ and Spg11$^{+/+}$ neurons (see **Figure 74**).

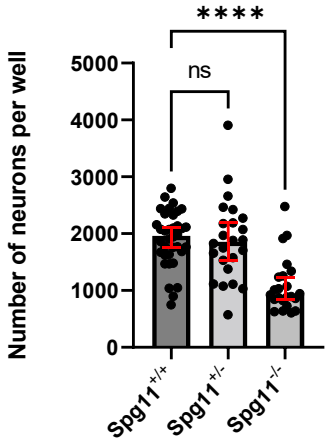

Figure 74: Survival rate of Spg11$^{-/-}$ neurons is altered after 15 days of culture. **** MW test p<0.0001

Although we know that neuronal cultures accumulate cholesterol like fibroblasts and present calcium homeostasis alterations (Boutry et al., 2019a), we did not observe tubular lysosomes in neurons. We also haven't studied the dynamics of their lysosomes in absence of spatacsin, which would be interesting to study.

b) The difficulty of working on endogenous spatacsin

Spatacsin and its binding partners AP5z1 and spastizin are expressed at very low endogenous levels (Hirst et al., 2021b). Moreover, the antibodies available for spatacsin are poorly specific, except from the one manufactured by ProteinTech (see Experimental Procedures) which is acceptable for western blot applications. Therefore, detecting spatacsin on western blot assays always required loading an $Spg11^{-/-}$ control to see which band corresponds to spatacsin as there are so many that are marked by the anti-spatacsin antibody.

In our study, we had to over-express tagged proteins to observe them. If it allowed us to study their localization for example, as it was not representing their real level of expression in the cell, it might have created artifacts. Although protein over-expression is not ideal, it has the advantage to be easily obtained, images can be acquired in less than 12 hours after transfection of cells. Again, working on a model that has an endogenous tagged spatacsin would have been interesting, this was recently achieved and seems promising for spatacsin study (Krumm et al., 2021).

c) Cellular biology and reductionism

Emergence of complexity

In cell biology, it appears impossible to explain all phenomena that are taking place. Moreover, there is a difference between "naming the parts" that are involved in a mechanism and explaining how the mechanism works. Most of the times, we deal with an input parameter that will affect a "black box" mechanism that will produce an output parameter (Nurse, 1998). In this study on spatacsin molecular role, we are getting closer to the explanation, but we are not there yet. We were able to cut the mechanisms into parts by invalidating some genes, but can we reconstruct the mechanisms by just a sum of the parts? There could be layers of interaction that we did not anticipate like redundancy between our parameters for example.

Moreover, the emergence of complexity in "simple" mechanisms applies to cellular biology and models that don't include many parameters can behave in very complex patterns (Kauffman and Kauffman, 1993). This goes with the notion of chaos, also known as "butterfly effect", emerging in the variability of simple phenomena (Gleick, 1987). Indeed, there are so many interconnected pathways of regulations interacting with one another, that a minor change at one end of the mechanism could result in drastic changes at the other end in an unpredictable fashion. This is preventing us to draw simple boundaries and to oversimplify mechanisms or think that they will always be accurately describing the reality. However, this does not prevent us to try to build as accurate as possible models that will capture a good part of the information, even being by essence unable to capture the whole complexity of biological mechanisms. Recent examples highlighted the limitations of reductionism in approaches of regulation of organisms development (Green and Batterman, 2017).

These are the reasons that motivated us to limit the study of spatacsin molecular role to a few proteins despite identifying several interesting interactors of the protein, as the more elements there are in a mechanism, the more complexity there will be. The advantages we had in this study were that first, we were working on "intact" cells with live-imaging, and we did not limit our approach to only in vitro assays such as western blot analysis of cell lysates. Moreover, in our study, we tried to introduce the notion of time, indeed even if it was just for a few minutes of imaging, we followed the cell for more than a single snapshot at a given time point, which allowed us to extract additional information on the behavior of the lysosomes. Finally, using the siRNA technology allowed us to precisely downregulate genes one by one, limiting the number of parameters involved.

The scale dilemma

At which scale should we model a biological problem? When we study a biological phenomenon, this question might be difficult to answer. Indeed, if we take the example of our study on spatacsin molecular role, what is indeed causing the neurodegeneration? Is it the unfulfilled molecular role of spatacsin at the ER-Lysosomes interface? Is it an impairment of the lysosomal compartment at the subcellular level due to spatacsin absence? Is it an impairment of the general cell metabolism caused by an imbalance of the lysosomal function? Is it a specific cell type malfunctioning in a tissue that results in an alteration of the whole functioning of an organ? All scales are connected but identifying the one that is the most important for the development of neurodegeneration is not an easy task.

If we consider the example of the gain of resolution provided by STED imaging (see **Figure 75**), when we look at the interaction between Endoplasmic Reticulum and Lysosomes, we realize that we completely miss the complexity of this interaction at low resolution. STED imaging reveals how tightly entangled the compartments are.

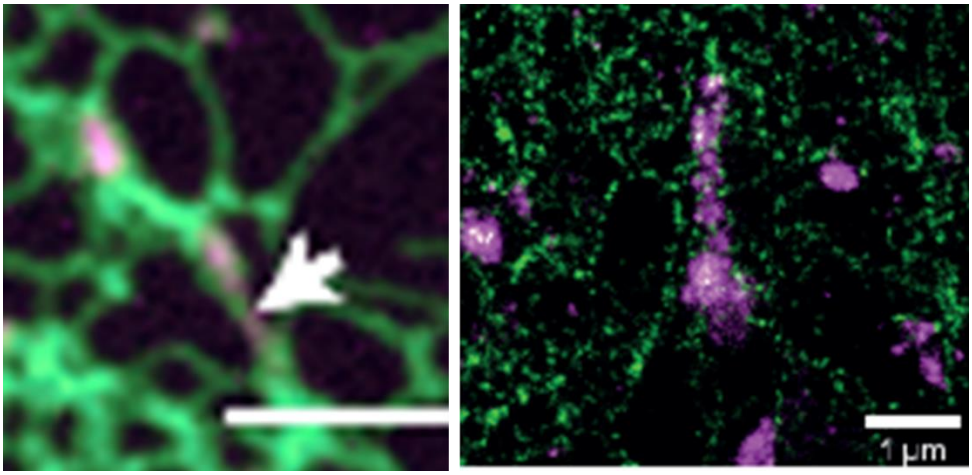

Figure 75: The gain of resolution from spinning disk imaging (left) compared to STED imaging (right) changes the dimension of ER-Lysosome connection. Magenta: lamp1-mcherry. Green: ER staining (sec61/RTN2). Scale bars: Left 5 µm, Right 1 µm.

It is as if it is not the same question anymore for ER-Lysosome interaction, we can wonder if it does make sense to distinguish between compartments at this interface? When we see there is so much proximity in the contact between them and how they appear so tightly bound.

Limits of reductionism

The general reductionist approach of cellular biology is reflected by the existence of many subdisciplines: regulation of autophagy, of cellular traffic, of cellular signaling etc. This might cause problems of inapplicability and of identifying clear cut effects (Brigandt and Love, 2017). Indeed, models get so specialized that it is sometimes difficult to find the way back to the original scientific question that motivated the design of the model. This might explain the difficulty to go back to the patient level from a cellular biology finding. It first requires an as accurate as possible understanding of the studied mechanism to see if we can find any way to rescue eventual defaults. Then going back, in our example, to the neuronal level is necessary and challenging, then bringing up the solution to the mice model requires additional testing of the model and then eventually, at the end of the process, if all steps are correctly overcome the patient might benefit from it.

According to (Brigandt and Love, 2017), it would be interesting to mix up more disciplines in the design of our models in an attempt to capture more information. In our study this evokes to me the use of more precise physics for lysosomal deformation or movement modelling, the use of automation to collect large data sets bearing more statistical power and the use of machine learning to pick parameters that might be too complex for the human brain to imagine. As reductionism is likely an imperfect way to study biological phenomena, it is however the least bad available option to study them and has produced great successes over the years of cellular biology history. That said, it is important that we remain careful in our scientific practice and humble in our conclusions as we ignore far more than we know.

VI. Importance of this work

a) Better understanding of spatacsin molecular function

In this study on spatacsin molecular role, we produced original data. Indeed, the sub-cellular fractionation of mouse brain revealed spatacsin sub-cellular localization and had never been performed before, likely due to the difficulty of performing spatacsin detection by Western Blot. We managed to extract a lot of information from these assays that helped us to learn more on spatacsin localization and ultimately on its function. This was combined with microscopy approaches to take advantages of super-resolution imaging (STED) which revealed the localization of spatacsin-V5 to endoplasmic reticulum staining.

Moreover, we showed that spatacsin function was important to regulate the tubular lysosomes dynamics, a role that was never identified before, even if spatacsin involvement in the regulation of lysosomal compartment had been studied. We also showed that spatacsin function in the regulation of tubular lysosome dynamics was dependent on spatacsin$^{32\text{-}34}$ domain. The importance of this domain for SPG11 HSP is highlighted by the neurodegenerative phenotype that is affecting mice that have a truncated spatacsin$^{\Delta 32\text{-}34}$.

Spatacsin interaction with proteins of the ubiquitin depedent pathway to regulate tubular lysosome formation is a new feature of spatacsin role that we discovered. This is also an interesting example of regulation of a lysosomal function that is based on ubiquitin signaling.

The ability of spatacsin to promote UBR4-dependent degradation is a new role for spatacsin and the involvement of this degradation in promoting the localization of spastizin to lysosomes confirms recent findings (Hirst et al., 2021b).

b) Contribution to the field of tubular lysosomes

While lysosomal and endosomal tubulation for compartment recycling is extensively studied, the field of tubular lysosomes is rather modest. We have confirmed that tubular lysosomes are particles that are more mobile than round lysosomes. We have shown that this motility is under a ubiquitin and spatacsin dependent regulation. We have confirmed that tubular lysosomes are indeed acidic compartments that represent a population of catalytically acidic lysosomes. We have shown that these tubular lysosomes can be observed in basal conditions in mouse embryonic fibroblasts, without requiring stimulation by cellular stress.

We have identified a new role of ubiquitin-proteasome pathway in the regulation of tubular lysosome formation and lysosomal dynamics which was not expected and unknown. We have shown that kinesin KI13A is involved in tubular lysosome formation and dynamics, adding KIF13A to the list of kinesins regulating lysosomal movement.

c) Validating the use of automated tracking and image analysis to study lysosomes

Our original approach combining the precise technology of siRNA, yeast 2 hybrid screening for exploratory discovery of interactors and live imaging using a well-defined parameter showed to be an efficient method to study the role of potential interactors of a protein. We reduced its time-consuming cost by taking advantage as much as possible of automation in image analysis.

Our use of the neural network directed analysis that reinforced our results showed that unsupervised classification is possible and beneficial in the screening of potential interactors.

d) Contribution to the functions of spastizin and AP5z1

We confirmed a lysosomal localization for AP5z1 and spastizin and confirmed that spastizin localization at the lysosomes was dependent of spatacsin. We have shown that spatacsin dependent recruitment of spastizin to lysosomes could be negatively regulated by competitive interaction of AP5z1 with spatacsin. We have identified a mechanism for AP5z1 ubiquitin dependent degradation via UBR4 and spatacsin regulation. We have also shown the cooperation of spastizin and AP5z1 with spatacsin to regulate the formation and dynamic of tubular lysosomes

We have confirmed the interaction of spastizin with KIF13A and showed that they were both involved in tubular lysosomes dynamics regulation.

e) A new function for ER-lysosome contacts

As spatacsin-spastizin interaction was happening only at the level of lysosomes, we have identified a new protein-protein contact materialized by spatacsin and spastizin at ER-lysosomes contact sites. This interaction is involved in the promotion of tubular lysosomes formation and dynamics. It is under regulation of a ubiquitin-dependent signaling pathway that degrades AP5z1.

Moreover, it appears that this ER-Lysosomes contact is dependent of ER-architecture integrity and was perturbed upon ER-architecture disruption. This resulted in an alteration of the promoting role of the protein-protein interaction for tubular lysosomes dynamics. Ubiquitin signaling and ER architecture remodeling being very dynamic, it is likely that this new type of ER-Lysosomes contact is also very dynamic and adaptive to changes in cellular environment.

f) A better understanding of mechanisms linked to Hereditary Spastic Paraplegia

Thanks to the identification of this spatacsin-based mechanism of regulation of the lysosomal function we have a better understanding of the "ER-Lysosomes connection" that is happening in the context of Hereditary Spastic Paraplegia. Indeed it is a thematic that has been evoked before (Allison et al., 2017b; Lee and Blackstone, 2020), proteins that are located at the ER regulate the lysosomal function via ER-Lysosomes contact. Spatacsin, is likely present at ER-Lysosomes contacts, therefore joining the family of proteins that are mutated in forms of HSP, located at the ER and involved in endolysosomal compartment regulation along with Spastin, REEP1 and Strumpellin.

As the endolysosomal pathway appears to be dysregulated at many levels due to the mutation of proteins linked to HSP (see **Figure 76**), it is therefore important to continue to dig for an eventual unifying mechanism of endolysosomal compartment regulation by ER proteins for hereditary spastic paraplegias. Moreover, the involvement of endolysosomal defects in neurodegenerative diseases has been shown to be broader than HSP so it important to investigate the mechanisms regulating them for the understanding of the cellular biology of neurodegenerative diseases in general.

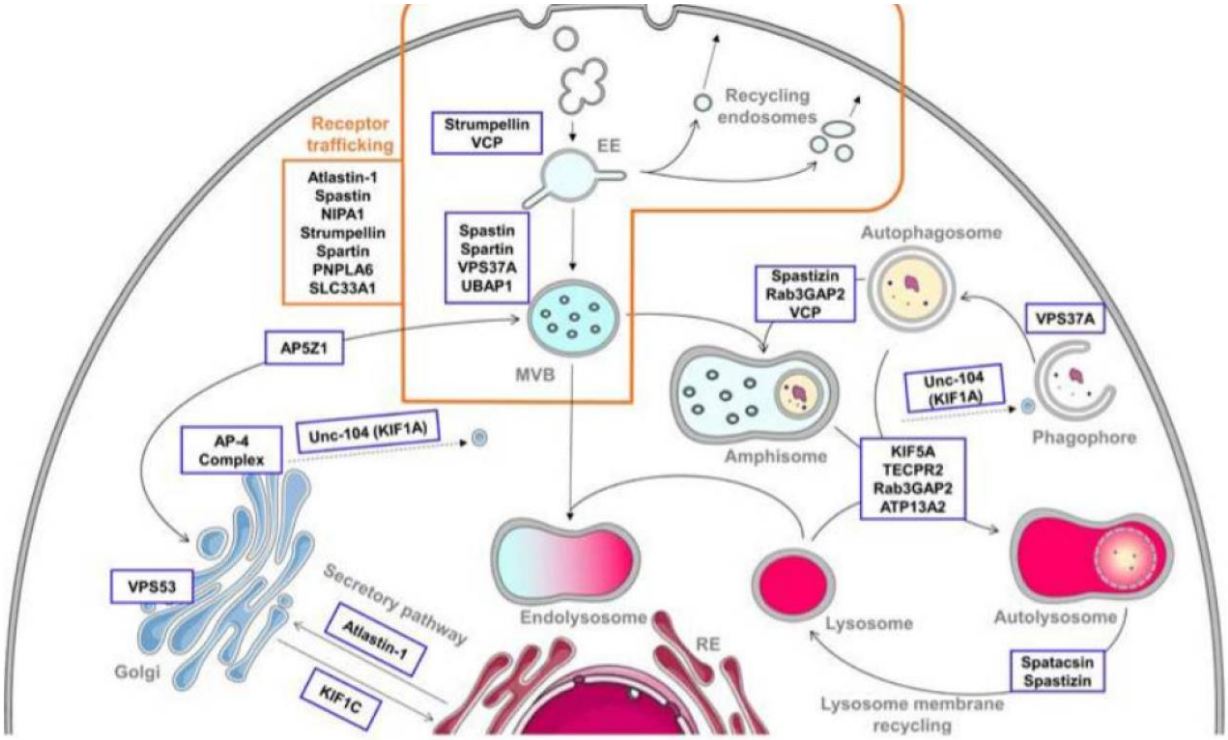

Figure 76 : Involvement of hereditary spastic paraplegia proteins in the regulation of the endolysosomal pathway (Toupenet Marchesi et al., 2021)

VII. Next challenges & perspectives:

a) Can we regulate tubular lysosome formation in a positive way?

As we have seen in this study, spatacsin regulates tubular lysosome formation and their dynamics. We have identified several proteins involved in this mechanism as we have shown that they were necessary for the tubular lysosomes to form. It will also be interesting to identify positive regulators of tubular lysosome formation that could help us rescue spatacsin loss of function and potentially find a path to prevent neurodegeneration caused by spatacsin loss.

Expressing spatacsin

Rescuing spatacsin loss in Spg11$^{-/-}$ cells by re-expressing spatacsin has proven to be a difficult task. Indeed, it is very difficult to express spatacsin in cells, the efficiency of transfection is extremely low. I was unable to observe any spatacsin-GFP cells in live imaging as the signal was too low, making it difficult to observe tubular lysosome formation or tubular lysosome dynamics. The few cells that we can observe expressing a tagged spatacsin require the use of anti-tag antibodies. By using fixations techniques that conserve tubular lysosomes and expressing tagged spatacsin, I did not observe a significant rescue of the tubular lysosome formation.

We must consider that Spg11$^{-/-}$ cells have almost no spastizin and reduced level of AP5z1, so to have a positive effect on tubular lysosome formation, it is possible that we need to express the 3 proteins. As they all have low transfection efficacy, it is an almost impossible task, unless changing the transfection method and using a more efficient method like lentiviral infection. However, Spg11 cDNA is too large for insertion in classical viral vectors used for gene therapy (up to 6.5kb while Spg11 cDNA is 7.7kb) (Bulcha et al., 2021)

Stimulating ubiquitin-dependent degradation

Besides trying to express spatacsin in cells, we could target other levels of the mechanism regulating tubular lysosome formation. This could be done for example by targeting the ubiquitin dependent degradation and promoting the degradation of substrates by using PROTAC technology (Huang and Dixit, 2016) (see **Figure 77**).

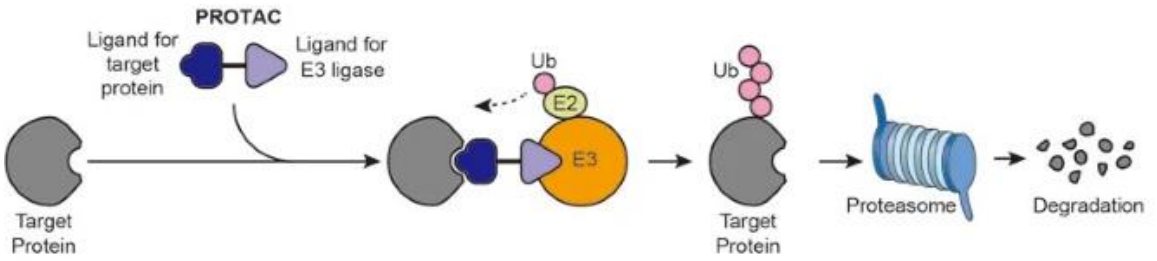

Figure 77: The principles of PROTAC technology to specifically promote the ubiquitin-dependent degradation of a substrate (Huang and Dixit, 2016).

This technology is based on the design of proteins that will promote the ubiquitination of substrates thanks to their capacity to bind the target protein and E3 ligases (see **Figure 77**). Similar results can be achieved by tagging unwanted proteins with a hydrophobic ligand that will be recognized by the chaperone machinery and targeted for degradation. However, the challenge here would be to identify which proteins should be degraded to have a positive impact on tubular lysosome formation.

Stimulating spatacsin/spastizin/AP5z1 recruitment to lysosomes

We observed an enhancement of the tubular lysosome formation in starvation conditions, coinciding with the recruitment of spatacsin/spastizin/AP5z1 to the endolysosomes. It would be interesting to test the effect on tubular lysosomes formation of short exposition of cells to YM2016-36 and of expression of GDP-locked RagC, two conditions that stimulate spatacsin/spastizin/AP5z1 recruitment to lysosomes, (Hirst et al., 2021).

Testing a DNA nanodevice promoting tubulation

A recent study described the promoting tubulation effects of *Tudor*, a DNA nanodevice that triggers lysosomes tubulation in macrophages without activating them. *Tudor* is designed to be internalized by endocytic uptake and to display a fluorescent reporter. Its activity seems to be also independent of autophagy activation (Suresh et al., 2021). Testing the effect of *Tudor* on tubular lysosome formation in Spg11$^{-/-}$ cells could eventually restore it.

Expressing kinesins to restore tubulation and movement

Overexpressing kinesins such as KIF13A or KIF5B to compensate for the loss of tubular lysosomes dynamics could be tested as they are important for lysosome dynamics. The P180 protein, a KIF5B-binding protein enriched in ER tubules seems to have a promoting role for ER mediated transport of lysosomes (Özkan et al., 2021). Expressing P180 in Spg11$^{-/-}$ fibroblasts may compensate the effect of loss of spatacsin on tubular lysosome formation and dynamics.

b) Digging into the mechanism complexity

The results we obtained allowed us to propose a role for spatacsin in regulating lysosome dynamics. However, several questions have still not been explored and may refine the mechanisms of action of spatacsin.

Precising spatacsin cellular localization at ER-lysosomes contacts

Why is it important for spatacsin to be at the interface between ER and lysosomes? The ER is a very dynamic compartment, in constant remodeling. Moreover, as most late endosomes and lysosomes are in contact with the ER, being present at ER-Lysosomes contact sites allows for a precise access to lysosomes to regulate their function even at the low expression levels of spatacsin. This is therefore a strategic position to regulate endolysosomal function for spatacsin.

To precisely obtain the exact position of spatacsin at ER-lysosomes contacts, we could try to locate V5-tagged spatacsin in electronic microscopy images by using biotin-conjugated antibodies against V5 tag or by using an APEX-spatacsin construct (Lam et al., 2015). Electron microscopy resolution would allow us to obtain a very precise spatacsin subcellular localization. However, as spatacsin is very poorly expressed, this approach requires a correlative microscopy set up to identify the position of the few cells expressing tagged-spatacsin before proceeding to electron microscopy preparation. Another alternative would be to perform three colors STED imaging to observe the interaction between the ER, the lysosomes and V5-tagged spatacsin.

Modulating the ER tubular network

Could we play on the ER tubular network to modulate tubular lysosome dynamics? Indeed, we have shown that preventing homotypic fusion of ER tubules altered the formation of tubular lysosomes and their general dynamics, but what about promoting this homotypic fusion?

However, it is difficult to find ways to do so, overexpression of ER-tubular morphology regulators RTN3 or ATL3 do not seem to create more junctions between ER tubules (Chen et al., 2019, p. 3; Grumati et al., 2017, p. 3). Moreover, it has been shown that, upon starvation, because of the peri-nuclear clustering of lysosomes toward the cell center, there is a reduction of the number of three way junctions and of ER-tubular network complexity (Spits et al., 2021b). As we have seen that starvation had a positive effect on tubular lysosome formation, this constitutes a mechanism independent of spatacsin action or, as this change in ER morphology is not drastic, the balance between ER tubule network branching and tubular lysosome dynamics is more complex than we thought.

Lunapark is localized at three-way ER-junctions (Zhao et al., 2020) and its presence stabilizes the ER tubular junctions (Chen et al., 2015). Could Lunapark expression in cells modulate the tubular lysosome dynamics, and would it be a spatacsin dependent effect? As we have seen no major alteration of the ER tubular network in absence of spatacsin, we should not expect a strong effect.

Identifying the complete AP5z1 degradation mechanism

We have seen that AP5z1 degradation promoted by spatacsin was dependent on UBR4 and on poly-ubiquitination. However, UBR4 has no E3 ligase activity. Then, which E3 ligase is ubiquitinating AP5z1? UBR4 interacts with KCMF1 (E3 ligase) and RAD6 (E2) to regulate N-end rule substrates lysosome mediated degradation (J. H. Hong et al., 2015). It would then be interesting to test the involvement of KCMF1-RAD6 in AP5z1 degradation as it appears that this process is

taking place at the lysosomes. The lysosomal degradation of AP5z1 is further supported by the fact that UBR4 associates with several substrates to degrade them by autophagy, and that its absence is linked to LC3 accumulation (Tasaki et al., 2013).

Measuring lipid transport at ER-lysosomes contacts in absence of spatacsin

We have previously shown by using fluorescent cholesterol that the export of cholesterol from lysosomes was altered in absence of spatacsin (Boutry et al., 2019a). Several mechanisms of cholesterol export out of lysosome occur at contact sites between the ER and Lysosomes. Since we showed that spatacsin is present at this interface, I would like to test now, using the same fluorescent cholesterol, if there is an impairment in cholesterol transfer from the ER to the lysosomes in absence of spatacsin. This would refine the mechanism of import/export of cholesterol at the lysosomes.

On a broader exploratory perspective, there are probably other functions of spatacsin to discover besides the regulation of tubular lysosome formation, indeed it has been recently shown that there were mitochondrial alterations in axons of neurons that lack spatacsin (Güner et al., 2021).

c) Going back to neuronal model

Since loss of spatacsin is responsible for a neurodegenerative disease, it will be important to evaluate whether the observations we made in fibroblasts are also valid in neuronal models.

The ER tubular network is extremely important in polarized neurons

There are multiple ER-Lysosome contacts formed in neurons similarly to what was observed in other cell types (Wu et al., 2017). It appears that in neurons, the ER is polarized: the ER cisternae are localized mostly in the cellular body of the cell while axons contain mostly a tubular ER network. The architecture of this axonal ER network is very important and its disruption could lead to axon degenerative diseases (Öztürk et al., 2020). Moreover, hereditary spastic paraplegia reticulon and REEP proteins are involved in the shaping and maintenance of this axonal tubular network (Yalçın et al., 2017). It would be interesting to evaluate in these models whether the formation of tubular lysosomes, or even the dynamics of lysosomes in axons is disturbed.

Are there tubular lysosomes in neurons?

Furthermore, a recent study showed that ER-lysosome contacts are important for lysosomal movement and axonal lysosome availability (Özkan et al., 2021). In this study, it appears that there are tubular lysosomes in neurons. It would be interesting to see if we can indeed observe tubular lysosomes in our neuronal model. To avoid electroporating these sensitive cells, we could use dyes that we have identified as staining tubular lysosomes in our fibroblast model such as fluorescent dextran and lysotracker. Then, analyzing the dynamics of the lysosomal compartment in neurons in absence of spatacsin will be necessary to look for alterations like the ones we have observed in our fibroblast model.

Is tubular lysosome dynamics loss causing lipid accumulations?

We know that loss of spatacsin leads to accumulation of gangliosides and cholesterol in lysosomes, and that the ganglioside accumulation is linked to neuronal death (Boutry et al., 2018). It would be interesting to evaluate whether the alteration of lysosome dynamics linked to formation of tubular lysosome contributes to the accumulation of lipids in lysosomes. We could first evaluate in fibroblasts if accumulation of cholesterol in lysosomes is modulated by the parameters that we identified as important for tubular lysosome formation and dynamics, such as overexpression of mutant ubiquitin k0, overexpression of AP5z1-GFP, of motor-less KIF13A-ST and of mutant Atlastin-K80A. If these parameters trigger a cholesterol accumulation, it will likely be showing that cholesterol export from lysosomes is reliant on tubular lysosomes formation and dynamics.

Promoting lysosome fusion with other compartments

Moreover, it will be also interesting to investigate the hypothesis of the preferred role of tubular lysosomes in fusion with autophagosomes and endosomes and if such defects could be linked to lipid accumulation. Maybe promoting autophagosomes-lysosome fusion in Spg11$^{-/-}$ cells using c-Src (Suzuki et al., 2020) or overexpressing ATG14 (Zhang et al., 2021, p. 14) could have a beneficial effect on lysosomal accumulations.

If we ultimately find a way to promote tubular lysosome formation and if this is applicable to the better clearance of the lysosomal content in lysosomes of neurons, it will be interesting to test if it could improve their survival in absence of spatacsin.

References

Agromayor, M., Soler, N., Caballe, A., Kueck, T., Freund, S.M., Allen, M.D., Bycroft, M., Perisic, O., Ye, Y., McDonald, B., Scheel, H., Hofmann, K., Neil, S.J.D., Martin-Serrano, J., Williams, R.L., 2012. The UBAP1 subunit of ESCRT-I interacts with ubiquitin via a SOUBA domain. Struct. Lond. Engl. 1993 20, 414–428. https://doi.org/10.1016/j.str.2011.12.013

Ahmed, Z., Sheng, H., Xu, Y., Lin, W.-L., Innes, A.E., Gass, J., Yu, X., Hou, H., Chiba, S., Yamanouchi, K., Leissring, M., Petrucelli, L., Nishihara, M., Hutton, M.L., McGowan, E., Dickson, D.W., Lewis, J., 2010. Accelerated Lipofuscinosis and Ubiquitination in Granulin Knockout Mice Suggest a Role for Progranulin in Successful Aging. Am. J. Pathol. 177, 311–324. https://doi.org/10.2353/ajpath.2010.090915

Allison, R., Edgar, J.R., Pearson, G., Rizo, T., Newton, T., Günther, S., Berner, F., Hague, J., Connell, J.W., Winkler, J., Lippincott-Schwartz, J., Beetz, C., Winner, B., Reid, E., 2017a. Defects in ER–endosome contacts impact lysosome function in hereditary spastic paraplegia. J. Cell Biol. 216, 1337–1355. https://doi.org/10.1083/jcb.201609033

Allison, R., Edgar, J.R., Pearson, G., Rizo, T., Newton, T., Günther, S., Berner, F., Hague, J., Connell, J.W., Winkler, J., Lippincott-Schwartz, J., Beetz, C., Winner, B., Reid, E., 2017b. Defects in ER–endosome contacts impact lysosome function in hereditary spastic paraplegia. J. Cell Biol. 216, 1337–1355. https://doi.org/10.1083/jcb.201609033

Allison, R., Lumb, J.H., Fassier, C., Connell, J.W., Ten Martin, D., Seaman, M.N.J., Hazan, J., Reid, E., 2013. An ESCRT-spastin interaction promotes fission of recycling tubules from the endosome. J. Cell Biol. 202, 527–543. https://doi.org/10.1083/jcb.201211045

Alpy, F., Rousseau, A., Schwab, Y., Legueux, F., Stoll, I., Wendling, C., Spiegelhalter, C., Kessler, P., Mathelin, C., Rio, M.-C., Levine, T.P., Tomasetto, C., 2013. STARD3 or STARD3NL and VAP form a novel molecular tether between late endosomes and the ER. J. Cell Sci. 126, 5500–5512. https://doi.org/10.1242/jcs.139295

Area-Gomez, E., Del Carmen Lara Castillo, M., Tambini, M.D., Guardia-Laguarta, C., de Groof, A.J.C., Madra, M., Ikenouchi, J., Umeda, M., Bird, T.D., Sturley, S.L., Schon, E.A., 2012. Upregulated function of mitochondria-associated ER membranes in Alzheimer disease. EMBO J. 31, 4106–4123. https://doi.org/10.1038/emboj.2012.202

Arribat, Y., Grepper, D., Lagarrigue, S., Qi, T., Cohen, S., Amati, F., 2020. Spastin mutations impair coordination between lipid droplet dispersion and reticulum. PLoS Genet. 16, e1008665. https://doi.org/10.1371/journal.pgen.1008665

Arruda, A.P., Pers, B.M., Parlakgül, G., Güney, E., Inouye, K., Hotamisligil, G.S., 2014. Chronic enrichment of hepatic endoplasmic reticulum-mitochondria contact leads to mitochondrial dysfunction in obesity. Nat. Med. 20, 1427–1435. https://doi.org/10.1038/nm.3735

Atakpa, P., Thillaiappan, N.B., Mataragka, S., Prole, D.L., Taylor, C.W., 2018. IP3 Receptors Preferentially Associate with ER-Lysosome Contact Sites and Selectively Deliver Ca2+ to Lysosomes. Cell Rep. 25, 3180-3193.e7. https://doi.org/10.1016/j.celrep.2018.11.064

Azizieh, R., Orduz, D., Van Bogaert, P., Bouschet, T., Rodriguez, W., Schiffmann, S.N., Pirson, I., Abramowicz, M.J., 2011. Progressive myoclonic epilepsy-associated gene KCTD7 is a regulator of potassium conductance in neurons. Mol. Neurobiol. 44, 111–121. https://doi.org/10.1007/s12035-011-8194-0

Ba, Q., Raghavan, G., Kiselyov, K., Yang, G., 2018. Whole-Cell Scale Dynamic Organization of Lysosomes Revealed by Spatial Statistical Analysis. Cell Rep. 23, 3591–3606. https://doi.org/10.1016/j.celrep.2018.05.079

Babu, J.R., Geetha, T., Wooten, M.W., 2005. Sequestosome 1/p62 shuttles polyubiquitinated tau for proteasomal degradation. J. Neurochem. 94, 192–203. https://doi.org/10.1111/j.1471-4159.2005.03181.x

Bach, G., 2001. Mucolipidosis Type IV. Mol. Genet. Metab. 73, 197–203. https://doi.org/10.1006/mgme.2001.3195

Ballabio, A., Bonifacino, J.S., 2020. Lysosomes as dynamic regulators of cell and organismal homeostasis. Nat. Rev. Mol. Cell Biol. 21, 101–118. https://doi.org/10.1038/s41580-019-0185-4

Beacham, G.M., Partlow, E.A., Hollopeter, G., 2019. Conformational regulation of AP1 and AP2 clathrin adaptor complexes. Traffic 20, 741–751. https://doi.org/10.1111/tra.12677

Belinson, H., Lev, D., Masliah, E., Michaelson, D.M., 2008. Activation of the amyloid cascade in apolipoprotein E4 transgenic mice induces lysosomal activation and neurodegeneration resulting in marked cognitive deficits. J. Neurosci. Off. J. Soc. Neurosci. 28, 4690–4701. https://doi.org/10.1523/JNEUROSCI.5633-07.2008

Belzil, C., Neumayer, G., Vassilev, A.P., Yap, K.L., Konishi, H., Rivest, S., Sanada, K., Ikura, M., Nakatani, Y., Nguyen, M.D., 2013. A Ca2+-dependent mechanism of neuronal survival mediated by the microtubule-associated protein p600. J. Biol. Chem. 288, 24452–24464. https://doi.org/10.1074/jbc.M113.483107

Berke, S.J.S., Paulson, H.L., 2003. Protein aggregation and the ubiquitin proteasome pathway: gaining the UPPer hand on neurodegeneration. Curr. Opin. Genet. Dev. 13, 253–261. https://doi.org/10.1016/S0959-437X(03)00053-4

Bissig, C., Hurbain, I., Raposo, G., van Niel, G., 2017. PIKfyve activity regulates reformation of terminal storage lysosomes from endolysosomes. Traffic 18, 747–757. https://doi.org/10.1111/tra.12525

Bjørkøy, G., Lamark, T., Brech, A., Outzen, H., Perander, M., Øvervatn, A., Stenmark, H., Johansen, T., 2005. p62/SQSTM1 forms protein aggregates degraded by autophagy and has a protective effect on huntingtin-induced cell death. J. Cell Biol. 171, 603–614. https://doi.org/10.1083/jcb.200507002

Blackstone, C., 2012. Cellular pathways of hereditary spastic paraplegia. Annu. Rev. Neurosci. 35, 25–47. https://doi.org/10.1146/annurev-neuro-062111-150400

Blackstone, C., O'Kane, C.J., Reid, E., 2011. Hereditary spastic paraplegias: membrane traffic and the motor pathway. Nat. Rev. Neurosci. 12, 31–42. https://doi.org/10.1038/nrn2946

Boes, M., Cerny, J., Massol, R., Op den Brouw, M., Kirchhausen, T., Chen, J., Ploegh, H.L., 2002. T-cell engagement of dendritic cells rapidly rearranges MHC class II transport. Nature 418, 983–988. https://doi.org/10.1038/nature01004

Bomont, P., Cavalier, L., Blondeau, F., Ben Hamida, C., Belal, S., Tazir, M., Demir, E., Topaloglu, H., Korinthenberg, R., Tüysüz, B., Landrieu, P., Hentati, F., Koenig, M., 2000. The gene encoding gigaxonin, a new member of the cytoskeletal BTB/kelch repeat family, is mutated in giant axonal neuropathy. Nat. Genet. 26, 370–374. https://doi.org/10.1038/81701

Bonifacino, J.S., Neefjes, J., 2017. Moving and positioning the endolysosomal system. Curr. Opin. Cell Biol. 47, 1–8. https://doi.org/10.1016/j.ceb.2017.01.008

Bord, 2016. A Tether Is a Tether Is a Tether: Tethering at Membrane Contact Sites. Dev. Cell 39, 395–409. https://doi.org/10.1016/j.devcel.2016.10.022

Boukhris, A., Stevanin, G., Feki, I., Denis, E., Elleuch, N., Miladi, M.I., Truchetto, J., Denora, P., Belal, S., Mhiri, C., Brice, A., 2008. Hereditary Spastic Paraplegia With Mental Impairment and Thin Corpus Callosum in Tunisia: SPG11, SPG15, and Further Genetic Heterogeneity. Arch. Neurol. 65. https://doi.org/10.1001/archneur.65.3.393

Boutet, S.C., Disatnik, M.-H., Chan, L.S., Iori, K., Rando, T.A., 2007. Regulation of Pax3 by Proteasomal Degradation of Monoubiquitinated Protein in Skeletal Muscle Progenitors. Cell 130, 349–362. https://doi.org/10.1016/j.cell.2007.05.044

Boutry, M., Branchu, J., Lustremant, C., Pujol, C., Pernelle, J., Matusiak, R., Seyer, A., Poirel, M., Chu-Van, E., Pierga, A., Dobrenis, K., Puech, J.-P., Caillaud, C., Durr, A., Brice, A., Colsch, B., Mochel, F., El Hachimi, K.H., Stevanin, G., Darios, F., 2018. Inhibition of Lysosome Membrane Recycling Causes Accumulation of Gangliosides that Contribute to Neurodegeneration. Cell Rep. 23, 3813–3826. https://doi.org/10.1016/j.celrep.2018.05.098

Boutry, M., Kim, P.K., 2021. ORP1L mediated PI(4)P signaling at ER-lysosome-mitochondrion three-way contact contributes to mitochondrial division. Nat. Commun. 12, 5354. https://doi.org/10.1038/s41467-021-25621-4

Boutry, M., Pierga, A., Matusiak, R., Branchu, J., Houllegatte, M., Ibrahim, Y., Balse, E., El Hachimi, K.-H., Brice, A., Stevanin, G., Darios, F., 2019a. Loss of spatacsin impairs cholesterol trafficking and calcium homeostasis. Commun. Biol. 2. https://doi.org/10.1038/s42003-019-0615-z

Boutry, M., Pierga, A., Matusiak, R., Branchu, J., Houllegatte, M., Ibrahim, Y., Balse, E., El Hachimi, K.-H., Brice, A., Stevanin, G., Darios, F., 2019b. Loss of spatacsin impairs cholesterol trafficking and calcium homeostasis. Commun. Biol. 2, 380. https://doi.org/10.1038/s42003-019-0615-z

Bozidis, P., Williamson, C.D., Colberg-Poley, A.M., 2007. Isolation of Endoplasmic Reticulum, Mitochondria, and Mitochondria-Associated Membrane Fractions from Transfected Cells and from Human Cytomegalovirus-Infected Primary Fibroblasts. Curr. Protoc. Cell Biol. 37. https://doi.org/10.1002/0471143030.cb0327s37

Brady, O.A., Zheng, Y., Murphy, K., Huang, M., Hu, F., 2013. The frontotemporal lobar degeneration risk factor, TMEM106B, regulates lysosomal morphology and function. Hum. Mol. Genet. 22, 685–695. https://doi.org/10.1093/hmg/dds475

Branchu, J., Boutry, M., Sourd, L., Depp, M., Leone, C., Corriger, A., Vallucci, M., Esteves, T., Matusiak, R., Dumont, M., Muriel, M.-P., Santorelli, F.M., Brice, A., El Hachimi, K.H., Stevanin, G., Darios, F., 2017. Loss of spatacsin function alters lysosomal lipid clearance leading to upper and lower motor neuron degeneration. Neurobiol. Dis. 102, 21–37. https://doi.org/10.1016/j.nbd.2017.02.007

Breiden, B., Sandhoff, K., 2019. Lysosomal Glycosphingolipid Storage Diseases 28.

Brigandt, I., Love, A., 2017. Reductionism in Biology, in: Zalta, E.N. (Ed.), The Stanford Encyclopedia of Philosophy. Metaphysics Research Lab, Stanford University.

Brocchieri, L., Karlin, S., 2005. Protein length in eukaryotic and prokaryotic proteomes. Nucleic Acids Res. 33, 3390–3400. https://doi.org/10.1093/nar/gki615

Brunk, U.T., Terman, A., 2002. Lipofuscin: mechanisms of age-related accumulation and influence on cell function. Free Radic. Biol. Med. 33, 611–619. https://doi.org/10.1016/s0891-5849(02)00959-0

Budenholzer, L., Cheng, C.L., Li, Y., Hochstrasser, M., 2017. Proteasome Structure and Assembly. J. Mol. Biol. 429, 3500–3524. https://doi.org/10.1016/j.jmb.2017.05.027

Bulcha, J.T., Wang, Y., Ma, H., Tai, P.W.L., Gao, G., 2021. Viral vector platforms within the gene therapy landscape. Signal Transduct. Target. Ther. 6, 1–24. https://doi.org/10.1038/s41392-021-00487-6

Caballero Oteyza, A., Battaloğlu, E., Ocek, L., Lindig, T., Reichbauer, J., Rebelo, A.P., Gonzalez, M.A., Zorlu, Y., Ozes, B., Timmann, D., Bender, B., Woehlke, G., Züchner, S., Schöls, L., Schüle, R., 2014. Motor protein mutations cause a new form of hereditary spastic paraplegia. Neurology 82, 2007–2016. https://doi.org/10.1212/WNL.0000000000000479

Cabukusta, B., Neefjes, J., 2018a. Mechanisms of lysosomal positioning and movement. Traffic Cph. Den. 19, 761–769. https://doi.org/10.1111/tra.12587

Cabukusta, B., Neefjes, J., 2018b. Mechanisms of lysosomal positioning and movement. Traffic 19, 761–769. https://doi.org/10.1111/tra.12587

Carstea, E.D., Morris, J.A., Coleman, K.G., Loftus, S.K., Zhang, D., Cummings, C., Gu, J., Rosenfeld, M.A., Pavan, W.J., Krizman, D.B., Nagle, J., Polymeropoulos, M.H., Sturley, S.L., Ioannou, Y.A., Higgins, M.E., Comly, M., Cooney, A., Brown, A., Kaneski, C.R., Blanchette-Mackie, E.J., Dwyer, N.K., Neufeld, E.B., Chang, T.-Y., Liscum, L., Strauss, J.F., Ohno, K., Zeigler, M., Carmi, R., Sokol, J., Markie, D., O'Neill, R.R., van Diggelen, O.P., Elleder, M., Patterson, M.C., Brady, R.O., Vanier, M.T., Pentchev, P.G., Tagle, D.A., 1997. Niemann-Pick C1 Disease Gene: Homology to Mediators of Cholesterol Homeostasis. Science 277, 228–231. https://doi.org/10.1126/science.277.5323.228

Casari, G., De Fusco, M., Ciarmatori, S., Zeviani, M., Mora, M., Fernandez, P., De Michele, G., Filla, A., Cocozza, S., Marconi, R., Dürr, A., Fontaine, B., Ballabio, A., 1998. Spastic paraplegia and OXPHOS impairment caused by mutations in paraplegin, a nuclear-encoded mitochondrial metalloprotease. Cell 93, 973–983. https://doi.org/10.1016/s0092-8674(00)81203-9

Chang, C.-L., Liou, J., 2015. Phosphatidylinositol 4,5-Bisphosphate Homeostasis Regulated by Nir2 and Nir3 Proteins at Endoplasmic Reticulum-Plasma Membrane Junctions*. J. Biol. Chem. 290, 14289–14301. https://doi.org/10.1074/jbc.M114.621375

Chang, C.-L., Weigel, A.V., Ioannou, M.S., Pasolli, H.A., Xu, C.S., Peale, D.R., Shtengel, G., Freeman, M., Hess, H.F., Blackstone, C., Lippincott-Schwartz, J., 2019. Spastin tethers lipid droplets to peroxisomes and directs fatty acid trafficking through ESCRT-III. J. Cell Biol. 218, 2583–2599. https://doi.org/10.1083/jcb.201902061

Chang, J., Lee, S., Blackstone, C., 2014a. Spastic paraplegia proteins spastizin and spatacsin mediate autophagic lysosome reformation. J. Clin. Invest. 124, 5249–5262. https://doi.org/10.1172/JCI77598

Chang, J., Lee, S., Blackstone, C., 2014b. Spastic paraplegia proteins spastizin and spatacsin mediate autophagic lysosome reformation. J. Clin. Invest. 124, 5249–5262. https://doi.org/10.1172/JCI77598

Chang, J., Lee, S., Blackstone, C., 2013. Protrudin binds atlastins and endoplasmic reticulum-shaping proteins and regulates network formation. Proc. Natl. Acad. Sci. U. S. A. 110, 14954–14959. https://doi.org/10.1073/pnas.1307391110

Chen, Q., Xiao, Y., Chai, P., Zheng, P., Teng, J., Chen, J., 2019. ATL3 Is a Tubular ER-Phagy Receptor for GABARAP-Mediated Selective Autophagy. Curr. Biol. 29, 846-855.e6. https://doi.org/10.1016/j.cub.2019.01.041

Chen, S., Desai, T., McNew, J.A., Gerard, P., Novick, P.J., Ferro-Novick, S., 2015. Lunapark stabilizes nascent three-way junctions in the endoplasmic reticulum. Proc. Natl. Acad. Sci. 112, 418–423. https://doi.org/10.1073/pnas.1423026112

Chen, Y., Yu, L., 2017. Recent progress in autophagic lysosome reformation. Traffic 18, 358–361. https://doi.org/10.1111/tra.12484

Chiapparino, A., Maeda, K., Turei, D., Saez-Rodriguez, J., Gavin, A.-C., 2016. The orchestra of lipid-transfer proteins at the crossroads between metabolism and signaling. Prog. Lipid Res. 61, 30–39. https://doi.org/10.1016/j.plipres.2015.10.004

Chino, H., Mizushima, N., 2020. ER-Phagy: Quality Control and Turnover of Endoplasmic Reticulum. Trends Cell Biol. 30, 384–398. https://doi.org/10.1016/j.tcb.2020.02.001

Chiurchiù, V., Maccarrone, M., Orlacchio, A., 2014. The role of reticulons in neurodegenerative diseases. Neuromolecular Med. 16, 3–15. https://doi.org/10.1007/s12017-013-8271-9

Chondrogianni, N., Sakellari, M., Lefaki, M., Papaevgeniou, N., Gonos, E.S., 2014. Proteasome activation delays aging in vitro and in vivo. Free Radic. Biol. Med. 71, 303–320. https://doi.org/10.1016/j.freeradbiomed.2014.03.031

Chu, B.-B., Liao, Y.-C., Qi, W., Xie, C., Du, X., Wang, J., Yang, H., Miao, H.-H., Li, B.-L., Song, B.-L., 2015. Cholesterol Transport through Lysosome-Peroxisome Membrane Contacts. Cell 161, 291–306. https://doi.org/10.1016/j.cell.2015.02.019

Chung, J., Torta, F., Masai, K., Lucast, L., Czapla, H., Tanner, L.B., Narayanaswamy, P., Wenk, M.R., Nakatsu, F., De Camilli, P., 2015. PI4P/phosphatidylserine countertransport at ORP5- and ORP8-mediated ER-plasma membrane contacts. Science 349, 428–432. https://doi.org/10.1126/science.aab1370

Ciechanover, A., Kwon, Y.T., 2015. Degradation of misfolded proteins in neurodegenerative diseases: therapeutic targets and strategies. Exp. Mol. Med. 47, e147. https://doi.org/10.1038/emm.2014.117

Citterio, A., Arnoldi, A., Panzeri, E., Merlini, L., D'Angelo, M.G., Musumeci, O., Toscano, A., Bondi, A., Martinuzzi, A., Bresolin, N., Bassi, M.T., 2015. Variants in KIF1A gene in dominant and sporadic forms of hereditary spastic paraparesis. J. Neurol. 262, 2684–2690. https://doi.org/10.1007/s00415-015-7899-9

Coen, K., Flannagan, R.S., Baron, S., Carraro-Lacroix, L.R., Wang, D., Vermeire, W., Michiels, C., Munck, S., Baert, V., Sugita, S., Wuytack, F., Hiesinger, P.R., Grinstein, S., Annaert, W., 2012. Lysosomal calcium homeostasis defects, not proton pump defects, cause endo-lysosomal dysfunction in PSEN-deficient cells. J. Cell Biol. 198, 23–35. https://doi.org/10.1083/jcb.201201076

Cogo, S., Tomkins, J.E., Vavouraki, N., Forcellato, F., Franchin, C., Tessari, I., Arrigoni, G., Cendron, L., Manzoni, C., Civiero, L., Lewis, P.A., Greggio, E., 2020. PKA-mediated phosphorylation of SPG11/spatacsin regulates binding with a subset of 14-3-3 proteins. bioRxiv 2020.09.09.289009. https://doi.org/10.1101/2020.09.09.289009

Cohen-Kaplan, V., Livneh, I., Avni, N., Cohen-Rosenzweig, C., Ciechanover, A., 2016. The ubiquitin-proteasome system and autophagy: Coordinated and independent activities. Int. J. Biochem. Cell Biol. 79, 403–418. https://doi.org/10.1016/j.biocel.2016.07.019

Connell, J.W., Allison, R.J., Rodger, C.E., Pearson, G., Zlamalova, E., Reid, E., 2020. ESCRT-III-associated proteins and spastin inhibit protrudin-dependent polarised membrane traffic. Cell. Mol. Life Sci. CMLS 77, 2641–2658. https://doi.org/10.1007/s00018-019-03313-z

Connell, J.W., Lindon, C., Luzio, J.P., Reid, E., 2009. Spastin couples microtubule severing to membrane traffic in completion of cytokinesis and secretion. Traffic Cph. Den. 10, 42–56. https://doi.org/10.1111/j.1600-0854.2008.00847.x

Conroy, J., McGettigan, P., Murphy, R., Webb, D., Murphy, S.M., McCoy, B., Albertyn, C., McCreary, D., McDonagh, C., Walsh, O., Lynch, S., Ennis, S., 2014. A novel locus for episodic ataxia:UBR4 the likely candidate. Eur. J. Hum. Genet. EJHG 22, 505–510. https://doi.org/10.1038/ejhg.2013.173

Cordonnier, M.-N., Dauzonne, D., Louvard, D., Coudrier, E., 2001. Actin Filaments and Myosin I Alpha Cooperate with Microtubules for the Movement of Lysosomes. Mol. Biol. Cell 12, 4013–4029. https://doi.org/10.1091/mbc.12.12.4013

Cremer, T., Jongsma, M.L.M., Trulsson, F., Vertegaal, A.C.O., Neefjes, J., Berlin, I., 2021. The ER-embedded UBE2J1/RNF26 ubiquitylation complex exerts spatiotemporal control over the endolysosomal pathway. Cell Rep. 34, 108659. https://doi.org/10.1016/j.celrep.2020.108659

Cui, Y., Parashar, S., Zahoor, M., Needham, P.G., Mari, M., Zhu, M., Chen, S., Ho, H.-C., Reggiori, F., Farhan, H., Brodsky, J.L., Ferro-Novick, S., 2019. A COPII subunit acts with an autophagy receptor to target endoplasmic reticulum for degradation. Science 365, 53–60. https://doi.org/10.1126/science.aau9263

Cummings, J.L., 2004. Alzheimer's disease. N. Engl. J. Med. 351, 56–67. https://doi.org/10.1056/NEJMra040223

Dammer, E.B., Na, C.H., Xu, P., Seyfried, N.T., Duong, D.M., Cheng, D., Gearing, M., Rees, H., Lah, J.J., Levey, A.I., Rush, J., Peng, J., 2011. Polyubiquitin Linkage Profiles in Three Models of Proteolytic Stress Suggest the Etiology of Alzheimer Disease*. J. Biol. Chem. 286, 10457–10465. https://doi.org/10.1074/jbc.M110.149633

Darios, F., Coarelli, G., Durr, A., 2022. Genetics in hereditary spastic paraplegias: Essential but not enough. Curr. Opin. Neurobiol. 72, 8–14. https://doi.org/10.1016/j.conb.2021.07.005

David, C., Koch, J., Oeljeklaus, S., Laernsack, A., Melchior, S., Wiese, S., Schummer, A., Erdmann, R., Warscheid, B., Brocard, C., 2013. A Combined Approach of Quantitative Interaction Proteomics and Live-cell Imaging Reveals a Regulatory Role for Endoplasmic Reticulum (ER) Reticulon Homology Proteins in Peroxisome Biogenesis*. Mol. Cell. Proteomics 12, 2408–2425. https://doi.org/10.1074/mcp.M112.017830

Davis, L.J., Bright, N.A., Edgar, J.R., Parkinson, M.D.J., Wartosch, L., Mantell, J., Peden, A.A., Luzio, J.P., 2021. Organelle tethering, pore formation and SNARE compensation in the late endocytic pathway. J. Cell Sci. 134. https://doi.org/10.1242/jcs.255463

Dawson, P.A., 2015. Impact of Inhibiting Ileal Apical versus Basolateral Bile Acid Transport on Cholesterol Metabolism and Atherosclerosis in Mice. Dig. Dis. Basel Switz. 33, 382–387. https://doi.org/10.1159/000371691

de Brito, O.M., Scorrano, L., 2008. Mitofusin 2 tethers endoplasmic reticulum to mitochondria. Nature 456, 605–610. https://doi.org/10.1038/nature07534

De Leonibus, C., Cinque, L., Settembre, C., 2019. Emerging lysosomal pathways for quality control at the endoplasmic reticulum. FEBS Lett. 593, 2319–2329. https://doi.org/10.1002/1873-3468.13571

de Sainte Agathe, J.-M., Mercier, S., Mahé, J.-Y., Péréon, Y., Buratti, J., Tissier, L., Kol, B., Said, S.A., Leguern, É., Banneau, G., Stévanin, G., 2021. RNF170-Related Hereditary Spastic Paraplegia: Confirmation by a Novel Mutation. Mov. Disord. 36, 771–774. https://doi.org/10.1002/mds.28371

de Souza, P.V.S., de Rezende Pinto, W.B.V., de Rezende Batistella, G.N., Bortholin, T., Oliveira, A.S.B., 2017. Hereditary Spastic Paraplegia: Clinical and Genetic Hallmarks. The Cerebellum 16, 525–551. https://doi.org/10.1007/s12311-016-0803-z

DeConinck, A., 2014. ajdecon/gradschool_matlab.

Delevoye, C., Heiligenstein, X., Ripoll, L., Gilles-Marsens, F., Dennis, M.K., Linares, R.A., Derman, L., Gokhale, A., Morel, E., Faundez, V., Marks, M.S., Raposo, G., 2016. BLOC-1 Brings Together the Actin and Microtubule Cytoskeletons to Generate Recycling Endosomes. Curr. Biol. 26, 1–13. https://doi.org/10.1016/j.cub.2015.11.020

Delevoye, C., Hurbain, I., Tenza, D., Sibarita, J.-B., Uzan-Gafsou, S., Ohno, H., Geerts, W.J.C., Verkleij, A.J., Salamero, J., Marks, M.S., Raposo, G., 2009. AP-1 and KIF13A coordinate endosomal sorting and positioning during melanosome biogenesis. J. Cell Biol. 187, 247–264. https://doi.org/10.1083/jcb.200907122

Delevoye, C., Miserey-Lenkei, S., Montagnac, G., Gilles-Marsens, F., Paul-Gilloteaux, P., Giordano, F., Waharte, F., Marks, M.S., Goud, B., Raposo, G., 2014a. Recycling endosome tubule morphogenesis

from sorting endosomes requires the kinesin motor KIF13A. Cell Rep. 6, 445–454. https://doi.org/10.1016/j.celrep.2014.01.002

Delevoye, C., Miserey-Lenkei, S., Montagnac, G., Gilles-Marsens, F., Paul-Gilloteaux, P., Giordano, F., Waharte, F., Marks, M.S., Goud, B., Raposo, G., 2014b. Recycling Endosome Tubule Morphogenesis from Sorting Endosomes Requires the Kinesin Motor KIF13A. Cell Rep. 6, 445–454. https://doi.org/10.1016/j.celrep.2014.01.002

Deluca, G.C., Ebers, G.C., Esiri, M.M., 2004. The extent of axonal loss in the long tracts in hereditary spastic paraplegia. Neuropathol. Appl. Neurobiol. 30, 576–584. https://doi.org/10.1111/j.1365-2990.2004.00587.x

Denora, P.S., Smets, K., Zolfanelli, F., Ceuterick-de Groote, C., Casali, C., Deconinck, T., Sieben, A., Gonzales, M., Zuchner, S., Darios, F., Peeters, D., Brice, A., Malandrini, A., De Jonghe, P., Santorelli, F.M., Stevanin, G., Martin, J.-J., El Hachimi, K.H., 2016a. Motor neuron degeneration in spastic paraplegia 11 mimics amyotrophic lateral sclerosis lesions. Brain J. Neurol. 139, 1723–1734. https://doi.org/10.1093/brain/aww061

Denora, P.S., Smets, K., Zolfanelli, F., Ceuterick-de Groote, C., Casali, C., Deconinck, T., Sieben, A., Gonzales, M., Zuchner, S., Darios, F., Peeters, D., Brice, A., Malandrini, A., De Jonghe, P., Santorelli, F.M., Stevanin, G., Martin, J.-J., El Hachimi, K.H., 2016b. Motor neuron degeneration in spastic paraplegia 11 mimics amyotrophic lateral sclerosis lesions. Brain aww061. https://doi.org/10.1093/brain/aww061

Denton, K., Mou, Y., Xu, C.-C., Shah, D., Chang, J., Blackstone, C., Li, X.-J., 2018. Impaired mitochondrial dynamics underlie axonal defects in hereditary spastic paraplegias. Hum. Mol. Genet. 27, 2517–2530. https://doi.org/10.1093/hmg/ddy156

Di Mattia, T., Martinet, A., Ikhlef, S., McEwen, A.G., Nominé, Y., Wendling, C., Poussin-Courmontagne, P., Voilquin, L., Eberling, P., Ruffenach, F., Cavarelli, J., Slee, J., Levine, T.P., Drin, G., Tomasetto, C., Alpy, F., 2020. FFAT motif phosphorylation controls formation and lipid transfer function of inter-organelle contacts. EMBO J. 39, e104369. https://doi.org/10.15252/embj.2019104369

Di Mattia, T., Wilhelm, L.P., Ikhlef, S., Wendling, C., Spehner, D., Nominé, Y., Giordano, F., Mathelin, C., Drin, G., Tomasetto, C., Alpy, F., 2018. Identification of MOSPD2, a novel scaffold for endoplasmic reticulum membrane contact sites. EMBO Rep. 19, e45453. https://doi.org/10.15252/embr.201745453

Di Paola, S., Scotto-Rosato, A., Medina, D.L., 2018. TRPML1: The Ca(2+)retaker of the lysosome. Cell Calcium 69, 112–121. https://doi.org/10.1016/j.ceca.2017.06.006

Dickson, E.J., Hille, B., 2019. Understanding phosphoinositides: rare, dynamic, and essential membrane phospholipids. Biochem. J. 476, 1–23. https://doi.org/10.1042/BCJ20180022

DiVincenzo, C., Elzinga, C.D., Medeiros, A.C., Karbassi, I., Jones, J.R., Evans, M.C., Braastad, C.D., Bishop, C.M., Jaremko, M., Wang, Z., Liaquat, K., Hoffman, C.A., York, M.D., Batish, S.D., Lupski, J.R., Higgins, J.J., 2014. The allelic spectrum of Charcot-Marie-Tooth disease in over 17,000 individuals with neuropathy. Mol. Genet. Genomic Med. 2, 522–529. https://doi.org/10.1002/mgg3.106

Dolese, D.A., Junot, M.P., Ghosh, B., Butsch, T.J., Johnson, A.E., Bohnert, K.A., 2021. Degradative tubular lysosomes link pexophagy to starvation and early aging in C. elegans. Autophagy 0, null. https://doi.org/10.1080/15548627.2021.1990647

Dong, J., Du, X., Wang, H., Wang, J., Lu, C., Chen, X., Zhu, Z., Luo, Z., Yu, L., Brown, A.J., Yang, H., Wu, J.-W., 2019. Allosteric enhancement of ORP1-mediated cholesterol transport by PI(4,5)P2/PI(3,4)P2. Nat. Commun. 10, 829. https://doi.org/10.1038/s41467-019-08791-0

Dong, R., Saheki, Y., Swarup, S., Lucast, L., Harper, J.W., De Camilli, P., 2016. Endosome-ER Contacts Control Actin Nucleation and Retromer Function through VAP-Dependent Regulation of PI4P. Cell 166, 408–423. https://doi.org/10.1016/j.cell.2016.06.037

Dou, Z., Xu, C., Donahue, G., Shimi, T., Pan, J.-A., Zhu, J., Ivanov, A., Capell, B.C., Drake, A.M., Shah, P.P., Catanzaro, J.M., Daniel Ricketts, M., Lamark, T., Adam, S.A., Marmorstein, R., Zong, W.-X., Johansen, T., Goldman, R.D., Adams, P.D., Berger, S.L., 2015. Autophagy mediates degradation of nuclear lamina. Nature 527, 105–109. https://doi.org/10.1038/nature15548

Du, H., Sheriff, S., Bezerra, J., Leonova, T., Grabowski, G.A., 1998. Molecular and enzymatic analyses of lysosomal acid lipase in cholesteryl ester storage disease. Mol. Genet. Metab. 64, 126–134. https://doi.org/10.1006/mgme.1998.2707

Du, W., Su, Q.P., Chen, Y., Zhu, Y., Jiang, D., Rong, Y., Zhang, S., Zhang, Y., Ren, H., Zhang, C., Wang, X., Gao, N., Wang, Y., Sun, L., Sun, Y., Yu, L., 2016. Kinesin 1 Drives Autolysosome Tubulation. Dev. Cell 37, 326–336. https://doi.org/10.1016/j.devcel.2016.04.014

Eastman, S.W., Yassaee, M., Bieniasz, P.D., 2009. A role for ubiquitin ligases and Spartin/SPG20 in lipid droplet turnover. J. Cell Biol. 184, 881–894. https://doi.org/10.1083/jcb.200808041

Eden, E.R., Sanchez-Heras, E., Tsapara, A., Sobota, A., Levine, T.P., Futter, C.E., 2016. Annexin A1 Tethers Membrane Contact Sites that Mediate ER to Endosome Cholesterol Transport. Dev. Cell 37, 473–483. https://doi.org/10.1016/j.devcel.2016.05.005

Edwards, T.L., Clowes, V.E., Tsang, H.T.H., Connell, J.W., Sanderson, C.M., Luzio, J.P., Reid, E., 2009. Endogenous spartin (SPG20) is recruited to endosomes and lipid droplets and interacts with the ubiquitin E3 ligases AIP4 and AIP5. Biochem. J. 423, 31–39. https://doi.org/10.1042/BJ20082398

Elsasser, S., Gali, R.R., Schwickart, M., Larsen, C.N., Leggett, D.S., Müller, B., Feng, M.T., Tübing, F., Dittmar, G.A.G., Finley, D., 2002. Proteasome subunit Rpn1 binds ubiquitin-like protein domains. Nat. Cell Biol. 4, 725–730. https://doi.org/10.1038/ncb845

Enchev, R.I., Schulman, B.A., Peter, M., 2015. Protein neddylation: beyond cullin–RING ligases. Nat. Rev. Mol. Cell Biol. 16, 30–44. https://doi.org/10.1038/nrm3919

Erfanian Omidvar, M., Torkamandi, S., Rezaei, S., Alipoor, B., Omrani, M.D., Darvish, H., Ghaedi, H., 2021. Genotype–phenotype associations in hereditary spastic paraplegia: a systematic review and meta-analysis on 13,570 patients. J. Neurol. 268, 2065–2082. https://doi.org/10.1007/s00415-019-09633-1

Fang, S., Ferrone, M., Yang, C., Jensen, J.P., Tiwari, S., Weissman, A.M., 2001. The tumor autocrine motility factor receptor, gp78, is a ubiquitin protein ligase implicated in degradation from the endoplasmic reticulum. Proc. Natl. Acad. Sci. 98, 14422–14427. https://doi.org/10.1073/pnas.251401598

Ferguson, S.M., 2019. Neuronal lysosomes. Neurosci. Lett. 697, 1–9. https://doi.org/10.1016/j.neulet.2018.04.005

Fink, J.K., 2013. Hereditary spastic paraplegia: clinico-pathologic features and emerging molecular mechanisms. Acta Neuropathol. (Berl.) 126, 307–328. https://doi.org/10.1007/s00401-013-1115-8

Fink, J.K., 2001. Progressive spastic paraparesis: hereditary spastic paraplegia and its relation to primary and amyotrophic lateral sclerosis. Semin. Neurol. 21, 199–207. https://doi.org/10.1055/s-2001-15265

Fischer, D., Schabhüttl, M., Wieland, T., Windhager, R., Strom, T.M., Auer-Grumbach, M., 2014. A novel missense mutation confirms ATL3 as a gene for hereditary sensory neuropathy type 1. Brain 137, e286. https://doi.org/10.1093/brain/awu091

Forrester, A., 2019. A selective ER-phagy exerts procollagen quality control via a Calnexin-FAM134B complex. EMBO J. 38, e99847. https://doi.org/10.15252/embj.201899847

Freeman, S.A., Grinstein, S., 2018. Resolution of macropinosomes, phagosomes and autolysosomes: Osmotically driven shrinkage enables tubulation and vesiculation. Traffic 19, 965–974. https://doi.org/10.1111/tra.12614

Fregno, I., Molinari, M., 2021. N-glycan processing selects ERAD-resistant misfolded proteins for ER-to-lysosome-associated degradation. EMBO J. 40, e107240. https://doi.org/10.15252/embj.2020107240

Fregno, I., Molinari, M., 2019. Proteasomal and lysosomal clearance of faulty secretory proteins: ER-associated degradation (ERAD) and ER-to-lysosome-associated degradation (ERLAD) pathways. Crit. Rev. Biochem. Mol. Biol. 54, 153–163. https://doi.org/10.1080/10409238.2019.1610351

Friedman, J.R., DiBenedetto, J.R., West, M., Rowland, A.A., Voeltz, G.K., 2013. Endoplasmic reticulum–endosome contact increases as endosomes traffic and mature. Mol. Biol. Cell 24, 1030–1040. https://doi.org/10.1091/mbc.E12-10-0733

Friedman, J.R., Lackner, L.L., West, M., DiBenedetto, J.R., Nunnari, J., Voeltz, G.K., 2011. ER tubules mark sites of mitochondrial division. Science 334, 358–362. https://doi.org/10.1126/science.1207385

Friedman, J.R., Webster, B.M., Mastronarde, D.N., Verhey, K.J., Voeltz, G.K., 2010. ER sliding dynamics and ER–mitochondrial contacts occur on acetylated microtubules. J. Cell Biol. 190, 363–375. https://doi.org/10.1083/jcb.200911024

Fumagalli, F., Noack, J., Bergmann, T.J., Cebollero, E., Pisoni, G.B., Fasana, E., Fregno, I., Galli, C., Loi, M., Soldà, T., D'Antuono, R., Raimondi, A., Jung, M., Melnyk, A., Schorr, S., Schreiber, A., Simonelli, L.,

Varani, L., Wilson-Zbinden, C., Zerbe, O., Hofmann, K., Peter, M., Quadroni, M., Zimmermann, R., Molinari, M., 2016. Translocon component Sec62 acts in endoplasmic reticulum turnover during stress recovery. Nat. Cell Biol. 18, 1173–1184. https://doi.org/10.1038/ncb3423

Gallastegui, N., Groll, M., 2010. The 26S proteasome: assembly and function of a destructive machine. Trends Biochem. Sci. 35, 634–642. https://doi.org/10.1016/j.tibs.2010.05.005

Garfield, A.S., 2010. Derivation of Primary Mouse Embryonic Fibroblast (PMEF) Cultures, in: Ward, A., Tosh, D. (Eds.), Mouse Cell Culture: Methods and Protocols, Methods in Molecular Biology. Humana Press, Totowa, NJ, pp. 19–27. https://doi.org/10.1007/978-1-59745-019-5_2

Gavilán, E., Pintado, C., Gavilan, M.P., Daza, P., Sánchez-Aguayo, I., Castaño, A., Ruano, D., 2015. Age-related dysfunctions of the autophagy lysosomal pathway in hippocampal pyramidal neurons under proteasome stress. Neurobiol. Aging 36, 1953–1963. https://doi.org/10.1016/j.neurobiolaging.2015.02.025

Gillard, B.K., Clement, R.G., Marcus, D.M., 1998. Variations among cell lines in the synthesis of sphingolipids in de novo and recycling pathways. Glycobiology 8, 885–890. https://doi.org/10.1093/glycob/8.9.885

Giordano, F., Saheki, Y., Idevall-Hagren, O., Colombo, S.F., Pirruccello, M., Milosevic, I., Gracheva, E.O., Bagriantsev, S.N., Borgese, N., De Camilli, P., 2013. PI(4,5)P2-Dependent and Ca2+-Regulated ER-PM Interactions Mediated by the Extended Synaptotagmins. Cell 153, 1494–1509. https://doi.org/10.1016/j.cell.2013.05.026

Gleick, J., 1987. Chaos: Making a New Science. Viking.

Goldberg, A.L., 2003. Protein degradation and protection against misfolded or damaged proteins. Nature 426, 895–899. https://doi.org/10.1038/nature02263

Gomez, T.S., Gorman, J.A., Artal-Martinez de Narvajas, A., Koenig, A.O., Billadeau, D.D., 2012. Trafficking defects in *WASH*- knockout fibroblasts originate from collapsed endosomal and lysosomal networks. Mol. Biol. Cell 23, 3215–3228. https://doi.org/10.1091/mbc.e12-02-0101

Graham, J.M., 2000. Isolation of Lysosomes from Tissues and Cells by Differential and Density Gradient Centrifugation. Curr. Protoc. Cell Biol. 7. https://doi.org/10.1002/0471143030.cb0306s07

Green, S., Batterman, R., 2017. Biology meets physics: Reductionism and multi-scale modeling of morphogenesis. Stud. Hist. Philos. Sci. Part C Stud. Hist. Philos. Biol. Biomed. Sci. 61, 20–34. https://doi.org/10.1016/j.shpsc.2016.12.003

Grumati, P., Morozzi, G., Hölper, S., Mari, M., Harwardt, M.-L.I., Yan, R., Müller, S., Reggiori, F., Heilemann, M., Dikic, I., 2017. Full length RTN3 regulates turnover of tubular endoplasmic reticulum via selective autophagy. eLife 6, e25555. https://doi.org/10.7554/eLife.25555

Guardia, C.M., De Pace, R., Mattera, R., Bonifacino, J.S., 2018. Neuronal Functions of Adaptor Complexes Involved in Protein Sorting. Curr. Opin. Neurobiol. 51, 103–110. https://doi.org/10.1016/j.conb.2018.02.021

Guardia, C.M., Farías, G.G., Jia, R., Pu, J., Bonifacino, J.S., 2016. BORC Functions Upstream of Kinesins 1 and 3 to Coordinate Regional Movement of Lysosomes along Different Microtubule Tracks. Cell Rep. 17, 1950–1961. https://doi.org/10.1016/j.celrep.2016.10.062

Guardia-Laguarta, C., Area-Gomez, E., Rüb, C., Liu, Y., Magrané, J., Becker, D., Voos, W., Schon, E.A., Przedborski, S., 2014. α-Synuclein is localized to mitochondria-associated ER membranes. J. Neurosci. Off. J. Soc. Neurosci. 34, 249–259. https://doi.org/10.1523/JNEUROSCI.2507-13.2014

Guha, P., Kaptan, E., Gade, P., Kalvakolanu, D.V., Ahmed, H., 2017. Tunicamycin induced endoplasmic reticulum stress promotes apoptosis of prostate cancer cells by activating mTORC1. Oncotarget 8, 68191–68207. https://doi.org/10.18632/oncotarget.19277

Güner, F., Pozner, T., Krach, F., Prots, I., Loskarn, S., Schlötzer-Schrehardt, U., Winkler, J., Winner, B., Regensburger, M., 2021. Axon-Specific Mitochondrial Pathology in SPG11 Alpha Motor Neurons. Front. Neurosci. 15, 680572. https://doi.org/10.3389/fnins.2021.680572

Guo, Y., Li, Di, Zhang, S., Yang, Y., Liu, J.-J., Wang, X., Liu, C., Milkie, D.E., Moore, R.P., Tulu, U.S., Kiehart, D.P., Hu, J., Lippincott-Schwartz, J., Betzig, E., Li, Dong, 2018. Visualizing Intracellular Organelle and Cytoskeletal Interactions at Nanoscale Resolution on Millisecond Timescales. Cell 175, 1430-1442.e17. https://doi.org/10.1016/j.cell.2018.09.057

Hamasaki, M., Furuta, N., Matsuda, A., Nezu, A., Yamamoto, A., Fujita, N., Oomori, H., Noda, T., Haraguchi, T., Hiraoka, Y., Amano, A., Yoshimori, T., 2013. Autophagosomes form at ER–mitochondria contact sites. Nature 495, 389–393. https://doi.org/10.1038/nature11910

Hanein, S., Martin, E., Boukhris, A., Byrne, P., Goizet, C., Hamri, A., Benomar, A., Lossos, A., Denora, P., Fernandez, J., Elleuch, N., Forlani, S., Durr, A., Feki, I., Hutchinson, M., Santorelli, F.M., Mhiri, C., Brice, A., Stevanin, G., 2008a. Identification of the SPG15 gene, encoding spastizin, as a frequent cause of complicated autosomal-recessive spastic paraplegia, including Kjellin syndrome. Am. J. Hum. Genet. 82, 992–1002. https://doi.org/10.1016/j.ajhg.2008.03.004

Hanein, S., Martin, E., Boukhris, A., Byrne, P., Goizet, C., Hamri, A., Benomar, A., Lossos, A., Denora, P., Fernandez, J., Elleuch, N., Forlani, S., Durr, A., Feki, I., Hutchinson, M., Santorelli, F.M., Mhiri, C., Brice, A., Stevanin, G., 2008b. Identification of the SPG15 Gene, Encoding Spastizin, as a Frequent Cause of Complicated Autosomal-Recessive Spastic Paraplegia, Including Kjellin Syndrome. Am. J. Hum. Genet. 82, 992–1002. https://doi.org/10.1016/j.ajhg.2008.03.004

Hara, T., Nakamura, K., Matsui, M., Yamamoto, A., Nakahara, Y., Suzuki-Migishima, R., Yokoyama, M., Mishima, K., Saito, I., Okano, H., Mizushima, N., 2006. Suppression of basal autophagy in neural cells causes neurodegenerative disease in mice. Nature 441, 885–889. https://doi.org/10.1038/nature04724

Harding, A.E., 1983. Classification of the hereditary ataxias and paraplegias. Lancet Lond. Engl. 1, 1151–1155. https://doi.org/10.1016/s0140-6736(83)92879-9

Hariharan, N., Zhai, P., Sadoshima, J., 2011. Oxidative stress stimulates autophagic flux during ischemia/reperfusion. Antioxid. Redox Signal. 14, 2179–2190. https://doi.org/10.1089/ars.2010.3488

Helle, S.C.J., Kanfer, G., Kolar, K., Lang, A., Michel, A.H., Kornmann, B., 2013. Organization and function of membrane contact sites. Biochim. Biophys. Acta BBA - Mol. Cell Res., Functional and structural diversity of the endoplasmic reticulum 1833, 2526–2541. https://doi.org/10.1016/j.bbamcr.2013.01.028

Hipolito, V.E.B., Ospina-Escobar, E., Botelho, R.J., 2018. Lysosome remodelling and adaptation during phagocyte activation. Cell. Microbiol. 20, e12824. https://doi.org/10.1111/cmi.12824

Hirst, J., Borner, G.H.H., Edgar, J., Hein, M.Y., Mann, M., Buchholz, F., Antrobus, R., Robinson, M.S., 2013a. Interaction between AP-5 and the hereditary spastic paraplegia proteins SPG11 and SPG15. Mol. Biol. Cell 24, 2558–2569. https://doi.org/10.1091/mbc.e13-03-0170

Hirst, J., D. Barlow, L., Francisco, G.C., Sahlender, D.A., Seaman, M.N.J., Dacks, J.B., Robinson, M.S., 2011a. The Fifth Adaptor Protein Complex. PLoS Biol. 9, e1001170. https://doi.org/10.1371/journal.pbio.1001170

Hirst, J., D. Barlow, L., Francisco, G.C., Sahlender, D.A., Seaman, M.N.J., Dacks, J.B., Robinson, M.S., 2011b. The Fifth Adaptor Protein Complex. PLoS Biol. 9, e1001170. https://doi.org/10.1371/journal.pbio.1001170

Hirst, J., Edgar, J.R., Esteves, T., Darios, F., Madeo, M., Chang, J., Roda, R.H., Dürr, A., Anheim, M., Gellera, C., Li, J., Züchner, S., Mariotti, C., Stevanin, G., Blackstone, C., Kruer, M.C., Robinson, M.S., 2015. Loss of AP-5 results in accumulation of aberrant endolysosomes: defining a new type of lysosomal storage disease. Hum. Mol. Genet. 24, 4984–4996. https://doi.org/10.1093/hmg/ddv220

Hirst, J., Hesketh, G.G., Gingras, A.-C., Robinson, M.S., 2021a. Rag GTPases and phosphatidylinositol 3-phosphate mediate recruitment of the AP-5/SPG11/SPG15 complex. J. Cell Biol. 220, e202002075. https://doi.org/10.1083/jcb.202002075

Hirst, J., Hesketh, G.G., Gingras, A.-C., Robinson, M.S., 2021b. Rag GTPases and phosphatidylinositol 3-phosphate mediate recruitment of the AP-5/SPG11/SPG15 complex. J. Cell Biol. 220, e202002075. https://doi.org/10.1083/jcb.202002075

Hirst, J., Irving, C., Borner, G.H.H., 2013b. Adaptor Protein Complexes AP-4 and AP-5: New Players in Endosomal Trafficking and Progressive Spastic Paraplegia: AP-4 and AP-5: Functions and Genetic Disorders. Traffic 14, 153–164. https://doi.org/10.1111/tra.12028

Hirst, J., Itzhak, D.N., Antrobus, R., Borner, G.H.H., Robinson, M.S., 2018a. Role of the AP-5 adaptor protein complex in late endosome-to-Golgi retrieval. PLoS Biol. 16. https://doi.org/10.1371/journal.pbio.2004411

Hirst, J., Itzhak, D.N., Antrobus, R., Borner, G.H.H., Robinson, M.S., 2018b. Role of the AP-5 adaptor protein complex in late endosome-to-Golgi retrieval. PLOS Biol. 16, e2004411. https://doi.org/10.1371/journal.pbio.2004411

Höglinger, D., Burgoyne, T., Sanchez-Heras, E., Hartwig, P., Colaco, A., Newton, J., Futter, C.E., Spiegel, S., Platt, F.M., Eden, E.R., 2019. NPC1 regulates ER contacts with endocytic organelles to mediate cholesterol egress. Nat. Commun. 10. https://doi.org/10.1038/s41467-019-12152-2

Hollenbeck, P.J., Swanson, J.A., 1990. Radial extension of macrophage tubular lysosomes supported by kinesin. Nature 346, 864–866. https://doi.org/10.1038/346864a0

Hong, J.H., Kaustov, L., Coyaud, E., Srikumar, T., Wan, J., Arrowsmith, C., Raught, B., 2015. KCMF1 (potassium channel modulatory factor 1) Links RAD6 to UBR4 (ubiquitin N-recognin domain-containing E3 ligase 4) and Lysosome-Mediated Degradation. Mol. Cell. Proteomics MCP 14, 674–685. https://doi.org/10.1074/mcp.M114.042168

Hong, N.H., Qi, A., Weaver, A.M., 2015. PI(3,5)P2 controls endosomal branched actin dynamics by regulating cortactin–actin interactions. J. Cell Biol. 210, 753–769. https://doi.org/10.1083/jcb.201412127

Hong, Z., Pedersen, N.M., Wang, L., Torgersen, M.L., Stenmark, H., Raiborg, C., 2017. PtdIns3P controls mTORC1 signaling through lysosomal positioning. J. Cell Biol. 216, 4217–4233. https://doi.org/10.1083/jcb.201611073

Hooper, C., Puttamadappa, S.S., Loring, Z., Shekhtman, A., Bakowska, J.C., 2010. Spartin activates atrophin-1-interacting protein 4 (AIP4) E3 ubiquitin ligase and promotes ubiquitination of adipophilin on lipid droplets. BMC Biol. 8, 72. https://doi.org/10.1186/1741-7007-8-72

Hoyer, M.J., Chitwood, P.J., Ebmeier, C.C., Striepen, J.F., Qi, R.Z., Old, W.M., Voeltz, G.K., 2018. A Novel Class of ER Membrane Proteins Regulates ER-Associated Endosome Fission. Cell 175, 254-265.e14. https://doi.org/10.1016/j.cell.2018.08.030

Hsu, F., Spannl, S., Ferguson, C., Hyman, A.A., Parton, R.G., Zerial, M., 2018. Rab5 and Alsin regulate stress-activated cytoprotective signaling on mitochondria. eLife 7, e32282. https://doi.org/10.7554/eLife.32282

Hu, A., Zhao, X.-T., Tu, H., Xiao, T., Fu, T., Wang, Y., Liu, Y., Shi, X.-J., Luo, J., Song, B.-L., 2018. PIP4K2A regulates intracellular cholesterol transport through modulating PI(4,5)P2 homeostasis. J. Lipid Res. 59, 507–514. https://doi.org/10.1194/jlr.M082149

Hu, J., Shibata, Y., Zhu, P.-P., Voss, C., Rismanchi, N., Prinz, W.A., Rapoport, T.A., Blackstone, C., 2009. A Class of Dynamin-like GTPases Involved in the Generation of the Tubular ER Network. Cell 138, 549–561. https://doi.org/10.1016/j.cell.2009.05.025

Hua, R., Cheng, D., Coyaud, É., Freeman, S., Di Pietro, E., Wang, Y., Vissa, A., Yip, C.M., Fairn, G.D., Braverman, N., Brumell, J.H., Trimble, W.S., Raught, B., Kim, P.K., 2017. VAPs and ACBD5 tether peroxisomes to the ER for peroxisome maintenance and lipid homeostasis. J. Cell Biol. 216, 367–377. https://doi.org/10.1083/jcb.201608128

Huang, X., Dixit, V.M., 2016. Drugging the undruggables: exploring the ubiquitin system for drug development. Cell Res. 26, 484–498. https://doi.org/10.1038/cr.2016.31

Huo, Y., Khatri, N., Hou, Q., Gilbert, J., Wang, G., Man, H.-Y., 2015. The deubiquitinating enzyme USP46 regulates AMPA receptor ubiquitination and trafficking. J. Neurochem. 134, 1067–1080. https://doi.org/10.1111/jnc.13194

Isabel, S., David, V., 2014. The Mechanistic Links Between Proteasome Activity, Aging and Agerelated Diseases. Curr. Genomics 15, 38–51.

Ishida, Y., Yamamoto, A., Kitamura, A., Lamandé, S.R., Yoshimori, T., Bateman, J.F., Kubota, H., Nagata, K., 2009. Autophagic Elimination of Misfolded Procollagen Aggregates in the Endoplasmic Reticulum as a Means of Cell Protection. Mol. Biol. Cell 20, 2744–2754. https://doi.org/10.1091/mbc.E08-11-1092

Ito, D., 1993. BSCL2-Related Neurologic Disorders/Seipinopathy, in: Adam, M.P., Ardinger, H.H., Pagon, R.A., Wallace, S.E., Bean, L.J., Mirzaa, G., Amemiya, A. (Eds.), GeneReviews®. University of Washington, Seattle, Seattle (WA).

Ito, D., Fujisawa, T., Iida, H., Suzuki, N., 2008. Characterization of seipin/BSCL2, a protein associated with spastic paraplegia 17. Neurobiol. Dis. 31, 266–277. https://doi.org/10.1016/j.nbd.2008.05.004

Ito, D., Suzuki, N., 2009. Seipinopathy: a novel endoplasmic reticulum stress-associated disease. Brain J. Neurol. 132, 8–15. https://doi.org/10.1093/brain/awn216

Jeyakumar, M., Dwek, R.A., Butters, T.D., Platt, F.M., 2005. Storage solutions: treating lysosomal disorders of the brain. Nat. Rev. Neurosci. 6, 713–725. https://doi.org/10.1038/nrn1725

Ji, C.H., Kim, H.Y., Heo, A.J., Lee, S.H., Lee, M.J., Kim, S.B., Srinivasrao, G., Mun, S.R., Cha-Molstad, H., Ciechanover, A., Choi, C.Y., Lee, H.G., Kim, B.Y., Kwon, Y.T., 2019. The N-Degron Pathway Mediates ER-phagy. Mol. Cell 75, 1058-1072.e9. https://doi.org/10.1016/j.molcel.2019.06.028

Jiang, P., Nishimura, T., Sakamaki, Y., Itakura, E., Hatta, T., Natsume, T., Mizushima, N., 2014. The HOPS complex mediates autophagosome-lysosome fusion through interaction with syntaxin 17. Mol. Biol. Cell 25, 1327–1337. https://doi.org/10.1091/mbc.E13-08-0447

Jin, L., Pahuja, K.B., Wickliffe, K.E., Gorur, A., Baumgärtel, C., Schekman, R., Rape, M., 2012. Ubiquitin-dependent regulation of COPII coat size and function. Nature 482, 495–500. https://doi.org/10.1038/nature10822

Johansson, M., Lehto, M., Tanhuanpää, K., Cover, T.L., Olkkonen, V.M., 2005. The Oxysterol-binding Protein Homologue ORP1L Interacts with Rab7 and Alters Functional Properties of Late Endocytic Compartments. Mol. Biol. Cell 16, 5480–5492. https://doi.org/10.1091/mbc.E05-03-0189

Johnson, A.E., Shu, H., Hauswirth, A.G., Tong, A., Davis, G.W., 2015. VCP-dependent muscle degeneration is linked to defects in a dynamic tubular lysosomal network in vivo. eLife 4. https://doi.org/10.7554/eLife.07366

Jongsma, M.L.M., Berlin, I., Wijdeven, R.H.M., Janssen, L., Janssen, G.M.C., Garstka, M.A., Janssen, H., Mensink, M., van Veelen, P.A., Spaapen, R.M., Neefjes, J., 2016a. An ER-Associated Pathway Defines Endosomal Architecture for Controlled Cargo Transport. Cell 166, 152–166. https://doi.org/10.1016/j.cell.2016.05.078

Jongsma, M.L.M., Berlin, I., Wijdeven, R.H.M., Janssen, L., Janssen, G.M.C., Garstka, M.A., Janssen, H., Mensink, M., van Veelen, P.A., Spaapen, R.M., Neefjes, J., 2016b. An ER-Associated Pathway Defines Endosomal Architecture for Controlled Cargo Transport. Cell 166, 152–166. https://doi.org/10.1016/j.cell.2016.05.078

Ju, J.-S., Weihl, C.C., 2010. p97/VCP at the intersection of the autophagy and the ubiquitin proteasome system. Autophagy 6, 283–285. https://doi.org/10.4161/auto.6.2.11063

Kainu, V., Hermansson, M., Hänninen, S., Hokynar, K., Somerharju, P., 2013. Import of phosphatidylserine to and export of phosphatidylethanolamine molecular species from mitochondria. Biochim. Biophys. Acta 1831, 429–437. https://doi.org/10.1016/j.bbalip.2012.11.003

Kanagaraj, P., Gautier-Stein, A., Riedel, D., Schomburg, C., Cerdà, J., Vollack, N., Dosch, R., 2014. Souffle/Spastizin Controls Secretory Vesicle Maturation during Zebrafish Oogenesis. PLoS Genet. 10, e1004449. https://doi.org/10.1371/journal.pgen.1004449

Kanapin, A., Batalov, S., Davis, M.J., Gough, J., Grimmond, S., Kawaji, H., Magrane, M., Matsuda, H., Schönbach, C., Teasdale, R.D., Group, R.G., Members, G.S.L., Yuan3, Z., 2003. Mouse Proteome Analysis. Genome Res. 13, 1335–1344. https://doi.org/10.1101/gr.978703

Karaca, I., Tamboli, I.Y., Glebov, K., Richter, J., Fell, L.H., Grimm, M.O., Haupenthal, V.J., Hartmann, T., Gräler, M.H., van Echten-Deckert, G., Walter, J., 2014. Deficiency of sphingosine-1-phosphate lyase impairs lysosomal metabolism of the amyloid precursor protein. J. Biol. Chem. 289, 16761–16772. https://doi.org/10.1074/jbc.M113.535500

Karle, K.N., Möckel, D., Reid, E., Schöls, L., 2012. Axonal transport deficit in a KIF5A(-/-) mouse model. Neurogenetics 13, 169–179. https://doi.org/10.1007/s10048-012-0324-y

Kauffman, S.A., Kauffman, M. of the S.F.I. and P. of B.S.A., 1993. The Origins of Order: Self-organization and Selection in Evolution. Oxford University Press.

Kawaguchi, K., Endo, A., Fukushima, T., Madoka, Y., Tanaka, T., Komada, M., 2018. Ubiquitin-specific protease 8 deubiquitinates Sec31A and decreases large COPII carriers and collagen IV secretion. Biochem. Biophys. Res. Commun. 499, 635–641. https://doi.org/10.1016/j.bbrc.2018.03.202

Kawamoto, R.M., Brunschwig, J.P., Kim, K.C., Caswell, A.H., 1986. Isolation, characterization, and localization of the spanning protein from skeletal muscle triads. J. Cell Biol. 103, 1405–1414. https://doi.org/10.1083/jcb.103.4.1405

Kawano, M., Kumagai, K., Nishijima, M., Hanada, K., 2006. Efficient trafficking of ceramide from the endoplasmic reticulum to the Golgi apparatus requires a VAMP-associated protein-interacting FFAT motif of CERT. J. Biol. Chem. 281, 30279–30288. https://doi.org/10.1074/jbc.M605032200

Khaminets, A., Heinrich, T., Mari, M., Grumati, P., Huebner, A.K., Akutsu, M., Liebmann, L., Stolz, A., Nietzsche, S., Koch, N., Mauthe, M., Katona, I., Qualmann, B., Weis, J., Reggiori, F., Kurth, I., Hübner, C.A., Dikic, I., 2015. Regulation of endoplasmic reticulum turnover by selective autophagy. Nature 522, 354–358. https://doi.org/10.1038/nature14498

Khundadze, M., Kollmann, K., Koch, N., Biskup, C., Nietzsche, S., Zimmer, G., Hennings, J.C., Huebner, A.K., Symmank, J., Jahic, A., Ilina, E.I., Karle, K., Schöls, L., Kessels, M., Braulke, T., Qualmann, B., Kurth, I., Beetz, C., Hübner, C.A., 2013a. A hereditary spastic paraplegia mouse model supports a role of ZFYVE26/SPASTIZIN for the endolysosomal system. PLoS Genet. 9, e1003988. https://doi.org/10.1371/journal.pgen.1003988

Khundadze, M., Kollmann, K., Koch, N., Biskup, C., Nietzsche, S., Zimmer, G., Hennings, J.C., Huebner, A.K., Symmank, J., Jahic, A., Ilina, E.I., Karle, K., Schöls, L., Kessels, M., Braulke, T., Qualmann, B., Kurth, I., Beetz, C., Hübner, C.A., 2013b. A Hereditary Spastic Paraplegia Mouse Model Supports a Role of ZFYVE26/SPASTIZIN for the Endolysosomal System. PLoS Genet. 9, e1003988. https://doi.org/10.1371/journal.pgen.1003988

Khundadze, M., Ribaudo, F., Hussain, A., Rosentreter, J., Nietzsche, S., Thelen, M., Winter, D., Hoffmann, B., Afzal, M.A., Hermann, T., de Heus, C., Piskor, E.-M., Kosan, C., Franzka, P., von Kleist, L., Stauber, T., Klumperman, J., Damme, M., Proikas-Cezanne, T., Hübner, C.A., 2019a. A mouse model for SPG48 reveals a block of autophagic flux upon disruption of adaptor protein complex five. Neurobiol. Dis. 127, 419–431. https://doi.org/10.1016/j.nbd.2019.03.026

Khundadze, M., Ribaudo, F., Hussain, A., Rosentreter, J., Nietzsche, S., Thelen, M., Winter, D., Hoffmann, B., Afzal, M.A., Hermann, T., de Heus, C., Piskor, E.-M., Kosan, C., Franzka, P., von Kleist, L., Stauber, T., Klumperman, J., Damme, M., Proikas-Cezanne, T., Hübner, C.A., 2019b. A mouse model for SPG48 reveals a block of autophagic flux upon disruption of adaptor protein complex five. Neurobiol. Dis. 127, 419–431. https://doi.org/10.1016/j.nbd.2019.03.026

Khundadze, M., Ribaudo, F., Hussain, A., Stahlberg, H., Brocke-Ahmadinejad, N., Franzka, P., Varga, R.-E., Zarkovic, M., Pungsrinont, T., Kokal, M., Ganley, I.G., Beetz, C., Sylvester, M., Hübner, C.A., 2021. Mouse models for hereditary spastic paraplegia uncover a role of PI4K2A in autophagic lysosome reformation. Autophagy 0, null. https://doi.org/10.1080/15548627.2021.1891848

Kiffin, R., Christian, C., Knecht, E., Cuervo, A.M., 2004. Activation of chaperone-mediated autophagy during oxidative stress. Mol. Biol. Cell 15, 4829–4840. https://doi.org/10.1091/mbc.e04-06-0477

Kilpatrick, B.S., Eden, E.R., Hockey, L.N., Yates, E., Futter, C.E., Patel, S., 2017. An Endosomal NAADP-Sensitive Two-Pore Ca2+ Channel Regulates ER-Endosome Membrane Contact Sites to Control Growth Factor Signaling. Cell Rep. 18, 1636–1645. https://doi.org/10.1016/j.celrep.2017.01.052

King, C., Sengupta, P., Seo, A.Y., Lippincott-Schwartz, J., 2020. ER membranes exhibit phase behavior at sites of organelle contact. Proc. Natl. Acad. Sci. U. S. A. 117, 7225–7235. https://doi.org/10.1073/pnas.1910854117

Kishida, T., Kostetskii, I., Zhang, Z., Martinez, F., Liu, P., Walkley, S.U., Dwyer, N.K., Blanchette-Mackie, E.J., Radice, G.L., Strauss, J.F., 2004. Targeted mutation of the MLN64 START domain causes only modest alterations in cellular sterol metabolism. J. Biol. Chem. 279, 19276–19285. https://doi.org/10.1074/jbc.M400717200

Kishino, T., Lalande, M., Wagstaff, J., 1997. UBE3A/E6-AP mutations cause Angelman syndrome. Nat. Genet. 15, 70–73. https://doi.org/10.1038/ng0197-70

Kitada, T., Asakawa, S., Hattori, N., Matsumine, H., Yamamura, Y., Minoshima, S., Yokochi, M., Mizuno, Y., Shimizu, N., 1998. Mutations in the parkin gene cause autosomal recessive juvenile parkinsonism. Nature 392, 605–608. https://doi.org/10.1038/33416

Kittler, J., Illingworth, J., 1986. Minimum error thresholding. Pattern Recognit. 19, 41–47. https://doi.org/10.1016/0031-3203(86)90030-0

Klemm, R.W., Norton, J.P., Cole, R.A., Li, C.S., Park, S.H., Crane, M.M., Li, L., Jin, D., Boye-Doe, A., Liu, T.Y., Shibata, Y., Lu, H., Rapoport, T.A., Farese, R.V., Blackstone, C., Guo, Y., Mak, H.Y., 2013. A Conserved Role for Atlastin GTPases in Regulating Lipid Droplet Size. Cell Rep. 3, 1465–1475. https://doi.org/10.1016/j.celrep.2013.04.015

Koch, G.L., 1990. The endoplasmic reticulum and calcium storage. BioEssays News Rev. Mol. Cell. Dev. Biol. 12, 527–531. https://doi.org/10.1002/bies.950121105

Korolchuk, V.I., Saiki, S., Lichtenberg, M., Siddiqi, F.H., Roberts, E.A., Imarisio, S., Jahreiss, L., Sarkar, S., Futter, M., Menzies, F.M., O'Kane, C.J., Deretic, V., Rubinsztein, D.C., 2011. Lysosomal positioning coordinates cellular nutrient responses. Nat. Cell Biol. 13, 453–460. https://doi.org/10.1038/ncb2204

Kravtsova-Ivantsiv, Y., Ciechanover, A., 2012. Non-canonical ubiquitin-based signals for proteasomal degradation. J. Cell Sci. 125, 539–548. https://doi.org/10.1242/jcs.093567

Kravtsova-Ivantsiv, Y., Cohen, S., Ciechanover, A., 2009. Modification by Single Ubiquitin Moieties Rather Than Polyubiquitination Is Sufficient for Proteasomal Processing of the p105 NF-κB Precursor. Mol. Cell 33, 496–504. https://doi.org/10.1016/j.molcel.2009.01.023

Krumm, L., Pozner, T., Kaindl, J., Regensburger, M., Günther, C., Turan, S., Asadollahi, R., Rauch, A., Winner, B., 2021. Generation and characterization of an endogenously tagged SPG11-human iPSC line by CRISPR/Cas9 mediated knock-in. Stem Cell Res. 56, 102520. https://doi.org/10.1016/j.scr.2021.102520

Kurth, I., Pamminger, T., Hennings, J.C., Soehendra, D., Huebner, A.K., Rotthier, A., Baets, J., Senderek, J., Topaloglu, H., Farrell, S.A., Nürnberg, G., Nürnberg, P., De Jonghe, P., Gal, A., Kaether, C., Timmerman, V., Hübner, C.A., 2009. Mutations in FAM134B, encoding a newly identified Golgi protein, cause severe sensory and autonomic neuropathy. Nat. Genet. 41, 1179–1181. https://doi.org/10.1038/ng.464

Kwon, Y.T., Ciechanover, A., 2017. The Ubiquitin Code in the Ubiquitin-Proteasome System and Autophagy. Trends Biochem. Sci. 42, 873–886. https://doi.org/10.1016/j.tibs.2017.09.002

Kwong, J.Q., Beal, M.F., Manfredi, G., 2006. The role of mitochondria in inherited neurodegenerative diseases. J. Neurochem. 97, 1659–1675. https://doi.org/10.1111/j.1471-4159.2006.03990.x

Lahiri, S., Chao, J.T., Tavassoli, S., Wong, A.K.O., Choudhary, V., Young, B.P., Loewen, C.J.R., Prinz, W.A., 2014. A conserved endoplasmic reticulum membrane protein complex (EMC) facilitates phospholipid transfer from the ER to mitochondria. PLoS Biol. 12, e1001969. https://doi.org/10.1371/journal.pbio.1001969

Lam, S.S., Martell, J.D., Kamer, K.J., Deerinck, T.J., Ellisman, M.H., Mootha, V.K., Ting, A.Y., 2015. Directed evolution of APEX2 for electron microscopy and proximity labeling. Nat. Methods 12, 51–54. https://doi.org/10.1038/nmeth.3179

Lauwers, E., Erpapazoglou, Z., Haguenauer-Tsapis, R., André, B., 2010. The ubiquitin code of yeast permease trafficking. Trends Cell Biol. 20, 196–204. https://doi.org/10.1016/j.tcb.2010.01.004

Lee, B.-H., Lee, M.J., Park, S., Oh, D.-C., Elsasser, S., Chen, P.-C., Gartner, C., Dimova, N., Hanna, J., Gygi, S.P., Wilson, S.M., King, R.W., Finley, D., 2010. Enhancement of proteasome activity by a small-molecule inhibitor of USP14. Nature 467, 179–184. https://doi.org/10.1038/nature09299

Lee, C.A., Blackstone, C., 2020. ER morphology and endo-lysosomal crosstalk: Functions and disease implications. Biochim. Biophys. Acta BBA - Mol. Cell Biol. Lipids 1865, 158544. https://doi.org/10.1016/j.bbalip.2019.158544

Lee, J.E., Westrate, L.M., Wu, H., Page, C., Voeltz, G.K., 2016. Multiple dynamin family members collaborate to drive mitochondrial division. Nature 540, 139–143. https://doi.org/10.1038/nature20555

Lescouzères, L., Bomont, P., 2020. E3 Ubiquitin Ligases in Neurological Diseases: Focus on Gigaxonin and Autophagy. Front. Physiol. 11, 1022. https://doi.org/10.3389/fphys.2020.01022

Lev, S., 2010. Non-vesicular lipid transport by lipid-transfer proteins and beyond. Nat. Rev. Mol. Cell Biol. 11, 739–750. https://doi.org/10.1038/nrm2971

Li, C., Wang, X., Li, X., Qiu, K., Jiao, F., Liu, Yidan, Kong, Q., Liu, Yan, Wu, Y., 2019. Proteasome Inhibition Activates Autophagy-Lysosome Pathway Associated With TFEB Dephosphorylation and Nuclear Translocation. Front. Cell Dev. Biol. 0. https://doi.org/10.3389/fcell.2019.00170

Li, P., Gu, M., Xu, H., 2019. Lysosomal Ion Channels as Decoders of Cellular Signals. Trends Biochem. Sci. 44, 110–124. https://doi.org/10.1016/j.tibs.2018.10.006

Li, X., Rydzewski, N., Hider, A., Zhang, X., Yang, J., Wang, W., Gao, Q., Cheng, X., Xu, H., 2016. A Molecular Mechanism to Regulate Lysosome Motility for Lysosome Positioning and Tubulation. Nat. Cell Biol. 18, 404–417. https://doi.org/10.1038/ncb3324

Liang, C.-C., Wang, C., Peng, X., Gan, B., Guan, J.-L., 2010. Neural-specific Deletion of FIP200 Leads to Cerebellar Degeneration Caused by Increased Neuronal Death and Axon Degeneration*. J. Biol. Chem. 285, 3499–3509. https://doi.org/10.1074/jbc.M109.072389

Lie, P.P.Y., Nixon, R.A., 2019. Lysosome trafficking and signaling in health and neurodegenerative diseases. Neurobiol. Dis. 122, 94–105. https://doi.org/10.1016/j.nbd.2018.05.015

Lim, Y., Cho, I.-T., Schoel, L.J., Cho, G., Golden, J.A., 2015. Hereditary spastic paraplegia-linked REEP1 modulates endoplasmic reticulum/mitochondria contacts. Ann. Neurol. 78, 679–696. https://doi.org/10.1002/ana.24488

Lin, X., Su, H.-Z., Dong, E.-L., Lin, X.-H., Zhao, M., Yang, C., Wang, C., Wang, J., Chen, Y.-J., Yu, H., Xu, J., Ma, L.-X., Xiong, Z.-Q., Wang, N., Chen, W.-J., 2019. Stop-gain mutations in UBAP1 cause pure autosomal-dominant spastic paraplegia. Brain 142, 2238–2252. https://doi.org/10.1093/brain/awz158

Liu, L.-K., Choudhary, V., Toulmay, A., Prinz, W.A., 2017. An inducible ER-Golgi tether facilitates ceramide transport to alleviate lipotoxicity. J. Cell Biol. 216, 131–147. https://doi.org/10.1083/jcb.201606059

Lloyd-Evans, E., Waller-Evans, H., Peterneva, K., Platt, F.M., 2010. Endolysosomal calcium regulation and disease. Biochem. Soc. Trans. 38, 1458–1464. https://doi.org/10.1042/BST0381458

Lo Giudice, T., Lombardi, F., Santorelli, F.M., Kawarai, T., Orlacchio, A., 2014. Hereditary spastic paraplegia: Clinical-genetic characteristics and evolving molecular mechanisms. Exp. Neurol. 261, 518–539. https://doi.org/10.1016/j.expneurol.2014.06.011

Lock, J.T., Sinkins, W.G., Schilling, W.P., 2012. Protein S-glutathionylation enhances Ca2+-induced Ca2+ release via the IP3 receptor in cultured aortic endothelial cells. J. Physiol. 590, 3431–3447. https://doi.org/10.1113/jphysiol.2012.232645

Loftus, S.K., Morris, J.A., Carstea, E.D., Gu, J.Z., Cummings, C., Brown, A., Ellison, J., Ohno, K., Rosenfeld, M.A., Tagle, D.A., Pentchev, P.G., Pavan, W.J., 1997. Murine Model of Niemann-Pick C Disease: Mutation in a Cholesterol Homeostasis Gene. Science 277, 232–235. https://doi.org/10.1126/science.277.5323.232

Loi, M., Raimondi, A., Morone, D., Molinari, M., 2019. ESCRT-III-driven piecemeal micro-ER-phagy remodels the ER during recovery from ER stress. Nat. Commun. 10, 5058. https://doi.org/10.1038/s41467-019-12991-z

López Sanjurjo, C.I., Tovey, S.C., Taylor, C.W., 2014. Rapid recycling of Ca2+ between IP3-sensitive stores and lysosomes. PloS One 9, e111275. https://doi.org/10.1371/journal.pone.0111275

Lu, J., Rashid, F., Byrne, P.C., 2006. The hereditary spastic paraplegia protein spartin localises to mitochondria. J. Neurochem. 98, 1908–1919. https://doi.org/10.1111/j.1471-4159.2006.04008.x

Lu, J.P., Wang, Y., Sliter, D.A., Pearce, M.M.P., Wojcikiewicz, R.J.H., 2011. RNF170 Protein, an Endoplasmic Reticulum Membrane Ubiquitin Ligase, Mediates Inositol 1,4,5-Trisphosphate Receptor Ubiquitination and Degradation*. J. Biol. Chem. 286, 24426–24433. https://doi.org/10.1074/jbc.M111.251983

Lu, M., van Tartwijk, F.W., Lin, J.Q., Nijenhuis, W., Parutto, P., Fantham, M., Christensen, C.N., Avezov, E., Holt, C.E., Tunnacliffe, A., Holcman, D., Kapitein, L., Schierle, G.S.K., Kaminski, C.F., 2020. The structure and global distribution of the endoplasmic reticulum network are actively regulated by lysosomes. Sci. Adv. 6, eabc7209. https://doi.org/10.1126/sciadv.abc7209

Magalhaes, J., Gegg, M.E., Migdalska-Richards, A., Doherty, M.K., Whitfield, P.D., Schapira, A.H.V., 2016. Autophagic lysosome reformation dysfunction in glucocerebrosidase deficient cells: relevance to Parkinson disease. Hum. Mol. Genet. 25, 3432–3445. https://doi.org/10.1093/hmg/ddw185

Mannan, A.U., Krawen, P., Sauter, S.M., Boehm, J., Chronowska, A., Paulus, W., Neesen, J., Engel, W., 2006. ZFYVE27 (SPG33), a novel spastin-binding protein, is mutated in hereditary spastic paraplegia. Am. J. Hum. Genet. 79, 351–357. https://doi.org/10.1086/504927

Marshall, A.G., Watson, J.A., Hallengren, J.J., Walters, B.J., Dobrunz, L.E., Francillon, L., Wilson, J.A., Phillips, S.E., Wilson, S.M., 2013. Genetic Background Alters the Severity and Onset of Neuromuscular Disease Caused by the Loss of Ubiquitin-Specific Protease 14 (Usp14). PLOS ONE 8, e84042. https://doi.org/10.1371/journal.pone.0084042

Martin, E., Yanicostas, C., Rastetter, A., Naini, S.M.A., Maouedj, A., Kabashi, E., Rivaud-Péchoux, S., Brice, A., Stevanin, G., Soussi-Yanicostas, N., 2012. Spatacsin and spastizin act in the same pathway required for proper spinal motor neuron axon outgrowth in zebrafish. Neurobiol. Dis. 48, 299–308. https://doi.org/10.1016/j.nbd.2012.07.003

Marwaha, R., Sharma, M., 2017. DQ-Red BSA Trafficking Assay in Cultured Cells to Assess Cargo Delivery to Lysosomes. BIO-Protoc. 7. https://doi.org/10.21769/BioProtoc.2571

Mateus, D., Marini, E.S., Progida, C., Bakke, O., 2018. Rab7a modulates ER stress and ER morphology. Biochim. Biophys. Acta BBA - Mol. Cell Res. 1865, 781–793. https://doi.org/10.1016/j.bbamcr.2018.02.011

Matsuoka, S., Ballif, B.A., Smogorzewska, A., McDonald, E.R., Hurov, K.E., Luo, J., Bakalarski, C.E., Zhao, Z., Solimini, N., Lerenthal, Y., Shiloh, Y., Gygi, S.P., Elledge, S.J., 2007. ATM and ATR substrate analysis reveals extensive protein networks responsive to DNA damage. Science 316, 1160–1166. https://doi.org/10.1126/science.1140321

McGourty, C.A., Akopian, D., Walsh, C., Gorur, A., Werner, A., Schekman, R., Bautista, D., Rape, M., 2016. Regulation of the CUL3 Ubiquitin Ligase by a Calcium-Dependent Co-adaptor. Cell 167, 525-538.e14. https://doi.org/10.1016/j.cell.2016.09.026

Mehrtash, A.B., Hochstrasser, M., 2019. Ubiquitin-dependent protein degradation at the endoplasmic reticulum and nuclear envelope. Semin. Cell Dev. Biol., SI: Viscoelasticity 93, 111–124. https://doi.org/10.1016/j.semcdb.2018.09.013

Meng, Y., Heybrock, S., Neculai, D., Saftig, P., 2020. Cholesterol Handling in Lysosomes and Beyond. Trends Cell Biol. 30, 452–466. https://doi.org/10.1016/j.tcb.2020.02.007

Mesmin, B., Bigay, J., Moser von Filseck, J., Lacas-Gervais, S., Drin, G., Antonny, B., 2013. A four-step cycle driven by PI(4)P hydrolysis directs sterol/PI(4)P exchange by the ER-Golgi tether OSBP. Cell 155, 830–843. https://doi.org/10.1016/j.cell.2013.09.056

Mijaljica, D., Devenish, R.J., 2013. Nucleophagy at a glance. J. Cell Sci. 126, 4325–4330. https://doi.org/10.1242/jcs.133090

Miller, A., Schafer, J., Upchurch, C., Spooner, E., Huynh, J., Hernandez, S., McLaughlin, B., Oden, L., Fares, H., 2015. Mucolipidosis Type IV Protein TRPML1-Dependent Lysosome Formation: TRPML1-Dependent Lysosome Formation. Traffic 16, 284–297. https://doi.org/10.1111/tra.12249

Mishra, H.K., Prots, I., Havlicek, S., Kohl, Z., Perez-Branguli, F., Boerstler, T., Anneser, L., Minakaki, G., Wend, H., Hampl, M., Leone, M., Brückner, M., Klucken, J., Reis, A., Boyer, L., Schuierer, G., Behrens, J., Lampert, A., Engel, F.B., Gage, F.H., Winkler, J., Winner, B., 2016. GSK3ß-dependent dysregulation of neurodevelopment in SPG11-patient iPSC model. Ann. Neurol. https://doi.org/10.1002/ana.24633

Mizushima, N., Komatsu, M., 2011. Autophagy: renovation of cells and tissues. Cell 147, 728–741. https://doi.org/10.1016/j.cell.2011.10.026

Molinari, M., Galli, C., Vanoni, O., Arnold, S.M., Kaufman, R.J., 2005. Persistent Glycoprotein Misfolding Activates the Glucosidase II/UGT1-Driven Calnexin Cycle to Delay Aggregation and Loss of Folding Competence. Mol. Cell 20, 503–512. https://doi.org/10.1016/j.molcel.2005.09.027

Molino, D., Nascimbeni, A.C., Giordano, F., Codogno, P., Morel, E., 2017. ER-driven membrane contact sites: Evolutionary conserved machineries for stress response and autophagy regulation? Commun. Integr. Biol. 10, e1401699. https://doi.org/10.1080/19420889.2017.1401699

Montecchiani, C., Pedace, L., Lo Giudice, T., Casella, A., Mearini, M., Gaudiello, F., Pedroso, J.L., Terracciano, C., Caltagirone, C., Massa, R., St George-Hyslop, P.H., Barsottini, O.G.P., Kawarai, T., Orlacchio, A., 2016. ALS5/SPG11/ *KIAA1840* mutations cause autosomal recessive axonal Charcot–Marie–Tooth disease. Brain 139, 73–85. https://doi.org/10.1093/brain/awv320

Montenegro, G., Rebelo, A.P., Connell, J., Allison, R., Babalini, C., D'Aloia, M., Montieri, P., Schüle, R., Ishiura, H., Price, J., Strickland, A., Gonzalez, M.A., Baumbach-Reardon, L., Deconinck, T., Huang, J., Bernardi, G., Vance, J.M., Rogers, M.T., Tsuji, S., De Jonghe, P., Pericak-Vance, M.A., Schöls, L., Orlacchio, A., Reid, E., Züchner, S., 2012. Mutations in the ER-shaping protein reticulon 2 cause the axon-degenerative disorder hereditary spastic paraplegia type 12. J. Clin. Invest. 122, 538–544. https://doi.org/10.1172/JCI60560

Mori, S., Honda, H., Hamasaki, H., Sasagasako, N., Suzuki, S.O., Furuya, H., Taniwaki, T., Iwaki, T., 2021. Transactivation response DNA-binding protein of 43 kDa proteinopathy and lysosomal abnormalities in spastic paraplegia type 11. Neuropathol. Off. J. Jpn. Soc. Neuropathol. 41, 253–265. https://doi.org/10.1111/neup.12733

Mortimore, G.E., Lardeux, B.R., Adams, C.E., 1988. Regulation of microautophagy and basal protein turnover in rat liver. Effects of short-term starvation. J. Biol. Chem. 263, 2506–2512. https://doi.org/10.1016/S0021-9258(18)69235-X

Mrakovic, A., Kay, J.G., Furuya, W., Brumell, J.H., Botelho, R.J., 2012. Rab7 and Arl8 GTPases are Necessary for Lysosome Tubulation in Macrophages. Traffic 13, 1667–1679. https://doi.org/10.1111/tra.12003

Multilevel image thresholds using Otsu's method - MATLAB multithresh - MathWorks France [WWW Document], n.d. URL https://fr.mathworks.com/help/images/ref/multithresh.html (accessed 6.6.17).

Murakawa, T., Kiger, A.A., Sakamaki, Y., Fukuda, M., Fujita, N., 2020. An autophagy-dependent tubular lysosomal network synchronizes degradative activity required for muscle remodeling. J. Cell Sci. 133. https://doi.org/10.1242/jcs.248336

Murley, A., Lackner, L.L., Osman, C., West, M., Voeltz, G.K., Walter, P., Nunnari, J., 2013. ER-associated mitochondrial division links the distribution of mitochondria and mitochondrial DNA in yeast. eLife 2, e00422. https://doi.org/10.7554/eLife.00422

Murmu, R.P., Martin, E., Rastetter, A., Esteves, T., Muriel, M.-P., El Hachimi, K.H., Denora, P.S., Dauphin, A., Fernandez, J.C., Duyckaerts, C., Brice, A., Darios, F., Stevanin, G., 2011a. Cellular distribution and subcellular localization of spatacsin and spastizin, two proteins involved in hereditary spastic paraplegia. Mol. Cell. Neurosci. 47, 191–202. https://doi.org/10.1016/j.mcn.2011.04.004

Murmu, R.P., Martin, E., Rastetter, A., Esteves, T., Muriel, M.-P., El Hachimi, K.H., Denora, P.S., Dauphin, A., Fernandez, J.C., Duyckaerts, C., Brice, A., Darios, F., Stevanin, G., 2011b. Cellular distribution and subcellular localization of spatacsin and spastizin, two proteins involved in hereditary spastic paraplegia. Mol. Cell. Neurosci. 47, 191–202. https://doi.org/10.1016/j.mcn.2011.04.004

Nakagawa, T., Setou, M., Seog, D.-H., Ogasawara, K., Dohmae, N., Takio, K., Hirokawa, N., 2000. A Novel Motor, KIF13A, Transports Mannose-6-Phosphate Receptor to Plasma Membrane through Direct Interaction with AP-1 Complex. Cell 103, 569–581. https://doi.org/10.1016/S0092-8674(00)00161-6

Nakatani, Y., Konishi, H., Vassilev, A., Kurooka, H., Ishiguro, K., Sawada, J., Ikura, T., Korsmeyer, S.J., Qin, J., Herlitz, A.M., 2005. p600, a unique protein required for membrane morphogenesis and cell survival. Proc. Natl. Acad. Sci. U. S. A. 102, 15093–15098. https://doi.org/10.1073/pnas.0507458102

Nanduri, P., Hao, R., Fitzpatrick, T., Yao, T.-P., 2015. Chaperone-mediated 26S Proteasome Remodeling Facilitates Free K63 Ubiquitin Chain Production and Aggresome Clearance*. J. Biol. Chem. 290, 9455–9464. https://doi.org/10.1074/jbc.M114.627950

Naujokat, C., Hoffmann, S., 2002. Role and Function of the 26S Proteasome in Proliferation and Apoptosis. Lab. Invest. 82, 965–980. https://doi.org/10.1097/01.LAB.0000022226.23741.37

Neefjes, J., van der Kant, R., 2014. Stuck in traffic: an emerging theme in diseases of the nervous system. Trends Neurosci. 37, 66–76. https://doi.org/10.1016/j.tins.2013.11.006

Nishimura, A.L., Mitne-Neto, M., Silva, H.C.A., Richieri-Costa, A., Middleton, S., Cascio, D., Kok, F., Oliveira, J.R.M., Gillingwater, T., Webb, J., Skehel, P., Zatz, M., 2004. A mutation in the vesicle-trafficking protein VAPB causes late-onset spinal muscular atrophy and amyotrophic lateral sclerosis. Am. J. Hum. Genet. 75, 822–831. https://doi.org/10.1086/425287

Nixon, R.A., 2013. The role of autophagy in neurodegenerative disease. Nat. Med. 19, 983–997. https://doi.org/10.1038/nm.3232

Novarino, G., Fenstermaker, A.G., Zaki, M.S., Hofree, M., Silhavy, J.L., Heiberg, A.D., Abdellateef, M., Rosti, B., Scott, E., Mansour, L., Masri, A., Kayserili, H., Al-Aama, J.Y., Abdel-Salam, G.M.H., Karminejad, A., Kara, M., Kara, B., Bozorgmehri, B., Ben-Omran, T., Mojahedi, F., Mahmoud, I.G.E.D., Bouslam, N., Bouhouche, A., Benomar, A., Hanein, S., Raymond, L., Forlani, S., Mascaro, M., Selim, L., Shehata, N., Al-Allawi, N., Bindu, P.S., Azam, M., Gunel, M., Caglayan, A., Bilguvar, K., Tolun, A., Issa, M.Y., Schroth, J., Spencer, E.G., Rosti, R.O., Akizu, N., Vaux, K.K., Johansen, A., Koh, A.A., Megahed, H., Durr, A., Brice, A., Stevanin, G., Gabriel, S.B., Ideker, T., Gleeson, J.G., 2014. Exome Sequencing Links Corticospinal Motor Neuron Disease to Common Neurodegenerative Disorders. Science 343, 506–511. https://doi.org/10.1126/science.1247363

Nurse, P., 1998. Reductionism and explanation in cell biology. Novartis Found. Symp. 213, 93–101; discussion 102-105. https://doi.org/10.1002/9780470515488.ch7

Olivo-Marin, J.-C., 2002. Extraction of spots in biological images using multiscale products. Pattern Recognit. 35, 1989–1996. https://doi.org/10.1016/S0031-3203(01)00127-3

Omari, S., Makareeva, E., Roberts-Pilgrim, A., Mirigian, L., Jarnik, M., Ott, C., Lippincott-Schwartz, J., Leikin, S., 2018. Noncanonical autophagy at ER exit sites regulates procollagen turnover. Proc. Natl. Acad. Sci. 115, E10099–E10108. https://doi.org/10.1073/pnas.1814552115

Omura, T., Siekevitz, P., Palade, G.E., 1967. Turnover of Constituents of the Endoplasmic Reticulum Membranes of Rat Hepatocytes. J. Biol. Chem. 242, 2389–2396. https://doi.org/10.1016/S0021-9258(18)95974-0

Onyike, C.U., Diehl-Schmid, J., 2013. The epidemiology of frontotemporal dementia. Int. Rev. Psychiatry Abingdon Engl. 25, 130–137. https://doi.org/10.3109/09540261.2013.776523

Orlacchio, A., Babalini, C., Borreca, A., Patrono, C., Massa, R., Basaran, S., Munhoz, R.P., Rogaeva, E.A., St George-Hyslop, P.H., Bernardi, G., Kawarai, T., 2010. SPATACSIN mutations cause autosomal recessive juvenile amyotrophic lateral sclerosis. Brain 133, 591–598. https://doi.org/10.1093/brain/awp325

Osellame, L.D., Rahim, A.A., Hargreaves, I.P., Gegg, M.E., Richard-Londt, A., Brandner, S., Waddington, S.N., Schapira, A.H.V., Duchen, M.R., 2013. Mitochondria and Quality Control Defects in a Mouse Model of Gaucher Disease—Links to Parkinson's Disease. Cell Metab. 17, 941–953. https://doi.org/10.1016/j.cmet.2013.04.014

Oslowski, C.M., Urano, F., 2011. Measuring ER stress and the unfolded protein response using mammalian tissue culture system. Methods Enzymol. 490, 71–92. https://doi.org/10.1016/B978-0-12-385114-7.00004-0

Otsu, N., 1979. A Threshold Selection Method from Gray-Level Histograms. IEEE Trans. Syst. Man Cybern. 9, 62–66. https://doi.org/10.1109/TSMC.1979.4310076

Oyarzún, J.E., Lagos, J., Vázquez, M.C., Valls, C., De la Fuente, C., Yuseff, M.I., Alvarez, A.R., Zanlungo, S., 2019. Lysosome motility and distribution: Relevance in health and disease. Biochim. Biophys. Acta BBA - Mol. Basis Dis. 1865, 1076–1087. https://doi.org/10.1016/j.bbadis.2019.03.009

Özkan, N., Koppers, M., van Soest, I., van Harten, A., Jurriens, D., Liv, N., Klumperman, J., Kapitein, L.C., Hoogenraad, C.C., Farías, G.G., 2021. ER – lysosome contacts at a pre-axonal region regulate axonal lysosome availability. Nat. Commun. 12, 4493. https://doi.org/10.1038/s41467-021-24713-5

Öztürk, Z., O'Kane, C.J., Pérez-Moreno, J.J., 2020. Axonal Endoplasmic Reticulum Dynamics and Its Roles in Neurodegeneration. Front. Neurosci. 14, 48. https://doi.org/10.3389/fnins.2020.00048

Pan, X., Roberts, P., Chen, Y., Kvam, E., Shulga, N., Huang, K., Lemmon, S., Goldfarb, D.S., 2000. Nucleus–Vacuole Junctions in Saccharomyces cerevisiae Are Formed Through the Direct Interaction of Vac8p with Nvj1p. Mol. Biol. Cell 11, 2445–2457. https://doi.org/10.1091/mbc.11.7.2445

Pankiv, S., Alemu, E.A., Brech, A., Bruun, J.-A., Lamark, T., Øvervatn, A., Bjørkøy, G., Johansen, T., 2010. FYCO1 is a Rab7 effector that binds to LC3 and PI3P to mediate microtubule plus end–directed vesicle transport. J. Cell Biol. 188, 253–269. https://doi.org/10.1083/jcb.200907015

Pankiv, S., Clausen, T.H., Lamark, T., Brech, A., Bruun, J.-A., Outzen, H., Øvervatn, A., Bjørkøy, G., Johansen, T., 2007. p62/SQSTM1 Binds Directly to Atg8/LC3 to Facilitate Degradation of Ubiquitinated Protein Aggregates by Autophagy *. J. Biol. Chem. 282, 24131–24145. https://doi.org/10.1074/jbc.M702824200

Papadopoulos, C., Orso, G., Mancuso, G., Herholz, M., Gumeni, S., Tadepalle, N., Jüngst, C., Tzschichholz, A., Schauss, A., Höning, S., Trifunovic, A., Daga, A., Rugarli, E.I., 2015. Spastin Binds to Lipid Droplets and Affects Lipid Metabolism. PLoS Genet. 11, e1005149. https://doi.org/10.1371/journal.pgen.1005149

Park, S.H., Zhu, P.-P., Parker, R.L., Blackstone, C., 2010. Hereditary spastic paraplegia proteins REEP1, spastin, and atlastin-1 coordinate microtubule interactions with the tubular ER network. J. Clin. Invest. 120, 1097–1110. https://doi.org/10.1172/JCI40979

Park, S.Y., Guo, X., 2014. Adaptor protein complexes and intracellular transport. Biosci. Rep. 34. https://doi.org/10.1042/BSR20140069

Parr, C., Carzaniga, R., Gentleman, S.M., Van Leuven, F., Walter, J., Sastre, M., 2012. Glycogen synthase kinase 3 inhibition promotes lysosomal biogenesis and autophagic degradation of the amyloid-β precursor protein. Mol. Cell. Biol. 32, 4410–4418. https://doi.org/10.1128/MCB.00930-12

Patto, Alexander L., O'Kane, C.J., 2020. Distant homologies and domain conservation of the Hereditary Spastic Paraplegia protein SPG11/ALS5/spatacsin. bioRxiv 2020.03.08.982389. https://doi.org/10.1101/2020.03.08.982389

Patto, Alexander L, O'Kane, C.J., 2020. Distant homologies and domain conservation of the Hereditary Spastic Paraplegia protein SPG11/ALS5/spatacsin (preprint). Neuroscience. https://doi.org/10.1101/2020.03.08.982389

Pearce, M.M.P., Wormer, D.B., Wilkens, S., Wojcikiewicz, R.J.H., 2009. An Endoplasmic Reticulum (ER) Membrane Complex Composed of SPFH1 and SPFH2 Mediates the ER-associated Degradation of Inositol 1,4,5-Trisphosphate Receptors*. J. Biol. Chem. 284, 10433–10445. https://doi.org/10.1074/jbc.M809801200

Peng, H., Yang, F., Hu, Q., Sun, J., Peng, C., Zhao, Y., Huang, C., 2019. The ubiquitin-specific protease USP8 directly deubiquitinates SQSTM1/p62 to suppress its autophagic activity. Autophagy 16, 698–708. https://doi.org/10.1080/15548627.2019.1635381

Peretti, D., Dahan, N., Shimoni, E., Hirschberg, K., Lev, S., 2008. Coordinated lipid transfer between the endoplasmic reticulum and the Golgi complex requires the VAP proteins and is essential for Golgi-mediated transport. Mol. Biol. Cell 19, 3871–3884. https://doi.org/10.1091/mbc.e08-05-0498

Pérez-Brangulí, F., Buchsbaum, I.Y., Pozner, T., Regensburger, M., Fan, W., Schray, A., Börstler, T., Mishra, H., Gräf, D., Kohl, Z., Winkler, J., Berninger, B., Cappello, S., Winner, B., 2019. Human SPG11 cerebral organoids reveal cortical neurogenesis impairment. Hum. Mol. Genet. 28, 961–971. https://doi.org/10.1093/hmg/ddy397

Pérez-Brangulí, F., Mishra, H.K., Prots, I., Havlicek, S., Kohl, Z., Saul, D., Rummel, C., Dorca-Arevalo, J., Regensburger, M., Graef, D., Sock, E., Blasi, J., Groemer, T.W., Schlötzer-Schrehardt, U., Winkler, J., Winner, B., 2014. Dysfunction of spatacsin leads to axonal pathology in SPG11-linked hereditary spastic paraplegia. Hum. Mol. Genet. 23, 4859–4874. https://doi.org/10.1093/hmg/ddu200

Phillips, M.J., Voeltz, G.K., 2016. Structure and function of ER membrane contact sites with other organelles. Nat. Rev. Mol. Cell Biol. 17, 69–82. https://doi.org/10.1038/nrm.2015.8

Platt, F.M., Boland, B., van der Spoel, A.C., 2012. Lysosomal storage disorders: The cellular impact of lysosomal dysfunction. J. Cell Biol. 199, 723–734. https://doi.org/10.1083/jcb.201208152

Pozner, T., Schray, A., Regensburger, M., Lie, D.C., Schlötzer-Schrehardt, U., Winkler, J., Turan, S., Winner, B., 2018. Tideglusib Rescues Neurite Pathology of SPG11 iPSC Derived Cortical Neurons. Front. Neurosci. 12. https://doi.org/10.3389/fnins.2018.00914

Prinz, W.A., 2014. Bridging the gap: Membrane contact sites in signaling, metabolism, and organelle dynamics. J. Cell Biol. 205, 759–769. https://doi.org/10.1083/jcb.201401126

Prinz, W.A., Toulmay, A., Balla, T., 2020. The functional universe of membrane contact sites. Nat. Rev. Mol. Cell Biol. 21, 7–24. https://doi.org/10.1038/s41580-019-0180-9

Pu, J., Guardia, C.M., Keren-Kaplan, T., Bonifacino, J.S., 2016. Mechanisms and functions of lysosome positioning. J. Cell Sci. jcs.196287. https://doi.org/10.1242/jcs.196287

Raiborg, C., Wenzel, E.M., Pedersen, N.M., Olsvik, H., Schink, K.O., Schultz, S.W., Vietri, M., Nisi, V., Bucci, C., Brech, A., Johansen, T., Stenmark, H., 2015a. Repeated ER–endosome contacts promote endosome translocation and neurite outgrowth. Nature 520, 234–238. https://doi.org/10.1038/nature14359

Raiborg, C., Wenzel, E.M., Pedersen, N.M., Olsvik, H., Schink, K.O., Schultz, S.W., Vietri, M., Nisi, V., Bucci, C., Brech, A., Johansen, T., Stenmark, H., 2015b. Repeated ER–endosome contacts promote endosome translocation and neurite outgrowth. Nature 520, 234–238. https://doi.org/10.1038/nature14359

Raimondi, M., Cesselli, D., Di Loreto, C., La Marra, F., Schneider, C., Demarchi, F., 2018. USP1 (ubiquitin specific peptidase 1) targets ULK1 and regulates its cellular compartmentalization and autophagy. Autophagy 15, 613–630. https://doi.org/10.1080/15548627.2018.1535291

Reggiori, F., Klumperman, J., 2016. Lysosome Biogenesis and Autophagy, in: Maxfield, F.R., Willard, J.M., Lu, S. (Eds.), Lysosomes: Biology, Diseases, and Therapeutics. John Wiley & Sons, Inc., Hoboken, NJ, USA, pp. 7–31. https://doi.org/10.1002/9781118978320.ch2

Reincke, M., Sbiera, S., Hayakawa, A., Theodoropoulou, M., Osswald, A., Beuschlein, F., Meitinger, T., Mizuno-Yamasaki, E., Kawaguchi, K., Saeki, Y., Tanaka, K., Wieland, T., Graf, E., Saeger, W., Ronchi, C.L., Allolio, B., Buchfelder, M., Strom, T.M., Fassnacht, M., Komada, M., 2015. Mutations in the deubiquitinase gene USP8 cause Cushing's disease. Nat. Genet. 47, 31–38. https://doi.org/10.1038/ng.3166

Renvoisé, B., Chang, J., Singh, R., Yonekawa, S., FitzGibbon, E.J., Mankodi, A., Vanderver, A., Schindler, A., Toro, C., Gahl, W.A., Mahuran, D.J., Blackstone, C., Pierson, T.M., 2014. Lysosomal abnormalities in hereditary spastic paraplegia types SPG15 and SPG11. Ann. Clin. Transl. Neurol. 1, 379–389. https://doi.org/10.1002/acn3.64

Ring, J., Rockenfeller, P., Abraham, C., Tadic, J., Poglitsch, M., Schimmel, K., Westermayer, J., Schauer, S., Achleitner, B., Schimpel, C., Moitzi, B., Rechberger, G.N., Sigrist, S.J., Carmona-Gutierrez, D., Kroemer, G., Büttner, S., Eisenberg, T., Madeo, F., 2017. Mitochondrial energy metabolism is required for lifespan extension by the spastic paraplegia-associated protein spartin. Microb. Cell Graz Austria 4, 411–422. https://doi.org/10.15698/mic2017.12.603

Ripoll, L., Heiligenstein, X., Hurbain, I., Domingues, L., Figon, F., Petersen, K.J., Dennis, M.K., Houdusse, A., Marks, M.S., Raposo, G., Delevoye, C., 2018. Myosin VI and branched actin filaments mediate membrane constriction and fission of melanosomal tubule carriers. J. Cell Biol. 217, 2709–2726. https://doi.org/10.1083/jcb.201709055

Rismanchi, N., Soderblom, C., Stadler, J., Zhu, P.-P., Blackstone, C., 2008. Atlastin GTPases are required for Golgi apparatus and ER morphogenesis. Hum. Mol. Genet. 17, 1591–1604. https://doi.org/10.1093/hmg/ddn046

Ritchie, K., Lovestone, S., 2002. The dementias. Lancet Lond. Engl. 360, 1759–1766. https://doi.org/10.1016/S0140-6736(02)11667-9

Ritz, D., Vuk, M., Kirchner, P., Bug, M., Schütz, S., Hayer, A., Bremer, S., Lusk, C., Baloh, R.H., Lee, H., Glatter, T., Gstaiger, M., Aebersold, R., Weihl, C.C., Meyer, H., 2011. Endolysosomal sorting of ubiquitylated caveolin-1 is regulated by VCP and UBXD1 and impaired by VCP disease mutations. Nat. Cell Biol. 13, 1116–1123. https://doi.org/10.1038/ncb2301

Rocha, N., Kuijl, C., van der Kant, R., Janssen, L., Houben, D., Janssen, H., Zwart, W., Neefjes, J., 2009a. Cholesterol sensor ORP1L contacts the ER protein VAP to control Rab7–RILP–p150Glued and late endosome positioning. J. Cell Biol. 185, 1209–1225. https://doi.org/10.1083/jcb.200811005

Rocha, N., Kuijl, C., van der Kant, R., Janssen, L., Houben, D., Janssen, H., Zwart, W., Neefjes, J., 2009b. Cholesterol sensor ORP1L contacts the ER protein VAP to control Rab7–RILP–p150Glued and late endosome positioning. J. Cell Biol. 185, 1209–1225. https://doi.org/10.1083/jcb.200811005

Rogowska, J., 2009. Overview and Fundamentals of Medical Image Segmentation. Handb. Med. Image Process. Anal. 73–90. https://doi.org/10.1016/B978-012373904-9.50013-1

Ron, D., Walter, P., 2007. Signal integration in the endoplasmic reticulum unfolded protein response. Nat. Rev. Mol. Cell Biol. 8, 519–529. https://doi.org/10.1038/nrm2199

Rong, Y., Liu, M., Ma, L., Du, W., Zhang, H., Tian, Y., Cao, Z., Li, Y., Ren, H., Zhang, C., Li, L., Chen, S., Xi, J., Yu, L., 2012. Clathrin and phosphatidylinositol-4,5-bisphosphate regulate autophagic lysosome reformation. Nat. Cell Biol. 14, 924–934. https://doi.org/10.1038/ncb2557

Rothenberg, C., Srinivasan, D., Mah, L., Kaushik, S., Peterhoff, C.M., Ugolino, J., Fang, S., Cuervo, A.M., Nixon, R.A., Monteiro, M.J., 2010. Ubiquilin functions in autophagy and is degraded by chaperone-mediated autophagy. Hum. Mol. Genet. 19, 3219–3232. https://doi.org/10.1093/hmg/ddq231

Row, P.E., Prior, I.A., McCullough, J., Clague, M.J., Urbé, S., 2006. The ubiquitin isopeptidase UBPY regulates endosomal ubiquitin dynamics and is essential for receptor down-regulation. J. Biol. Chem. 281, 12618–12624. https://doi.org/10.1074/jbc.M512615200

Rowland, A.A., Chitwood, P.J., Phillips, M.J., Voeltz, G.K., 2014a. ER Contact Sites Define the Position and Timing of Endosome Fission. Cell 159, 1027–1041. https://doi.org/10.1016/j.cell.2014.10.023

Rowland, A.A., Chitwood, P.J., Phillips, M.J., Voeltz, G.K., 2014b. ER Contact Sites Define the Position and Timing of Endosome Fission. Cell 159, 1027–1041. https://doi.org/10.1016/j.cell.2014.10.023

Saffi, G.T., Botelho, R.J., 2019. Lysosome Fission: Planning for an Exit. Trends Cell Biol. https://doi.org/10.1016/j.tcb.2019.05.003

Sagona, A.P., Nezis, I.P., Pedersen, N.M., Liestøl, K., Poulton, J., Rusten, T.E., Skotheim, R.I., Raiborg, C., Stenmark, H., 2010a. PtdIns(3)P controls cytokinesis through KIF13A-mediated recruitment of FYVE-CENT to the midbody. Nat. Cell Biol. 12, 362–371. https://doi.org/10.1038/ncb2036

Sagona, A.P., Nezis, I.P., Pedersen, N.M., Liestøl, K., Poulton, J., Rusten, T.E., Skotheim, R.I., Raiborg, C., Stenmark, H., 2010b. PtdIns(3)P controls cytokinesis through KIF13A-mediated recruitment of FYVE-CENT to the midbody. Nat. Cell Biol. 12, 362–371. https://doi.org/10.1038/ncb2036

Salo, V.T., Belevich, I., Li, S., Karhinen, L., Vihinen, H., Vigouroux, C., Magré, J., Thiele, C., Hölttä-Vuori, M., Jokitalo, E., Ikonen, E., 2016. Seipin regulates ER-lipid droplet contacts and cargo delivery. EMBO J. 35, 2699–2716. https://doi.org/10.15252/embj.201695170

Sandhoff, K., Harzer, K., 2013. Gangliosides and Gangliosidoses: Principles of Molecular and Metabolic Pathogenesis. J. Neurosci. 33, 10195–10208. https://doi.org/10.1523/JNEUROSCI.0822-13.2013

Sanger, A., Hirst, J., Davies, A.K., Robinson, M.S., 2019. Adaptor protein complexes and disease at a glance. J. Cell Sci. 132, jcs222992. https://doi.org/10.1242/jcs.222992

Sano, R., Annunziata, I., Patterson, A., Moshiach, S., Gomero, E., Opferman, J., Forte, M., d'Azzo, A., 2009. GM1-ganglioside accumulation at the mitochondria-associated ER membranes links ER stress to Ca(2+)-dependent mitochondrial apoptosis. Mol. Cell 36, 500–511. https://doi.org/10.1016/j.molcel.2009.10.021

Saric, A., Freeman, S.A., 2021. Endomembrane Tension and Trafficking. Front. Cell Dev. Biol. 8, 1736. https://doi.org/10.3389/fcell.2020.611326

Saric, A., Freeman, S.A., Williamson, C.D., Jarnik, M., Guardia, C.M., Fernandopulle, M.S., Gershlick, D.C., Bonifacino, J.S., 2021. SNX19 restricts endolysosome motility through contacts with the endoplasmic reticulum. Nat. Commun. 12, 4552. https://doi.org/10.1038/s41467-021-24709-1

Schreij, A.M.A., Fon, E.A., McPherson, P.S., 2016. Endocytic membrane trafficking and neurodegenerative disease. Cell. Mol. Life Sci. CMLS 73, 1529–1545. https://doi.org/10.1007/s00018-015-2105-x

Schröder, B., Wrocklage, C., Pan, C., Jäger, R., Kösters, B., Schäfer, H., Elsässer, H.-P., Mann, M., Hasilik, A., 2007. Integral and Associated Lysosomal Membrane Proteins. Traffic 8, 1676–1686. https://doi.org/10.1111/j.1600-0854.2007.00643.x

Schuberth, C., Buchberger, A., 2005. Membrane-bound Ubx2 recruits Cdc48 to ubiquitin ligases and their substrates to ensure efficient ER-associated protein degradation. Nat. Cell Biol. 7, 999–1006. https://doi.org/10.1038/ncb1299

Schuck, S., Gallagher, C.M., Walter, P., 2014. ER-phagy mediates selective degradation of endoplasmic reticulum independently of the core autophagy machinery. J. Cell Sci. 127, 4078–4088. https://doi.org/10.1242/jcs.154716

Schulze, R.J., Weller, S.G., Schroeder, B., Krueger, E.W., Chi, S., Casey, C.A., McNiven, M.A., 2013. Lipid droplet breakdown requires Dynamin 2 for vesiculation of autolysosomal tubules in hepatocytes. J. Cell Biol. 203, 315–326. https://doi.org/10.1083/jcb.201306140

Scorrano, L., De Matteis, M.A., Emr, S., Giordano, F., Hajnóczky, G., Kornmann, B., Lackner, L.L., Levine, T.P., Pellegrini, L., Reinisch, K., Rizzuto, R., Simmen, T., Stenmark, H., Ungermann, C., Schuldiner, M., 2019. Coming together to define membrane contact sites. Nat. Commun. 10, 1287. https://doi.org/10.1038/s41467-019-09253-3

Seaman, M.N.J., 2012. The retromer complex - endosomal protein recycling and beyond. J. Cell Sci. 125, 4693–4702. https://doi.org/10.1242/jcs.103440

Sekiguchi, T., Furuno, N., Ishii, T., Hirose, E., Sekiguchi, F., Wang, Y., Kobayashi, H., 2019. RagA, an mTORC1 activator, interacts with a hedgehog signaling protein, WDR35/IFT121. Genes Cells Devoted Mol. Cell. Mech. 24, 151–161. https://doi.org/10.1111/gtc.12663

Sherrington, R., Rogaev, E.I., Liang, Y., Rogaeva, E.A., Levesque, G., Ikeda, M., Chi, H., Lin, C., Li, G., Holman, K., Tsuda, T., Mar, L., Foncin, J.F., Bruni, A.C., Montesi, M.P., Sorbi, S., Rainero, I., Pinessi, L., Nee, L., Chumakov, I., Pollen, D., Brookes, A., Sanseau, P., Polinsky, R.J., Wasco, W., Da Silva, H.A., Haines, J.L., Perkicak-Vance, M.A., Tanzi, R.E., Roses, A.D., Fraser, P.E., Rommens, J.M., St George-Hyslop, P.H., 1995. Cloning of a gene bearing missense mutations in early-onset familial Alzheimer's disease. Nature 375, 754–760. https://doi.org/10.1038/375754a0

Shi, Yuan, Chen, X., Elsasser, S., Stocks, B.B., Tian, G., Lee, B.-H., Shi, Yanhong, Zhang, N., de Poot, S.A.H., Tuebing, F., Sun, S., Vannoy, J., Tarasov, S.G., Engen, J.R., Finley, D., Walters, K.J., 2016. Rpn1

provides adjacent receptor sites for substrate binding and deubiquitination by the proteasome. Science 351, 10.1126/science.aad9421 aad9421. https://doi.org/10.1126/science.aad9421

Shim, S.Y., Wang, J., Asada, N., Neumayer, G., Tran, H.C., Ishiguro, K., Sanada, K., Nakatani, Y., Nguyen, M.D., 2008. Protein 600 is a microtubule/endoplasmic reticulum-associated protein in CNS neurons. J. Neurosci. Off. J. Soc. Neurosci. 28, 3604–3614. https://doi.org/10.1523/JNEUROSCI.5278-07.2008

Shirane, M., Wada, M., Morita, K., Hayashi, N., Kunimatsu, R., Matsumoto, Y., Matsuzaki, F., Nakatsumi, H., Ohta, K., Tamura, Y., Nakayama, K.I., 2020. Protrudin and PDZD8 contribute to neuronal integrity by promoting lipid extraction required for endosome maturation. Nat. Commun. 11, 4576. https://doi.org/10.1038/s41467-020-18413-9

Shorten, C., Khoshgoftaar, T.M., 2019. A survey on Image Data Augmentation for Deep Learning. J. Big Data 6, 60. https://doi.org/10.1186/s40537-019-0197-0

Simonyan, K., Zisserman, A., 2015. Very Deep Convolutional Networks for Large-Scale Image Recognition. ArXiv14091556 Cs.

Sipione, S., Monyror, J., Galleguillos, D., Steinberg, N., Kadam, V., 2020. Gangliosides in the Brain: Physiology, Pathophysiology and Therapeutic Applications. Front. Neurosci. 14, 572965. https://doi.org/10.3389/fnins.2020.572965

Sitia, R., Braakman, I., 2003. Quality control in the endoplasmic reticulum protein factory. Nature 426, 891–894. https://doi.org/10.1038/nature02262

Sitte, N., Huber, M., Grune, T., Ladhoff, A., Doecke, W.D., Von Zglinicki, T., Davies, K.J., 2000. Proteasome inhibition by lipofuscin/ceroid during postmitotic aging of fibroblasts. FASEB J. Off. Publ. Fed. Am. Soc. Exp. Biol. 14, 1490–1498. https://doi.org/10.1096/fj.14.11.1490

Słabicki, M., Theis, M., Krastev, D.B., Samsonov, S., Mundwiller, E., Junqueira, M., Paszkowski-Rogacz, M., Teyra, J., Heninger, A.-K., Poser, I., Prieur, F., Truchetto, J., Confavreux, C., Marelli, C., Durr, A., Camdessanche, J.P., Brice, A., Shevchenko, A., Pisabarro, M.T., Stevanin, G., Buchholz, F., 2010a. A genome-scale DNA repair RNAi screen identifies SPG48 as a novel gene associated with hereditary spastic paraplegia. PLoS Biol. 8, e1000408. https://doi.org/10.1371/journal.pbio.1000408

Słabicki, M., Theis, M., Krastev, D.B., Samsonov, S., Mundwiller, E., Junqueira, M., Paszkowski-Rogacz, M., Teyra, J., Heninger, A.-K., Poser, I., Prieur, F., Truchetto, J., Confavreux, C., Marelli, C., Durr, A., Camdessanche, J.P., Brice, A., Shevchenko, A., Pisabarro, M.T., Stevanin, G., Buchholz, F., 2010b. A Genome-Scale DNA Repair RNAi Screen Identifies SPG48 as a Novel Gene Associated with Hereditary Spastic Paraplegia. PLoS Biol. 8, e1000408. https://doi.org/10.1371/journal.pbio.1000408

Sofou, K., Meier, K., Sanderson, L.E., Kaminski, D., Montoliu-Gaya, L., Samuelsson, E., Blomqvist, M., Agholme, L., Gärtner, J., Mühlhausen, C., Darin, N., Barakat, T.S., Schlotawa, L., van Ham, T., Asin Cayuela, J., Sterky, F.H., 2021. Bi-allelic VPS16 variants limit HOPS/CORVET levels and cause a mucopolysaccharidosis-like disease. EMBO Mol. Med. 13, e13376. https://doi.org/10.15252/emmm.202013376

Sohn, M., Korzeniowski, M., Zewe, J.P., Wills, R.C., Hammond, G.R.V., Humpolickova, J., Vrzal, L., Chalupska, D., Veverka, V., Fairn, G.D., Boura, E., Balla, T., 2018. PI(4,5)P2 controls plasma membrane PI4P and PS levels via ORP5/8 recruitment to ER-PM contact sites. J. Cell Biol. 217, 1797–1813. https://doi.org/10.1083/jcb.201710095

Spiegel, R., Soiferman, D., Shaag, A., Shalev, S., Elpeleg, O., Saada, A., 2017. Novel Homozygous Missense Mutation in SPG20 Gene Results in Troyer Syndrome Associated with Mitochondrial Cytochrome c Oxidase Deficiency. JIMD Rep. 33, 55–60. https://doi.org/10.1007/8904_2016_580

Spits, M., Heesterbeek, I.T., Voortman, L.M., Akkermans, J.J., Wijdeven, R.H., Cabukusta, B., Neefjes, J., 2021a. Mobile late endosomes modulate peripheral endoplasmic reticulum network architecture. EMBO Rep. 22, e50815. https://doi.org/10.15252/embr.202050815

Spits, M., Heesterbeek, I.T., Voortman, L.M., Akkermans, J.J., Wijdeven, R.H., Cabukusta, B., Neefjes, J., 2021b. Mobile late endosomes modulate peripheral endoplasmic reticulum network architecture. EMBO Rep. 22. https://doi.org/10.15252/embr.202050815

Sridhar, S., Patel, B., Aphkhazava, D., Macian, F., Santambrogio, L., Shields, D., Cuervo, A.M., 2012. The lipid kinase PI4KIIIβ preserves lysosomal identity. EMBO J. 32, 324–339. https://doi.org/10.1038/emboj.2012.341

Sriram, S.M., Kim, B.Y., Kwon, Y.T., 2011. The N-end rule pathway: emerging functions and molecular principles of substrate recognition. Nat. Rev. Mol. Cell Biol. 12, 735–747. https://doi.org/10.1038/nrm3217

Staropoli, J.F., Karaa, A., Lim, E.T., Kirby, A., Elbalalesy, N., Romansky, S.G., Leydiker, K.B., Coppel, S.H., Barone, R., Xin, W., MacDonald, M.E., Abdenur, J.E., Daly, M.J., Sims, K.B., Cotman, S.L., 2012. A homozygous mutation in KCTD7 links neuronal ceroid lipofuscinosis to the ubiquitin-proteasome system. Am. J. Hum. Genet. 91, 202–208. https://doi.org/10.1016/j.ajhg.2012.05.023

Steel, D., Zech, M., Zhao, C., Barwick, K.E.S., Burke, D., Demailly, D., Kumar, K.R., Zorzi, G., Nardocci, N., Kaiyrzhanov, R., Wagner, M., Iuso, A., Berutti, R., Škorvánek, M., Necpál, J., Davis, R., Wiethoff, S., Mankad, K., Sudhakar, S., Ferrini, A., Sharma, S., Kamsteeg, E.-J., Tijssen, M.A., Verschuuren, C., van Egmond, M.E., Flowers, J.M., McEntagart, M., Tucci, A., Coubes, P., Bustos, B.I., Gonzalez-Latapi, P., Tisch, S., Darveniza, P., Gorman, K.M., Peall, K.J., Bötzel, K., Koch, J.C., Kmieć, T., Plecko, B., Boesch, S., Haslinger, B., Jech, R., Garavaglia, B., Wood, N., Houlden, H., Gissen, P., Lubbe, S.J., Sue, C.M., Cif, L., Mencacci, N.E., Anderson, G., Kurian, M.A., Winkelmann, J., Genomics England Research Consortium, 2020. Loss-of-Function Variants in HOPS Complex Genes VPS16 and VPS41 Cause Early Onset Dystonia Associated with Lysosomal Abnormalities. Ann. Neurol. 88, 867–877. https://doi.org/10.1002/ana.25879

Steinman, R.M., Brodie, S.E., Cohn, Z.A., 1976. Membrane flow during pinocytosis. A stereologic analysis. J. Cell Biol. 68, 665–687. https://doi.org/10.1083/jcb.68.3.665

Stevanin, G., Azzedine, H., Denora, P., Boukhris, A., Tazir, M., Lossos, A., Rosa, A.L., Lerer, I., Hamri, A., Alegria, P., Loureiro, J., Tada, M., Hannequin, D., Anheim, M., Goizet, C., Gonzalez-Martinez, V., Le Ber, I., Forlani, S., Iwabuchi, K., Meiner, V., Uyanik, G., Erichsen, A.K., Feki, I., Pasquier, F., Belarbi, S., Cruz, V.T., Depienne, C., Truchetto, J., Garrigues, G., Tallaksen, C., Tranchant, C., Nishizawa, M., Vale, J., Coutinho, P., Santorelli, F.M., Mhiri, C., Brice, A., Durr, A., on behalf of the SPATAX consortium, 2008. Mutations in SPG11 are frequent in autosomal recessive spastic paraplegia with thin corpus callosum, cognitive decline and lower motor neuron degeneration. Brain 131, 772–784. https://doi.org/10.1093/brain/awm293

Stevanin, G., Santorelli, F.M., Azzedine, H., Coutinho, P., Chomilier, J., Denora, P.S., Martin, E., Ouvrard-Hernandez, A.-M., Tessa, A., Bouslam, N., Lossos, A., Charles, P., Loureiro, J.L., Elleuch, N., Confavreux, C., Cruz, V.T., Ruberg, M., Leguern, E., Grid, D., Tazir, M., Fontaine, B., Filla, A., Bertini, E., Durr, A., Brice, A., 2007a. Mutations in SPG11, encoding spatacsin, are a major cause of spastic paraplegia with thin corpus callosum. Nat. Genet. 39, 366–372. https://doi.org/10.1038/ng1980

Stevanin, G., Santorelli, F.M., Azzedine, H., Coutinho, P., Chomilier, J., Denora, P.S., Martin, E., Ouvrard-Hernandez, A.-M., Tessa, A., Bouslam, N., Lossos, A., Charles, P., Loureiro, J.L., Elleuch, N., Confavreux, C., Cruz, V.T., Ruberg, M., Leguern, E., Grid, D., Tazir, M., Fontaine, B., Filla, A., Bertini, E., Durr, A., Brice, A., 2007b. Mutations in SPG11, encoding spatacsin, are a major cause of spastic paraplegia with thin corpus callosum. Nat. Genet. 39, 366–372. https://doi.org/10.1038/ng1980

Strong, M.J., Gordon, P.H., 2005. Primary lateral sclerosis, hereditary spastic paraplegia and amyotrophic lateral sclerosis: discrete entities or spectrum? Amyotroph. Lateral Scler. Mot. Neuron Disord. Off. Publ. World Fed. Neurol. Res. Group Mot. Neuron Dis. 6, 8–16. https://doi.org/10.1080/14660820410021267

Sun, E.W., Guillén-Samander, A., Bian, X., Wu, Y., Cai, Y., Messa, M., De Camilli, P., 2019. Lipid transporter TMEM24/C2CD2L is a Ca2+-regulated component of ER-plasma membrane contacts in mammalian neurons. Proc. Natl. Acad. Sci. U. S. A. 116, 5775–5784. https://doi.org/10.1073/pnas.1820156116

Suresh, B., Saminathan, A., Chakraborty, K., Zajac, M., Cui, C., Becker, L., Krishnan, Y., 2021. Tubular lysosomes harbor active ion gradients and poise macrophages for phagocytosis. Proc. Natl. Acad. Sci. 118. https://doi.org/10.1073/pnas.2113174118

Suzuki, K., Honda, T., Akatsu, A., Yamaguchi, Noritaka, Yamaguchi, Naoto, 2020. The promoting role of lysosome-localized c-Src in autophagosome-lysosome fusion. Cell. Signal. 75, 109774. https://doi.org/10.1016/j.cellsig.2020.109774

Swanson, J, Burke, E., Silverstein, S.C., 1987. Tubular lysosomes accompany stimulated pinocytosis in macrophages. J. Cell Biol. 104, 1217–1222. https://doi.org/10.1083/jcb.104.5.1217

Swanson, J., Bushnell, A., Silverstein, S.C., 1987. Tubular lysosome morphology and distribution within macrophages depend on the integrity of cytoplasmic microtubules. Proc. Natl. Acad. Sci. U. S. A. 84, 1921–1925. https://doi.org/10.1073/pnas.84.7.1921

Swanson, J.A., Locke, A., Ansel, P., Hollenbeck, P.J., 1992. Radial movement of lysosomes along microtubules in permeabilized macrophages. J. Cell Sci. 103 (Pt 1), 201–209.

Szabadkai, G., Bianchi, K., Várnai, P., De Stefani, D., Wieckowski, M.R., Cavagna, D., Nagy, A.I., Balla, T., Rizzuto, R., 2006. Chaperone-mediated coupling of endoplasmic reticulum and mitochondrial Ca2+ channels. J. Cell Biol. 175, 901–911. https://doi.org/10.1083/jcb.200608073

Tasaki, T., Kim, S.T., Zakrzewska, A., Lee, B.E., Kang, M.J., Yoo, Y.D., Cha-Molstad, H.J., Hwang, J., Soung, N.K., Sung, K.S., Kim, S.-H., Nguyen, M.D., Sun, M., Yi, E.C., Kim, B.Y., Kwon, Y.T., 2013. UBR box N-recognin-4 (UBR4), an N-recognin of the N-end rule pathway, and its role in yolk sac vascular development and autophagy. Proc. Natl. Acad. Sci. U. S. A. 110, 3800–3805. https://doi.org/10.1073/pnas.1217358110

Taylor, C.W., Tovey, S.C., Rossi, A.M., Lopez Sanjurjo, C.I., Prole, D.L., Rahman, T., 2014. Structural organization of signalling to and from IP3 receptors. Biochem. Soc. Trans. 42, 63–70. https://doi.org/10.1042/BST20130205

Tesson, C., Koht, J., Stevanin, G., 2015. Delving into the complexity of hereditary spastic paraplegias: how unexpected phenotypes and inheritance modes are revolutionizing their nosology. Hum. Genet. 134, 511–538. https://doi.org/10.1007/s00439-015-1536-7

Toupenet Marchesi, L., Leblanc, M., Stevanin, G., 2021. Current Knowledge of Endolysosomal and Autophagy Defects in Hereditary Spastic Paraplegia. Cells 10, 1678. https://doi.org/10.3390/cells10071678

Tresse, E., Salomons, F.A., Vesa, J., Bott, L.C., Kimonis, V., Yao, T.-P., Dantuma, N.P., Taylor, J.P., 2010. VCP/p97 is essential for maturation of ubiquitin-containing autophagosomes and this function is impaired by mutations that cause IBMPFD. Autophagy 6, 217–227. https://doi.org/10.4161/auto.6.2.11014

Valdez, C., Wong, Y.C., Schwake, M., Bu, G., Wszolek, Z.K., Krainc, D., 2017. Progranulin-mediated deficiency of cathepsin D results in FTD and NCL-like phenotypes in neurons derived from FTD patients. Hum. Mol. Genet. 26, 4861–4872. https://doi.org/10.1093/hmg/ddx364

Valm, A.M., Cohen, S., Legant, W.R., Melunis, J., Hershberg, U., Wait, E., Cohen, A.R., Davidson, M.W., Betzig, E., Lippincott-Schwartz, J., 2017. Applying systems-level spectral imaging and analysis to reveal the organelle interactome. Nature 546, 162–167. https://doi.org/10.1038/nature22369

Van Bogaert, P., Azizieh, R., Désir, J., Aeby, A., De Meirleir, L., Laes, J.-F., Christiaens, F., Abramowicz, M.J., 2007. Mutation of a potassium channel-related gene in progressive myoclonic epilepsy. Ann. Neurol. 61, 579–586. https://doi.org/10.1002/ana.21121

Vance, J.E., 1990. Phospholipid synthesis in a membrane fraction associated with mitochondria. J. Biol. Chem. 265, 7248–7256.

Vanier, M.T., 2010. Niemann-Pick disease type C. Orphanet J. Rare Dis. 5, 16. https://doi.org/10.1186/1750-1172-5-16

Vantaggiato, C., Panzeri, E., Castelli, M., Citterio, A., Arnoldi, A., Santorelli, F.M., Liguori, R., Scarlato, M., Musumeci, O., Toscano, A., Clementi, E., Bassi, M.T., 2019. ZFYVE26/SPASTIZIN and SPG11/SPATACSIN mutations in hereditary spastic paraplegia types AR-SPG15 and AR-SPG11 have different effects on autophagy and endocytosis. Autophagy 15, 34–57. https://doi.org/10.1080/15548627.2018.1507438

Varga, R.-E., Khundadze, M., Damme, M., Nietzsche, S., Hoffmann, B., Stauber, T., Koch, N., Hennings, J.C., Franzka, P., Huebner, A.K., Kessels, M.M., Biskup, C., Jentsch, T.J., Qualmann, B., Braulke, T., Kurth, I., Beetz, C., Hübner, C.A., 2015. In Vivo Evidence for Lysosome Depletion and Impaired Autophagic Clearance in Hereditary Spastic Paraplegia Type SPG11. PLOS Genet. 11, e1005454. https://doi.org/10.1371/journal.pgen.1005454

Venditti, R., Wilson, C., De Matteis, M.A., 2021. Regulation and physiology of membrane contact sites. Curr. Opin. Cell Biol. 71, 148–157. https://doi.org/10.1016/j.ceb.2021.03.004

Voeltz, G.K., Prinz, W.A., Shibata, Y., Rist, J.M., Rapoport, T.A., 2006. A Class of Membrane Proteins Shaping the Tubular Endoplasmic Reticulum. Cell 124, 573–586. https://doi.org/10.1016/j.cell.2005.11.047

Walkley, S.U., Vanier, M.T., 2009. Secondary lipid accumulation in lysosomal disease. Biochim. Biophys. Acta BBA - Mol. Cell Res. 1793, 726–736. https://doi.org/10.1016/j.bbamcr.2008.11.014

Walther, T.C., Chung, J., Farese, R.V., 2017. Lipid Droplet Biogenesis. Annu. Rev. Cell Dev. Biol. 33, 491–510. https://doi.org/10.1146/annurev-cellbio-100616-060608

Wang, B., Yu, Y., Wei, L., Zhang, Y., 2020. Inhibition of ER stress improves progressive motor deficits in a REEP1-null mouse model of hereditary spastic paraplegia. Biol. Open 9, bio054296. https://doi.org/10.1242/bio.054296

Wang, W., Zhang, X., Gao, Q., Lawas, M., Yu, L., Cheng, X., Gu, M., Sahoo, N., Li, X., Li, P., Ireland, S., Meredith, A., Xu, H., 2017. A voltage-dependent K+ channel in the lysosome is required for refilling lysosomal Ca2+ stores. J. Cell Biol. 216, 1715–1730. https://doi.org/10.1083/jcb.201612123

Wang, Y., Metz, J., Costello, J.L., Passmore, J., Schrader, M., Schultz, C., Islinger, M., 2018. Intracellular redistribution of neuronal peroxisomes in response to ACBD5 expression. PloS One 13, e0209507. https://doi.org/10.1371/journal.pone.0209507

Wartosch, L., Günesdogan, U., Graham, S.C., Luzio, J.P., 2015. Recruitment of VPS33A to HOPS by VPS16 Is Required for Lysosome Fusion with Endosomes and Autophagosomes. Traffic Cph. Den. 16, 727–742. https://doi.org/10.1111/tra.12283

Watts, G.D.J., Thomasova, D., Ramdeen, S.K., Fulchiero, E.C., Mehta, S.G., Drachman, D.A., Weihl, C.C., Jamrozik, Z., Kwiecinski, H., Kaminska, A., Kimonis, V.E., 2007. Novel VCP mutations in inclusion body myopathy associated with Paget disease of bone and frontotemporal dementia. Clin. Genet. 72, 420–426. https://doi.org/10.1111/j.1399-0004.2007.00887.x

Wijdeven, R.H., Janssen, H., Nahidiazar, L., Janssen, L., Jalink, K., Berlin, I., Neefjes, J., 2016. Cholesterol and ORP1L-mediated ER contact sites control autophagosome transport and fusion with the endocytic pathway. Nat. Commun. 7. https://doi.org/10.1038/ncomms11808

Wilhelm, L.P., Wendling, C., Védie, B., Kobayashi, T., Chenard, M., Tomasetto, C., Drin, G., Alpy, F., 2017a. STARD3 mediates endoplasmic reticulum-to-endosome cholesterol transport at membrane contact sites. EMBO J. 36, 1412–1433. https://doi.org/10.15252/embj.201695917

Wilhelm, L.P., Wendling, C., Védie, B., Kobayashi, T., Chenard, M., Tomasetto, C., Drin, G., Alpy, F., 2017b. STARD 3 mediates endoplasmic reticulum-to-endosome cholesterol transport at membrane contact sites. EMBO J. 36, 1412–1433. https://doi.org/10.15252/embj.201695917

Williamson, C.D., Wong, D.S., Bozidis, P., Zhang, A., Colberg-Poley, A.M., 2015. Isolation of Endoplasmic Reticulum, Mitochondria, and Mitochondria-Associated Membrane and Detergent Resistant Membrane Fractions from Transfected Cells and from Human Cytomegalovirus-Infected Primary Fibroblasts. Curr. Protoc. Cell Biol. 68, 3.27.1-3.27.33. https://doi.org/10.1002/0471143030.cb0327s68

Wolfe, D.M., Lee, J.-H., Kumar, A., Lee, S., Orenstein, S.J., Nixon, R.A., 2013. Autophagy failure in Alzheimer's disease and the role of defective lysosomal acidification. Eur. J. Neurosci. 37, 1949–1961. https://doi.org/10.1111/ejn.12169

Wong, L.H., Gatta, A.T., Levine, T.P., 2019. Lipid transfer proteins: the lipid commute via shuttles, bridges and tubes. Nat. Rev. Mol. Cell Biol. 20, 85–101. https://doi.org/10.1038/s41580-018-0071-5

Wong, Y.C., Ysselstein, D., Krainc, D., 2018. Mitochondria-lysosome contacts regulate mitochondrial fission via RAB7 GTP hydrolysis. Nature 554, 382–386. https://doi.org/10.1038/nature25486

Wu, D., Pan, W., 2010. GSK3: a multifaceted kinase in Wnt signaling. Trends Biochem. Sci. 35, 161–168. https://doi.org/10.1016/j.tibs.2009.10.002

Wu, H., Carvalho, P., Voeltz, G.K., 2018. Here, There and Everywhere: The Importance of ER Membrane Contact Sites. Science 361, eaan5835. https://doi.org/10.1126/science.aan5835

Wu, W., Lin, C., Wu, K., Jiang, L., Wang, X., Li, W., Zhuang, H., Zhang, X., Chen, H., Li, S., Yang, Y., Lu, Y., Wang, J., Zhu, R., Zhang, L., Sui, S., Tan, N., Zhao, B., Zhang, J., Li, L., Feng, D., 2016. FUNDC1 regulates mitochondrial dynamics at the ER-mitochondrial contact site under hypoxic conditions. EMBO J. 35, 1368–1384. https://doi.org/10.15252/embj.201593102

Wu, Y., Whiteus, C., Xu, C.S., Hayworth, K.J., Weinberg, R.J., Hess, H.F., Camilli, P.D., 2017. Contacts between the endoplasmic reticulum and other membranes in neurons. Proc. Natl. Acad. Sci. 114, E4859–E4867. https://doi.org/10.1073/pnas.1701078114

Wu-Baer, F., Lagrazon, K., Yuan, W., Baer, R., 2003. The BRCA1/BARD1 Heterodimer Assembles Polyubiquitin Chains through an Unconventional Linkage Involving Lysine Residue K6 of Ubiquitin. J. Biol. Chem. 278, 34743–34746. https://doi.org/10.1074/jbc.C300249200

Wyant, G.A., Abu-Remaileh, M., Frenkel, E.M., Laqtom, N.N., Dharamdasani, V., Lewis, C.A., Chan, S.H., Heinze, I., Ori, A., Sabatini, D.M., 2018. NUFIP1 is a ribosome receptor for starvation-induced ribophagy. Science 360, 751–758. https://doi.org/10.1126/science.aar2663

Xu, L., Xie, Q., Qi, L., Wang, C., Xu, N., Liu, W., Yu, Y., Li, S., Xu, Y., 2018. Bcl-2 overexpression reduces cisplatin cytotoxicity by decreasing ER-mitochondrial Ca2+ signaling in SKOV3 cells. Oncol. Rep. 39, 985–992. https://doi.org/10.3892/or.2017.6164

Xu, N., Zhang, S.O., Cole, R.A., McKinney, S.A., Guo, F., Haas, J.T., Bobba, S., Farese, R.V., Mak, H.Y., 2012. The FATP1-DGAT2 complex facilitates lipid droplet expansion at the ER-lipid droplet interface. J. Cell Biol. 198, 895–911. https://doi.org/10.1083/jcb.201201139

Yalçın, B., Zhao, L., Stofanko, M., O'Sullivan, N.C., Kang, Z.H., Roost, A., Thomas, M.R., Zaessinger, S., Blard, O., Patto, A.L., Sohail, A., Baena, V., Terasaki, M., O'Kane, C.J., 2017. Modeling of axonal endoplasmic reticulum network by spastic paraplegia proteins. eLife 6, e23882. https://doi.org/10.7554/eLife.23882

Yin, J., Schoeffler, A.J., Wickliffe, K., Newton, K., Starovasnik, M.A., Dueber, E.C., Harris, S.F., 2015. Structural Insights into WD-Repeat 48 Activation of Ubiquitin-Specific Protease 46. Struct. Lond. Engl. 1993 23, 2043–2054. https://doi.org/10.1016/j.str.2015.08.010

Yu, L., McPhee, C.K., Zheng, L., Mardones, G.A., Rong, Y., Peng, J., Mi, N., Zhao, Y., Liu, Z., Wan, F., Hailey, D.W., Oorschot, V., Klumperman, J., Baehrecke, E.H., Lenardo, M.J., 2010. Termination of autophagy and reformation of lysosomes regulated by mTOR. Nature 465, 942–946. https://doi.org/10.1038/nature09076

Zaarur, N., Meriin, A.B., Bejarano, E., Xu, X., Gabai, V.L., Cuervo, A.M., Sherman, M.Y., 2014. Proteasome Failure Promotes Positioning of Lysosomes around the Aggresome via Local Block of Microtubule-Dependent Transport. Mol. Cell. Biol. 34, 1336–1348. https://doi.org/10.1128/MCB.00103-14

Zampese, E., Fasolato, C., Kipanyula, M.J., Bortolozzi, M., Pozzan, T., Pizzo, P., 2011. Presenilin 2 modulates endoplasmic reticulum (ER)-mitochondria interactions and Ca2+ cross-talk. Proc. Natl. Acad. Sci. U. S. A. 108, 2777–2782. https://doi.org/10.1073/pnas.1100735108

Zempel, H., Mandelkow, E.-M., 2015. Tau missorting and spastin-induced microtubule disruption in neurodegeneration: Alzheimer Disease and Hereditary Spastic Paraplegia. Mol. Neurodegener. 10. https://doi.org/10.1186/s13024-015-0064-1

Zhan, J., He, J., Zhou, Y., Wu, M., Liu, Y., Shang, F., Zhang, X., 2016. Crosstalk Between the Autophagy-Lysosome Pathway and the Ubiquitin-Proteasome Pathway in Retinal Pigment Epithelial Cells. Curr. Mol. Med. 16, 487–495. https://doi.org/10.2174/1566524016666160429121606

Zhang, H., Ge, S., Ni, B., He, K., Zhu, P., Wu, X., Shao, Y., 2021. Augmenting ATG14 alleviates atherosclerosis and inhibits inflammation via promotion of autophagosome-lysosome fusion in macrophages. Autophagy 0, 1–13. https://doi.org/10.1080/15548627.2021.1909833

Zhang, T., Xu, Y., Liu, Y., Ye, Y., 2015. gp78 functions downstream of Hrd1 to promote degradation of misfolded proteins of the endoplasmic reticulum. Mol. Biol. Cell 26, 4438–4450. https://doi.org/10.1091/mbc.E15-06-0354

Zhang, X., Ding, X., Marshall, R.S., Paez-Valencia, J., Lacey, P., Vierstra, R.D., Otegui, M.S., 2020. Reticulon proteins modulate autophagy of the endoplasmic reticulum in maize endosperm. eLife 9, e51918. https://doi.org/10.7554/eLife.51918

Zhang, Y., Gao, P., Yuan, J.S., 2010. Plant Protein-Protein Interaction Network and Interactome. Curr. Genomics 11, 40–46. https://doi.org/10.2174/138920210790218016

Zhao, K., Ridgway, N.D., 2017. Oxysterol-Binding Protein-Related Protein 1L Regulates Cholesterol Egress from the Endo-Lysosomal System. Cell Rep. 19, 1807–1818. https://doi.org/10.1016/j.celrep.2017.05.028

Zhao, Y., Feng, Z., Zou, Y., Liu, Y., 2020. The E3 Ubiquitin Ligase SYVN1 Ubiquitinates Atlastins to Remodel the Endoplasmic Reticulum Network. iScience 23, 101494. https://doi.org/10.1016/j.isci.2020.101494

Zheng, P., Chen, Q., Tian, X., Qian, N., Chai, P., Liu, B., Hu, J., Blackstone, C., Zhu, D., Teng, J., Chen, J., 2018. DNA damage triggers tubular endoplasmic reticulum extension to promote apoptosis by facilitating ER-mitochondria signaling. Cell Res. 28, 833–854. https://doi.org/10.1038/s41422-018-0065-z

Zhu, P.-P., Patterson, A., Lavoie, B., Stadler, J., Shoeb, M., Patel, R., Blackstone, C., 2003. Cellular Localization, Oligomerization, and Membrane Association of the Hereditary Spastic Paraplegia 3A (SPG3A) Protein Atlastin. J. Biol. Chem. 278, 49063–49071. https://doi.org/10.1074/jbc.M306702200

Ziv, I., Matiuhin, Y., Kirkpatrick, D.S., Erpapazoglou, Z., Leon, S., Pantazopoulou, M., Kim, W., Gygi, S.P., Haguenauer-Tsapis, R., Reis, N., Glickman, M.H., Kleifeld, O., 2011. A perturbed ubiquitin landscape distinguishes between ubiquitin in trafficking and in proteolysis. Mol. Cell. Proteomics MCP 10, M111.009753. https://doi.org/10.1074/mcp.M111.009753

Zou, Y., He, W., Wang, K., Han, H., Xiao, T., Chen, X., Zhou, B., Tan, J., Xia, K., Tang, B., Chen, C., Shen, L., Yan, R., Zhang, Z., 2018. Identification of rare RTN3 variants in Alzheimer's disease in Han Chinese. Hum. Genet. 137, 141–150. https://doi.org/10.1007/s00439-018-1868-1

Annex 1:

Article 2: Loss of spatacsin impairs cholesterol trafficking and calcium homeostasis (2019)

- Maxime Boutry
- Alexandre Pierga
- Raphaël Matusiak
- Julien Branchu
- Marc Houllegatte
- Yoan Ibrahim
- Elise Balse
- Khalid-Hamid El Hachimi
- Alexis Brice
- Giovanni Stevanin
- Frédéric Darios

Communications Biology **volume 2**, Article number : 380 (2019)

CONTRIBUTION :

For this work, I performed the experiments and analyses that were done on the cholesterol accumulation in the lysosomes of neurons in absence of spatacsin. I also performed the experiments & analyses with Frédéric on the role of calcineurin regulation of TFEB levels and the role of TFEB on cholesterol accumulation in lysosomes, this was during the reviewing process of the paper.

COMMUNICATIONS BIOLOGY

ARTICLE

https://doi.org/10.1038/s42003-019-0615-z OPEN

Loss of spatacsin impairs cholesterol trafficking and calcium homeostasis

Maxime Boutry[1,2,3,4,5,7], Alexandre Pierga[1,2,3,4], Raphaël Matusiak[1,2,3,4], Julien Branchu[1,2,3,4], Marc Houllegatte[1,2,3,4,5], Yoan Ibrahim[1,2,3,4], Elise Balse[6], Khalid-Hamid El Hachimi[1,2,3,4,5], Alexis Brice[1,2,3,4], Giovanni Stevanin[1,2,3,4,5] & Frédéric Darios[1,2,3,4*]

Mutations in *SPG11*, leading to loss of spatacsin function, impair the formation of membrane tubules in lysosomes and cause lysosomal lipid accumulation. However, the full nature of lipids accumulating in lysosomes and the physiological consequences of such accumulation are unknown. Here we show that loss of spatacsin inhibits the formation of tubules on lysosomes and prevents the clearance of cholesterol from this subcellular compartment. Accumulation of cholesterol in lysosomes decreases cholesterol levels in the plasma membrane, enhancing the entry of extracellular calcium by store-operated calcium entry and increasing resting cytosolic calcium levels. Higher cytosolic calcium levels promote the nuclear translocation of the master regulator of lysosomes TFEB, preventing the formation of tubules and the clearance of cholesterol from lysosomes. Our work reveals a homeostatic balance between cholesterol trafficking and cytosolic calcium levels and shows that loss of spatacsin impairs this homeostatic equilibrium.

[1] Sorbonne Université, UPMC Univ Paris 06, UMR S 1127, F-75013 Paris, France. [2] Inserm, U1127, F-75013 Paris, France. [3] CNRS, UMR 7225, F-75013 Paris, France. [4] Institut du Cerveau et de la Moelle Epinière, ICM, F-75013 Paris, France. [5] Ecole Pratique des Hautes Etudes, PSL Research University, Laboratoire de Neurogénétique, F-75013 Paris, France. [6] Sorbonne Université, UPMC Univ Paris 06, UMR S 1166, F-75013 Paris, France. [7] Present address: Cell Biology Program, Hospital for Sick Children, Peter Gilgan Centre for Research and Learning, Toronto, ON, Canada. *email: frederic.darios@upmc.fr

Mutations in the *SPG11* gene are responsible for a severe form of hereditary spastic paraplegia characterized by bilateral weakness, spasticity in the lower limbs, as well as ataxia or cognitive impairment[1,2]. Most mutations are truncating mutations, suggesting that the symptoms are due to loss of function of the *SPG11* product, spatacsin[3]. Accordingly, knockout of *Spg11* in the mouse reproduces the main motor and cognitive symptoms observed in patients[4]. Studies in SPG11 patient fibroblasts and in *Spg11* knockout mice suggested that loss of spatacsin led to impaired function of lysosomes[4–6]. Lysosomes are organelles containing hydrolytic enzymes that notably fuse with endosomes or autophagosomes to allow degradation of their content. After the degradation step, new lysosomes can be reformed from the hybrid organelles[7,8]. Recycling of the lysosomal membrane after the termination of autophagy, known as autophagic lysosome recovery (ALR), relies on the formation of tubules on the lysosomes. This mechanism involves proteins that participate in membrane trafficking, such as clathrin and dynamin[9,10], but it also relies on spatacsin[11].

Analysis of *Spg11* knockout mice showed that the loss of spatacsin function led to progressive accumulation of lipids in lysosomes, both in neuronal and non-neuronal cells[4]. In particular, it was shown that loss of spatacsin led to lysosomal accumulation of glycosphingolipids in neuronal models[12]. Most lipids such as triacylglycerols, phospholipids, and gangliosides are degraded by the lysosomal hydrolases into their basic building blocks. The latter are then exported in the cytosol to be further degraded to fuel energy metabolism or can re-enter biosynthetic pathways[13]. In contrast, cholesterol is not degraded in the endolysosomal pathway, but it is exported out of this subcellular compartment. It is redistributed to the membranes of other subcellular compartments, placing lysosomes at a crossroad of cholesterol metabolism[14]. However, the molecular mechanisms by which cholesterol leaves late endosomes/lysosomes and reaches other subcellular compartments have been only partially characterized[15]. Furthermore, alteration of cholesterol trafficking is associated with many pathological conditions[16]. It is therefore important to explore the downstream consequences for cellular physiology of impaired cholesterol trafficking. Cholesterol has long been known to influence cellular calcium homeostasis, but little is known about the molecular mechanisms coupling change in cholesterol concentration to alterations of calcium signaling[17].

Here, we show that the loss of spatacsin function and the associated inhibition of tubule formation in late endosomes/lysosomes leads to the accumulation of cholesterol in this compartment, due to its impaired export out of the organelle. This results in a decrease in the level of plasma membrane cholesterol that disturbs intracellular calcium homeostasis. We demonstrate that the resulting modification in cytosolic calcium levels contributes to the impairment of lysosome tubulation and accumulation of cholesterol in late endosomes/lysosomes and that this process is TFEB-dependent.

Results

Tubules on lysosomes contributes to cholesterol clearance. We analyzed the localization of lysosomes in control and spatacsin-deficient ($Spg11^{-/-}$) fibroblasts by LAMP1 immunostaining. $Spg11^{-/-}$ cells showed perinuclear accumulation of LAMP1-positive vesicles (Fig. 1a, b), a phenotype that has been linked to the accumulation of cholesterol in late endosomes and lysosomes[18,19]. We thus tested whether cholesterol accumulates in the late endosomes/lysosomes of $Spg11^{-/-}$ fibroblasts by monitoring intracellular localization of cholesterol with filipin, which stains free cholesterol (Fig. 1c), or the fluorescent probe derived from perfringolysin-O, GFP-D4[20] (Supplementary Fig. 1a). The mean fluorescence intensity of filipin staining of whole cells was the same in $Spg11^{+/+}$ and $Spg11^{-/-}$ fibroblasts (Fig. 1d), a result confirmed by the biochemical analysis of cellular cholesterol content (Supplementary Fig. 1b). However, the proportion of cholesterol colocalized with late endosomes/lysosomes was significantly higher in $Spg11^{-/-}$ than control fibroblasts when monitored with filipin or GFP-D4 (Fig. 1e, Supplementary Fig. 1c). Since mutations in *SPG11* cause neurodegeneration[3], we evaluated the impact of loss of spatacsin function on cholesterol distribution in neuronal models. Biochemical quantification showed that the amount of total cholesterol was similar in $Spg11^{+/+}$ and $Spg11^{-/-}$ neurons (Fig. 1f). We monitored whether cholesterol accumulates in the late endosomes/lysosomes of $Spg11^{-/-}$ neurons with the GFP-D4 probe or filipin staining (Fig. 1g, Supplementary Fig. 1d). Consistent with data obtained in fibroblasts, the proportion of cholesterol colocalized with late endosomes/lysosomes was significantly higher in $Spg11^{-/-}$ than control neurons, suggesting that cholesterol distribution was impaired in neurons in the absence of spatacsin (Fig. 1h, Supplementary Fig. 1d). We previously showed that loss of spatacsin induced the accumulation of gangliosides in lysosomes in neuronal models[12]. We tested whether cholesterol accumulation could be a consequence of the accumulation of gangliosides, by preventing their synthesis using miglustat. Inhibition of ganglioside synthesis did not prevent the accumulation of cholesterol in late endosomes/lysosomes (Supplementary Fig. 1d), suggesting that cholesterol accumulation is not a consequence of the accumulation of gangliosides.

Since the distribution of cholesterol, but not the total amount, was altered in the absence of spatacsin, we hypothesized that the trafficking of cholesterol could be disturbed. We monitored the trafficking of fluorescently labeled cholesterol. Control and $Spg11^{-/-}$ fibroblasts were incubated with low density lipoprotein (LDL) loaded with fluorescent cholesterol for two hours and chased for 24 h. We quantified the colocalization of fluorescent cholesterol with LAMP1 at several time points. During the first four hours, the proportion of fluorescent cholesterol colocalized with LAMP1 increased, consistent with the internalization of LDL, and there was no difference in the internalization of cholesterol between $Spg11^{+/+}$ and $Spg11^{-/-}$ fibroblasts. At longer chase times, there was a progressive decrease in the colocalization of fluorescent cholesterol and LAMP1 in control cells, consistent with the egress of cholesterol from late endosomes/lysosomes[21]. In contrast, the proportion remained stable in $Spg11^{-/-}$ cells (Fig. 1i), suggesting that the efflux of cholesterol from late endosomes/lysosomes was altered in the absence of spatacsin.

Spatacsin participates in the initiation of tubule formation on lysosomes[11]. Accordingly, we observed that $Spg11^{-/-}$ fibroblasts contained fewer lysosomes with tubules than $Spg11^{+/+}$ fibroblasts under basal condition when they were transfected with a vector expressing LAMP1-mCherry and analyzed by live imaging (Supplementary Fig. 2a, b). We tested whether the formation of tubules contributed to cholesterol clearance from lysosomes using siRNA to downregulate the clathrin heavy chain (Fig. 2a), a protein essential for the initiation of tubule formation on late endosomes/lysosomes[9]. Downregulation of the clathrin heavy chain in wild-type fibroblasts significantly decreased the number of tubules emanating from lysosomes and increased the proportion of cholesterol colocalized with the LAMP1-positive compartment under basal condition (Fig. 2b, c). Pulse-chase experiments of LDL loaded with fluorescent cholesterol showed that the efflux of cholesterol from late endosomes/lysosomes decreased when clathrin heavy chain was downregulated (Supplementary Fig. 2c). The scission of lysosome tubules requires dynamin[10], a binding partner of spatacsin[12]. The

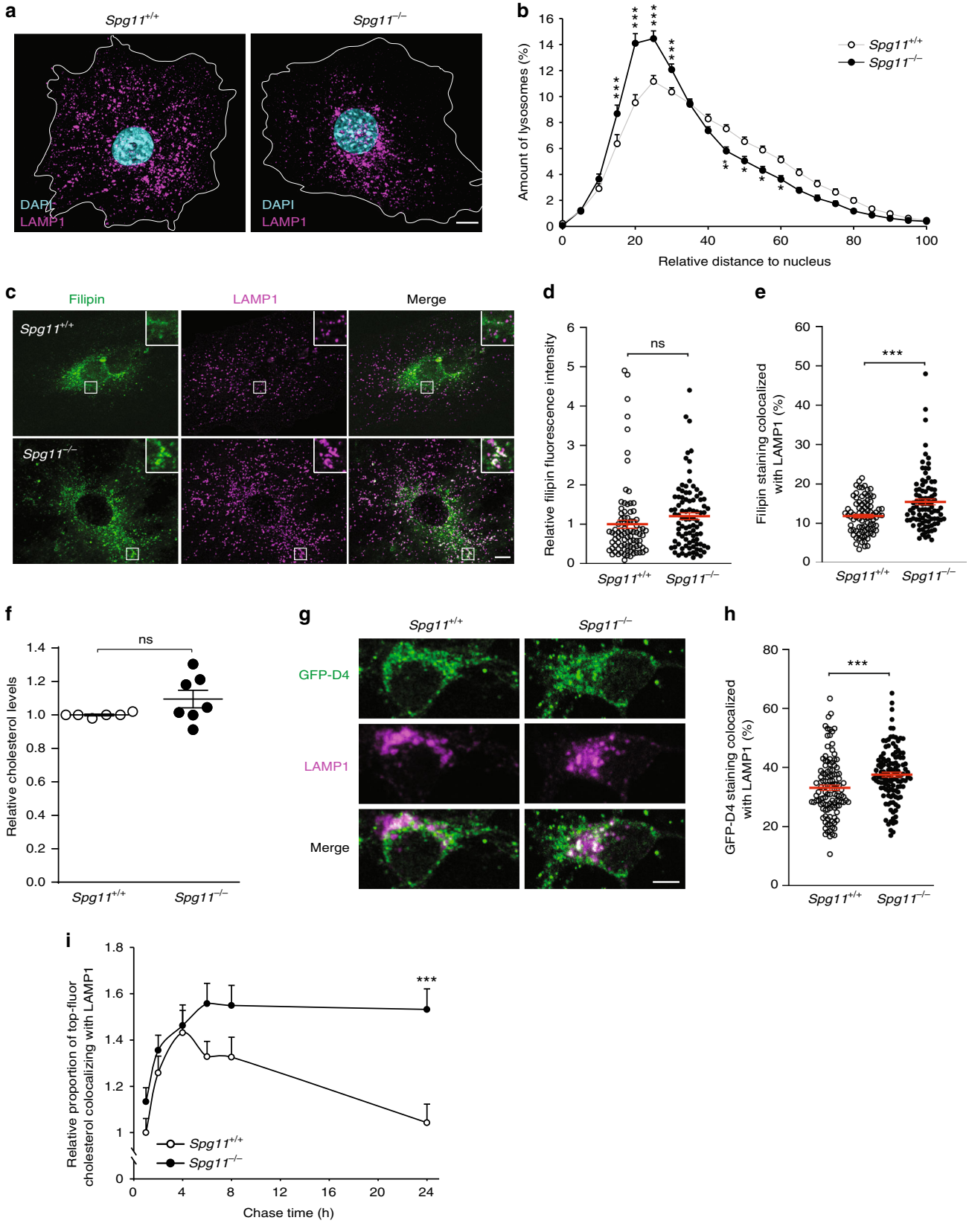

inhibition of dynamin by dynasore increased the proportion of cholesterol colocalized with late endosomes/lysosomes in control, but not in *Spg11*$^{-/-}$ fibroblasts (Fig. 2d). These data suggest that spatacsin and dynamin cooperate in a same pathway to clear cholesterol from late endosomes/lysosomes. Overall, these data suggest that the formation of tubules on lysosomes contributes to the clearance of cholesterol from lysosomes.

We investigated whether lysosomal tubules are used for cholesterol trafficking by transfecting fibroblasts with a vector expressing LAMP1-mCherry and incubating them with LDL

Fig. 1 The loss of spatacsin ($Spg11^{-/-}$) promotes the accumulation of cholesterol in late endosomes/lysosomes. **a** Immunostaining of $Spg11^{+/+}$ and $Spg11^{-/-}$ fibroblasts with the late endosome/lysosome marker LAMP1. Nuclei are stained with DAPI. White lines indicate the cell periphery. Scale bar: 10 µm. **b** Distribution of late endosomes/lysosomes in $Spg11^{+/+}$ and $Spg11^{-/-}$ fibroblasts. The maximum distance between particles and the nucleus was fixed at 100 for each cell. Late endosomes/lysosomes cluster more around the nuclei of $Spg11^{-/-}$ than $Spg11^{+/+}$ fibroblasts. The graph shows the mean ± SEM. $N = 65$ cells from three independent experiments. Two-way ANOVA: $^{***}p < 0.0001$; $^{**}p < 0.01$; $^{*}p < 0.05$. **c** Staining of cholesterol with filipin and late endosomes/lysosomes by the marker LAMP1 in $Spg11^{+/+}$ and $Spg11^{-/-}$ fibroblasts. Insets show a higher magnification of the zone highlighted by a white square. Scale bar: 10 µm. **d** Quantification of the intensity of filipin staining of whole cells showing no significant difference in the total amount of cholesterol in $Spg11^{+/+}$ and $Spg11^{-/-}$ fibroblasts. The graph shows the mean ± SEM. $N > 85$ cells from three independent experiments. *T*-test: $p = 0.83$. **e** Quantification of the amount of filipin staining colocalized with the marker LAMP1, showing more cholesterol in late endosomes/lysosomes in $Spg11^{-/-}$ than $Spg11^{+/+}$ fibroblasts. The graph shows the mean ± SEM. $N > 85$ cells from three independent experiments. *T*-test: $^{***}p < 0.0001$. **f** Biochemical quantification of total cholesterol levels in $Spg11^{+/+}$ ($N = 7$) and $Spg11^{-/-}$ ($N = 6$) neurons. The graph shows the mean ± SD. Mann–Whitney test: $p = 0.63$. **g** Staining of cholesterol with GFP-D4 probe and immunostaining of the late endosome/lysosome marker LAMP1 in $Spg11^{+/+}$ and $Spg11^{-/-}$ primary cortical neurons. Scale bar: 5 µm. **h** Quantification of the amount of GFP-D4 staining colocalized with the marker LAMP1, showing more cholesterol in late endosomes/lysosomes in $Spg11^{-/-}$ than $Spg11^{+/+}$ neurons. The graph shows the mean ± SEM. $N > 110$ cells from three independent experiments. *T*-test: $^{***}p < 0.001$. **i** Quantification of the amount of Top-Fluor cholesterol colocalized with the marker LAMP1 in $Spg11^{+/+}$ and $Spg11^{-/-}$ fibroblasts over time. The graph shows the mean ± SEM. $N > 95$ cells analyzed in three independent experiments. Two-way ANOVA: $^{***}p < 0.0001$

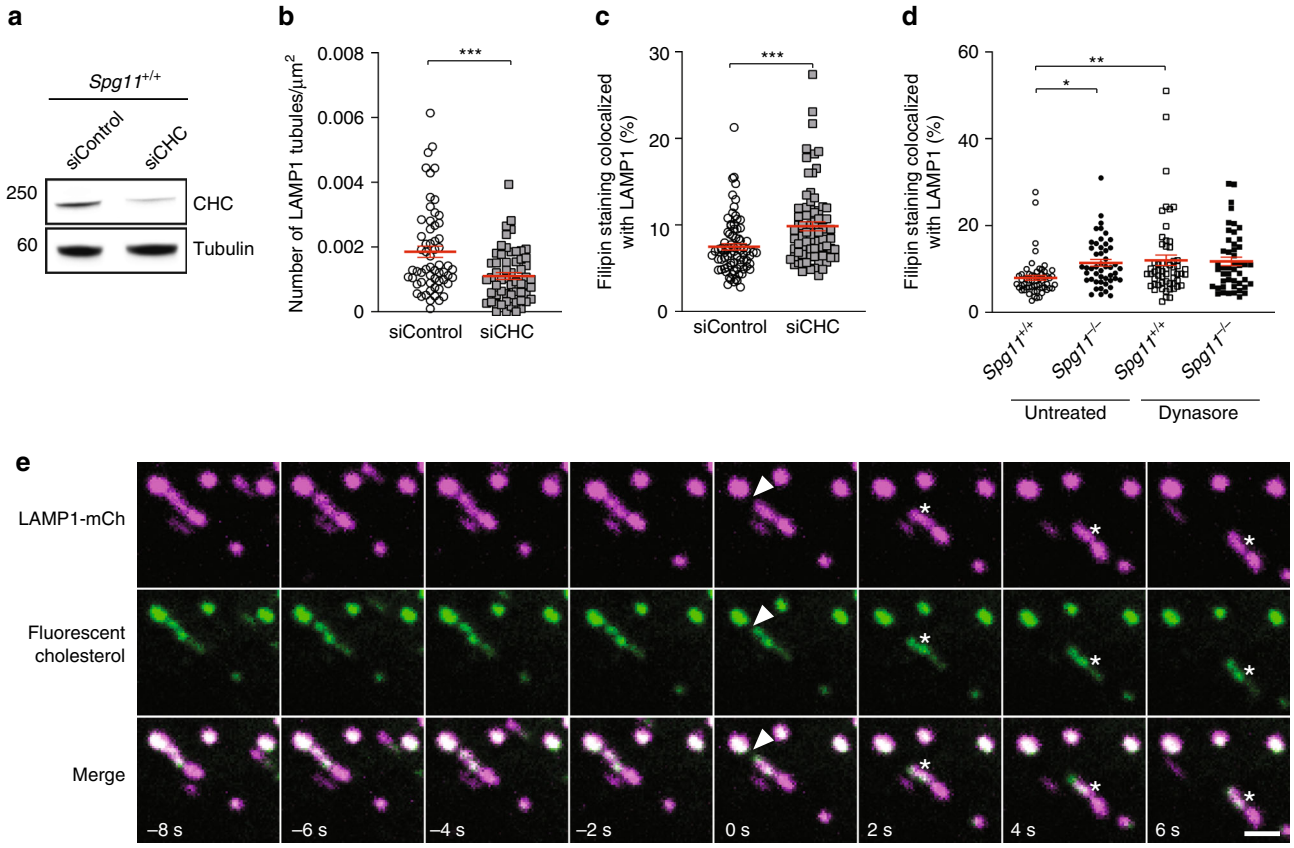

Fig. 2 Inhibition of tubule formation in late endososmes/lysosomes causes the accumulation of cholesterol. **a** Western blot showing the downregulation of clathrin heavy chain (CHC) in wild-type mouse embryonic fibroblasts transfected with siRNA targeting CHC. **b** Quantification of the number of LAMP1-positive tubules in wild-type fibroblasts transfected with a control siRNA or a siRNA that downregulates CHC and expressing LAMP1 fused to mCherry, analyzed by live imaging. The graph shows the mean ± SEM. $N > 58$ cells analyzed in three independent experiments. *T*-test: $^{***}p = 0.0004$. **c** Quantification of the amount of filipin staining colocalized with the LAMP1 marker in fibroblasts transfected with a control siRNA or a siRNA that downregulates CHC. Downregulation of CHC resulted in a higher amount of cholesterol in late endosomes/lysosomes. The graph shows the mean ± SEM. $N > 78$ cells analyzed in three independent experiments. *T*-test: $^{***}p = 0.0002$. **d** Two-hour treatment of fibroblasts with the dynamin inhibitor dynasore (40 µM) induces the accumulation of cholesterol in $Spg11^{+/+}$ but not $Spg11^{-/-}$ fibroblasts. The graph shows the mean ± SEM. $N > 78$ cells analyzed in three independent experiments. Two-way ANOVA: $^{*}p = 0.037$, $^{**}p = 0.0098$. **e** Live imaging of fibroblasts expressing LAMP1-mCherry and loaded with fluorescent cholesterol coupled to LDL. Note the presence of fluorescent cholesterol in tubules emanating from LAMP1-positive late endosomes/lysosomes (asterisk). Arrowheads point to a lysosomal tubule undergoing fission. Scale bar: 2 µm

loaded with fluorescent cholesterol for 2 h in the presence of U18666a. This compound promotes the strong accumulation of cholesterol in late endosomes and lysosomes[22]. Twenty minutes after U18666a washout, which allows cholesterol egress from lysosomes, live imaging showed the fluorescent cholesterol to be localized to lysosomal tubules (Fig. 2e). Occasionally, tubules fission gave rise to new vesicles containing cholesterol (Fig. 2e), suggesting that tubulation in late endosomes/lysosomes is involved in cholesterol trafficking.

Lysosome tubulation regulates plasma membrane cholesterol. In cells, cholesterol levels are high in the plasma membrane, intermediate in late endosome/lysosomes, and low in the endoplasmic reticulum (ER)[23]. We investigated whether the accumulation of cholesterol in late endosomes/lysosomes changes its concentration in the plasma membrane by staining cholesterol in the plasma membrane of live cells using the probe GFP-D4. Cholesterol levels in the plasma membrane were significantly lower in *Spg11*$^{-/-}$ than control cells (Fig. 3a, b). We confirmed this result by determining total and plasma membrane cholesterol levels by an enzymatic assay. The total amount of cholesterol was the same in *Spg11*$^{-/-}$ and *Spg11*$^{+/+}$ cells (Supplementary Fig. 1b), but it was lower in the plasma membrane of *Spg11*$^{-/-}$ than *Spg11*$^{+/+}$ cells (Fig. 3c). Similarly, the inhibition of tubule formation in late endosomes/lysosomes by downregulation of clathrin heavy chain or dynasore treatment led to the accumulation of cholesterol in late endosomes/lysosomes at the expense of the plasma membrane (Figs. 2 and 3d, e). Overall, these results show that impaired trafficking of cholesterol out of late endosomes/lysosomes due to alterations in the formation of tubules results in decreased levels of cholesterol in the plasma membrane.

Depletion of plasma membrane cholesterol increases store-operated calcium entry. We then investigated the consequences of impaired trafficking of cholesterol from lysosomes to the plasma membrane by analyzing cells deficient in spatacsin, which is required for the initiation of tubule formation[11]. On electron microscopy preparations, the loss of spatacsin significantly increased the number and size of the contacts between ER and the plasma membrane (Fig. 4a–c). Such close contacts play a role in various cellular functions and notably regulate transfer of lipids between the membranes, or homeostasis of calcium[24,25]. Upon depletion of the intracellular calcium store of the ER, the ER calcium sensor STIM1 oligomerizes and interacts with the plasma

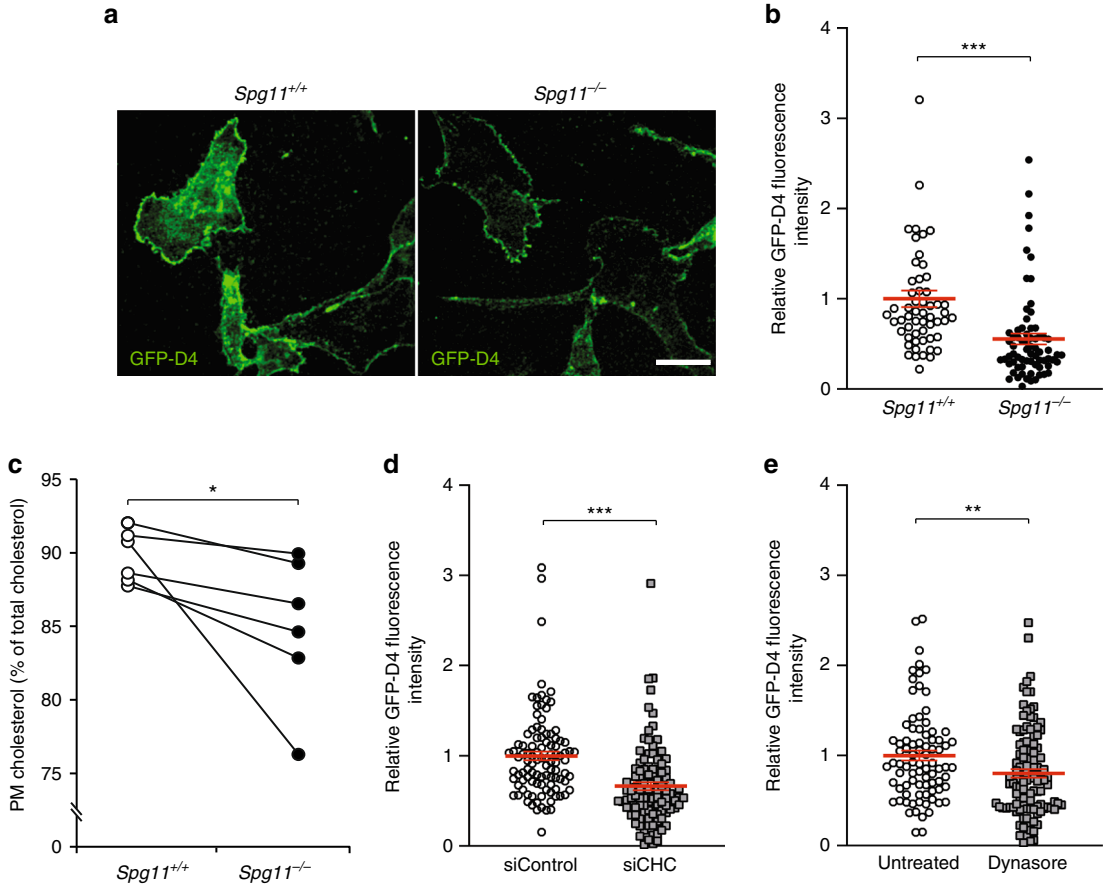

Fig. 3 The inhibition of tubule formation on late endosomes/lysosomes lowers cholesterol content in the plasma membrane. **a**. Staining of live fibroblasts with the probe GFP-D4, which allows staining of the plasma membrane cholesterol only. Scale bar: 10 µm. **b** Quantification of the intensity of GFP-D4 staining performed on live *Spg11*$^{+/+}$ and *Spg11*$^{-/-}$ fibroblasts, showing a lower level of plasma membrane cholesterol in *Spg11*$^{-/-}$ than *Spg11*$^{+/+}$ fibroblasts. The graphs show the mean ± SEM. $N > 95$ cells analyzed in at least three independent experiments. *T*-test: ***$p < 0.0001$. **c** Biochemical quantification of the proportion of cholesterol present in the plasma membrane in *Spg11*$^{+/+}$ and *Spg11*$^{-/-}$ fibroblasts, showing a lower level of plasma membrane cholesterol in *Spg11*$^{-/-}$ than *Spg11*$^{+/+}$ fibroblasts. $N = 6$ independent assays. Wilcoxon paired test: *$p = 0.031$. **d** Quantification of the intensity of GFP-D4 staining performed on live control fibroblasts transfected with control siRNA or siRNA targeting CHC. Downregulation of CHC decreases the amount of cholesterol in the plasma membrane. The graph shows the mean ± SEM. $N > 100$ cells analyzed in two independent experiments. *T*-test: ***$p < 0.0001$. **e** Quantification of the intensity of GFP-D4 staining performed on live control fibroblasts treated with dynasore (40 µM, 2 h). Inhibition of dynamin decreases the amount of cholesterol in the plasma membrane. The graph shows the mean ± SEM. $N > 80$ cells analyzed in three independent experiments. *T*-test: **$p = 0.0062$

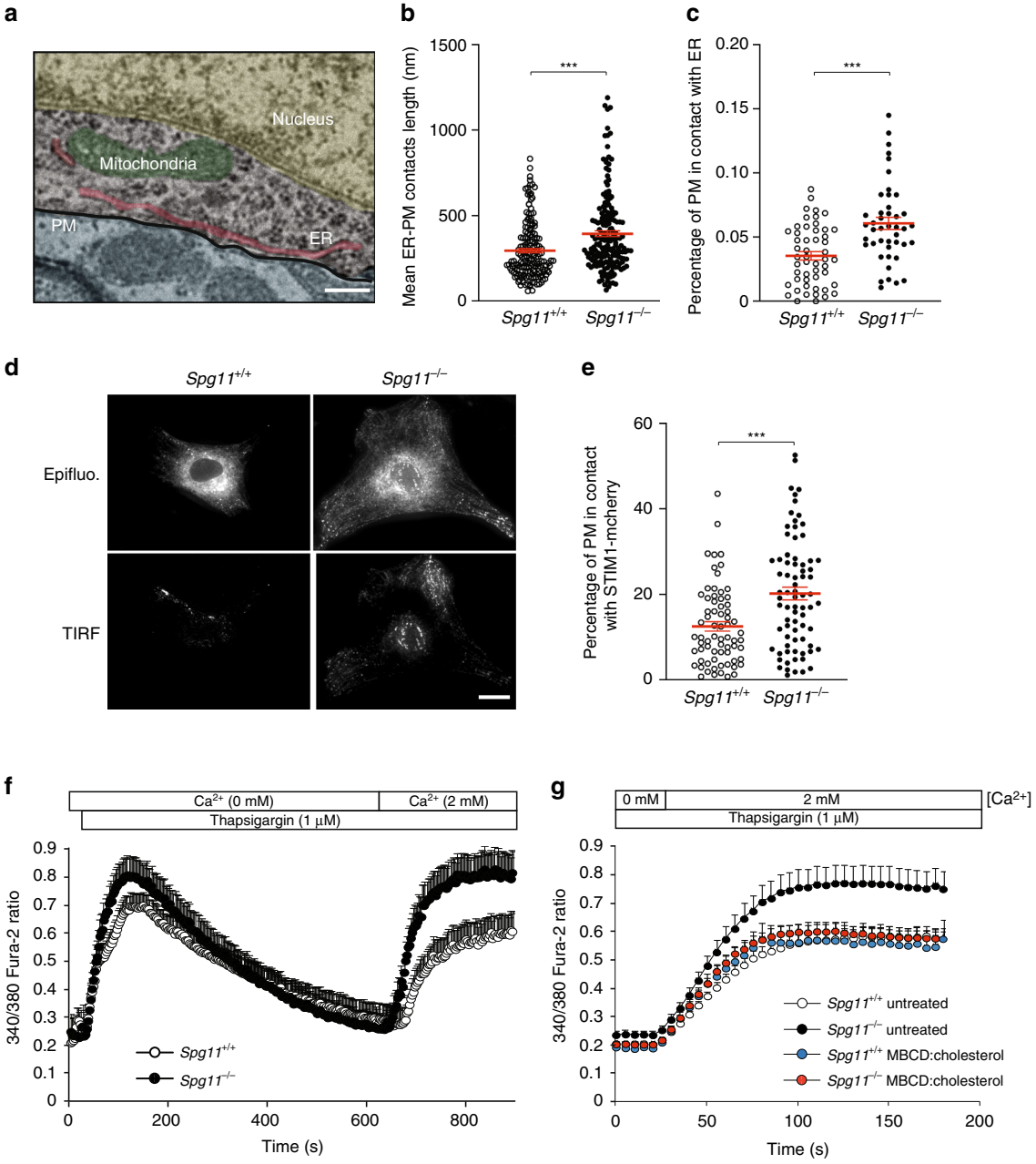

Fig. 4 The depletion of plasma membrane cholesterol promotes higher store-operated calcium entry. **a** Electron micrograph of neurons in the cortex of a 2-month-old *Spg11*$^{-/-}$ mouse, showing close contact between the endoplasmic reticulum (ER) and plasma membrane (PM). False colors highlight the various cellular compartments. Scale bar: 250 nm. **b**, **c** Quantification of contacts between the ER and plasma membrane, defined as the zone where the distance between the two membranes is lower than 30 nm. **b** Quantification of the mean length of individual contacts between the ER and plasma membrane in the cortex of 2-month-old *Spg11*$^{-/-}$ or *Spg11*$^{+/+}$ mice. **c** Quantification of the percentage of the plasma membrane in close contact with the ER in the cortex of 2-month-old *Spg11*$^{-/-}$ or *Spg11*$^{+/+}$ mice. The graphs represent the mean ± SEM. $N > 23$ cells analyzed in two independent mice for each group. *T*-test: ***$p < 0.0001$. **d** *Spg11*$^{-/-}$ or *Spg11*$^{+/+}$ mouse embryonic fibroblasts transfected with vectors expressing STIM1-mCherry imaged by epifluorescence or total internal reflection microscopy (TIRF). Scale bar: 10 µm. **e** Quantification of the percentage of the cellular area with STIM1-mCherry staining detected by TIRF microscopy, indicating close contact between STIM1-mCherry and the plasma membrane. The graph shows the mean ± SEM. $N > 60$ cells from three independent experiments. *T*-test: ***$p < 0.0001$. **f** Evaluation of extracellular calcium import by SOCE. Cytosolic calcium was measured with Fura-2 in the absence of extracellular calcium. The ER calcium store was depleted with thapsigargin, 2 mM $CaCl_2$ added to the extracellular medium, and the increase in cytosolic calcium measured with Fura-2, allowing the quantification of SOCE. The graph shows the mean ± SEM. $N > 35$ cells from three independent experiments. **g** Increasing cholesterol levels in the plasma membrane with methyl-β-cyclodextrin (MBCD) loaded with cholesterol decreases store-operated calcium entry in *Spg11*$^{-/-}$ fibroblasts, measured by the addition of 2 mM extracellular calcium after a 10-min treatment with thapsigargin. The graph shows the mean ± SEM. $N > 60$ cells from three independent experiments

membrane calcium channel Orai1, forming close contacts between the ER and the plasma membrane and allowing the import of extracellular calcium to restore normal intracellular calcium homeostasis[25]. This mechanism is known as store-operated calcium entry (SOCE). We analyzed the proximity of the ER calcium sensor STIM1 and the plasma membrane by total internal reflection fluorescence (TIRF) in cells transfected with a vector expressing STIM1-mCherry. TIRF microscopy performed on fibroblasts under basal conditions confirmed that the proportion of the plasma membrane in close contact with the ER calcium sensor STIM1 was higher in *Spg11*$^{-/-}$ than control cells (Fig. 4d, e).

Levels of cholesterol in the plasma membrane regulate SOCE[26,27]. We therefore tested whether lower levels of cholesterol in the plasma membrane, caused by the loss of spatacsin, altered SOCE. We treated fibroblasts in Ca^{2+}-free medium with the SERCA inhibitor thapsigargin to deplete the ER calcium store and trigger SOCE. We then added 2 mM calcium in the extracellular medium and calcium import was measured using the cytosolic calcium probe Fura-2. *Spg11*$^{-/-}$ cells imported more extracellular calcium than *Spg11*$^{+/+}$ cells (Fig. 4f), suggesting that the loss of spatacsin promoted SOCE under basal conditions.

We then investigated whether the increased SOCE observed in the absence of spatacsin was due to lower levels of cholesterol in the plasma membrane. We increased plasma membrane cholesterol levels by exposing *Spg11*$^{-/-}$ fibroblasts for 1 h to methyl-β-cyclodextrin loaded with cholesterol (Supplementary Fig. 3a, b). This restored normal SOCE in *Spg11*$^{-/-}$ fibroblasts (Fig. 4g), suggesting that cholesterol depletion from the plasma membrane due to impaired lysosomal tubulation is responsible for the increase in SOCE when spatacsin function is lost.

Plasma membrane cholesterol regulates cytosolic calcium levels. SOCE promotes the entry of extracellular calcium into the cytosol that is normally taken up by the ER[25,28]. We monitored whether the increased SOCE due to the loss of spatacsin modified cytosolic calcium levels in resting cells. Cytosolic calcium levels were slightly, but significantly, higher in *Spg11*$^{-/-}$ than *Spg11*$^{+/+}$ fibroblasts (Fig. 5a). We tested whether this increase in cytosolic calcium was a consequence of increased SOCE by reducing extracellular calcium levels to 0.4 mM by adding EGTA to the culture medium for 1 h. Under these conditions, resting cytosolic calcium levels were significantly reduced in both *Spg11*$^{+/+}$ and *Spg11*$^{-/-}$ fibroblasts (Fig. 5a). We confirmed this result by downregulating the expression of STIM1 by transfecting fibroblasts with specific siRNA (Fig. 5b). Downregulation of STIM1 decreased SOCE and restored normal cytosolic calcium levels in *Spg11*$^{-/-}$ cells (Fig. 5b, c), demonstrating that enhanced SOCE increases cytosolic calcium levels in the absence of spatacsin. Finally, we restored normal cytosolic calcium levels when we increased cholesterol levels in the plasma membrane of *Spg11*$^{-/-}$ fibroblasts (Supplementary Fig. 3), suggesting that the increase in SOCE, caused by lower plasma membrane cholesterol levels, is responsible for the alteration of cytosolic calcium levels (Fig. 5d).

Cytosolic calcium contributes to cholesterol accumulation in lysosomes. Among other cellular functions, the entry of extracellular calcium by SOCE has been proposed to regulate the nuclear translocation of TFEB[29], which is a major regulator of lysosome function[30]. We monitored the amount of nuclear TFEB, which represents the transcriptionally active protein[30], in *Spg11*$^{-/-}$ and *Spg11*$^{+/+}$ fibroblasts. The amount of nuclear TFEB was significantly higher in *Spg11*$^{-/-}$ than *Spg11*$^{+/+}$ fibroblasts, whereas cytosolic levels of TFEB were not significantly different (Fig. 6a). Decreasing cytosolic calcium levels using the intracellular chelator EGTA-AM or by lowering extracellular calcium levels decreased the amount of nuclear TFEB in *Spg11*$^{-/-}$ fibroblasts, suggesting that higher SOCE in *Spg11*$^{-/-}$ fibroblasts is responsible for the nuclear translocation of the transcription factor (Fig. 6a). Translocation of TFEB into the nucleus depends on its phosphorylation state[31], and it can be phosphorylated by mTOR. The levels of phosphorylated S6 protein and S6 kinase, two mTOR substrates, were similar in *Spg11*$^{-/-}$ and *Spg11*$^{+/+}$ fibroblasts (Supplementary Fig. 4a), suggesting that mTOR activity is not altered in absence of spatacsin and that it is not responsible for nuclear TFEB in *Spg11*$^{-/-}$ fibroblasts. We then examined whether the entry of calcium mediated by SOCE in *Spg11*$^{-/-}$ fibroblasts could promote the nuclear translocation of TFEB by regulating the calcium-dependent phosphatase calcineurin[32]. The amount of nuclear TFEB was partially restored in *Spg11*$^{-/-}$ fibroblasts upon transfection with a siRNA downregulating calcineurin compared to a control siRNA (Fig. 6b, c). Together, these data suggest that entry of calcium by SOCE in *Spg11*$^{-/-}$ fibroblasts mediates the calcium-dependent dephosphorylation of TFEB, allowing its nuclear translocation.

Since TFEB regulates many lysosome functions, we wondered whether the higher levels of nuclear TFEB due to higher cytosolic calcium levels could regulate the formation of tubules of late endosomes/lysosomes and modulate the cholesterol content in this compartment. We decreased SOCE by downregulating STIM1 or reducing extracellular free Ca^{2+} levels. These treatments partially restored tubule formation in the absence of spatacsin (Fig. 7a and Supplementary Fig. 4b). Similarly, treatment with the intracellular calcium chelator EGTA-AM, to decrease cytosolic calcium levels, increased the number of lysosomes with tubules in *Spg11*$^{-/-}$ fibroblasts (Supplementary Fig. 4c). We tested whether these effects where mediated by TFEB by downregulating its expression using siRNA, leading to lower levels of TFEB in both the cytoplasm and nucleus (Fig. 7b). Downregulation of TFEB in *Spg11*$^{-/-}$ fibroblasts partially restored the number of lysosomes with tubules (Fig. 7c). Overall, these data suggest that altered calcium homeostasis impairs the formation of tubules on lysosomes in the absence of spatacsin in a TFEB-dependent manner.

We showed that tubule formation is required for the clearance of cholesterol from lysosomes (Fig. 1). We thus investigated whether treatment that restores the formation of tubules in the absence of spatacsin also has an effect on cholesterol accumulation in late endosomes/lysosomes. Decreasing SOCE by downregulating STIM1 expression corrected the accumulation of cholesterol observed in lysosomes in *Spg11*$^{-/-}$ fibroblasts (Fig. 7d). Similarly, decreasing cytosolic calcium levels with EGTA-AM decreased cholesterol levels in late endosomes/lysosomes in *Spg11*$^{-/-}$ fibroblasts (Fig. 7e) and *Spg11*$^{-/-}$ neurons (Supplementary Fig. 4d). Downregulation of TFEB in *Spg11*$^{-/-}$ fibroblasts also decreased the proportion of cholesterol in late endosomes/lysosomes (Fig. 7f). Since TFEB was shown to regulate lipid metabolism in liver[33], we monitored whether downregulation of TFEB could activate the transcription factor SREBP that regulates cholesterol synthesis[34]. SREBP is activated by its cleavage, and we detected no change in the levels of activated SREBP between *Spg11*$^{+/+}$ and *Spg11*$^{-/-}$ fibroblasts, whether TFEB was downregulated or not (Supplementary Fig. 4e). Together, these data suggest that increased cytosolic calcium levels contributed to the accumulation of cholesterol in a TFEB-dependent manner.

We also showed that the accumulation of cholesterol in late endosomes/lysosomes slightly decreases cholesterol levels in the plasma membrane (Fig. 3). We reasoned the treatment that restores the distribution of cholesterol in late endosomes/lysosomes in *Spg11*$^{-/-}$ fibroblasts should also restore normal

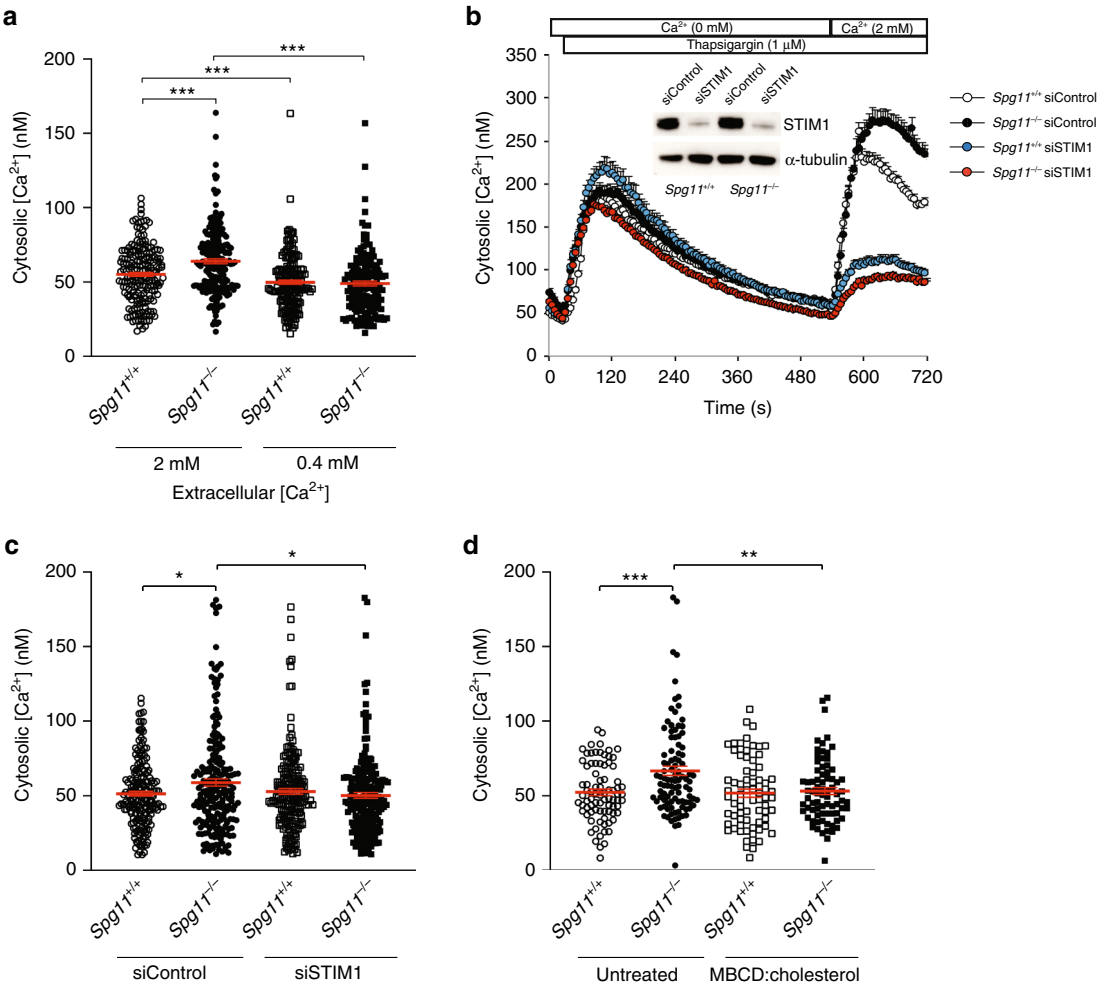

Fig. 5 High store-operated calcium entry in the absence of spatacsin increases cytoplasmic calcium levels. **a** Quantification of cytosolic calcium levels in *Spg11*$^{+/+}$ and *Spg11*$^{-/-}$ fibroblasts in normal medium or medium supplemented with EGTA to lower the extracellular calcium to 0.4 mM. The graphs represent the mean ± SEM. $N > 159$ cells from three independent experiments. Two-way ANOVA: ***$p < 0.0001$. **b** Downregulation of STIM1 strongly abrogates store-operated calcium entry in *Spg11*$^{+/+}$ and *Spg11*$^{-/-}$ fibroblasts. The graphs show the mean ± SEM. $N > 55$ cells from three independent experiments. Insert: western blot showing the downregulation of STIM1 in *Spg11*$^{+/+}$ and *Spg11*$^{-/-}$ fibroblasts transfected with siRNA directed against STIM1. **c** Downregulation of STIM1 decreases the levels of cytosolic calcium in *Spg11*$^{-/-}$ fibroblasts to those measured in *Spg11*$^{+/+}$ fibroblasts. The graph shows the mean ± SEM. $N > 190$ cells analyzed in three independent experiments. Two-way ANOVA: *$p < 0.05$. **d** Treatment of *Spg11*$^{+/+}$ or *Spg11*$^{-/-}$ fibroblasts with methyl-β-cyclodextrin (MBCD) loaded with cholesterol for 1 h restores normal cytosolic calcium levels in *Spg11*$^{-/-}$ cells. The graph shows the mean ± SEM. $N > 70$ cells from three independent experiments. Two-way ANOVA: **$p = 0.0017$, ***$p = 0.0006$

levels of cholesterol in the plasma membrane. Inhibiting SOCE via STIM1 downregulation indeed corrected cholesterol levels in the plasma membrane of *Spg11*$^{-/-}$ fibroblasts (Fig. 7g), showing that dysregulation of calcium homeostasis contributed to the observed alterations in cholesterol trafficking. This demonstrates that impaired calcium homeostasis due to the accumulation of cholesterol in late endosomes/lysosomes contributed to the maintenance or enhancement of the imbalanced cholesterol distribution.

Discussion

Loss of spatacsin leads to accumulation of lipids in lysosomes, both in neuronal and non-neuronal cells[4], but the mechanisms underlying the accumulation of lipids in this compartment are unknown. Here we show that spatacsin is implicated in the trafficking of cholesterol and demonstrate that alteration of this trafficking pathway has functional consequences for the plasma membrane and calcium homeostasis, affecting lysosome function.

Cholesterol is an essential constituent of cellular membranes, but is unevenly distributed within subcellular compartments[23,35]. The lipid composition of membranes, including the amount of cholesterol, affects their biological functions[36]. The mechanisms that regulate cholesterol transport between subcellular compartments thus appear to be critical for cellular functions[14]. The transport of cholesterol out of lysosomes requires the proteins Niemann Pick Type C (NPC) 1 and 2 that likely allow cholesterol to be integrated in the lysosomal membrane[14,23,37]. However, the dissection of mechanisms allowing cholesterol transport is complicated by the co-existence of vesicular transport of cholesterol[21] and non-vesicular trafficking of cholesterol at the levels of contact sites between lysosomes and other subcellular compartments[35,38].

The formation of tubules on lysosomes requires clathrin, spatacsin, and dynamin. These proteins are involved in the recycling of lysosome membranes after the termination of autophagy[9–11]. Although autophagic lysosome recovery occurs after the termination of autophagy, we show here that this machinery is also used to clear cholesterol from late endosomes/lysosomes by

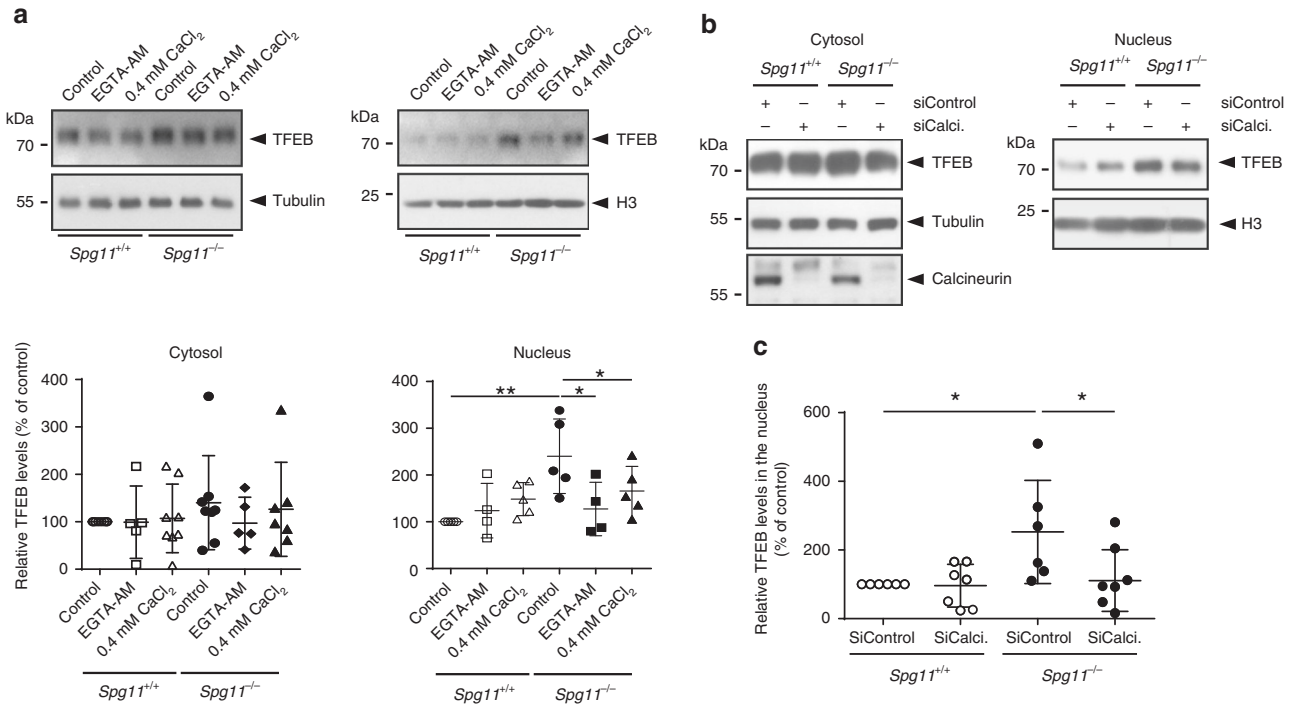

Fig. 6 High cytosolic calcium levels promotes nuclear translocation of TFEB in the absence of spatacsin. **a** Western blot of TFEB in cytosolic and nuclear fractions of *Spg11*$^{+/+}$ and *Spg11*$^{-/-}$ fibroblasts cultured for 2 h in normal medium or medium containing either 0.4 mM $CaCl_2$ or 0.5 µM EGTA-AM. Graphs show the quantification of the amount of TFEB normalized to the levels of α-tubulin (Cytosol) and Histone H3 (Nuclei). One-way ANOVA: *$p < 0.05$, **$p < 0.01$. **b** Western blots of TFEB in cytosolic and nuclear fractions of *Spg11*$^{+/+}$ and *Spg11*$^{-/-}$ fibroblasts transfected with control siRNA or a specific siRNA that downregulates calcineurin (Calci). Downregulation of calcineurin is evidenced by western blot in the cytosolic fraction. **c** Quantification of the amount of nuclear TFEB normalized to the levels of Histone H3 upon downregulation of calcineurin (SiCalci). One-way ANOVA: *$p < 0.05$

tubulation under basal conditions. Accordingly, downregulation of spatacsin was shown to decrease the formation of tubules on late endosomes/lysosomes under basal conditions[11]. The accumulation of cholesterol in late endosomes/lysosomes due to the inhibition of tubulation leads to lower cholesterol levels in the plasma membrane. shRNA screening consistently identified spatacsin as a regulator of cholesterol trafficking from lysosomes toward the plasma membrane[39]. The formation of tubules could give rise to vesicles that may participate in the vesicular trafficking of cholesterol from late endosomes/lysosomes to the plasma membrane. The mechanism that regulates such trafficking is not clear, but it may involve Rab8a and myosin5b, as previously observed[21].

Changes in the concentration of cholesterol in the plasma membrane enhance the entry of extracellular calcium by SOCE and leads to higher cytosolic calcium levels, which could contribute to alter calcium signaling[17]. Cholesterol affects SOCE in various cellular systems[26,40,41]. Global depletion of cholesterol in cells was shown to decrease SOCE[40,41]. In contrast, cholesterol depletion in the plasma membrane was shown to enhance SOCE[26], consistent with our observation that SOCE was higher when plasma membrane cholesterol levels were lower in absence of spatacsin. This effect could be mediated by the interaction of plasma membrane cholesterol with Orai1 channel, regulating its activity[26]. A recent study showed that the entry of calcium by SOCE promotes nuclear translocation of the master lysosomal gene TFEB, promoting its transcriptional activity[29] and thereby regulating autophagy, lysosome biogenesis, and metabolism of lipids[33]. In accordance with these results, we observed increased nuclear translocation of TFEB in absence of spatacsin. Decreasing calcium entry or cytosolic calcium levels was sufficient to restore normal nuclear TFEB levels in the absence of spatacsin. Thus, changes in plasma membrane composition could indirectly modulate lysosomal function through calcium-dependent regulation of TFEB. Nuclear translocation of TFEB depends on its phosphorylation state, and the calcium-dependent phosphatase calcineurin was shown to dephosphorylate TFEB allowing its nuclear translocation[32]. Our data suggest that calcium entry by SOCE allows calcineurin-dependent nuclear translocation of TFEB. Major kinases responsible for TFEB phosphorylation include mTOR, ERK, GSK3β, and AKT[31]. Loss of spatacsin has been shown to impair GSK3β phosphorylation[42], and this signaling pathway could also contribute to the higher nuclear translocation of TFEB in *Spg11*$^{-/-}$ cells.

TFEB activation has been proposed to promote cellular clearance in several lysosomal storage disorders[43]. It could be hypothesized that increased nuclear translocation of TFEB is a compensatory mechanism to restore lysosomal function in *Spg11*$^{-/-}$ cells. However, downregulation of TFEB or treatments that compensated the nuclear translocation of TFEB in *Spg11*$^{-/-}$ cells partially restored the formation of tubules on late endosomes/lysosomes, in the absence of spatacsin, and restored cholesterol homeostasis. These data therefore suggest that nuclear translocation of TFEB inhibited the formation of tubules and the clearance of cholesterol in lysosomes. Nuclear translocation of TFEB may induce the expression of proteins that block the tubulation of lysosomes and the recycling of lysosomal membrane, but the nature of such factors is still to be uncovered.

The interdependence of cholesterol trafficking and calcium homeostasis that we observed highlights a homeostatic equilibrium in which the impairment of cholesterol clearance from lysosomes modifies plasma membrane composition, thus affecting calcium homeostasis and lysosomal cholesterol content in a

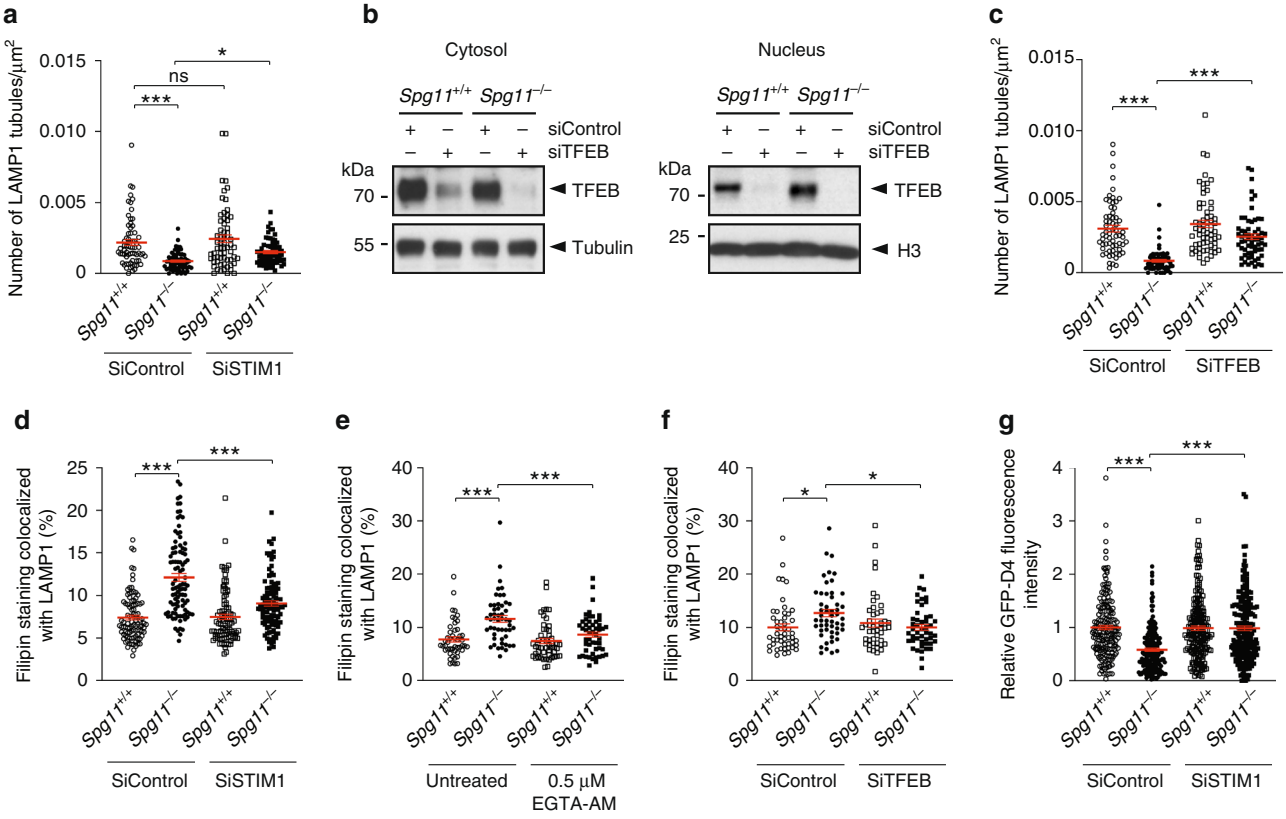

Fig. 7 High cytosolic calcium levels cause accumulation of cholesterol in late endosomes/lysosomes in the absence of spatacsin. **a** Quantification of the number of LAMP1-positive tubules in *Spg11*$^{+/+}$ and *Spg11*$^{-/-}$ fibroblasts expressing LAMP1-mCherry, analyzed by live imaging. The graphs show the mean ± SEM. $N > 60$ cells analyzed in four independent experiments. Two-way ANOVA: $^{*}p = 0.034$, $^{***}p < 0.0001$. **b** Western blots of TFEB in cytosolic and nuclear fractions of *Spg11*$^{+/+}$ and *Spg11*$^{-/-}$ fibroblasts transfected with control siRNA or a specific siRNA that downregulates TFEB. **c** Quantification of the number of LAMP1-positive tubules in *Spg11*$^{+/+}$ and *Spg11*$^{-/-}$ fibroblasts transfected with control siRNA or siRNA that downregulates TFEB. The graph shows the mean ± SEM. $N > 60$ cells analyzed in four independent experiments. Two-way ANOVA: $^{***}p < 0.0001$. **d** Downregulation of STIM1 decreases the amount of cholesterol colocalized with LAMP1 in *Spg11*$^{-/-}$ fibroblasts. The graph shows the mean ± SEM. $N > 95$ cells analyzed in three independent experiments. Two-way ANOVA: $^{***}p < 0.001$. **e** Lowering intracellular calcium levels with EGTA-AM (1 h) decreases the amount of cholesterol colocalized with LAMP1 in *Spg11*$^{-/-}$ fibroblasts. The graph shows the mean ± SEM. $N > 45$ cells analyzed in three independent experiments. Two-way ANOVA: $^{***}p < 0.001$. **f** Downregulation of TFEB decreases the amount of cholesterol colocalized with LAMP1 in *Spg11*$^{-/-}$ fibroblasts. The graph shows the mean ± SEM. $N > 45$ cells analyzed in three independent experiments. Two-way ANOVA: $^{*}p < 0.05$. **g** Quantification of plasma membrane cholesterol with the probe GFP-D4, performed on live *Spg11*$^{+/+}$ and *Spg11*$^{-/-}$ fibroblasts, showing that downregulation of STIM1 restores normal levels of cholesterol in the plasma membrane in *Spg11*$^{-/-}$ fibroblasts. The graph shows the mean ± SEM. $N > 180$ cells analyzed in three independent experiments. Two-way ANOVA: $^{***}p < 0.0001$

TFEB-dependent manner. The compensatory role of the down-regulation of TFEB or the decrease in cytosolic calcium levels on the formation of tubules in late endosomes/lysosomes suggest that spatacsin could be indirectly implicated in the formation of tubules or that alternative mechanisms could compensate for the absence of spatacsin. However, the exact role of spatacsin in the maintenance of the homeostasis of calcium and cholesterol still need to be elucidated.

Our data support the hypothesis that the loss of spatacsin leads to similar impairment of cholesterol and calcium homeostasis both in non-neuronal cells and in neurons. Hereditary spastic paraplegia SPG11 is characterized by neuronal death in various brain regions[4,44]. The persistent deregulation of cholesterol distribution could lead to a slight modification of calcium homeostasis. Calcium plays a central role in cellular physiology and neuronal transmission[45] and a persistent change in cytosolic calcium levels could explain the behavioral alterations that were observed in *Spg11*$^{-/-}$ mice long before neurodegeneration occurred[4]. Alternatively, alteration in calcium homeostasis in absence of spatacsin, could also contribute, in the long term, to neurodegeneration[46].

In conclusion, we demonstrate that loss of spatacsin function impairs trafficking of cholesterol leading to a strong alteration of cellular homeostasis that could contribute to neuronal dysfunction. Since SPG15 patients are indistinguishable from SPG11 patients[47], it would be interesting to investigate whether similar phenotype are observed in absence of spastizin. Atlastin that is mutated in the SPG3 form of HSP has also been proposed to modulate SOCE and lipid metabolism[48]. It would be interesting to investigate the role of atlastin in the distribution of cholesterol. Conversely, alterations of cholesterol trafficking in endosomes and lysosomes have also been described in models of Alzheimer's disease[49], and impaired distribution of cholesterol seems to play a crucial role in neurodegeneration in the case of Alzheimer's disease[50]. It may be informative to test whether the deregulation of cholesterol homeostasis in late endosomes in this disease also induces an alteration of cellular homeostasis that could contribute to persistent and deleterious impairment of lysosomal function.

Methods

Antibodies and chemicals. Thapsigargin, filipin, $CaCl_2$, EDTA, and cholesterol were purchased from Sigma. EGTA-AM was purchased from Thermo Scientific. Dynasore was purchased from Abcam. Miglustat was purchased from Tocris. Antibodies used in the study were: mouse anti-α-tubulin (Abcam); rat anti-LAMP1 (Clone 1D4B, Development Studies Hybridoma Bank), mouse anti clathrin heavy chain (BD Biosciences), mouse anti-STIM1 (Cell Signalling), rabbit anti-TFEB (Proteintech), rabbit anti-calcineurin (Abcam), rabbit anti-histone H3 (Cell Signalling), and rabbit anti SREBP (Abcam). For immunoblotting, the secondary antibodies were conjugated to horseradish peroxidase (Jackson Laboratories) or fluorochromes (IR-dye 800 or IR-dye 680; LI-COR). Secondary antibodies used for immunofluorescence were purchased from Thermo Scientific.

Mouse embryonic fibroblast cultures. *Spg11*$^{-/-}$ mice in C57BL/6 N background were described previously[4]. Mouse embryonic fibroblasts (MEFs) were prepared using E14.5 embryos obtained from the breeding of heterozygous mice. After removing the head and inner organs, the body was minced with a razor blade and incubated in 0.25% trypsin/EDTA (Gibco) for 15 min at 37 °C. Cells were dissociated and grown in DMEM medium (Gibco) supplemented with 10% FBS and 1% penicillin/streptomycin. All experiments were performed between passages 4 and 6. At least three independent preparations of fibroblasts were used for each experiment.

Primary cultures of cortical neurons. Cortices of E14.5 embryos were mechanically dissociated in HBSS medium and plated at 25,000 neurons cm^{-2} on poly-D-Lysine (250 µg ml^{-1}) coated glass coverslips. The neurons were grown in Neurobasal medium supplemented with 2% B27 (Gibco), 2 mM L-glutamine and 2% fetal bovine serum. Half of the medium was changed every 2 days and neurons were fixed after 6 days in vitro with 4% paraformaldehyde (PFA). When required, neurons were treated with miglustat (100 µM) from the second day after plating.

Electron microscopy. Two-month-old male and female *Spg11*$^{+/+}$ and *Spg11*$^{-/-}$ mice were anaesthetized and killed by intracardiac perfusion with a solution of 4% PFA in 0.1 M phosphate buffer at pH 7.4. Samples from the frontal cortex were fixed in 1% glutaraldehyde in the same buffer, post-fixed in 2% osmium tetroxyde, dehydrated, and embedded in Araldite. Ultrathin sections were stained with uranyl acetate and lead citrate and examined using a Hitashi transmission electron microscope. Images were analyzed using ImageJ.

Calcium imaging. Cells grown in Lab-Tek™ (Nunc) were washed with HCSS buffer (120 mM NaCl, 5.4 mM KCl, 0.8 mM $MgCl_2$, 15 mM glucose, and 20 mM Hepes [pH 7.4]) and incubated with 2.5 µM Fura-2-AM (Life Technologies) for 30 min at room temperature in the dark. Cells were washed with HCSS and incubated 15 min at room temperature to allow Fura-2 de-esterification. Images were recorded with a Nikon Eclipse Ti-E inverted microscope, with excitation of Fura-2-AM loaded cells alternately at 340 and 380 nm. Emission at 510 nm was recorded. Conversion of Fura-2 ratios into cytosolic calcium concentrations was performed as previously described[51].

Plasmids and transfection. LAMP1-mCherry was obtained from Addgene (#45147). STIM1-mcherry was obtained from R. Lewis[52]. Fibroblasts were transfected with the Neon transfection system (Invitrogen), according to the manufacturer's instructions, using the following parameters: 1350 V, 30 ms, and one pulse. For overexpression studies, we used 0.5 µg DNA per 50×10^3 cells and the analysis was performed 24 h after transfection. For silencing studies, 50×10^3 cells were transfected with 1 pmol siRNA (Invitrogen) and analyzed 48 h later. The sequence of siRNA targeting STIM1 was 5′-GCAAGGAUGUUAUAUUUGATT-3′, that targeting clathrin heavy chain, 5′-CAUUGUCUGUGAUCGGUUUTT-3′, that targeting TFEB, 5′-CAACCUAAUUGAGAGAAGATT-3′, and that targeting calcineurin, 5′-GGGUUUGGAUAGGAUCAAUTT-3′.

Immunofluorescence. After fixation with 4% PFA, cells were incubated with PBS containing 10 mM NH_4Cl for 10 min at 22 °C to quench autofluorescence. Cells were incubated with a solution of 5% BSA/ 0.1% Triton X-100 in PBS for 30 min at 22 °C and then with primary antibodies in 5% BSA/0.1% Triton X-100 in PBS overnight at 4 °C. After washing, the cells were incubated with the secondary antibodies for 45 min at room temperature and mounted in Prolong Gold reagent (Thermo Scientific). Images were acquired with a Zeiss upright microscope equipped with a Plan-APOCHROMAT objective (×63; NA: 1.4), allowing acquisition of optical section images (Apotome 2 microscope).

Lysosome positioning. The position of lysosomes was assessed using ImageJ and MATLAB software. Signals from the nucleus (DAPI) and lysosomes (LAMP1) from an optical section were acquired with an Apotome 2 microscope. The centroid of the nucleus was determined using the DAPI signal and centroids of each lysosome were determined as the pixel with the highest intensity for each LAMP1-positive vesicle. The distance between lysosome centroids and the nucleus centroid was calculated. The results were expressed as the relative distance to the nucleus with 100 being the distance between the nucleus and the farthest lysosome.

Live-cell imaging. The formation of tubules in late endosomes/lysosomes was followed by live imaging of cells expressing LAMP1-mcherry at 37 °C and 5% CO2 using a Leica DMi8 microscope equipped with a Yokogawa Confocal Spinning Disk module. Cells were chosen randomly, with the only criterion being LAMP1-mCherry levels sufficiently high to detect lysosomal tubules.

Cholesterol staining. Cells were fixed with 4% PFA for 30 min at 22 °C. They were then incubated with filipin (50 µg ml^{-1}) in PBS supplemented with 10% FBS for 2 h at room temperature in the dark, without prior permeabilization. Cells were then processed for immunostaining when required. Cholesterol levels were quantified as the mean gray value using ImageJ. Colocalization of cholesterol staining with lysosomes was quantified using ImageJ on randomly chosen images of cultured fibroblasts. First, we created a mask corresponding to LAMP1 staining using the automatic threshold in Image J. The mask was copied to the corresponding fluorescence image of cholesterol. We quantified the total intensity of cholesterol fluorescence in the lysosome mask and expressed it as the percentage of total cholesterol fluorescence in every cell. A preparation of domain D4 of prefringolysin O fused to GFP (GFP-D4) was produced and purified as previously described[53]. Labeling of total cholesterol was performed by incubating fixed and permeabilized cells with 20 µg ml^{-1} recombinant GFP-D4 for 20 min at 22 °C. Cholesterol of the outer leaflet of the plasma membrane was labeled by incubating live cells for 15 min at 22 °C with 20 µg ml^{-1} GFP-D4 diluted in PBS containing 2 mM $CaCl_2$ and 0.8 mM $MgCl_2$. Cells were then fixed with 4% PFA for 20 min and processed for imaging.

Cholesterol measurement. Cells cultured in 60 mm petri dishes were harvested and lysed by incubation in 100 mM NaCl, 10 mM Tris HCl pH 7.4, 1 mM EGTA, 2 mM $MgCl_2$, 1% Triton X-100, and Halt™ Protease Inhibitor Cocktail (Thermo Scientific) for 30 min at 4 °C. The total cellular cholesterol concentration was measured using the Amplex® Red Cholesterol Assay Kit (Thermo Scientific). The values were normalized to total cellular protein concentration, which was determined by BCA assay (Thermo Scientific).

The cholesterol content of the plasma membrane was measured using a protocol modified from Chu et al.[39]. In brief, cells were extensively washed with ice-cold assay buffer (310 mM sucrose, 1 mM $MgSO_4$, 0.5 mM Sodium phosphate [pH 7.4]) and then incubated with or without 1 U ml^{-1} cholesterol oxidase for 3 min at room temperature. The buffer was removed and the cells washed once with ice-cold assay buffer. Cells were lysed and the cholesterol concentration measured as described above. The plasma membrane cholesterol concentration was calculated by subtracting the amount of intracellular cholesterol (cells incubated with cholesterol oxidase) from the total amount of cholesterol (cells incubated in the absence of cholesterol oxidase). The values were normalized to total cellular protein concentration determined by BCA assay.

Cholesterol trafficking. Unlabeled LDL (1 mg) from human plasma (Thermo Scientific) was incubated with 50 nmol cholesterol (Top-Fluor cholesterol, Avanti Polar Lipids) for 2 h at 40 °C and dialyzed overnight in PBS supplemented with 1 mM EDTA. LDL-deprived serum was prepared as described previously[54]. Cells were cultured in medium prepared with LDL-deprived serum for 24 h. Cholesterol trafficking was monitored by adding LDL complexed with Top-Fluor Cholesterol to the cells followed by incubation for 2 h. Cells were washed with culture medium and fixed with 4% PFA after various times of incubation in LDL-free medium.

Cholesterol loading of plasma membrane. Methyl-β-cyclodextrin (150 mg, MBCD, Sigma) was mixed with 5 mg cholesterol (Sigma) in 1 ml PBS and sonicated for 5 min (45% duty cycle, Branson Sonifier 250). Cells were incubated for 1 h at 37 °C with 1.5 mg ml^{-1} MBCD and 50 µg ml^{-1} cholesterol in serum-free DMEM medium.

Western blot analysis. Downregulation of clathrin heavy chain or STIM1 was evaluated by lysing cells in 100 mM NaCl, 10 mM Tris HCl pH 7.4, 1 mM EGTA, 2 mM $MgCl_2$, 1% Triton X-100, and Halt™ Protease Inhibitor Cocktail (Thermo Scientific) for 15 min at 4 °C. Lysates were cleared by a 15-min centrifugation at 16,000 × *g* at 4 °C. The subcellular localization of TFEB was evaluated by preparing the cells as described previously[55]. Protein concentration was determined with the BCA assay kit. Western blots were performed as described previously[56]. Signals were visualized with a chemiluminescence substrate (SuperSignal West Dura) or acquired with an Odyssey ClX (Li-COR) instrument. Signal intensities were quantified using ImageJ software. Uncroped western blots are presented in Supplementary Fig. 5.

Total internal reflection fluorescence microscopy. TIRF experiments were performed on fibroblasts transfected with vectors expressing STIM1-mCherry, using a previously described protocol[57]. Analyses were performed using ImageJ

software. The TIRF signal was obtained by thresholding and the area containing the TIRF signal normalized to the surface for each cell.

Statistics and data analysis. All statistical tests were performed using GraphPad Prism 6 and the tests are described in the figure legends. Multiple comparisons were performed using ANOVA when data had a normal distribution. Holm–Sidak multiple comparison tests allowed to compare the means of the different sets of data. $P < 0.05$ was considered to be statistically significant.

Ethical approval. The care and treatment of animals followed European legislation (N° 2010/63/UE) and national (Ministère de l'Agriculture, France) guidelines for the detention, use, and ethical treatment of laboratory animals. All experiments on animals were approved by the local ethics committee (approval APAFIS-5199) and conducted by authorized personnel.

Reporting summary. Further information on research design is available in the Nature Research Reporting Summary linked to this article.

Data availability

The data that support the findings of this study are available in Supplementary Data 1.

Received: 19 April 2019; Accepted: 17 September 2019;
Published online: 17 October 2019

References

1. Stevanin, G. et al. Mutations in SPG11 are frequent in autosomal recessive spastic paraplegia with thin corpus callosum, cognitive decline and lower motor neuron degeneration. *Brain* **131**, 772–784 (2008).
2. Paisan-Ruiz, C., Dogu, O., Yilmaz, A., Houlden, H. & Singleton, A. SPG11 mutations are common in familial cases of complicated hereditary spastic paraplegia. *Neurology* **70**, 1384–1389 (2008).
3. Stevanin, G. et al. Mutations in SPG11, encoding spatacsin, are a major cause of spastic paraplegia with thin corpus callosum. *Nat. Genet.* **39**, 366–372 (2007).
4. Branchu, J. et al. Loss of spatacsin function alters lysosomal lipid clearance leading to upper and lower motor neuron degeneration. *Neurobiol. Dis.* **102**, 21–37 (2017).
5. Varga, R. E. et al. In vivo evidence for lysosome depletion and impaired autophagic clearance in hereditary spastic paraplegia type SPG11. *PLoS Genet.* **11**, e1005454 (2015).
6. Renvoise, B. et al. Lysosomal abnormalities in hereditary spastic paraplegia types SPG15 and SPG11. *Ann. Clin. Transl. Neurol.* **1**, 379–389 (2014).
7. Bright, N. A., Reaves, B. J., Mullock, B. M. & Luzio, J. P. Dense core lysosomes can fuse with late endosomes and are re-formed from the resultant hybrid organelles. *J. Cell Sci.* **110**(Pt 17), 2027–2040 (1997).
8. Yu, L. et al. Termination of autophagy and reformation of lysosomes regulated by mTOR. *Nature* **465**, 942–946 (2010).
9. Rong, Y. et al. Clathrin and phosphatidylinositol-4,5-bisphosphate regulate autophagic lysosome reformation. *Nat. Cell Biol.* **14**, 924–934 (2012).
10. Schulze, R. J. et al. Lipid droplet breakdown requires dynamin 2 for vesiculation of autolysosomal tubules in hepatocytes. *J. Cell Biol.* **203**, 315–326 (2013).
11. Chang, J., Lee, S. & Blackstone, C. Spastic paraplegia proteins spastizin and spatacsin mediate autophagic lysosome reformation. *J. Clin. Invest.* **124**, 5249–5262 (2014).
12. Boutry, M. et al. Inhibition of lysosome membrane recycling causes accumulation of gangliosides that contribute to neurodegeneration. *Cell Rep.* **23**, 3813–3826 (2018).
13. Schulze, H., Kolter, T. & Sandhoff, K. Principles of lysosomal membrane degradation: Cellular topology and biochemistry of lysosomal lipid degradation. *Biochim. Biophys. Acta* **1793**, 674–683 (2009).
14. Thelen, A. M. & Zoncu, R. Emerging roles for the lysosome in lipid metabolism. *Trends Cell Biol.* **27**, 833–850 (2017).
15. Luo, J., Jiang, L., Yang, H. & Song, B. L. Routes and mechanisms of post-endosomal cholesterol trafficking: a story that never ends. *Traffic* **18**, 209–217 (2017).
16. Soffientini, U. & Graham, A. Intracellular cholesterol transport proteins: roles in health and disease. *Clin. Sci.* **130**, 1843–1859 (2016).
17. Mackrill, J. J. Oxysterols and calcium signal transduction. *Chem. Phys. Lipids* **164**, 488–495 (2011).
18. Li, X. et al. A molecular mechanism to regulate lysosome motility for lysosome positioning and tubulation. *Nat. Cell Biol.* **18**, 404–417 (2016).
19. Rocha, N. et al. Cholesterol sensor ORP1L contacts the ER protein VAP to control Rab7-RILP-p150 Glued and late endosome positioning. *J. Cell Biol.* **185**, 1209–1225 (2009).
20. Ohno-Iwashita, Y. et al. Perfringolysin O, a cholesterol-binding cytolysin, as a probe for lipid rafts. *Anaerobe* **10**, 125–134 (2004).
21. Kanerva, K. et al. LDL cholesterol recycles to the plasma membrane via a Rab8a-Myosin5b-actin-dependent membrane transport route. *Dev. Cell* **27**, 249–262 (2013).
22. Lu, F. et al. Identification of NPC1 as the target of U18666A, an inhibitor of lysosomal cholesterol export and Ebola infection. *Elife* **4**, e12177 (2015).
23. Mesmin, B., Antonny, B. & Drin, G. Insights into the mechanisms of sterol transport between organelles. *Cell Mol. Life Sci.* **70**, 3405–3421 (2013).
24. Saheki, Y. & De Camilli, P. Endoplasmic reticulum-plasma membrane contact sites. *Annu. Rev. Biochem.* **86**, 659–684 (2017).
25. Prakriya, M. & Lewis, R. S. Store-operated calcium channels. *Physiol. Rev.* **95**, 1383–1436 (2015).
26. Derler, I. et al. Cholesterol modulates Orai1 channel function. *Sci. Signal.* **9**, ra10 (2016).
27. Pacheco, J., Dominguez, L., Bohorquez-Hernandez, A., Asanov, A. & Vaca, L. A cholesterol-binding domain in STIM1 modulates STIM1-Orai1 physical and functional interactions. *Sci. Rep.* **6**, 29634 (2016).
28. Smyth, J. T. et al. Activation and regulation of store-operated calcium entry. *J. Cell. Mol. Med.* **14**, 2337–2349 (2010).
29. Zhu, Z. D., Yu, T., Liu, H. J., Jin, J. & He, J. SOCE induced calcium overload regulates autophagy in acute pancreatitis via calcineurin activation. *Cell Death Dis.* **9**, 50 (2018).
30. Settembre, C. et al. A lysosome-to-nucleus signalling mechanism senses and regulates the lysosome via mTOR and TFEB. *EMBO J.* **31**, 1095–1108 (2012).
31. Puertollano, R., Ferguson, S. M., Brugarolas, J. & Ballabio, A. The complex relationship between TFEB transcription factor phosphorylation and subcellular localization. *EMBO J.* **37**, e98804 (2018).
32. Medina, D. L. et al. Lysosomal calcium signalling regulates autophagy through calcineurin and TFEB. *Nat. Cell Biol.* **17**, 288–299 (2015).
33. Settembre, C. et al. TFEB controls cellular lipid metabolism through a starvation-induced autoregulatory loop. *Nat. Cell Biol.* **15**, 647–658 (2013).
34. Robichon, C. & Dugail, I. De novo cholesterol synthesis at the crossroads of adaptive response to extracellular stress through SREBP. *Biochimie* **89**, 260–264 (2007).
35. Ikonen, E. Mechanisms of cellular cholesterol compartmentalization: recent insights. *Curr. Opin. Cell Biol.* **53**, 77–83 (2018).
36. Harayama, T. & Riezman, H. Understanding the diversity of membrane lipid composition. *Nat. Rev. Mol. Cell Biol.* **19**, 281–296 (2018).
37. Kwon, H. J. et al. Structure of N-terminal domain of NPC1 reveals distinct subdomains for binding and transfer of cholesterol. *Cell* **137**, 1213–1224 (2009).
38. Holthuis, J. C. & Menon, A. K. Lipid landscapes and pipelines in membrane homeostasis. *Nature* **510**, 48–57 (2014).
39. Chu, B. B. et al. Cholesterol transport through lysosome-peroxisome membrane contacts. *Cell* **161**, 291–306 (2015).
40. Gwozdz, T., Dutko-Gwozdz, J., Schafer, C. & Bolotina, V. M. Overexpression of Orai1 and STIM1 proteins alters regulation of store-operated Ca2+ entry by endogenous mediators. *J. Biol. Chem.* **287**, 22865–22872 (2012).
41. Zhang, B., Naik, J. S., Jernigan, N. L., Walker, B. R. & Resta, T. C. Reduced membrane cholesterol limits pulmonary endothelial Ca(2+) entry after chronic hypoxia. *Am. J. Physiol. Heart Circ. Physiol.* **312**, H1176–H1184 (2017).
42. Mishra, H. K. et al. GSK3ss-dependent dysregulation of neurodevelopment in SPG11-patient induced pluripotent stem cell model. *Ann. Neurol.* **79**, 826–840 (2016).
43. Bajaj, L. et al. Lysosome biogenesis in health and disease. *J. Neurochem.* **148**, 573–589 (2019).
44. Denora, P. S. et al. Motor neuron degeneration in spastic paraplegia 11 mimics amyotrophic lateral sclerosis lesions. *Brain* **139**, 1723–1734 (2016).
45. Gleichmann, M., Chow, V. W. & Mattson, M. P. Homeostatic disinhibition in the aging brain and Alzheimer's disease. *J. Alzheimers Dis.* **24**, 15–24 (2011).
46. Mattson, M. P. Calcium and neurodegeneration. *Aging Cell* **6**, 337–350 (2007).
47. Hanein, S. et al. Identification of the SPG15 gene, encoding spastizin, as a frequent cause of complicated autosomal-recessive spastic paraplegia, including Kjellin syndrome. *Am. J. Hum. Genet.* **82**, 992–1002 (2008).
48. Li, J. et al. Atlastin regulates store-operated calcium entry for nerve growth factor-induced neurite outgrowth. *Sci. Rep.* **7**, 43490 (2017).
49. Yang, D. S. et al. Defective macroautophagic turnover of brain lipids in the TgCRND8 Alzheimer mouse model: prevention by correcting lysosomal proteolytic deficits. *Brain* **137**, 3300–3318 (2014).

50. Arenas, F., Garcia-Ruiz, C. & Fernandez-Checa, J. C. Intracellular cholesterol trafficking and impact in neurodegeneration. *Front. Mol. Neurosci.* **10**, 382 (2017).
51. Grynkiewicz, G., Poenie, M. & Tsien, R. Y. A new generation of Ca2+ indicators with greatly improved fluorescence properties. *J. Biol. Chem.* **260**, 3440–3450 (1985).
52. Luik, R. M., Wu, M. M., Buchanan, J. & Lewis, R. S. The elementary unit of store-operated Ca2+ entry: local activation of CRAC channels by STIM1 at ER-plasma membrane junctions. *J. Cell Biol.* **174**, 815–825 (2006).
53. Abe, M. & Kobayashi, T. Dynamics of sphingomyelin- and cholesterol-enriched lipid domains during cytokinesis. *Methods Cell Biol.* **137**, 15–24 (2017).
54. Goldstein, J. L., Basu, S. K. & Brown, M. S. Receptor-mediated endocytosis of low-density lipoprotein in cultured cells. *Methods Enzymol.* **98**, 241–260 (1983).
55. Medina, D. L., Settembre, C. & Ballabio, A. Methods to monitor and manipulate TFEB activity during autophagy. *Methods Enzymol.* **588**, 61–78 (2017).
56. Esteves, T. et al. Loss of association of REEP2 with membranes leads to hereditary spastic paraplegia. *Am. J. Hum. Genet.* **94**, 268–277 (2014).
57. Eichel, C. A. et al. Lateral membrane-specific MAGUK CASK down-regulates NaV1.5 channel in cardiac myocytes. *Circ. Res.* **119**, 544–556 (2016).

Acknowledgements

We thank Phenoparc, IGenSeq, Celis, and the ICM.quant facilities of the Institut du Cerveau et de la Moelle Épinière for their contributions. The 1D4B monoclonal antibody was obtained from the Developmental Studies Hybridoma Bank (University of Iowa, Department of Biology, IA 52242). This work was supported by the "Investissements d'avenir" program grants [ANR-10-IAIHU-06] and [ANR-11-INBS-0011] and received funding from the Verum Foundation (to A.B. and G.S.), the French Agency for Research (ANR) (to G.S.), the GIS-Maladies Rares Foundation (to G.S.), the Fondation Roger de Spoelberch (to A.B.), and the European Union with the ANR (to A.B., Seventh Framework Programme - FP7, Omics call; to G.S., the E-Rare programme) and the European Research Council (European Research Council Starting [grant No 311149] to F.D.). M.B. received a fellowship from the French Ministry of Research (Doctoral School ED3C). A. P. received an ARDoC fellowship (17012953) from the Région Ile de France (Doctoral School ED3C).

Author contributions

M.B., A.P., A.B., G.S., and F.D. conceived and designed the experiments. M.B., A.P., R.M., J.B., M.H., Y.I., E.B., K.H.E.H., and F.D. performed the experiments. M.B., A.P., R.M., and F.D. analyzed the data. M.B. and F.D. wrote the paper with comments of all co-authors.

Competing interests

The authors declare no competing interests.

Additional information

Supplementary information is available for this paper at https://doi.org/10.1038/s42003-019-0615-z.

Correspondence and requests for materials should be addressed to F.D.

Reprints and permission information is available at http://www.nature.com/reprints

Publisher's note Springer Nature remains neutral with regard to jurisdictional claims in published maps and institutional affiliations.

Annex 2: MATLAB code of programs used for image analysis

In green are the explanations of the code.

a) Tubular lysosome detection

```
close all
location='C:\Users\alexandre.pierga\Documents\Folder';


% The absolute path to where your data folders are, here its an example
%path

fileList = dir(location); %obtaining the list of subfolders
fileList = fileList([fileList.isdir]); %testing that the subfolders
%are indeed subfolders
numfiles = numel(fileList); % Number of folders in the directory
name = {fileList.name}.';%obtaining the name of the folders
CorrectOrder=natsortfiles(name);%sorting the folders in order

A=[];%variables initialization
B=[];
TableFinal=[];
TailleFinal=[];

for i = 1 : numfiles %opening a loop that will go through each subfolder

    if length(char(CorrectOrder(i)))>=4 %this condition is necessary to
        %remove phantom files named . and .. present in every file list

            disp(['Reading folder ', char(CorrectOrder(i))]);
            % giving you the information in the command window of which
            % folder in being processed

            directory=[char(location), '\', char(CorrectOrder(i)), '\'];
            % Opening the current subfolder & Concatenating strings
            %to obtain the absolute path to the pictures

            fileList2 = dir(directory); % obtaining the list of images
            %in the subfolder
            fileList2 = fileList2(~[fileList2.isdir]); % removes . and ..
            numfiles2 = numel(fileList2); % Number of images in the directory
            %normally =2

                for j = 1 : numfiles2    % going through images

                   nom = fileList2(j).name; % list of images name

                    CANAL1 = 'w2'; % defining the label that will identify
                    %the first channel, which the one marking the cell area
                    % in my example, it is cell tracker and w2 corresponds
                    % to 'wavelength 2'
                    CANAL2 = 'w1'; % defining the label that will identify
                    %the second channel, which the one marking the
                    %lysosomes
```

```
                    % in my example, it is dextran and w1 corresponds
                    % to 'wavelegnth 1'

                    if regexp(nom,CANAL1) ~= 0

                        loc1=strcat(directory, nom);
                        image1 = imread(loc1);

                        % if the image name contains the label 'w2' then it
                        % is defined as the image containing the cell


                    elseif regexp(nom,CANAL2) ~= 0

                        loc2=strcat(directory, nom);
                        image2 = imread(loc2);

                        % if the image name contains the label 'w1' then it
                        % is defined as the image containing the lysosomes

                    end
                end  %closing the images loop


[TableResultats,Tailletubules]=FonctionAnalyseTubules(image1,image2);
                    %here we open an inner function that performs the
                    %analysis of the number of lysosomes in the cell
                    % its input parameters are the two images of the
                    % subfolder and it will give as an output the number of
                    % tubes per cell stacked in atable

                    A=TableResultats;
                    B=Tailletubules;

                    TableFinal=[TableFinal,A]; % results from different cells
                    %are stacked on the same table
                    TailleFinal=[TailleFinal;B];
    end


end % closing the subfolder loop

 Parametres = {'Aire Cellule';'Nbe de Tubule';'Nbe de tubules/Aire'};
 TableFinal=table(TableFinal,'RowNames',Parametres);
 %building the final output table that contains the output values
```

```
function[TableResultats,Tailletubules]=FonctionAnalyseTubules(image1,image2)

% Inputs : image 1 -> Cell tracker
% Image 2 : lysosomes

% Outputs :
% Result Table: 1 column per cell

[f]=(image1);
imagesc(f);%visualizing the image
thresh =kittler(f);%calculating kittler thrshold value

a=(f>thresh);
%Thresholding the image
imshow(a);%visualizing the thresholding

b=imclean(a);%filling holes and cleaning the image
imshow(b);
% visualizing the cleaning

c=remove(b,3000,1048576);
%removing cellular debris based on their (inferior to 3000 pixels)

imshow(c);
%visualizing the cleaned image

A= regionprops(c,'area');%c is a binary image of the cell(s)
A=struct2table(A);%
A=table2array(A); % A is now an array containing all areas of detected cells

B=regionprops(c,'PixelList');% B contains the list of pixel of detected cells
C=[];

TableResultats=NaN(3,1); % variable initialization
Tailletubules=[];

for i=1:length(A) % initiating a loop going through cells
       if A(i)>3000
           C=[B(i)]; % C contains all pixels of a cell
           E=[];
           D=[];

            for j=1:size(C,1)
                D=struct2table(C(j));
                D=table2array(D);
                E=[E;D]; %E contains the pixels of the same cell but
                %concatenated in an array

            end

            AireCell=length(C.PixelList);
            % the area of the cell in pixels corresponds to the number of
            % pixels of the cell

            thresh2=multitresh(image2);
            %calculation of threshold for lysosomal detection
            g=(image2>thresh2);
            %thresholding of the image containing lysosomal staining

           [m]=select(g,E);% selecting the lysosomes that are inside
           %the detected cell
           imshow(m);
           %visualization of the lysosomes
```

```
A2=m;

B2=regionprops(A2,'area');%area extraction of individual lysosomes
B2=struct2table(B2);
B2=table2array(B2);

C2=regionprops(A2,'perimeter');%perimeter extraction
C2=struct2table(C2);
C2=table2array(C2);

D2=regionprops(A2,'PixelList');%pixels extraction
N=0;

EX=regionprops(A2,'Eccentricity');%eccentricity extraction
EX=struct2table(EX);
EX=table2array(EX);

MAX=regionprops(A2,'MajorAxisLength');%Major Axis length extraction
MAX=struct2table(MAX);
MAX=table2array(MAX);

MIX=regionprops(A2,'MinorAxisLength');%Minor Axis length extraction
MIX=struct2table(MIX);
MIX=table2array(MIX);

H2=[]; %variables initialization
G2=[];
Nbetubules=[];
T=[];

for j2=1:length(B2) %going through every lysosome of the cell

        if B2(j2)>20 % lysosomes need to be bigger than 20pixels

          Circularity=2*3.14116*B2(j2)/((C2(j2))^2);
          %Circlarity computation B(j): area C(j): perimeter
          F2=[];
          E2=[];


          if Circularity < 0.5 && EX(j2)>0.9 && (MAX(j2))/(MIX(j2))>4
             N=N+1;
             %conditions that need to be fulfilled to be
             %considered tubular

             for k=1:size(D2,1)
                E2=struct2table(D2(j2));
                E2=table2array(E2);
                F2=[F2;E2];
                %F2 contains pixels of a selected tubular
                %lysosomes
             end

             G2=F2;
             H2=[H2;G2];
             %H2 contains pixels of all selected tubular
             %lysosomes of the cell
             T=[T;MAX(j2)];
             %is the length of each tubular lysosome in column

          end
        end
end
```

```
            [m2]=select2(m,H2);
            % selecting tubular lysosomes of the cell
            imshow(m2);
            %visualizing the tubular lysosomes

            M=N;
            Nbetubules=[Nbetubules;M];
            %number of tubules per cell
            Tailletubules=[Tailletubules;T];
            %length of the tubules per cell

            Ratio= Nbetubules/AireCell;
            %ratio between the number of tubules and the cell area to
            %obtain the number of tubes per unit area
        end



    TableResultats(1)=AireCell;
    TableResultats(2)=Nbetubules;
    TableResultats(3)=Ratio;
          %building the results table

end
```

Other functions used in this program :

- Function select:

```
function[h]=select(image,E)
  % selecting the pixels of the image contained in the E array

h=NaN(size(image));
k=image;

for i=1:size(E,1)
    h(E(i,2),E(i,1))=k(E(i,2),E(i,1));

end
```

- Function imclean :

```
function[BWfinal]=imclean(BWs)

se90 = strel('line', 5, 90);%creates a vertical line length 5 pixels
se0 = strel('line', 5, 0);%creates an horizontal line length 5 pixels
BWsdil = imdilate(BWs, [se90 se0]);
%of the cell border is dilated horizontally and vertically by 5 pixels
BWdfill = imfill(BWsdil, 'holes');
%holes that are surrounded by pixels are filled
seD = strel('diamond',1);%creates a diamond shape that has a radius of 1
BWfinal = imerode(BWdfill,seD);
%the imag eiis eroded on its border by the shape of the diamond

end
```

b) Tubular lysosomes tracking

```
close all
clear
location='C:\Users\a'; % The absolute path to where your data folders are
fileList = dir(location);
fileList = fileList([fileList.isdir]); %
numfiles = numel(fileList); % Number of folders in the directory


BB=[];
BBB=[];
for i1 = 1 : numfiles

    if length(fileList(i1).name)>=4

            display(['Reading folder ', char(fileList(i1).name)]);
            directory=[char(location), '\', char(fileList(i1).name), '\'];
            % Concatenate strings to obtain the absolute path to the
pictures
            fileList2 = dir(directory); % Opens all the files in directory
            %and finds the center of the exit site for each image
            fileList2 = fileList2(~[fileList2.isdir]); % utlisé pour
retirer les 2 . et ..
            name = {fileList2.name}.';
            CorrectOrder=natsortfiles(name);
            numfiles2 = numel(fileList2); % Number of files in the
directory

            for j1 = 1 : numfiles2

                   nom = CorrectOrder(j1);
                   display(['Reading image', char(nom)]);
%                    nom = fileList2(j1).name;
                   loc1=strcat(directory, nom);
                   loc1=char(loc1);
                   image = imread(loc1);


                     A=imbinarize(image);%binarization de l'image
                     A = imclearborder(A, 8);
                     %retire ce qui touche le bord
%                      imshow(A);

                     B=regionprops(A,'centroid');%extraction des centroide
et formatage
                     B=struct2table(B);
                     B=table2array(B);
                     J=j1*ones(size(B,1),1);
                     BB=[B,J];
                     BBB=[BBB;BB];
            end

    end


end
```

```
tracks = track(BBB,30);

X=tracks;
Y=zeros(size(X,1),1);

for i=2:length(X(:,4))
    Y(i)=sqrt((X(i-1,1)-X(i,1))^2)+sqrt((X(i-1,2)-X(i,2))^2);
end

X=[X,Y];
Results=zeros(1,3);

for i2=1:max(X(:,4))
    Z=zeros(1,5);
    for j2=1:length(X(:,4))
        if X(j2,4)==i2
           Z=[Z;X(j2,:)];
        end
    end

if size(Z,1)>10
Distancetot=sum(Z(:,5))-(Z(2,5));
Tempstot=size(Z,1)-1;
Vitesse=Distancetot/Tempstot;
Results=[Results;[Distancetot,Tempstot,Vitesse]];


    end
end

TotNumberofParticles=size(tracks,1);
TotNumberofTrajectories=max(tracks(:,4));
TrajectoriesFollowed=size(Results,1)-1;
```

c) Area overlap between masks

```
close all
location='C:\iphérie'; % The absolute path to where your data folders are
fileList = dir(location);
fileList = fileList([fileList.isdir]); %
numfiles = numel(fileList); % Number of folders in the directory
name = {fileList.name}.';
CorrectOrder=natsortfiles(name);

TableFinal=[];

for i = 1 : numfiles

  if length(char(CorrectOrder(i)))>=4

            display(['Reading folder ', char(CorrectOrder(i))]);
            directory=[char(location), '\', char(CorrectOrder(i)), '\']; %
Concatenate strings to obtain the absolute path to the pictures

            fileList2 = dir(directory); % Opens all the files in directory
and finds the center of the exit site for each image
            fileList2 = fileList2(~[fileList2.isdir]); % utlisé pour
retirer les 2 . et ..
            numfiles2 = numel(fileList2); % Number of files in the
directory

                for j = 1 : numfiles2

                    nom = fileList2(j).name;

                    CANAL1 = 'c1'; % cell tracker
                    CANAL2 = 'Tubes'; % canal lyso
                    CANAL3 = 'c3'; % reticulum

                    if regexp(nom,CANAL1) ~= 0

                        loc1=strcat(directory, nom);
                        image1 = imread(loc1);

                    elseif regexp(nom,CANAL2) ~= 0

                        loc2=strcat(directory, nom);
                        image2 = imread(loc2);

                    elseif regexp(nom,CANAL3) ~= 0

                        loc3=strcat(directory, nom);
                        image3 = imread(loc3);

                    end
                end


[TableResultats]=FonctionAnalyseFibroRETICULUM(image1,image2,image3);
                  A=TableResultats;
```

```
                    TableFinal=[TableFinal,A];
%
    end


end

 Parametres = {'Aire Cellule';'Aire lysosomes';'Ratio aire lysosomes / aire
cellule';'Aire reticulum';'Aire RE/ Aire Cellule';'Aire Lyso contact
RE';'Aire lyso contact/aire totale';'Nombre lysos';'Nombre lysos RE'};
 TableFinal=table(TableFinal,'RowNames',Parametres);

function[TableResultats,p]=FonctionAnalyseFibroRETICULUM(image1,image2,imag
e3)

% %Paramètres d'entrée : image 1 -> cell tracker
% Image 2 : Marquage Lysosomal
% Image 3 : sec61 gfp

% Paramètre de sortie :
% Tableau de résultat : 1 colonne par cellule

[f]=traitementFibro(image1);%traitement de l'image

A= regionprops(f,'area');%f est une image binaire avec les cellules
sélectionnées
A=struct2table(A);%
A=table2array(A); % conversion de A en un vecteur répertoriant les aires

B=regionprops(f,'PixelList');% B répertorie les pixels associées aux aires
C=[];

TableResultats=NaN(9,length(A)); % initiation de la table de résultat

for i=1:length(A) % C contient les pixels associés aux aires des cellules
       if A(i)>3000
           C=[B(i)]; % C contient les coordonnées des pixels d'une cellule
           E=[];
           D=[];

            for j=1:size(C,1) % E répertorie toutes les coordonnées des
pixels des aires dans une matrice N*2
                D=struct2table(C(j));
                D=table2array(D);
                E=[E;D];

            end

            AireCell=length(C.PixelList);
            % aire totale de la cellule

                    [n]=select(image2,E);% sélection des lysosomes avec
seuil
%
                    G=regionprops(n,'area');

                    G=struct2table(G);
                    G=table2array(G);%  vecteur avec aire des lysosomes
```

```
                    AireLysosomes=sum(G); % somme de l'aire des lysosomes
                    NombreLysos=length(G);

                    RatioAireLysCell=AireLysosomes/AireCell;%ratio Aire
lysosomes sur aire de la cellule

                    [n2]=select3(image3,E);% sélection du reticulum
(kittler)
                    G2=regionprops(n2,'area');
                    G2=struct2table(G2);
                    G2=table2array(G2);%  vecteur avec aire des lysosomes

                    AireRE=sum(G2); % somme de l'aire des lysosomes

                    RatioAireRECell=AireRE/AireCell;%ratio Aire lysosomes
sur aire de la cellule
                    H=[];
                    I=[];
                    J=[];

                    H=regionprops(n2,'PixelList'); %Pixels du marquage
reticulum
                    for i2=1:size(H,1) % H répertorie toutes les
coordonnées des pixels des aires dans une matrice N*2
                         I=struct2table(H(i2));
                         I=table2array(I);
                         J=[J;I];

                    end

                    [p]=select(image2,J); % sélection des pixels lyso dans
le reticulum

                    G3=regionprops(p,'area');
                    G3=struct2table(G3);
                    G3=table2array(G3);
                    G3=find(G3>=5);%  vecteur avec aire des lysosomes

                    AireLysosomesRE=sum(G3); % somme de l'aire des
lysosomes
                    NombreLysoRE=length(G3);

                    RatioAireLysRE=AireLysosomesRE/AireLysosomes;

    TableResultats(1,i)=AireCell;
    TableResultats(2,i)=AireLysosomes;
    TableResultats(3,i)=RatioAireLysCell;
    TableResultats(4,i)=AireRE;
    TableResultats(5,i)=RatioAireRECell;
    TableResultats(6,i)=AireLysosomesRE;
    TableResultats(7,i)=RatioAireLysRE;
    TableResultats(8,i)=NombreLysos;
    TableResultats(9,i)=NombreLysoRE;
       imshow(n);
       imshow(n2);
       imshow(p);

       end
end
```

d) Clustering of particles

```
tic
close all

clear all
% clc

% Déclaration de variable %


x = 1;
donneescell = {};
distancelysonoyau = [];
DAPI = 'w1'; %% name of the image that has the center
LAMP = 'Nouveau';%% name of the lamp1 image binarized

location='C:\Users\alexandre.pierga\Desktop\10-09-2021-tubulation-334-
atlk80a\atlk80a\save\clustering'; % The absolute path to where your data
folders are
fileList = dir(location);
fileList = fileList([fileList.isdir]); % retire les . et ..
numfiles = numel(fileList);
name = {fileList.name}.';
CorrectOrder=natsortfiles(name);% Number of folders in the directory


%%%%%%%%%%%%%%%% OUVERTURE DES DOSSIERS ET FICHIERS %%%%%%%%%%%%%


for i = 1:numfiles

%     if length(fileList(i).name)>=4

      if length(char(CorrectOrder(i)))>=4
      disp(['Reading folder ', char(CorrectOrder(i))]);
      directory=[char(location), '\', char(CorrectOrder(i)), '\'];

%             directory=[char(location), '\', char(fileList(i).name), '\'];
% Concatenate strings to obtain the absolute path to the pictures

            fileList2 = dir(directory); % Opens all the files in directory
and finds the center of the exit site for each image
            fileList2 = fileList2(~[fileList2.isdir]); % utlisé pour
retirer les 2 . et ..
            numfiles2 = numel(fileList2); % Number of files in the
directory


            for j = 1 : numfiles2


                nom = fileList2(j).name;


                %%%%%%%%%%%%%%%% ANALYSE DU SIGNAL DAPI %%%%%%%%%%%%%
```

```
                if regexp(nom,DAPI) ~= 0 % si le nom du fichier contient
DAPI %

                    loc=strcat(directory, nom);
                    image=imread(loc); % lit l'image à partir de la
localisation
%                     image=thresh(image);
                    image=imbinarize(image); % transforme l'image en binary
(255 en 1)

                    a  = regionprops(image, 'Centroid', 'Area');
                    s = [];
                    s(:,1:2) = (cat(1,a.Centroid));
                    s(:,3) = (cat(1,a.Area));
                    m = max(s(:,3));

                    for k = 1 : length(s(:,1))
                        if s(k,3) == m
                            centrenoyau(1,1:2) = s(k,1:2);
                        end
                    end

                end


                    %%%%%%%%%%%%%%%% ANALYSE DU SIGNAL LAMP1 %%%%%%%%%%%%%


                if regexp(nom,LAMP) ~= 0

                    loc=strcat(directory, nom);
                    image = imread(loc);


                    I = bpass(image,1,5);
                    r = round(I);
                    thresh = multithresh(r);
                    position = pkfnd(r,thresh,5);

                    figure;
                    imagesc(r);
                    axis image;
                    hold on;
                    title('Image lysosomes')
                    plot(position(:,1),position(:,2),'g+');
                    hold off



                end

            end
            donneescell{x,1} = centrenoyau;
            donneescell{x,2} = position;
            position = [];
            x = x + 1;

    end
```

```
end

%%%%%%%%%%%%%%%% calcul des distances noyau - lysosomes %%%%%%%%%%%%%%%%%%


for i = 1 : length(donneescell(:,1))

    for j = 1 : length(donneescell{i,2}(:,1))

        donneescell{i,2}(j,3)=sqrt((donneescell{i,1}(1,1)-
donneescell{i,2}(j,1))^2+(donneescell{i,1}(1,2)-donneescell{i,2}(j,2))^2);

    end
end

M=[];
for i = 1 : length(donneescell(:,1))

    m = max(donneescell{i,2}(:,3));

    for j = 1 : length(donneescell{i,2}(:,1))

        donneescell{i,2}(j,4) = donneescell{i,2}(j,3);
        distancelysonoyau(j,i) = donneescell{i,2}(j,4)/m*100;

    end
    M=[M,m];
end

clear x thresh signalLAMP signalDAPI s r donneescell fileList fileList2 i I
image is_filtered j k LAMP loc location m nom numfiles numfiles2 o position
directory a centrenoyau DAPI
%
[TableFinal,Table1]=traitementdonnees(distancelysonoyau);
```

e) Fluorescence ratio

```
close all
location='C:\Users\alexandre'; % The absolute path to where your data
folders are
fileList = dir(location);
fileList = fileList([fileList.isdir]); %
numfiles = numel(fileList); % Number of folders in the directory

%%%%%%%%%%%%%%%% OUVERTURE DES DOSSIERS ET FICHIERS %%%%%%%%%%%%%

TableFinal=[];

for i = 1 : numfiles

    if length(fileList(i).name)>=4

            display(['Reading folder ', char(fileList(i).name)]);
            directory=[char(location), '\', char(fileList(i).name), '\']; %
Concatenate strings to obtain the absolute path to the pictures

            fileList2 = dir(directory); % Opens all the files in directory
and finds the center of the exit site for each image
            fileList2 = fileList2(~[fileList2.isdir]); % utlisé pour
retirer les 2 . et ..
            numfiles2 = numel(fileList2); % Number of files in the
directory

                for j = 1 : numfiles2

                    nom = fileList2(j).name;

                    CANAL1 = 'w2'; % canal GM2/p62/GFPd4
                    CANAL2 = 'w1'; % canal lyso
                    CANAL3 = 'cell'; %canal cell tracker

                    if regexp(nom,CANAL1) ~= 0

                        loc1=strcat(directory, nom);
                        image1 = imread(loc1);

                    elseif regexp(nom,CANAL2) ~= 0

                        loc2=strcat(directory, nom);
                        image2 = imread(loc2);

                    elseif regexp(nom,CANAL3) ~= 0

                        loc3=strcat(directory, nom);
                        image3 = imread(loc3);

                    end
                end

[TableResultats]=FonctionAnalyseFibro(image1,image2,image3);
                  A=TableResultats;
                   TableFinal=[TableFinal,A];
    end
```

```
end

 Parametres = {'Aire Cellule';'Intensité moyenne cellule';'Aire
lysosomes';'intensité moyenne lysosomes';'Ratio aire lysosomes / aire
cellule';'Bruit de Fond';'RatioIntensite avec BF';};
 TableFinal=table(TableFinal,'RowNames',Parametres);

function[TableResultats]=FonctionAnalyseFibro(image1,image2,image3)

% %Paramètres d'entrée : image 1 -> Marquage GM2/P62/gfpd4 dans les
% lysosomes
% Image 2 : Marquage Lysosomal
% Image 3 : Marquage du corps cellulaire

% Paramètre de sortie :
% Tableau de résultat : 1 colonne par cellule

[f]=traitementFibro(image3);%traitement de l'image

BF=noise(image1); % calcul du bruit de fond avec double seuillage otsu

A= regionprops(f,'area');%f est une image binaire avec les cellules
sélectionnées
A=struct2table(A);%
A=table2array(A); % conversion de A en un vecteur répertoriant les aires

B=regionprops(f,'PixelList');% B répertorie les pixels associées aux aires
C=[];

TableResultats=NaN(7,length(A)); % initiation de la table de résultat

for i=1:length(A) % C contient les pixels associés aux aires des cellules
       if A(i)>35000
           C=[B(i)]; % C contient les coordonnées des pixels d'une cellule
           E=[];
           D=[];

            for j=1:size(C,1) % E répertorie toutes les coordonnées des
pixels des aires dans une matrice N*2
                D=struct2table(C(j));
                D=table2array(D);
                E=[E;D];

            end

            AireCell=length(C.PixelList);
            % aire totale de la cellule

           [m]=select2(image1,E);% marquage du canal 1 (GM2 ou p62 ou
gfpd4)

            M=[];%matrice des intensités - Calcul de l'intensité de signal
moyenne

                for k=1:size(m,2)
                    M=[M;m(:,k)];
                end
                    Intensitemoyennecellule= mean(M,'omitnan')-BF;
```

```
                    [n]=select(image2,E);% sélection des lysosomes avec
seuillage
%                     nb=imclean(n);
%
                    G=regionprops(n,'area');
                    G=struct2table(G);
                    G=table2array(G);%  vecteur avec aire des lysosomes

                    AireLysosomes=sum(G); % somme de l'aire des lysosomes

                    RatioAireLysCell=(AireLysosomes)/AireCell;%ratio Aire
lysosomes sur aire de la cellule

                    H=[];
                    I=[];
                    J=[];

                    H=regionprops(n,'PixelList'); %Pixels du marquage
Lysosomal

                    for i2=1:size(H,1) % H répertorie toutes les
coordonnées des pixels des aires dans une matrice N*2
                        I=struct2table(H(i2));
                        I=table2array(I);
                        J=[J;I];

                     end

            [p]=select2(image1,J); % sélection des pixels du canal 1
(GM2/p62)qui sont dans le marquage lysosomal = colocalisation

               O=[];%matrice des intensités - Calcul de l'intensité de
signal moyenne

            for i3=1:size(p,2)
                O=[O;p(:,i3)];
            end

            IntensitemoyenneLyso= mean(O,'omitnan')-BF;


RatioIntensite=(AireLysosomes*(IntensitemoyenneLyso))/(AireCell*(Intensitem
oyennecellule));

                    TableResultats(1,i)=AireCell;
                    TableResultats(2,i)=Intensitemoyennecellule;
                    TableResultats(3,i)=AireLysosomes;
                    TableResultats(4,i)=IntensitemoyenneLyso;
                    TableResultats(5,i)=RatioAireLysCell;
                    TableResultats(6,i)=BF;
                    TableResultats(7,i)=RatioIntensite;
       imshow(m); %cellules détectées
       imshow(n);
%        imshow(nb);
       % lysosomes sélectionnés
       end
end
```